Radiative Corrections for ZH Production at Electron-Positron Collider

by

Qian Song

Bachelor of Science, Xi'an Jiaotong University, 2018

Submitted to the Graduate Faculty of

the Dietrich School of Arts and Sciences in partial fulfillment

of the requirements for the degree of

Doctor of Philosophy

University of Pittsburgh

2023

UNIVERSITY OF PITTSBURGH

DIETRICH SCHOOL OF ARTS AND SCIENCES

This dissertation was presented

by

Qian Song

It was defended on

June 2nd 2023

and approved by

Ayres Freitas, Department of Physics and Astronomy

Brian Batell, Department of Physics and Astronomy

Joseph Boudreau, Department of Physics and Astronomy

Wensheng Vincent Liu, Department of Physics and Astronomy

Colin Morningstar, Department of Physics

Radiative Corrections for ZH Production at Electron-Positron Collider

Qian Song, PhD

University of Pittsburgh, 2023

Current experimental measurements on Higgs boson properties are consistent with the Standard Model(SM) predictions, but large experimental uncertainties still leave room for the possibility of new physics. To reduce experimental uncertainties, a so-called "Higgs factory" including the International Linear Collider (ILC) [1, 2], Future Circular Collider (FCC-ee)[3], and Circular Electron-Positron Collider (CEPC) [4], has been proposed. The main production channel of Higgs boson in these e^+e^- colliders is the Higgsstrahlung process, $e^+e^- \to ZH$, which is projected to be measured with sub-percent level precision at these facilities (1.2% at ILC, 0.4% at FCC-ee, and 0.5% at CEPC). Reducing the theoretical uncertainty to the same level as the experimental one is crucial to prevent theoretical errors from dominating when extracting Higgs couplings, and this constitutes a significant part of this thesis, in which the largest missing contribution, the next-to-next-to-leading order(NNLO) electroweak corrections, will be presented. Moreover, the increasing experimental accuracy will impose stringent bounds on new physics. The thesis also investigates one specific class of new physics, fermionic dark matter, as a possible explanation for potential deviations on the cross section of the Higgsstrahlung process, and explores the parameter space that may be probed at future Large Hadron Collider(LHC).

Table of Contents

List of Tables

List of Figures

Preface

First and foremost, I would like to express my sincere gratitude to my PhD supervisor, Dr. Ayres Freitas, for his unwavering support and guidance throughout my doctoral studies. His expertise, patience, and encouragement have inspired me to pursue in academia. I am truly grateful for the opportunity to work with such a dedicated and inspiring mentor.

I would like to express my sincere appreciation to the members of my PhD committee, Dr. Brian Batell, Dr. Joseph Boudreau, Dr. Wensheng Vincent Liu and Dr. Colin Morningstar, for their invaluable guidance and feedback throughout my doctoral studies. I am also grateful for their time and effort spent in reviewing my thesis and participating in my defense. Thank you for being a vital part of my academic journey.

I would like to express my sincere gratitude to my friends and colleagues at Pitt for their unwavering support throughout my Ph.D. life. I would like to extend a special thanks to Lisong Chen, whose guidance in the early stages of my research were invaluable. I am also indebted to Hongbo Cai, Iris Leung, and Keping Xie for their insightful discussions on research and stimulating conversations beyond academia. Additionally, I am grateful to Pengshan Pan, Shu Liu, Bomin Zhang, Shan Hao, Zehua Wang, and Tianping Gu for their assistance in my life. I would like to express my appreciation to Erfei Wang for the thoughtful gift from Japan. Last but not least, I am grateful to my roommate Sicheng Lan and his cat DanHuang, for bringing some entertainment and joy during quarantine.

Lastly, I would like to thank my parents for their encouragement and support support throughout my life.

1.0 Introduction

The Standard Model(SM) of particle physics is a theoretical framework that describes the behavior of fundamental particles and their interactions through three of the four fundamental forces: the strong interaction is described by Quantum Chromodynamics (QCD)[5, 6, 7, 8], and the description of the electromagnetic and weak interactions is unified in the Glashow-Salam-Weinberg (GSW) model of the electroweak (EW) interaction[9, 10, 11], also called the Electroweak Standard Model (EWSM). The obstacle that EW gauge theory predicts massless gauge bosons, but experimental facts require the force carriers of weak interactions to be massive, was overcome by spontaneous symmetry breaking - a mechanism nowadays known as Brout-Englert-Higgs or simply Higgs mechanism [12, 13, 14, 15]. Owing to the observation of parity violation, fermions are chiral, i.e. left- and right-handed fermions interact differently with weak gauge bosons, which forbids the introduction of plain fermion mass terms due to gauge invariance. The so-called Yukawa interaction terms, which describe the interaction between chiral fermion and Higgs field, introduce the fermion masses in a consistent manner. This chapter depicts the main features of the SM and its renormalization, which is required to make precise predictions for EW phenomena that can be tested at colliders. Since perturbation theory is a method of choice in such precision calculations, some basic techniques for evaluating EW radiative corrections is also included in this chapter.

1.1 the Standard Model

The mathematical framework of the SM is the quantum field theory featuring a non-Abelian gauge group structure, referred to as $\mathrm{SU(3)_C} \times \mathrm{SU(2)_L} \times \mathrm{U(1)_Y}$. The $\mathrm{SU(3)_C}$ group corresponds to QCD, which describes the strong nuclear force responsible for color symmetry. The $\mathrm{SU(2)_L} \times \mathrm{U(1)_Y}$ group corresponds to the EWSM, which describes the electroweak interactions responsible for the symmetry of isospin and hypercharge. Gauge bosons, which emerge from the generators of the gauge group, mediate the interaction between fermions. According to gauge symmetry, all particles should be massless.

The masses of weak gauge bosons are generated by spontaneously breaking the EW $\mathrm{SU(2)_L} \times \mathrm{U(1)_Y}$ gauge symmetry down to electromagnetic $\mathrm{U(1)_{em}}$ invariance. The symmetry breaking is driven by the gauge interaction with a scalar field with non-vanishing vacuum expectation value (vev). Specially, the SM employs a complex scalar $\mathrm{SU(2)_L}$ doublet to break the EW gauge symmetry, so that three out of four scalar degrees of freedom deliver the longitudinal polarizations of the massive gauge boson. The fourth scalar corresponds to a neutral, massive boson, the so-called SM Higgs boson.

The introduction of fermion masses through Yukawa interaction terms mixes the flavour eigenstates of quarks, while leptons do not mix as long as neutrinos are massless. The mixing of quark generations is well described by the Cabbino-Kobayashi-Maskawa (CKM) matrix [16, 17], which contains the only source of CP violation in the SM.

Thus, the Lagrangian of the SM can be decomposed into gauge, fermion and

scalar sector

$$\mathcal{L}_{\mathrm{SM}} = \mathcal{L}_{\mathrm{G}} + \mathcal{L}_{\mathrm{F}} + \mathcal{L}_{\mathrm{S}}, \tag{1}$$

where the lowerscripts G, F, S denote gauge, fermion and scalar sector respectively, and the Yukawa interaction term is included into the scalar part.

We will start by writing the explicit form of symmetry unbroken Lagrangian, i.e. Higgs sector with vanishing vev, and the non-vanishing vev case will be incorporated afterwards. Specifically, we will discuss the Higgs mechanism and CP violation in detail.

1.1.1 Gauge Sector

According to the dimension of SM gauge group $\mathrm{SU(3)_C} \times \mathrm{SU(2)_L} \times \mathrm{U(1)_Y}$, there are eight QCD gauge fields and four EW gauge fields. The gauge fields belonging to the color group $\mathrm{SU(3)_C}$ are denoted as G^a_μ, the one belonging to weak-isospin group $\mathrm{SU(2)_L}$ is denoted as W^i_μ and the one belonging to weak-hypercharge group $\mathrm{U(1)_Y}$ is called B_μ. The dynamics of gauge boson are encoded in the Lagrangian in terms of the field strength tensors:

$$\mathcal{L}_{\mathrm{G}} = -\frac{1}{4} B_{\mu\nu} B^{\mu\nu} - \sum_{i=1}^{3} \frac{1}{4} W^i_{\mu\nu} W^{\mu\nu,i} - \sum_{a=1}^{8} \frac{1}{4} G^a_{\mu\nu} G^{\mu\nu,a} \tag{2}$$

where the indices i and a correspond to the number of generators in the gauge group. It is important to note that gauge boson mass terms such as $m_B^2 B_\mu B^\mu$ are forbidden due to gauge symmetry.

The corresponding field strength tensors are given by

$$B_{\mu\nu} = \partial_\mu B_\nu - \partial_\nu B_\mu \tag{3}$$

$$W^i_{\mu\nu} = \partial_\mu W^i_\nu - \partial_\nu W^i_\mu + g\epsilon^{ijk} W^j_\mu W^k_\nu \tag{4}$$

$$G^a_{\mu\nu} = \partial_\mu G^a_\nu - \partial_\nu G^a_\mu + g_s f^{abc} G^b_\mu G^c_\nu \tag{5}$$

where g and g_s are the gauge coupling constant for weak isospin and color groups, respectively. ϵ^{ijk}, f^{abc} are the structure constants of $\mathrm{SU(2)_L}$ and $\mathrm{SU(3)_C}$, which is defined through the anti-commutation relation between gauge group generators. The gauge coupling constant for weak hypercharge is denoted as $g^{'}$, and it is not shown in field strength tensor since the structure constant for Abelian group is zero.

We denote the eight generators of color by t^a, and these generators are Gell-Mann matrices for color triplet. The generator of weak hypercharge, denoted as Y_W, is a constant. The three generators of weak isospin are represented by T^i. For isospin doublet, the generators are $T^i = \sigma^i/2$, where σ^i are the Pauli matrices. For triplet fermion, the generators have the following form

$$T^1 = \frac{1}{\sqrt{2}} \begin{pmatrix} 0 & 1 & 0 \\ 1 & 0 & 1 \\ 0 & 1 & 0 \end{pmatrix}, T^2 = \frac{1}{\sqrt{2}} \begin{pmatrix} 0 & -i & 0 \\ i & 0 & -i \\ 0 & i & 0 \end{pmatrix}, T^3 = \frac{1}{\sqrt{2}} \begin{pmatrix} 1 & 0 & 0 \\ 0 & 0 & 0 \\ 0 & 0 & -1 \end{pmatrix} \tag{6}$$

The generators of triplet can also be chosen to be in the fundamental representation.

1.1.2 Fermion Sector

The SM contains three generations (copies) of chiral fermion fields with different gauge transformation properties under $\mathrm{SU(3)_C} \times \mathrm{SU(2)_L} \times \mathrm{U(1)_Y}$. Table. 1 lists the first generation of fermions and its corresponding gauge transformation properties, where u, d, ν, l stand for up-type quarks, down-type quarks, neutrinos and leptons.

The subscript L(R) denotes left-handed(right-handed) fields, which are obtained with projection operators:

$$L_{\rm L} = P_{\rm L}\ L = P_{\rm L} \begin{pmatrix} \nu \\ l \end{pmatrix}, Q_{\rm L} = P_{\rm L}\ Q = P_{\rm L} \begin{pmatrix} u \\ d \end{pmatrix}, \tag{7}$$

$$l_{\rm R} = P_{\rm R}\ l, u_{\rm R} = P_{\rm R} u, d_R = P_{\rm R} d \tag{8}$$

where $P_{L,R} = (1 \mp \gamma_5)/2$.

Quarks are color triplets, while leptons are color singlets. Additionally, the left-handed quark Q_L and lepton L_L transforms as doublets under $\mathrm{SU(2)_L}$, while the remaining right-handed fields transform like singlets. Right-handed neutrino is not included[1]. The weak hypercharges of right- and left-handed fermions are chosen in such a way that the known electric charge of the fermions are reproduced by the Gell-Mann-Nishijima relation

$$Q = I_W^3 + \frac{Y_W}{2} \tag{9}$$

The Lagrangian of the fermion sector, in terms of chiral fermion field, reads

$$\mathcal{L}_F = \sum_j (i\bar{L}_{\rm L}^j \not{D} L_{\rm L}^j + i\bar{Q}_{\rm L}^j \not{D} Q_{\rm L}^j + i\bar{l}_{\rm R}^j \not{D} l_{\rm R}^j + i\bar{u}_{\rm R}^j \not{D} u_{\rm R}^j + i\bar{d}_{\rm R}^j \not{D} d_{\rm R}^j) \tag{10}$$

Similar to the gauge mass term, the fermion mass term $m\bar{L}_{\rm L} L_{\rm L}$ is also not allowed due to gauge invariance. D^μ is the covariant derivative, which contains the interaction with gauge bosons

$$D_\mu = \partial_\mu - ig' \frac{Y_W}{2} B_\mu - igW_\mu^i T^i - ig_s G_\mu^a t^a \tag{11}$$

[1]In the Standard Model (SM), neutrinos are considered to be massless as the SM does not include right-handed neutrinos. However, the discovery of neutrino oscillation, as observed in experiments such as Super-Kamiokande [18], SNO [19], and KamLAND [20], has provided strong evidence that neutrinos have non-zero masses. This discovery implies that an extension of the SM is required to accommodate massive neutrinos.

	$Q_L^1 = \begin{pmatrix} u_L^1 \\ d_L^1 \end{pmatrix}$	u_R^1	d_R^1	$L_L^1 = \begin{pmatrix} \nu_L^1 \\ l_L^1 \end{pmatrix}$	l_R^2
hypercharge Y_W	$\frac{1}{3}$	$\frac{4}{3}$	$-\frac{2}{3}$	-1	-2
isospin I_W	$\frac{1}{2}$	0	0	$\frac{1}{2}$	0
color	triplet	triplet	triplet	singlet	singlet

Table 1: The chiral fermion content for the first generation, denoted by the superscript 1, of fermions in the SM. L and R denote left-handed and right-handed.

where we adopt the convention of Peskin and Schroeder [21] and Schwartz [22]. Different sign conventions are used in other literature. For example, the form $D_\mu = \partial_\mu + ig^{'}Y_W/2B_\mu + igW_\mu^i T^i$ is used in [23]. Different sign conventions lead to sign changes of the mixing matrix, Feynman rules and Green function, while the physical observables are not influenced. A resource for different sign conventions of the Standard Model is summarized in [24].

1.1.3 Higgs Sector

The scalar field Φ transforms as a $\mathrm{SU(2)_L}$ doublet and color singlet. To allow for an electrically neutral component, the scalar field must have hypercharge $Y_W = \pm 1$, which are the charge conjugate field with each other. Here we assume $Y_W = +1$. Under this convention, the Higgs doublet can be written as

$$\Phi = \begin{pmatrix} \phi^+ \\ \phi^0 \end{pmatrix} \tag{12}$$

where the upper indices indicate the electric charge of the components. The corresponding charge conjugate field with $Y_W = -1$ is defined as

$$\tilde{\Phi} \equiv i\sigma_2 \Phi^* = i \begin{pmatrix} 0 & -i \\ i & 0 \end{pmatrix} \begin{pmatrix} \phi^- \\ \phi^{0*} \end{pmatrix} = \begin{pmatrix} \phi^{0*} \\ -\phi^- \end{pmatrix} \tag{13}$$

The Lagrangian of the scalar sector is

$$\mathcal{L}_S = (D^\mu \Phi)^\dagger (D_\mu \Phi) - V(\Phi) + \mathcal{L}_Y \tag{14}$$

The Higgs potential V and the Yukawa interaction term $\mathcal{L}_Y$ are

$$V = -\mu^2 \Phi^\dagger \Phi + \lambda (\Phi^\dagger \Phi)^2 \tag{15}$$

$$\mathcal{L}_Y = -\sum_{j,k} (\bar{L}_L^j Y_{jk}^l l_R^k \Phi + \bar{Q}_L^j Y_{jk}^u u_R^k \tilde{\Phi} + \bar{Q}_L^j Y_{jk}^d d_R^k \Phi + \text{h.c}) \tag{16}$$

where μ, λ are the scalar field quadratic and quartic coupling constant, and they must be real to make the Higgs potential Hermitian.$Y_{jk}^{l,u,d}$ are Yukawa couplings for lepton, up quark and down quark respectively, and they are 3×3 matrices. The Hermition conjugate part, denoted as h.c, is required to ensure the Hermicity of $\mathcal{L}_Y$.

1.1.4 Gauge Invariance

Plugging the explicit expressions for gauge, fermion and scalar sectors, Eq. 1 becomes

$$\begin{aligned}
\mathcal{L}_{\rm SM} = & -\frac{1}{4}B_{\mu\nu}B^{\mu\nu} - \sum_{i=1}^{3}\frac{1}{4}W^{i}_{\mu\nu}W^{\mu\nu,i} - \sum_{a=1}^{8}\frac{1}{4}G^{a}_{\mu\nu}G^{\mu\nu,a} \\
& + \sum_{j}(i\bar{L}^{j}_{\rm L}\not{D}L^{j}_{\rm L} + i\bar{Q}^{j}_{\rm L}\not{D}Q^{j}_{\rm L} + i\bar{l}^{j}_{\rm R}\not{D}l^{j}_{\rm R} + i\bar{u}^{j}_{\rm R}\not{D}u^{j}_{\rm R} + i\bar{d}^{j}_{\rm R}\not{D}d^{j}_{\rm R}) \\
& + (D^{\mu}\Phi)^{\dagger}(D_{\mu}\Phi) + \mu^{2}\Phi^{\dagger}\Phi - \lambda(\Phi^{\dagger}\Phi)^{2} \\
& - \sum_{j,k}(\bar{L}^{j}_{L}Y^{l}_{jk}l^{k}_{R}\Phi + \bar{Q}^{j}_{L}Y^{u}_{jk}u^{k}_{R}\tilde{\Phi} + \bar{Q}^{j}_{L}Y^{d}_{jk}d^{k}_{R}\Phi + \text{h.c})
\end{aligned} \tag{17}$$

which is invariant under the infinitesimal gauge transformations assuming vanishing vev

$$\begin{aligned}
B_{\mu} &\to B_{\mu} + \partial_{\mu}\delta\theta^{y} \\
W^{i}_{\mu} &\to W^{i}_{\mu} + \partial_{\mu}\delta\theta^{i} + g\epsilon^{ijk}W^{j}_{\mu}\delta\theta^{k} \\
G^{a}_{\mu} &\to G^{a}_{\mu} + \partial_{\mu}\delta\theta^{a} + g_{s}f^{abc}G^{b}_{\mu}\delta\theta^{c} \\
F_{\rm L} &\to \Big[1 - i\frac{Y^{F}_{W}}{2}g^{'}\delta\theta^{y} - ig\frac{T^{i}}{2}\delta\theta^{i} - ig_{s}t^{a}\delta\theta^{a}|_{F=Q}\Big]F_{\rm L},\ F = L, Q \\
f_{\rm R} &\to \Big[1 - i\frac{Y^{f}_{W}}{2}g^{'}\delta\theta^{y} - ig_{s}t^{a}\delta\theta^{a}|_{F=u,d}\Big]F_{\rm L},\ F = l, u, d \\
\Phi &\to \Big[1 - i\frac{Y_{W}}{2}g^{'}\delta\theta^{y} - ig\frac{T^{i}}{2}\delta\theta^{i}\Big]\Phi
\end{aligned} \tag{18}$$

where $\delta\theta^{y(i,a)}$ is the minimal gauge field transformation to the $\mathrm{U(1)_Y(SU(2)_L, SU(3)_C)}$ group.

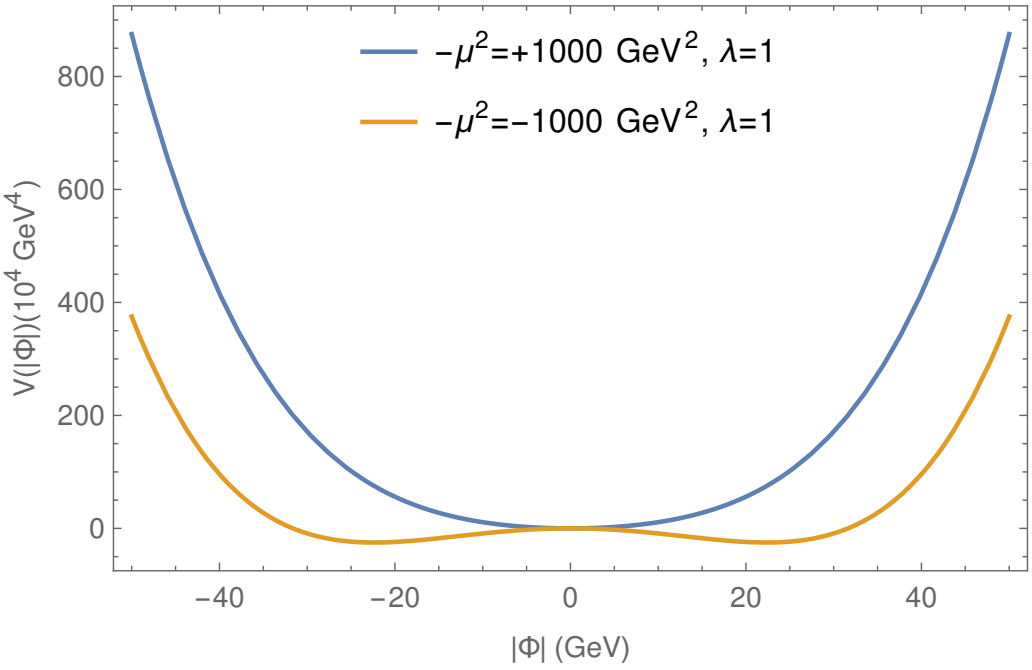

Figure 1: Distribution of Higgs potential $V(|\Phi|) = -\mu^2|\Phi|^2 + \lambda|\Phi|^4$ for $\lambda = 1, |\mu^2| = 1000(\text{GeV})^2$.

1.1.5 Higgs Mechanism

The gauge invariance of Eq.1 is realized by the scalar field with vanishing vev, which depends on the choice of the two parameters, μ and λ. Generally, they are real numbers and can be either positive or negative. If $\lambda < 0$, V is unbounded from below, i.e. this is no minimum value of the potential, such that scalar field is not stable. The left two possibilities are $\lambda > 0, \mu^2 < 0$ and $\lambda > 0, \mu^2 > 0$. If $\lambda > 0, \mu^2 < 0$, the

true minimum of the potential locates at

$$\frac{\partial V(|\Phi|)}{\partial(|\Phi|)} = 0 \;\Rightarrow\; |\Phi| = \pm\sqrt{\frac{\mu^2}{2\lambda}} \tag{19}$$

This minimum is denoted as $v^2 = \mu^2/(2\lambda)$, the so-called vacuum expectation value (vev). The corresponding value of the potential is

$$V(|\Phi| = \pm\sqrt{\frac{\mu^2}{2\lambda}}) = -\frac{\mu^4}{4\lambda} < 0 \tag{20}$$

The distributions of $V(\Phi)$ with respect to $|\Phi|$ for positive and negative μ^2 are shown in Fig.1, where we have chosen $|\mu^2| = 1000(\mathrm{GeV})^2$ and $\lambda = 1$.

The scalar doublet Φ contains four real scalar fields. We choose the charged state to have vanishing vev so that the remaining unbroken symmetry is $\mathrm{U}(1)_{\mathrm{em}}$. Thus, the scalar doublet can be parametrized as

$$\Phi = \begin{pmatrix} \phi^+ \\ (v + h + i\chi)/\sqrt{2} \end{pmatrix} \tag{21}$$

where χ and ϕ^+ have vanishing vev. The field χ, ϕ^+ and its Hermition conjugate field ϕ^-, are the would-be Goldstone fields, which are unphysical degrees of freedom and can be eliminated by a transition to unitary gauge, where $\phi^\pm = \chi = 0$. The derivation of physical fields will be much simpler under unitary gauge, thus in the following the scalar doublet is

$$\Phi = \begin{pmatrix} 0 \\ (v + h)/\sqrt{2} \end{pmatrix} \tag{22}$$

1.1.5.1 Physical Fields

The masses of gauge bosons and fermions are generated from spontaneous breaking of the $\mathrm{SU(2)_L \times U(1)_Y}$ gauge symmetry due to non-vanishing vev. Under unitary gauge, explicit form of the kinetic term in $\mathcal{L}_S$ is

$$
\begin{aligned}
(D^\mu\Phi)^\dagger(D^\mu\Phi) &= \left((\partial_\mu - i\frac{g'}{2}B_\mu - igW_\mu^a\frac{\sigma_a}{2})\Phi\right)^\dagger\left((\partial^\mu - i\frac{g'}{2}B^\mu - igW_\mu^a\frac{\sigma_a}{2})\Phi\right) \\
&= \frac{1}{2}\begin{pmatrix} i\frac{g}{2}(W_\mu^1 + iW_\mu^2)(v+h) \\ \partial_\mu h - \frac{i}{2}(gW_\mu^3 - g'B_\mu)(v+h)\end{pmatrix}^T \times \begin{pmatrix} -i\frac{g}{2}(W_\mu^1 - iW_\mu^2)(v+h) \\ \partial_\mu h + \frac{i}{2}(gW_\mu^3 - g'B_\mu)(v+h)\end{pmatrix} \\
&= \frac{1}{2}(\partial_\mu h)(\partial^\mu h) + \frac{1}{8}g^2(v+h)^2(W_\mu^1 - iW_\mu^2)(W^{\mu,1} + iW^{\mu,2}) \\
&+ \frac{1}{8}(v+h)^2(-g'B_\mu + gW_\mu^3)(-g'B^\mu + gW^{\mu,3})
\end{aligned} \tag{23}
$$

where we have replaced Higgs hypercharge by $y = 1$. The first term is the kinetic term for the real scalar field h. The second and third terms generate gauge bosons masses and interaction between scalar and gauge boson, which can be clearly seen by diagonalizing the gauge eigenstates to physical mass eigenstates

$$
\begin{aligned}
&\begin{pmatrix} W_\mu^+ \\ W_\mu^- \end{pmatrix} = \frac{1}{\sqrt{2}}\begin{pmatrix} 1 & -i \\ 1 & i \end{pmatrix}\begin{pmatrix} W_\mu^1 \\ W_\mu^2 \end{pmatrix} \ , \\
&\begin{pmatrix} Z_\mu \\ A_\mu \end{pmatrix} = \frac{1}{\sqrt{g^2 + g'^2}}\begin{pmatrix} g & -g' \\ g' & g \end{pmatrix}\begin{pmatrix} W_\mu^3 \\ B_\mu \end{pmatrix} = \begin{pmatrix} c_W & -s_W \\ s_W & c_W \end{pmatrix}\begin{pmatrix} W_\mu^3 \\ B_\mu \end{pmatrix}
\end{aligned} \tag{24}
$$

where $c_W = \cos\theta_W = g/\sqrt{g^2 + g'^2}$, and θ_W is called the weak mixing angle or Weinberg angle. The kinetic term in terms of mass eigenstates is

$$
\begin{aligned}
\mathcal{L}_{\text{kin}} =& \frac{1}{2}(\partial_\mu h)(\partial^\mu h) + \frac{1}{4}g^2(v+h)^2W_\mu^+W^{-\mu} + \frac{1}{8}(g^2 + g'^2)(v+h)^2Z_\mu Z^\mu \\
=& \frac{1}{2}(\partial_\mu h)(\partial^\mu h) + \frac{v^2g^2}{4}W_\mu^+W^{-\mu} + \frac{(g^2 + g'^2)v^2}{8}Z_\mu Z^\mu
\end{aligned}
$$

$$+\frac{vg^2}{2}hW_\mu^+W^{-\mu}+\frac{g^2}{4}hhW_\mu^+W^{-\mu}$$
$$+\frac{(g^2+g'^2)v^2}{4}hZ_\mu Z^\mu+\frac{(g^2+g'^2)}{8}hhZ_\mu Z^\mu \tag{25}$$

Masses of W and Z boson are

$$m_W^2=\frac{v^2g^2}{2}\ ,\ m_Z^2=\frac{(g^2+g'^2)v^2}{4} \tag{26}$$

The gauge boson A^μ is massless. Higgs mass and self-interactions of Higgs are generated by the scalar potential. Under unitary gauge, the scalar potential reads

$$\begin{aligned}\mathcal{L}_V^h&=\mu^2\Phi^\dagger\Phi-\lambda(\Phi^\dagger\Phi)^2=\frac{\mu^2}{2}(h+v)^2-\frac{\lambda}{4}(h+v)^4\\&=-\lambda v^2h^2-\lambda vh^3-\frac{\lambda}{4}h^4+f(\mu,v,\lambda)\end{aligned} \tag{27}$$

where $f(\mu,v,\lambda)$ is a constant. Higgs mass is

$$m_h^2=2\lambda v^2 \tag{28}$$

With mass eigenstates, the covariant derivative becomes

$$\begin{aligned}D_\mu=&\partial_\mu-ig_sG_\mu^at^a-i\frac{g}{\sqrt{2}}(W_\mu^+T^++W_\mu^-T^-)\\&-iZ_\mu(gc_WT^3-g's_WY)-iA_\mu(gs_WT^3+g'c_WY)\end{aligned} \tag{29}$$

The coupling constant of A_μ is

$$gs_WT^3+g'c_WY=\frac{gg'}{\sqrt{g^2+g'^2}}\equiv eQ \tag{30}$$

where we have introduced two parameters: e is the electromagnetic coupling and Q is the electric charge operator since the Lagrangian is invariant under $\mathrm{U}(1)_{\mathrm{em}}$ after EWSB.

With this convention, the couplings of W_μ and Z_μ gauge field become

$$\frac{g}{\sqrt{2}} = \frac{e}{\sqrt{2}s_W} \ , \ gc_W T^3 - g' s_W Y = \frac{e}{s_W c_w}(T^3 - s_W^2 Q) \tag{31}$$

Thus the new form of the covariant derivative is

$$\begin{aligned} D_\mu =& \partial_\mu - i g_s G_\mu^a t^a - i\frac{e}{\sqrt{2}s_W}(W_\mu^+ T^+ + W_\mu^- T^-) \\ & - i\frac{e}{s_W c_w}(T^3 - s_W^2 Q) Z_\mu - ieQA_\mu \end{aligned} \tag{32}$$

Masses of fermions are generated by the Yukawa interaction terms. Motivated by the observation of neutrino oscillation [18, 19, 20], which indicates neutrinos are massive, we choose to incorporate the right-handed neutrinos ν_{R}^i, where i stands for the generation. Right-handed neutrino transforms like a $\mathrm{SU}(2)_{\mathrm{L}}$ singlet, color singlet and has hypercharge $Y_W = 0$.[2] With the extension of right-handed neutrinos, the Yukawa interaction term becomes

$$\mathcal{L}_Y = -\sum_{j,k}(\bar{L}_L^j Y_{jk}^l l_R^k \Phi + \bar{L}_L^j Y_{jk}^\nu \nu_R^k \tilde{\Phi} + \bar{Q}_L^j Y_{jk}^d d_R^k \Phi + \bar{Q}_L^j Y_{jk}^u u_R^k \tilde{\Phi} + \mathrm{h.c}) \tag{33}$$

$Y_{ij}^{l,\nu,u,d}$ are dimensionless couplings and 3×3 complex matrix for leptons, neutrinos, up-quark and down quark. The sum over j, k considers all fermion generations. Lepton and quark doublets are defined as follows

$$\begin{aligned} L_L^1 = \begin{pmatrix} \nu_L^1 \\ l_L^1 \end{pmatrix} \ , \ L_L^2 = \begin{pmatrix} \nu_L^2 \\ l_L^2 \end{pmatrix} \ , \ L_L^3 = \begin{pmatrix} \nu_L^3 \\ l_L^3 \end{pmatrix} \ , \\ Q_L^1 = \begin{pmatrix} u_L^1 \\ d_L^1 \end{pmatrix} \ , \ Q_L^2 = \begin{pmatrix} u_L^2 \\ d_L^1 \end{pmatrix} \ , \ Q_L^3 = \begin{pmatrix} u_L^3 \\ d_L^3 \end{pmatrix} \end{aligned} \tag{34}$$

[2]For $Y_W = 0$, it is possible that neutrinos are Majorana fermions. We restrict ourselfes that all right-handed neutrinos are Dirac fermion because Majorana fermions could be forbidden by assuming lepton number conservation.

The singlets are

$$l_R = \begin{pmatrix} l_R^1 \\ l_R^2 \\ l_R^3 \end{pmatrix} \ , \ \nu_R = \begin{pmatrix} \nu_R^1 \\ \nu_R^2 \\ \nu_R^3 \end{pmatrix} \ , \ u_R = \begin{pmatrix} u_R^1 \\ u_R^2 \\ u_R^3 \end{pmatrix} \ , \ d_R = \begin{pmatrix} d_R^1 \\ d_R^2 \\ d_R^3 \end{pmatrix} \tag{35}$$

The right-handed fermions are written in the form like triplets, which is for the sake of brevity. f_R^i is the i-th component of f_R.

The first and second term in Eq.33 generate masses for leptons, and the third and forth one generate masses for quarks. Similar to gauge boson generation, fermion masses are also proportional to Higgs boson vacuum expectation value v

$$\begin{aligned} \mathcal{L}_{\rm y}^{\rm mass} \subset & - \begin{pmatrix} \bar{\nu}_R^1 & \bar{\nu}_R^2 & \bar{\nu}_R^3 \end{pmatrix} M^\nu \begin{pmatrix} \nu_L^1 \\ \nu_L^2 \\ \nu_L^3 \end{pmatrix} - \begin{pmatrix} \bar{l}_R^1 & \bar{l}_R^2 & \bar{l}_R^3 \end{pmatrix} M^l \begin{pmatrix} l_L^1 \\ l_L^2 \\ l_L^3 \end{pmatrix} \\ & - \begin{pmatrix} \bar{u}_R^1 & \bar{u}_R^2 & \bar{u}_R^3 \end{pmatrix} M^u \begin{pmatrix} u_L^1 \\ u_L^2 \\ u_L^3 \end{pmatrix} - \begin{pmatrix} \bar{d}_R^1 & \bar{d}_R^2 & \bar{d}_R^3 \end{pmatrix} M^d \begin{pmatrix} d_L^1 \\ d_L^2 \\ d_L^3 \end{pmatrix} + \text{h.c.} \end{aligned} \tag{36}$$

where $M^f = vY^f/\sqrt{2}$, which are non-diagonalized and contains 9 complex numbers. To find the fermion mass eigenstates, four mass matrices are needed to be diagonalized. Eight unitary rotational matrices are defined

$$\begin{aligned} \begin{pmatrix} \nu_1^m \\ \nu_2^m \\ \nu_3^m \end{pmatrix}_{L,R} &= V_{L,R} \begin{pmatrix} \nu_1 \\ \nu_2 \\ \nu_3 \end{pmatrix}_{L,R} , \begin{pmatrix} l_1^m \\ l_2^m \\ l_3^m \end{pmatrix}_{L,R} = E_{L,R} \begin{pmatrix} l_1 \\ l_2 \\ l_3 \end{pmatrix}_{L,R} , \\ \begin{pmatrix} u_1^m \\ u_2^m \\ u_3^m \end{pmatrix}_{L,R} &= U_{L,R} \begin{pmatrix} u_1 \\ u_2 \\ u_3 \end{pmatrix}_{L,R} , \begin{pmatrix} d_1^m \\ d_2^m \\ d_3^m \end{pmatrix}_{L,R} = D_{L,R} \begin{pmatrix} d_1 \\ d_2 \\ d_3 \end{pmatrix}_{L,R} \end{aligned} \tag{37}$$

such that

$$V_R^{-1}M^\nu V_L = \begin{pmatrix} m_{\nu_1^m} & 0 & 0 \\ 0 & m_{\nu_2^m} & 0 \\ 0 & 0 & m_{\nu_3^m} \end{pmatrix} \ , \ E_R^{-1}M^l E_L = \begin{pmatrix} m_{l_1^m} & 0 & 0 \\ 0 & m_{l_2^m} & 0 \\ 0 & 0 & m_{l_3^m} \end{pmatrix} \tag{38}$$

$$U_R^{-1}M^u U_L = \begin{pmatrix} m_{u_1^m} & 0 & 0 \\ 0 & m_{u_2^m} & 0 \\ 0 & 0 & m_{u_3^m} \end{pmatrix} \ , \ D_R^{-1}M^d D_L = \begin{pmatrix} m_{d_1^m} & 0 & 0 \\ 0 & m_{d_2^m} & 0 \\ 0 & 0 & m_{d_3^m} \end{pmatrix} \tag{39}$$

1.1.5.2 Fermion Mixing Matrix

Due to these rotational matrices, fermions in different generations can interact with each other. To demonstrate this, Let's write down the charge currents for leptons and quarks

$$J_L^{\mu,\text{lep}} = \begin{pmatrix} \bar{\nu}_1 & \bar{\nu}_2 & \bar{\nu}_3 \end{pmatrix}_L \gamma^\mu \begin{pmatrix} l_1 \\ l_2 \\ l_3 \end{pmatrix}_L = \begin{pmatrix} \bar{\nu}_1^m & \bar{\nu}_2^m & \bar{\nu}_3^m \end{pmatrix}_L V_L^\dagger E_L \gamma^\mu \begin{pmatrix} l_1^m \\ l_2^m \\ l_3^m \end{pmatrix}_L \tag{40}$$

$$J_L^{\mu,\text{quark}} = \begin{pmatrix} \bar{u}_1 & \bar{u}_2 & \bar{u}_3 \end{pmatrix}_L \gamma^\mu \begin{pmatrix} d_1 \\ d_2 \\ d_3 \end{pmatrix}_L = \begin{pmatrix} \bar{u}_1^m & \bar{u}_2^m & \bar{u}_3^m \end{pmatrix}_L U_L^\dagger D_L \gamma^\mu \begin{pmatrix} d_1^m \\ d_2^m \\ d_3^m \end{pmatrix}_L \tag{41}$$

The combination $V_L^\dagger E_L$ is the Maki-Nakagawa-Sakata-Pontecorvo(MNSP) matrix, and the combination $U_L^\dagger D_L$ is the Cabibbo-Kobayashi-Maskawa(CKM) matrix. These matrix are unitary:

$$\begin{aligned} \left(V_L^\dagger E_L\right)^\dagger \left(V_L^\dagger E_L\right) &= E_L^\dagger V_L V_L \dagger E_L = E_L^\dagger E_L = 1 \ , \\ \left(U_L^\dagger D_L\right)^\dagger \left(U_L^\dagger D_L\right) &= U_L^\dagger D_L D_L \dagger U_L = U_L^\dagger U_L = 1 \end{aligned} \tag{42}$$

The CKM and MNSP matrix are complex matrix and contain 18 variables each, but the matrix only contains four free variables. The unitarity, $X^{\dagger}_{ab}X_{bc} = \delta_{ac}$, reduces the number of variables into 9. Besides, we are free to absorb a phase when diagonalizing the gauge eigenstates, namely $f_L \to e^{i\alpha_f} f_L$, therefore, extra six phases can be generated for three columns and rows of each generations. But a common phase redefinition of all columns has no effect on matrix, so the variables of each matrix is reduced to 9-5=4. A complex unitary matrix with four variables can be written as a matrix with three real Euler angles and one complex phase. For example, the CKM matrix can be parameterized as

$$
\begin{aligned}
&V_{\rm CKM} = U_L^{\dagger} D_L \\
&= \begin{pmatrix} 1 & 0 & 0 \\ 0 & \cos\theta_{23} & \sin\theta_{23} \\ 0 & -\sin\theta_{23} & \cos\theta_{23} \end{pmatrix} \begin{pmatrix} \cos\theta_{13} & 0 & \sin\theta_{13} e^{-i\delta_{13}} \\ 0 & 1 & 0 \\ -\sin\theta_{13} e^{i\delta_{13}} & 0 & \cos\theta_{13} \end{pmatrix} \begin{pmatrix} \cos\theta_{12} & \sin\theta_{12} & 0 \\ -\sin\theta_{12} & \cos\theta_{12} & 0 \\ 1 & 0 & 0 \end{pmatrix}
\end{aligned}
\tag{43}
$$

This complex phase δ_{13} breaks CP symmetry, thus it gives rise to the CP violations in the SM EW interactions.

If there is no right-handed neutrinos, neutrinos are massless, which means that neutrino gauge eigenstates is always its mass eigenstates, thus V_L can be arbitrary matrix. We can choose $V_L = E_L$ such that $V_L^{\dagger} E_L = 1$. So there is no mixing between different generations of leptons in charge current in the SM.

The neutral current interactions of quark and leptons are

$$
J_L^{\mu,\rm lep} = \begin{pmatrix} \bar{l}_1 & \bar{l}_2 & \bar{l}_3 \end{pmatrix}_L \gamma^{\mu} \begin{pmatrix} l_1 \\ l_2 \\ l_3 \end{pmatrix}_L = \begin{pmatrix} l_1^m & l_2^m & l_3^m \end{pmatrix}_L E_L^{\dagger} E_L \gamma^{\mu} \begin{pmatrix} l_1^m \\ l_2^m \\ l_3^m \end{pmatrix}_L \tag{44}
$$

$$J_L^{\mu,\text{quark}} = \begin{pmatrix} \bar{u}_1 & \bar{u}_2 & \bar{u}_3 \end{pmatrix}_L \gamma^\mu \begin{pmatrix} u_1 \\ u_2 \\ u_3 \end{pmatrix}_L = \begin{pmatrix} \bar{u}_1^m & \bar{u}_2^m & \bar{u}_3^m \end{pmatrix}_L U_L^\dagger U_L \gamma^\mu \begin{pmatrix} u_1^m \\ u_2^m \\ u_3^m \end{pmatrix}_L \tag{45}$$

The fact that $U^\dagger U = E^\dagger E = 1$ forbids the mixing of different generations. As a result, there is no flavor changing neutral current(FCNC) at tree level in the SM.

Besides, the right-handed neutrinos are added in the Yukawa Lagrangian though the SM does not contain right-handed neutrinos. The purpose of adding right-handed neutrinos is to show one mechanism of generating neutrino mass in the SM, albeit at the expense of violating naturalness due to extremely small Y_{ij}^ν,

$$m_\nu = \frac{y_\nu v}{\sqrt{2}} \sim 10^{-10}\text{GeV} \ \rightarrow y_\nu = 10^{-13} \tag{46}$$

This coupling is too small such that it seems unnatural to appear in the SM.

Besides generating neutrino masses by introducing right-handed neutrinos, the other possibility is to introducing a Majorana mass term for the SM left-handed neutrinos, namely

$$\mathcal{L}_\nu = m_\nu \bar{\nu}_L \nu_L = m_\nu \nu_L \nu_L \tag{47}$$

Such a term violates $\text{SU(2)}_\text{L} \times \text{U(1)}_\text{Y}$, but it causes no problems by adding this term to SM Lagrangian after electroweak symmetry breaking, which can be realized by adding the dimension $d = 5$ Weinberg operator [25]

$$\mathcal{L}_5 = \frac{C_5^{ij}}{\Lambda}[\bar{L}_L^{i,c}\Phi][\Phi^{c,\dagger}L_L^j] + \text{h.c.} \ , \ L_L = \begin{pmatrix} \nu_l \\ l \end{pmatrix} \ , \ L_L^c = \begin{pmatrix} l^c \\ -\nu_l^c \end{pmatrix} \tag{48}$$

where $\bar{L}_L^c$ is the charge conjugate spinor, and it transforms in the same way as a right-handed spinor under Lorentz group. The Wilson coefficient C_5^{ij} allows the

mixing of neutrinos between different generations, thus this operator violates Lepton number(LN) conservation. Λ is the energy scale at which the particles responsible for LN violation become relevant. This Lagrangian has dimension 5 thus is not renormalizable. After EWSB, this term yields a neutrino mass

$$\begin{aligned}\mathcal{L}_5 &= \frac{C_5^{ij}}{\Lambda}\begin{pmatrix}\bar{l}^{i,c} & -\overline{\nu_l^{i,c}}\end{pmatrix}\begin{pmatrix}0\\ \frac{1}{\sqrt{2}}(v+h)\end{pmatrix}\begin{pmatrix}\frac{1}{\sqrt{2}}(v+h) & 0\end{pmatrix}\begin{pmatrix}\nu_l^j\\ l^j\end{pmatrix} + \text{h.c}\\ &\supset -\frac{C_5^{ij}}{2\Lambda}v^2\overline{\nu_l^{i,c}}\nu_l^j + \text{h.c}\end{aligned} \tag{49}$$

where we have adopted the unitary gauge for the scalar doublet.

1.2 Renormalization of the Electroweak Standard Model

The free parameters in the SM Lagrangian are chosen to have physical meaning such as mass, couplings, and relate to experimental quantities. Firstly, the relationship is modified through higher order radiative corrections. Moreover, the original parameters in the Lagrangian, the so-called bare parameters, differ from the physical quantities by UV divergent contributions. These divergences are canceled in renormalized theory, thus allowing meaningful predictions. The renormalizability of non-Abelian gauge theory with spontaneous symmetry breaking, that is the SM, was proven by 't Hooft and Veltman[26, 27] and Lee and Zinn-Justin[28, 29, 30, 31].

One of the renormalization procedures can be summarized as follows:

- choose a set of free parameters, which are bare parameters
- separate the bare parameters into renormalized parameters and counterterms, the so-called renormalization constants

- choose renormalization conditions to fix the counterterms, i.e. counterterms are functions of other renormalized parameters
- express physical observables as a function of renormalized parameters

To compare the theoretical predictions and experimental measurements, the following steps are needed:

- choose a set of input parameters, which have been measured precisely
- fix the value of renormalized parameters with input parameters
- evaluate theoretical predictions for physical observables with input data
- compare with experimental measurement

These steps highlight that there is a flexibility in selecting the free parameters, renormalization conditions, and input parameters that all affect the theoretical predictions of physical observables. However, if we were able to calculate the physical observables to an infinite order, then the differences between the various choices of parameters would vanish. On the other side, theoretical predictions at fixed order under different choices of free parameter set, renormalization conditions and input parameter sets differ by higher order term, which is a possible strategy to estimate the theory error from missing higher order corrections.

This section focuses on the renormalization process with a specific choice of free parameters and renormalization conditions. We will go into detail on how the process works and what steps are involved. Additionally, we will explore multiple input parameter sets, which can be helpful in estimating missing higher-order corrections.

According to the renormalization process, we need to choose a set of free parameters firstly. In the EWSM Lagrangian, there are 5 types of free parameters, namely

$$g' \ , \ g \ , \ \mu \ , \ \lambda \ , \ y^f \tag{50}$$

where g', g are the $\mathrm{U(1)_Y}$ and $\mathrm{SU(2)_L}$ gauge couplings respectively. μ, λ are from the scalar potential. y^f is the Yukawa coupling. The Yukawa coupling matrix is a 3×3 matrix and varies for leptons and quarks. However, for the purposes of renormalization, we treat it as a single parameter because the procedure for renormalizing the Yukawa couplings is the same for all fermions.

Instead, one can choose the free parameter set to be

$$M_W, M_Z, M_H, m_f, e \tag{51}$$

The advantage of this choice is that all parameters have a clear physical meaning and can be measured directly in suitable experiments.

Furthermore, radiative corrections give rise to two main issues. Firstly, the vacuum expectation value $v^2 = \mu^2/(2\lambda)$ is no longer the true minimum of the scalar potential. Secondly, radiative corrections provide non-diagonal corrections to the CKM matrices, thus the original bare eigenstates are no longer the actual physical mass eigenstates.

In order to let vev always be the minimum of the Higgs potential, a counterterm $\delta\nu$ is introduced to the vev of the Higgs field. Or equivalently, introduce a counterterm δt, which cancels all radiative corrections to Higgs field T^H, the so-called tadpole diagrams, i.e.the Higgs potential contains no linear term, namely

$$T^H + \delta t = 0 \tag{52}$$

By applying this condition, all tadpole contributions are exactly cancelled by the counterterms so that no tadpoles need to be taken into account in actual calculations.

In order to rediagonal the mass matrices, one has to introduce matrix valued field renormalization constants δV , which allow to define the renormalized fields in such a way that the mass eigenstates in bare Lagrangian are the correct physical mass

eigenstates in all orders of perturbation theory. However at high-energy scale, it is appropriate to take all quarks except the top quark massless and ignore the quark mixing. Thus we will omit the renormalization of CKM matrix. One can find the renormalization of CKM matrix in other literature, such as [32].

The renormalized parameters and counterterms are defined as follows

$$\begin{aligned} e_0 &= Z_e e = (1 + \delta Z_e) e, \\ M^2_{W,0} &= M^2_W + \delta M^2_W \\ M^2_{Z,0} &= M^2_Z + \delta M^2_Z \\ M^2_{H,0} &= M^2_H + \delta M^2_H \\ m_{f,0} &= m_f + \delta m_f \\ V_{ij,0} &= V_{ij} + \delta V_{ij} \end{aligned} \tag{53}$$

where bare quantities are denoted with a lower index 0.

These parameters lead to a finite S-matrix element, but leaves Green's functions divergent. Thus, besides renormalizing those input parameters, we also need to renormalize particle fields. Renormalization of these fields does not affect physical predictions. They are only relevant for Green's function and drop out when calculating S-matrix. On-shell renormalization for the fields is very convenient since it can eliminate the wave function correction of external fields, thus simplifying the calculation of S-matrix.

In EW sector of the SM, physical fields include gauge boson field, Higgs field, fermion field. Unphysical ghost and Goldstone files do not affect Green's function of physical fields, thus not relevant for our calculations. Furthermore, the renormalization of unphysical sector are governed by the Slavnov-Taylor identities.

The renormalization of fields with mass eigenstate are defined in the following way:

$$
\begin{aligned}
&W_0^{\pm} = Z_W^{1/2} W^{\pm} = (1 + \frac{1}{2}\delta Z_W) W^{\pm}, \\
&\begin{pmatrix} Z_0 \\ A_0 \end{pmatrix} = \begin{pmatrix} Z_{ZZ}^{1/2} & Z_{ZA}^{1/2} \\ Z_{AZ}^{1/2} & Z_{ZZ}^{1/2} \end{pmatrix} \begin{pmatrix} Z \\ A \end{pmatrix} = \begin{pmatrix} 1 + \frac{1}{2}\delta Z_{ZZ} & \frac{1}{2}\delta Z_{ZA} \\ \frac{1}{2}\delta Z_{AZ} & 1 + \frac{1}{2}\delta Z_{AA} \end{pmatrix} \begin{pmatrix} Z \\ A \end{pmatrix}, \\
&H_0 = Z_H^{1/2} H = (1 + \frac{1}{2}\delta Z_H) H, \\
&f_{i,0}^L = Z_{ij}^{1/2,f,L} f_{j,L} = (\delta_{ij} + \frac{1}{2} Z_{ij}^{f,L}) f_{j,L} \\
&f_{i,0}^R = Z_{ij}^{1/2,f,R} f_{j,R} = (\delta_{ij} + \frac{1}{2} Z_{ij}^{f,R}) f_{j,R}
\end{aligned} \tag{54}
$$

where the one without(with) subscript "0" denotes renormalized(bare) fields.

In terms of Eq.53 and Eq.54, the SM bare Lagrangian $\mathcal{L}_0$ can be splitted into the renormalized Lagrangian $\mathcal{L}$ and the counterterm Lagrangian $\delta\mathcal{L}$

$$\mathcal{L}_0 = \mathcal{L} + \delta\mathcal{L} \tag{55}$$

$\mathcal{L}_0$ and $\mathcal{L}$ have the same form, but the former(latter) depends on renormalized(bare) parameters.

1.2.1 Renormalization Schemes

The notion "Renormalization scheme" is used in two different senses of the word. Often the term is used in a more technique sense as

- a specific way of performing renormalization at intermediate steps. This includes the choice of regularization, the way field renormalizations and/or parameter renormalizations are organized. If the same physical quantity is calculated in terms of the same parameters to the same order in perturbation theory the result does not depend on the choice of the scheme. The first kind of distinctions of different schemes is therefore not relevant for the physics.

Renormalization conditions determine the relation between renormalized parameters and counterterms, and different choices of these conditions give rise to different renormalization schemes.

The second possible distinctions of renormalization schemes, also called input parameter scheme, is more physical, namely as characterizing

- a specific choice of input parameters. Perturbative predictions in terms of different input parameter sets are scheme dependent.

In Sec.1.2.2 and Sec.1.2.3, the renormalization scheme both refers to the first case.

1.2.2 On-shell Renormalization Condition at one-loop

The renormalization constants introduced in Eq.53 and Eq.54 are fixed by imposing renormalization conditions. Renormalization of free parameter in Eq.53 affects physical predictions, while renormalization of fields in Eq.54 is only relevant for making Green's function finite and has no effect in calculating S-matrix elements as discussed before. Nevertheless, renormalization of fields leads to simple forms of the renormalization conditions for free parameters.

In the on-shell renormalization scheme, the renormalized parameters in Eq.53

are equal to the physical mass and couplings. Additionally, the field renormalization is chosen in such a way that the residues of all renormalized propagators are equal to one. This ensures that the contributions from Feynman diagrams with external self-energies and their corresponding counterterm diagrams cancel out. Therefore, in practical calculations using the on-shell renormalization scheme, there is no need to include radiative corrections to external particles.

In the on-shell renormalization scheme, all renormalization conditions are formulated for on mass-shell external fields. Thus the field and mass renormalization constants as well as quark mixing matrix introduced in Eq.53 and Eq.54 are fixed using the one particle irreducible(1PI) two-point functions. Electric charge renormalization is fixed with three-point functions. In this section, we restrict to the on-shell renormalization of the EWSM at one-loop level. Two-loop renormalization of the EWSM can be found in Refs. [33, 34].

1.2.2.1 Physical Fields and Masses

Firstly, let us start with the definition of gauge boson 1PI two-point function. Consider the Green's function of gauge boson

$$\begin{aligned} G_{\mu\nu}(k^2) &= iD_{\mu\nu}(k^2) + iD_{\mu\rho}(k^2)\Sigma^{\rho\sigma}(k^2)D_{\rho\nu}(k^2) + ... \\ &= \frac{iD_{\mu\nu}}{1 - \Sigma^{\rho\sigma}D_{\rho\sigma}} \\ &= iD_{\mu\rho}\frac{-i}{D_{\rho\sigma} - D_{\rho\eta}\Sigma^{\eta\xi}D_{\xi\sigma}}iD_{\rho\nu} \\ &= iD_{\mu\rho}(\Gamma^{\rho\sigma})iD_{\rho\nu} \end{aligned} \tag{56}$$

All quantities shown above are unrenormalized. $D_{\mu\nu}$ is the gauge boson propagator, and Σ is the self-energy correction. In 't Hooft Feynman gauge, the gauge boson

propagator is written as

$$\frac{1}{D_{\mu\nu}} = g_{\mu\nu}(k^2 - M_0^2) \ , \tag{57}$$

The self-energy correction can be decomposed into the transverse and longitudinal part

$$\Sigma_{\mu\nu} = (g_{\mu\nu} - \frac{k_\mu k_\nu}{k^2})\Sigma_T + \frac{k_\mu k_\nu}{k^2}\Sigma_L, \tag{58}$$

denoted as Σ_T and Σ_L separately.

$\Gamma^{\mu\nu}$ is the 1PI two-point function, and it can be calculated perturbatively by expanding the self-energy correction

$$\begin{aligned} \Gamma &= \frac{-i}{D - D\Sigma D} \\ &= -\frac{i}{D} - i\Sigma - iD\Sigma D - \cdots \end{aligned} \tag{59}$$

where we have dropped all the indices.

The Green's function for fermions has the following form

$$\begin{aligned} iG^f(p) &= iS(p) + iS\Sigma S + iS\Sigma S\Sigma S + \cdots \\ &= \frac{iS(p)}{1 - \Sigma S} \\ &= iS(p)\frac{-i}{S - S\Sigma S}iS(p) \\ &= iS(p)(\Gamma^f)iS(p) \end{aligned} \tag{60}$$

All quantities shown above are unrenormalized. S is the fermion propagator, and Σ is the self-energy corrections. The explicit expressions are

$$-\frac{1}{S} = \not{p} - m_0 + i\epsilon \ , \ \Sigma(p) = \not{p}\Sigma_V + m_0\Sigma_S = \not{p}P_L\Sigma_L + \not{p}P_R\Sigma_R + m_0\Sigma_S \tag{61}$$

where we have decomposed the self-energy correction into the scalar part, Σ_S, and vector part, Σ_V. The latter can be further decomposed into the right-handed and left-handed contributions by inserting the left-handed and right-handed projectors, $P_{L,R}$.

Γ^f is the 1PI two-point function of fermion. Similarly, it can also be calculated perturbatively by expanding the self-energy correction

$$\begin{aligned}\Gamma^f &= \frac{-i}{S - S\Sigma S} \\ &= -\frac{i}{S} - i\Sigma - iS\Sigma S - \cdots\end{aligned} \tag{62}$$

At 1-loop level, 1PI two-point functions for physical fields listed in Eq.54 have the following form

$$\begin{aligned}
&\Gamma^W_{\mu\nu}(k) = -ig_{\mu\nu}(k^2 - M^2_{W,0}) - i(g_{\mu\nu} - \frac{k_\mu k_\nu}{k^2})\Sigma^W_T(k^2) - i\frac{k_\mu k_\nu}{k^2}\Sigma^W_L(k^2), \\
&\Gamma^{ZZ}_{\mu\nu}(k) = -ig_{\mu\nu}(k^2 - M^2_{Z,0}) - i(g_{\mu\nu} - \frac{k_\mu k_\nu}{k^2})\Sigma^{ZZ}_T(k^2) - i\frac{k_\mu k_\nu}{k^2}\Sigma^{ZZ}_L(k^2), \\
&\Gamma^{ZA}_{\mu\nu}(k) = \Gamma^{AZ}_{\mu\nu}(k) = -i(g_{\mu\nu} - \frac{k_\mu k_\nu}{k^2})\Sigma^{ZA}_T(k^2) - i\frac{k_\mu k_\nu}{k^2}\Sigma^{ZA}_L(k^2), \\
&\Gamma^{AA}_{\mu\nu}(k) = -ig_{\mu\nu}(k^2) - i(g_{\mu\nu} - \frac{k_\mu k_\nu}{k^2})\Sigma^{AA}_T(k^2) - i\frac{k_\mu k_\nu}{k^2}\Sigma^{AA}_L(k^2), \\
&\Gamma^H(k) = i(k^2 - M^2_{H,0}) + i\Sigma^H(k^2), \\
&\Gamma_f(p) = i(\not{p} - m_{f,0}) + i[\not{p}P_L\Sigma_{f,L}(p^2) + \not{p}P_R\Sigma_{f,R}(p^2) + m_{f,0}\Sigma_{f,S}(p^2)]
\end{aligned} \tag{63}$$

The renormalized 1PI two-point functions are obtained by replacing all bare parameter into the renormalized ones. Thus we obtain

$$\begin{aligned}
&\hat{\Gamma}^W_{\mu\nu}(k) = -ig_{\mu\nu}(k^2 - M^2_W) - i(g_{\mu\nu} - \frac{k_\mu k_\nu}{k^2})\hat{\Sigma}^W_T(k^2) - i\frac{k_\mu k_\nu}{k^2}\hat{\Sigma}^W_L(k^2), \\
&\hat{\Gamma}^{ZZ}_{\mu\nu}(k) = -ig_{\mu\nu}(k^2 - M^2_Z) - i(g_{\mu\nu} - \frac{k_\mu k_\nu}{k^2})\hat{\Sigma}^{ZZ}_T(k^2) - i\frac{k_\mu k_\nu}{k^2}\hat{\Sigma}^{ZZ}_L(k^2), \\
&\hat{\Gamma}^{ZA}_{\mu\nu}(k) = \hat{\Gamma}^{AZ}_{\mu\nu}(k) = -i(g_{\mu\nu} - \frac{k_\mu k_\nu}{k^2})\hat{\Sigma}^{ZA}_T(k^2) - i\frac{k_\mu k_\nu}{k^2}\hat{\Sigma}^{ZA}_L(k^2),
\end{aligned}$$

$$
\begin{aligned}
&\hat{\Gamma}^{AA}_{\mu\nu}(k) = -ig_{\mu\nu}(k^2) - i(g_{\mu\nu} - \frac{k_\mu k_\nu}{k^2})\hat{\Sigma}^{AA}_T(k^2) - i\frac{k_\mu k_\nu}{k^2}\hat{\Sigma}^{AA}_L(k^2), \\
&\hat{\Gamma}^{H}(k) = i(k^2 - M_H^2) + i\hat{\Sigma}^{H}(k^2), \\
&\hat{\Gamma}_f(p) = i(\not{p} - m_f) + i[\not{p}P_L\hat{\Sigma}_{f,L}(p^2) + \not{p}P_R\hat{\Sigma}_{f,R}(p^2) + m_f\hat{\Sigma}_{f,S}(p^2)]
\end{aligned} \tag{64}
$$

where $\hat{\Sigma}$ denotes renormalized self-energies. Explicit forms of them are obtained by performing following replacements

$$
\begin{aligned}
&D_{VV} = k^2 - M^2_{V,0} \to (k^2 - M_V^2 - \delta M_V^2) + \delta Z_{VV}(k^2 - M_V^2) \\
&D_f = \not{p} - m_f \to (\not{p} - m_f - \delta m_f) + (\delta Z_{f,L} + \delta Z_{f,R})(\not{p} - m_f) \\
&D_{VV'} = 0 \to \frac{1}{2}\delta Z_{VV'}(k^2 - M_V^2) + \frac{1}{2}\delta Z_{V'V}(k^2 - M_{V'}^2)
\end{aligned} \tag{65}
$$

where corrections proportional to $\delta Z \delta m$ have been neglected since we calculate $\hat{\Gamma}$ at one-loop order. Plugging Eq.65 into Eq.64, the transverse part of the renormalized self-energies can be simply derived

$$
\begin{aligned}
&\hat{\Sigma}^W_T(k^2) = \Sigma^W_T(k^2) + (k^2 - M_W^2)\delta Z_W - \delta M_W^2, \\
&\hat{\Sigma}^H(k^2) = \Sigma^H(k^2) + (k^2 - M_H^2)\delta Z_H - \delta M_H^2, \\
&\hat{\Sigma}^{ZZ}_T(k^2) = \Sigma^{ZZ}_T(k^2) + (k^2 - M_Z^2)\delta Z_{ZZ} - \delta M_Z^2, \\
&\hat{\Sigma}^{AZ}_T(k^2) = \Sigma^{AZ}_T(k^2) + \frac{1}{2}(k^2 - M_Z^2)\delta Z^{AZ} - \frac{1}{2}\delta Z^{AZ}k^2, \\
&\hat{\Sigma}^{AA}_T(k^2) = \Sigma^{AA}_T(k^2) - \delta Z^{AA}k^2, \\
&\hat{\Sigma}_{f,L} = \Sigma_{f,L} + \delta Z_{f,L}, \\
&\hat{\Sigma}_{f,R} = \Sigma_{f,R} + \delta Z_{f,R}, \\
&\hat{\Sigma}_{f,S} = \Sigma_{f,S} - \frac{1}{2}(\delta Z_{f,L} + \delta Z_{f,R}) - \frac{\delta m_f}{m_f}.
\end{aligned} \tag{66}
$$

Note that the unphysical longitudinal part of gauge boson self-energies drops out for on-shell external gauge boson. Since only transverse parts relate to renormalization

constant, it's convenient for practical calculation to project transverse part out with the following equations

$$\begin{aligned}
&\Sigma^{V_1V_2}_{\mu\nu} = -(g_{\mu\nu} - \frac{k_\mu k_\nu}{k^2})\Sigma^{V_1V_2}_T + \frac{k_\mu k_\nu}{k^2}\Sigma^{V_1V_2}_L \\
\Rightarrow\ &\Sigma^{V_1V_2}_T = \frac{-1}{D-1}(g^{\mu\nu} - \frac{k^\mu k^\nu}{k^2})\Sigma^{V_1V_2}_{\mu\nu}\ ,\ \Sigma^{V_1V_2}_L = \frac{k^\mu k^\nu}{k^2}\Sigma^{V_1V_2}_{\mu\nu}
\end{aligned} \tag{67}$$

where $\Sigma^{V_1V_2}_{\mu\nu}$ denotes the self-energy of the gauge bosons.

The renormalized mass parameters of physical particles are fixed by on-shell renormalization condition, which states that the renormalized mass parameters are equal to their physical masses, i.e. zeros of the 1PI two-point functions. Since the propagators are the inverse of 1PI two-point functions, physical masses are also the real parts of the poles of the corresponding propagators: $\mathrm{Re}(D^{-1})|_{p^2=m^2} = 0$. Due to the reason that only transverse part of the gauge boson propagator D^V_T is physical, the on-shell renormalization conditions read

$$(D^V_T)^{-1}(p^2 = M^2_V) = 0, \tag{68}$$

The field renormalization constants are determined by demanding the residues of the poles equal 1, thus we arrive at the following on-shell renormalization conditions

$$\mathrm{Re}\left\{\frac{\partial}{\partial p^2}(D^V_T)^{-1}|_{p^2=M^2_V}\right\} = i, \tag{69}$$

Replacing the propagator D^V_T with renormalized 1PI two-point functions, Eq. 68 and Eq. 69 has the following form

$$\begin{aligned}
&\mathrm{Re}\hat{\Gamma}^W_{\mu\nu}(k)\varepsilon^\nu(k)|_{k^2=M^2_W} = 0\ ,\ \lim_{k^2\to M^2_W}\frac{1}{k^2 - M^2_W}\mathrm{Re}\hat{\Gamma}^W_{\mu\nu}(k)\varepsilon^\nu(k) = -i\varepsilon_\mu(k) \\
&\mathrm{Re}\hat{\Gamma}^{ZZ}_{\mu\nu}(k)\varepsilon^\nu(k)|_{k^2=M^2_Z} = 0\ ,\ \lim_{k^2\to M^2_Z}\frac{1}{k^2 - M^2_Z}\mathrm{Re}\hat{\Gamma}^{ZZ}_{\mu\nu}(k)\varepsilon^\nu(k) = -i\varepsilon_\mu(k) \\
&\mathrm{Re}\hat{\Gamma}^{AA}_{\mu\nu}(k)\varepsilon^\nu(k)|_{k^2=0} = 0\ ,\ \lim_{k^2\to 0}\frac{1}{k^2}\mathrm{Re}\hat{\Gamma}^{AA}_{\mu\nu}(k)\varepsilon^\nu(k) = -i\varepsilon_\mu(k)
\end{aligned}$$

$$
\begin{aligned}
&\mathrm{Re}\hat{\Gamma}^{H}(k)|_{k^2=M_H^2}=0\ ,\ \lim_{k^2\to M_H^2}\frac{1}{k^2-M_H^2}\mathrm{Re}\hat{\Gamma}^{H}(k)=i\\
&\mathrm{Re}\hat{\Gamma}_f(p)u(p)|_{p^2=m_f^2}=0\ ,\ \lim_{p^2\to m_f^2}\frac{\not{p}+m_f}{p^2-m_f^2}\mathrm{Re}\hat{\Gamma}_f(p)=iu(p),\\
&\mathrm{Re}\hat{\Gamma}^{ZA}_{\mu\nu}(k)\varepsilon^{\nu}(k)|_{k^2=M_Z^2}=\mathrm{Re}\hat{\Gamma}^{AZ}_{\mu\nu}(k)\varepsilon^{\nu}(k)|_{k^2=0}=0.
\end{aligned}
\tag{70}
$$

where $\varepsilon(k), u(p)$ are the external polarization vectors for gauge fields, external fermion polarization.

Renormalization conditions allow to express the counterterms by the renormalized parameters. The expressions of counterterms for gauge boson fields and masses at one-loop order are

$$
\begin{aligned}
&\delta M_W^2=\mathrm{Re}\Sigma_T^W\left(M_W^2\right)\ ,\ \delta Z_W=-\,\mathrm{Re}\frac{\partial\Sigma_T^W\left(k^2\right)}{\partial k^2}\bigg|_{k^2=M_W^2},\\
&\delta M_Z^2=\mathrm{Re}\Sigma_T^{ZZ}\left(M_Z^2\right)\ ,\ \delta Z_{ZZ}=-\,\mathrm{Re}\frac{\partial\Sigma_T^{ZZ}\left(k^2\right)}{\partial k^2}\bigg|_{k^2=M_Z^2},\\
&\delta Z_{AZ}=-2\mathrm{Re}\frac{\Sigma_T^{AZ}\left(M_Z^2\right)}{M_Z^2}\ ,\ \delta Z_{ZA}=2\frac{\Sigma_T^{AZ}(0)}{M_Z^2}\ ,\ \delta Z_{AA}=-\,\frac{\partial\Sigma_T^{AA}\left(k^2\right)}{\partial k^2}\bigg|_{k^2=0}\\
&\delta M_H^2=\mathrm{Re}\Sigma^{H}\left(M_H^2\right)\ ,\ \delta Z_H=-\,\mathrm{Re}\frac{\partial\Sigma^{H}\left(k^2\right)}{\partial k^2}\bigg|_{k^2=M_H^2}
\end{aligned}
\tag{71}
$$

The expressions of counterterms for fermions fields and masses are

$$
\begin{aligned}
&\delta m_f=\frac{m_f}{2}\mathrm{Re}(\Sigma_{f,L}\left(m_f^2\right)+\Sigma_{f,R}(m_f^2)+2\Sigma_{f,S}(m_f^2)),\\
&\delta Z_{f,L}=-\mathrm{Re}\Sigma_{f,L}(m_f^2)-m_f^2\frac{\partial}{\partial p^2}\mathrm{Re}[\Sigma_{f,L}(p^2)+\Sigma_{f,R}(p^2)+2\Sigma_{f,S}(p^2)]\Big|_{p^2=m_f^2}\\
&\delta Z_{f,R}=-\mathrm{Re}\Sigma_{f,R}(m_f^2)-m_f^2\frac{\partial}{\partial p^2}\mathrm{Re}[\Sigma_{f,L}(p^2)+\Sigma_{f,R}(p^2)+2\Sigma_{f,S}(p^2)]\Big|_{p^2=m_f^2}
\end{aligned}
\tag{72}
$$

1.2.2.2 Electric Charge

Electric charge is renormalized through 1PI three point function. Generally, any three-point function can be chosen, and the final result should be independent on this choice. For generality, we choose $f\bar{f}A$ vertex to derive the renormalization condition for electric charge. The renormalized $f\bar{f}A$ vertex has the following form

$$\hat{\Gamma}_{\mu}^{f\bar{f}A}(p,p') = -ieQ_f\gamma_\mu + ie\hat{\Lambda}_{\mu}^{f\bar{f}A}(p,p') \tag{73}$$

where p, p' is the momentum of external fermions. Under on-shell renormalization condition, the renormalized 1PI three-point function is same as the tree level one, i.e higher order corrections are zero. Besides, photon momentum vanishes in on-shell limit. Thus the on-shell renormalization condition tells us

$$0 = \bar{u}(p)\hat{\Lambda}_{\mu}^{f\bar{f}A}(p,p)u(p) \tag{74}$$

At one-loop level, $\hat{\Lambda}_{\mu}^{f\bar{f}A}$ is written as

$$\begin{aligned} 0 = {} & \bar{u}(p)\gamma_\mu u(p)\left[-Q_f\left(\delta Z_e + \delta Z_{f,V} + \frac{1}{2}\delta Z_{AA}\right) + \Lambda_V^f(0) + \Lambda_S^f(0) + v_f\frac{1}{2}\delta Z_{ZA}\right] \\ & - \bar{u}(p)\gamma_\mu\gamma_5 u(p)\left[-Q_f\delta Z_{f,A} + \Lambda_A^f(0) + a_f\frac{1}{2}\delta Z_{ZA}\right] \end{aligned} \tag{75}$$

where $\hat{\Lambda}_{V(S,A)}^f$ is the vector(scalar, axial-vector) part of $\hat{\Lambda}_{\mu}^{f\bar{f}A}$, and

$$\delta Z_{f,V} = \frac{1}{2}(\delta Z_{f,L} + \delta Z_{f,R})\ ,\ \delta Z_{f,A} = \frac{1}{2}(\delta Z_{f,L} - \delta Z_{f,R}) \tag{76}$$

a_f, v_f are the vector and axial-vector couplings of Z boson to fermion f. Eq.75 yields

$$-Q_f\left(\delta Z_e + \delta Z_{f,V} + \frac{1}{2}\delta Z_{AA}\right) + \Lambda_V^f(0) + \Lambda_S^f(0) + v_f\frac{1}{2}\delta Z_{ZA} = 0 \tag{77}$$

$$-Q_f\delta Z_{f,A} + \Lambda_A^f(0) + a_f\frac{1}{2}\delta Z_{ZA} = 0 \tag{78}$$

Eq.77 fixes the charge renormalization constant, and it can be further simplified with the following equation [32]

$$\Lambda_V^f(0) + \Lambda_S^f(0) - Q_f \delta Z_{f,V} + a_f \frac{1}{2} \delta Z_{ZA} = 0, \tag{79}$$

which comes from the Ward identity. Thus, Eq.77 becomes

$$\delta Z_e = -\frac{1}{2} \delta Z_{AA} - \frac{s_W}{c_W} \frac{1}{2} \delta Z_{ZA} \tag{80}$$

One can notice that the explicit form of electric charge renormalization condition is independent of the fermion species, reflecting electric charge universality. Insert the expressions of field renormalization constant, the charge renormalization constant becomes

$$\delta Z_e = \frac{1}{2} \frac{\partial \Sigma_T^{AA}(k^2)}{\partial k^2}\Big|_{k^2=0} - \frac{s_W}{c_W} \frac{\Sigma_T^{AZ}(0)}{M_Z^2} \tag{81}$$

Remember this formula is derived from Eq.75, which is valid only at one-loop level, thus Eq.81 is also valid at one-loop level.

1.2.2.3 Weak Mixing Angle

In the on-shell scheme the weak mixing angle is a derived quantity. Following Sirlin [35], the on-shell weak mixing angle is defined as

$$\sin^2\theta_W = s_W^2 = 1 - \frac{M_W^2}{M_Z^2} \tag{82}$$

This definition is independent of a specific process and valid to all orders of perturbation theory.

Since the dependent parameters s_W and c_W frequently appear, it is useful to introduce the corresponding counterterms

$$c_{W,0} = c_W + \delta c_W \ , \ s_{W,0} = s_W + \delta s_W \tag{83}$$

There is another type of definition for the counterterms

$$c_{W,0}^2 = c_W^2 + \delta c_W^2 \ , \ s_{W,0}^2 = s_W^2 + \delta s_W^2 \tag{84}$$

Eq.83 and Eq.84 are equivalent since the explicit expressions of on-shell weak mixing angle counterterms are both derived from Eq.82, in other words, weak mixing angle counterterms are directly related to gauge boson counterterms. Adopting the definition in Eq.83, we obtain

$$\begin{aligned}
\frac{\delta c_W}{c_W} &= \frac{1}{2}\left(\frac{\delta M_W^2}{M_W^2} - \frac{\delta M_Z^2}{M_Z^2}\right) = \frac{1}{2}\mathrm{Re}\left(\frac{\Sigma_T^W(M_W^2)}{M_W^2} - \frac{\Sigma_T^{ZZ}(M_Z^2)}{M_Z^2}\right), \\
\frac{\delta s_W}{s_W} &= -\frac{c_W^2}{s_W^2}\frac{\delta c_W}{c_W} = \frac{1}{2}\frac{c_W^2}{s_W^2}\mathrm{Re}\left(\frac{\Sigma_T^W(M_W^2)}{M_W^2} - \frac{\Sigma_T^{ZZ}(M_Z^2)}{M_Z^2}\right).
\end{aligned} \tag{85}$$

1.2.2.4 Summary of Renormalization Constants at One-Loop

For future use, here we summarize the expressions for EW fields, masses and coupling constant at one-loop level under on-shell scheme.

fields	W	$\delta Z^W = -\mathrm{Re}[\frac{\partial \Sigma_T^W(p^2)}{\partial p^2}\|_{p^2=M_W^2}]$
	Z	$\delta Z^{ZZ} = -\mathrm{Re}[\frac{\partial \Sigma_T^{ZZ}(p^2)}{\partial p^2}\|_{p^2=M_Z^2}]$
		$\delta Z^{ZA} = 2\frac{\Sigma_T^{ZA}(p^2=0)}{M_Z^2}$
	A	$\delta Z^{AZ} = -2\mathrm{Re}[\frac{\Sigma_T^{AZ}(p^2=M_Z^2)}{M_Z^2}]$
		$\delta Z^{AA} = -\frac{\partial \Sigma_T^{AA}(p^2)}{\partial p^2}\|_{p^2=0}$
	H	$\delta Z^H = -\mathrm{Re}[\frac{\partial \Sigma^H(p^2)}{\partial p^2}\|_{p^2=M_H^2}]$
	f	$\delta Z^{f,L} = -\mathrm{Re}\Sigma^{f,L}\left(m_f^2\right) - m_f^2 \frac{\partial \mathrm{Re}\left[\Sigma^{f,L}\left(p^2\right)+\Sigma^{f,R}\left(p^2\right)+2\Sigma^{f,S}\left(p^2\right)\right]}{\partial p^2}\Big\|_{p^2=m_f^2}$
		$\delta Z^{f,R} = -\mathrm{Re}\Sigma^{f,R}\left(m_f^2\right) - m_f^2 \frac{\partial \mathrm{Re}\left[\Sigma^{f,L}\left(p^2\right)+\Sigma^{f,R}\left(p^2\right)+2\Sigma^{f,S}\left(p^2\right)\right]}{\partial p^2}\Big\|_{p^2=m_f^2}$
masses	W	$\delta M_W^2 = \mathrm{Re}[\Sigma_T^W(p^2=M_W^2)]$
	Z	$\delta M_Z^2 = \mathrm{Re}[\Sigma_T^Z(p^2=M_Z^2)]$
	H	$\delta M_H^2 = \mathrm{Re}[\Sigma^H(p^2=M_H^2)]$
	f	$\delta m_{f,i} = \frac{m_{f,i}}{2}\mathrm{Re}\left(\Sigma_{ii}^{f,L}\left(m_{f,i}^2\right) + \Sigma_{ii}^{f,R}\left(m_{f,i}^2\right) + 2\Sigma_{ii}^{f,S}\left({m_{f,i}}^2\right)\right)$
coupling	e	$\delta Z_e = -\frac{1}{2}\delta Z^{AA} - \frac{s_W}{2c_W}\delta Z^{ZA}$
	θ_W	$\frac{\delta s_W}{s_W} = -\frac{c_W^2}{s_W^2}\frac{\delta c_W}{c_W}$, $\frac{\delta c_W}{c_W} = \frac{1}{2}\mathrm{Re}\left(\frac{\Sigma_T^W(M_W^2)}{M_W^2} - \frac{\Sigma_T^{ZZ}(M_Z^2)}{M_Z^2}\right)$

Table 2: Summary of the renormalization constant for SM fields, masses and coupling constant at one-loop level under on-shell scheme.

1.2.3 Renormalization Schemes of Electric Charge

In Sec.1.2.2.2, the electric charge is renormalized in the Thomason limit, where photon momentum transfer Q equals zero. This leads to the renormalized value $\alpha = \alpha(Q^2 = 0)$ in the $\alpha(0)$ scheme. When applied to processes at energies scale of EW gauge boson or above, this scheme leads to large logarithmic corrections of the form $\ln m_f/m_{Z,W}$, which originates from light fermion loops. These large logarithmic contributions can be absorbed into a non-perturbative quantity, which will be discussed in Sec.1.2.3.1.

In addition to the $\alpha(0)$ scheme, there are two other commonly used renormalization schemes for electric charge: $\alpha(M_Z^2)$ scheme, where $\alpha(0)$ is evolved via renormalization-group equation from $Q^2 = 0$ to the Z-pole energy scale, and the G_μ scheme, where α is derived from the Fermi constant G_μ from the equation [32]:

$$\frac{G_\mu}{\sqrt{2}} = \frac{\pi\alpha}{2M_W^2(1 - M_W^2/M_Z^2)}(1 + \Delta r) \tag{86}$$

where Δr incorporates radiative corrections that are determined by matching the muon decay matrix element in the Fermi theory and the SM.

These two schemes will be discussed in Sec.1.2.3.2 and Sec.1.2.3.3.

1.2.3.1 $\alpha(0)$ Scheme

An explicit expression of δZ^{AA} in Eq.81 with fermion loop corrections is

$$\frac{\partial\Sigma_T^{AA}}{\partial p^2}\Big|_{p^2=0} = \Pi(0) = N_c^f Q_f^2 \frac{\alpha}{3\pi}\left(\frac{2}{4-D} - \gamma_E - \log\frac{m_f^2}{4\pi\mu^2}\right) \tag{87}$$

Dimensional regularization [27] is adopted to regularize the UV divergence at one-loop, which behaves as $1/(4 - D)$. Π stands for the photonic vacuum polarized induced by fermions. μ is the regularization scale, γ_E is Euler's constant, N_c^f is the

color number of fermion (1 for $f = l$ and 3 for $f = q$), and Q_f is the charge of fermion.

A problem of Eq.87 is that light quark mass($m_{u,d,s}$) are ill-defined because QCD at the energy scale of light fermion quark is non-perturbative. Thus a perturbative calculation of Eq.87 is adequate. This problem can be circumvented by implementing the following subtraction:

$$\Pi(0) = \Pi_{\text{top}}(0) + \Pi_{\text{light-f}}(0), \tag{88}$$

$$\Pi_{\text{light-f}}(0) = \underbrace{\Pi_{\text{light-f}}(0) - \text{Re}\Pi_{\text{light-f}}(p^2)}_{\equiv\Delta\alpha(p^2)} + \text{Re}\Pi_{\text{light-f}}(p^2) \ , \ \Pi(p^2) = \frac{\Sigma_T^{AA}(p^2)}{p^2}, \tag{89}$$

$$\Delta\alpha(p^2) = \underbrace{\Pi(0)_{\text{lepton}} - \text{Re}\Pi(p^2)_{\text{lepton}}}_{\Delta\alpha_{\text{lepton}}} + \underbrace{\Pi(0)_{\text{hadron}} - \text{Re}\Pi(p^2)_{\text{hadron}}}_{\Delta\alpha_{\text{hadron}}\, i.e. q\neq t} \tag{90}$$

with $p^2 = m_Z^2$, but this choice of m_Z is arbitrary. The only requirement is that the scale p^2 should be larger than QCD scale.

$\Pi_{\text{light-f}}(p^2)$ depends on quark mass through m_q^2/p^2, and the quark mass can be neglected in the perturbative calculation of $\Pi_{\text{light-f}}(p^2)$ if $p^2 \gg m^2_{\text{light-f}}$. $\Delta\alpha(p^2)$ is divided into a leptonic and hadronic part. The leptonic part,$\Delta\alpha_{\text{lepton}}$, can also be calculated using perturbation theory[36, 37]. The evaluation of hadronic contribution, $\Delta\alpha_{\text{hadron}}$, can be related to the process $e^+e^- \to$ hadron using a dispersion integral[38, 39, 40]:

$$\Delta\alpha_{\text{hadron}}(m_Z^2) = -\frac{\alpha}{3}\int_0^\infty ds' \frac{R(s')}{s'(s' - m_Z^2 - i\epsilon)} \ , \ R(s) = \frac{\sigma[e^+e^- \to \text{hadrons}]}{\sigma[e^+e^- \to \mu^+\mu^-]} \tag{91}$$

where we have chosen $p^2 = M_Z^2$.

Combining Eq.90 and Eq.81, the explicit expression for δZ_e under $\alpha(0)$ scheme at 1-loop level can be written as

$$\delta Z_e|_{\alpha(0)} = \frac{1}{2}\Pi_{\text{light-f}}(0) + \frac{1}{2}\Pi_{\text{top}}(0) + \frac{1}{2}\Pi_{\text{bos}}(0) - \frac{s_W}{2c_W}\delta Z^{Z\gamma(1)}$$

$$= \frac{1}{2}(\Delta\alpha(m_Z^2) + \mathrm{Re}\Pi_{\text{light-f}}(m_Z^2)) + \frac{1}{2}\Pi_{\text{top}}(0) + \frac{1}{2}\Pi_{bos}(0) - \frac{s_W}{2c_W}\delta Z^{Z\gamma(1)} \quad (92)$$

with $\Delta\alpha(m_Z^2) = \Delta\alpha_{\text{lepton}}(m_Z^2) + \Delta\alpha_{\text{hadron}}(m_Z^2)$.

1.2.3.2 $\alpha(M_Z)$ Scheme

At one-loop level, fine structure constant in $\alpha(M_Z)$ scheme can be converted from the $\alpha(0)$ scheme with following equations:

$$\alpha(m_Z) = \frac{\alpha(0)}{1 - \Delta\alpha(m_Z^2)} \quad (93)$$

Charge renormalization constant in $\alpha(M_Z)$ scheme relates to the one in $\alpha(0)$ scheme according to

$$\delta Z_e|_{\alpha(m_Z)} = \delta Z_e|_{\alpha(0)} - \frac{1}{2}\Delta\alpha(m_Z^2) \quad (94)$$

Comparing Eq.92 and Eq.94, one can find that $\alpha(M_Z)$ scheme guarantees the complete cancellation of light-fermion contributions, i.e. removes all large logarithmic dependence on small fermion masses.

1.2.3.3 G_μ Scheme

The fine structure constant in G_μ and $\alpha(0)$ schemes are related according to

$$\alpha_{G_\mu} = \frac{\sqrt{2}}{\pi} G_\mu m_W^2 (1 - \frac{m_W^2}{m_Z^2}) = \alpha(0)(1 + \Delta r) \tag{95}$$

The numerical value for G_μ is extracted from the measured muon lifetime [41]. The quantity Δr contains radiative corrections that are determined by matching the muon decay matrix element in the Fermi theory and the full SM. Note that this scheme does not depend on the shift $\Delta\alpha$ of the running electromagnetic coupling.

At one-loop level, the charge renormalization constant in G_μ scheme can be converted from the $\alpha(0)$ scheme according to:

$$\delta Z_{e(1)}|_{G_\mu} = \delta Z_{e(1)}|_{\alpha(0)} - \frac{1}{2}\Delta r \tag{96}$$

1.3 Method for Feynman Diagram Evaluation

In order to express physical observables as a function of the chosen free parameter set, perturbative calculations are required. However, such calculations at one-loop and higher orders involve the evaluation of Feynman diagrams with loops, which require integration over momenta. We start by introducing the basic techniques for evaluating one-loop Feynman integrals.

Consider a one-loop Feynman diagram with N external momenta q_i and N internal propagators, the masses of which are denoted as m_i. The Feynman integral is expressed as

$$I_N(q_i; m_i) = \frac{(2\pi\mu)^{4-D}}{i\pi^2} \int d^D l \frac{F(l, q_i)}{D_0 D_1 \cdots D_{N-1}}, \tag{97}$$

where l is the loop momenta. $F(l, q_i)$ denotes the numerator and is a function of loop momentum l and external momenta q_i. The denominators are

$$D_i = (l + p_i)^2 - m_i^2 + i\varepsilon \ , \ p_i = \sum_{j=0}^{i} q_j \ , \ q_0 = 0 \ , \tag{98}$$

where $i\varepsilon$ is an infinitesimal imaginary part which is needed to shift branch points away from integration axis. This specific choice ensures causality. After loop integral, $i\varepsilon$ determines the correct imaginary parts of the logrithms and dilogrithms.

The one-loop Feynman integral can be either UV divergent or finite, depending on the number of loop momenta l in the numerator, denoted as P. If $P+D-2N \geq 0$, the integral is UV-divergent. To regularize this divergence, we calculate the integrals in a general dimension $D \neq 4$, using the technique of dimensional regularization. The divergence, which is in the form of $1/(D-4)$, cancels out in the renormalized quantities.

The numerator in a loop integral can be independent of the loop momentum l, i.e. F is a constant or a dot product between external momenta $q_i \cdot q_j$. In this case, the loop integral is called a scalar integral, and its analytical expression is known, as we will discuss in Sec.1.3.3. On the other hand, if F depends on the loop momentum l, for example $F = p_i \cdot l$ or $F = l \cdot l$, the loop integral is called a tensor integral.

In practice, the tensor integrals can be reduced to a combination of scalar integrals. This is done using a technique known as tensor reduction, which involves decomposing the tensor integrals into linear combinations of scalar integrals. The scalar integrals are evaluated using known analytical expressions, while the coefficients of the scalar integrals are obtained by solving a system of linear equations. The resulting expression for the tensor integral can then be used to compute the loop contribution to a physical process.

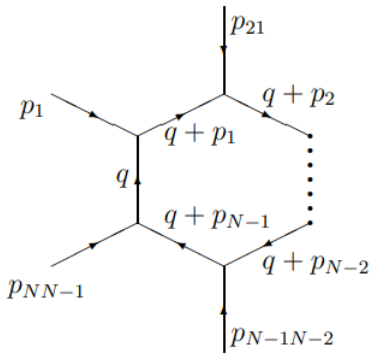

Figure 2: Feynman diagram for one-loop N-point integral, where $p_{ij} = p_i - p_j$

This section covers the methods for reducing tensor integrals to scalar integrals based on Refs. [42, 43]. The analytical formulas for one-loop scalar integrals will also be provided, following the methods presented in [44, 45]. Additionally, techniques for evaluating two-loop integrals are also discussed based on [46, 47].

1.3.1 Tensor Decomposition

The general one-loop tensor integral with P indices can be written as

$$\begin{aligned} T^N_{\mu_1,\cdots,\mu_P} &= \frac{(2\pi\mu)^{4-D}}{i\pi^2}\int d^Dq \frac{q_{\mu_1}\cdots q_{\mu_P}}{D_0 D_1 \cdots D_{N-1}} \\ &= \frac{(2\pi\mu)^{4-D}}{i\pi^2}\int d^Dq \frac{q_{\mu_1}\cdots q_{\mu_P}}{[(q^2-m_0^2)][(q+p_1)^2-m_1^2]\cdots[(q+p_{N-1})^2-m_{N-1}^2]} \end{aligned} \tag{99}$$

where μ has mass dimension and serves to keep the dimension of the integral fixed for varying D. There is an infinitesimal imaginary parts in association with the mass squared in the denominator, namely

$$(q+p_j)^2 - m_j^2 = (q+p_j)^2 - m_j^2 + i\varepsilon \tag{100}$$

For brevity, we will not write $i\varepsilon$ explicitly.

The representative Feynman diagram for this 1-loop N-point function is shown in Fig.2. Conventionally T^N is denoted by the Nth character of the alphabet, i.e. $T^1 \equiv A, T^2 \equiv B$ and etc. The scalar integrals carry an index 0, i.e. $P = 0$.

Power counting indicates that the integral is UV divergent if $P+D-2N \geq 0$. UV divergences are regularized as poles of $1/(D-4)$ with dimensional regularization and drop out in renormalized quantities. Besides, renormalized theory, which contains a finite number of UV divergences, requires that $P \leq N$. Otherwise, the number of UV divergences is infinite thus contradicts with renormlaized theory.

Lorentz covariance of the integrals allows to decompose the tensor integrals into tensors constructed from external momentum p_i and metric tensor $g_{\mu\nu}$ with totally symmetric coefficient function $T^N_{i_1,\cdots,i_p}$, namely

$$T^N_{\mu_1,\cdots,\mu_P} = \sum_{i_1,\cdots,i_P=0}^{N-1} T^N_{i_1,\cdots,i_p} p_{i_1,\mu_1} \cdots p_{i_P,\mu_P} \tag{101}$$

where artificially momentum p_0 is introduced in order to write the metric tensor in a compact way. The metric tensor is recovered by omitting terms with odd p_0's and replacing products of even p_0's by

$$\begin{aligned} p_{0,\mu_1} p_{0,\mu_2} &\to g_{\mu_1\mu_2} \\ p_{0,\mu_1} p_{0,\mu_2} p_{0,\mu_3} p_{0,\mu_4} &\to \{gg\}_{\mu_1\mu_2\mu_3\mu_4} \\ p_{0,\mu_1} p_{0,\mu_2} p_{0,\mu_3} p_{0,\mu_4} p_{0,\mu_5} p_{0,\mu_6} &\to \{ggg\}_{\mu_1\mu_2\mu_3\mu_4\mu_5\mu_6} \end{aligned} \tag{102}$$

where $\{g\cdots g\}_{\ldots}$ denotes all permutation possibilities of indices. Similarly, we define $\{p\cdots p\}_{\ldots}, \{p\cdots g\cdots\}_{\ldots}$ to stand for all permutation possibilities of indices from

external momenta and metric tensor. For example, the explicit forms of $\{gg\}_{\mu_1\mu_2\mu_3\mu_4}$ and $\{pg\}_{\mu_1\mu_2\mu_3}$ are

$$\begin{aligned}\{gg\}_{\mu_1\mu_2\mu_3\mu_4} &= g_{\mu_1\mu_2}g_{\mu_3\mu_4} + g_{\mu_1\mu_3}g_{\mu_2\mu_4} + g_{\mu_1\mu_4}g_{\mu_2\mu_3},\\ \{pg\}_{\mu_1\mu_2\mu_3} &= p_{\mu_1}g_{\mu_2\mu_3} + p_{\mu_2}g_{\mu_1\mu_3} + p_{\mu_3}g_{\mu_1\mu_2}\end{aligned} \tag{103}$$

For later use, here we summarize the explicit Lorentz decomposition for $T_P^N, N \leq 4$. For 1-point function:

$$A_\mu(m_0) = 0 \tag{104}$$

For 2-point functions: $B_{\dots} = B_{\dots}(p_1; m_0, m_1)$

$$\begin{aligned}B_\mu &= p_{1\mu}B_0\ ,\\ B_{\mu\nu} &= g_{\mu\nu}B_{00} + p_{1\mu}p_{1\nu}B_{11}\ ,\\ B_{\mu\nu\rho} &= (gp)_{\mu\nu\rho}B_{001} + p_{1\mu}p_{1\nu}p_{1\rho}B_{111}.\end{aligned} \tag{105}$$

For 3-point functions: $C_{\dots} = C_{\dots}(p_1, p_2; m_0, m_1, m_2)$

$$\begin{aligned}C_\mu &= p_{1\mu}C_1 + p_{2\mu}C_2 = \sum_{i=1}^{2} p_{i\mu}C_i\\ C_{\mu\nu} &= g_{\mu\nu}C_{00} + p_{1\mu}p_{1\nu}C_{11} + p_{1\mu}p_{2\nu}C_{12} + p_{2\mu}p_{1\nu}C_{21} + p_{2\mu}p_{2\nu}C_{22}\\ &= g_{\mu\nu}C_{00} + \sum_{i,j=1}^{2} p_{i\mu}p_{j\nu}C_{ij}\\ C_{\mu\nu\rho} &= \{gp_1\}_{\mu\nu\rho}C_{001} + \{gp_2\}_{\mu\nu\rho}C_{002} + \{p_1p_1p_2\}_{\mu\nu\rho}C_{112} + \{p_1p_2p_2\}_{\mu\nu\rho}C_{122}\\ &\quad + p_{1\mu}p_{1\nu}p_{1\rho}C_{111} + p_{2\mu}p_{2\nu}p_{2\rho}C_{222}\\ &= \sum_{i=1}^{2}\Big(g_{\mu\nu}p_{i\rho} + g_{\mu\rho}p_{i\nu} + g_{\nu\rho}p_{i\mu}\Big)C_{00i} + \sum_{i,j,k=1}^{2} p_{i\mu}p_{j\nu}p_{k\rho}C_{ijk}\end{aligned} \tag{106}$$

For 4-point functions: $D_{\cdots} = D_{\cdots}(p_1, p_2, p_3; m_0, m_1, m_2, m_3)$

$$
\begin{aligned}
D_\mu &= \sum_{i=1}^{3} p_{i\mu} D_i, \\
D_{\mu\nu} &= g_{\mu\nu} D_{00} + \sum_{i,j=1}^{3} p_{i\mu} p_{j\nu} D_{ij} \\
D_{\mu\nu\rho} &= \sum_{i=1}^{3} \Big(g_{\mu\nu} p_{i\rho} + g_{\mu\rho} p_{i\nu} + g_{\nu\rho} p_{i\mu} \Big) D_{00i} + \sum_{i,j,k=1}^{3} p_{i\mu} p_{j\nu} p_{k\rho} D_{ijk} \\
D_{\mu\nu\rho\sigma} &= \{gg\}_{\mu\nu\rho\sigma} D_{0000} + \sum_{i,j}^{3} \{gp_i p_i\}_{\mu\nu\rho\sigma} D_{00ij} + \sum_{i,j,k,l=1}^{3} p_{i\mu} p_{j\nu} p_{k\rho} p_{l\sigma} D_{ijkl}
\end{aligned}
\tag{107}
$$

There are no such terms like $C_{\mu_1 \cdots \mu_4}, D_{\mu_1 \cdots \mu_5}$ due to renormalizability.

The Lorentz decomposition for tensor integral with $N \geq 5$ is simply

$$
T^N_{\mu_1, \cdots, \mu_P} = \sum_{i_1, \cdots, i_P = 1}^{4} T^N_{i_1, \cdots, i_p} p_{i_1, \mu_1} \cdots p_{i_P, \mu_P} \tag{108}
$$

which is different from the tensor decomposition Eq.101. There are two differences: (a) metric tensor $g_{\mu\nu}$ disappears; (b) Only four momenta, instead of $N-1$ momenta is used. The latter can be thought as in four dimensional space, only four momenta are linearly independent, which can be viewed as the basis of the $\{p_i\}$ space. All the other momenta can be expressed as the linear combination of the basis momenta.

The symmetric coefficient function $T^N_{i_1, \cdots, i_p}$ can be reduced to a linear combination of scalar functions T^N_0 with $N \leq 4$. The coefficients of the scalar integrals are obtained by solving a linear system, which will be discussed in the next section.

1.3.2 Reduction of Tensor Integrals to Scalar Integrals

To provide a general understanding of the reduction method, it is better to begin by examining the reduction of T^N_μ before delving into the complex expressions for the reductions of $T^N_{\mu_1\cdots\mu_P}$.

For future use, here we define some new variables.

f_k, Y_{ij} are defined as follows:

$$f_k \equiv p_k^2 - m_k^2 + m_0^2 \ , \ Y_{ij} = m_i^2 + m_j^2 - (p_i - p_j)^2 \tag{109}$$

This quantities will appear frequently for the simplification of $q \cdot p_k$.

$T^{N-1}_{\mu_1\cdots\mu_P}(k)$ is defined as

$$T^{N-1}_{\mu_1\cdots\mu_P}(k) \equiv \frac{(2\pi\mu)^{4-D}}{i\pi^2}\int d^D q \frac{q_{\mu_1}\cdots q_{\mu_P}}{D_0\cdots D_{k-1}D_{k+1}\cdots D_{N+1}} \tag{110}$$

which can be thought as the kth propagator is removed from $T^N_{\mu_1\cdots\mu_P}$. Note that the first propagator of $T^{N-1}_{\mu_1\cdots\mu_P}(0)$ is $D_1 = (q+p_1)^2 - m_1^2$, which contains an external momentum. To bring back to the form in Eq.99, a shift of the integration momentum has to be performed, namely $q \to q - p_{i\neq k}$.

$R^{N,k}_{\mu_1\cdots\mu_{P-1}}$ is defined as

$$\begin{aligned} R^{N,k}_{\mu_1\cdots\mu_{P-1}} \equiv T^N_{\mu_1\cdots\mu_P} p_k^{\mu_P} &= \sum_{i_1,\cdots,i_{P-1}}^{M} R^{N,k}_{i_1,\cdots,i_{P-1}} p_{i_1\mu_1}\cdots p_{i_{P-1}\mu_{P-1}} \\ &= \frac{1}{2}\Big[T^{N-1}_{\mu_1\cdots\mu_{P-1}}(k) - T^{N-1}_{\mu_1\cdots\mu_{P-1}}(0) - f_k T^N_{\mu_1\cdots\mu_P}\Big] \end{aligned} \tag{111}$$

All tensor integrals on the right-hand side (RHS) have one Lorentz index less that the original tensor integral. Besides the first two have one propagator eliminated.

Similarly, $R^{N,00}_{\mu_1\cdots\mu_{P-2}}$ is

$$R^{N,00}_{\mu_1\cdots\mu_{P-2}} \equiv T^N_{\mu_1\cdots\mu_P} g_k^{\mu_{P-1}\mu_P} = \sum_{i_1,\cdots,i_{P-2}}^{M} R^{N,00}_{i_1,\cdots,i_{P-2}} p_{i_1\mu_1}\cdots p_{i_{P-2}\mu_{P-2}}$$
$$= \left[T^{N-1}_{\mu_1\cdots\mu_{P-2}}(0) + m_0^2 T^N_{\mu_1\cdots\mu_{P-2}}\right] \tag{112}$$

where two indices are eliminated for the functions on the RHS.

1.3.2.1 Reduction of T^N_μ

The expression of T^N_μ is

$$T^N_{\mu_1} = \frac{(2\pi\mu)^{4-D}}{i\pi^2}\int d^Dq \frac{q_{\mu_1}}{D_0 D_1\cdots D_{N-1}} \tag{113}$$
$$= \sum_{i_1=1}^{N-1} T^N_{i_1} p_{i_1,\mu_1} \tag{114}$$

Contracting Eq.113 with $p_k^{\mu_1}$, we obtain

$$R^{N,k} = T^N_{\mu_1}\cdot p_k^{\mu_1} = \frac{(2\pi\mu)^{4-D}}{i\pi^2}\int d^Dq \frac{q\cdot p_k}{D_0 D_1\cdots D_{N-1}}$$
$$= \frac{(2\pi\mu)^{4-D}}{i\pi^2}\int d^Dq \frac{1}{2}\times\frac{D_k - D_0 - f_k}{D_0 D_1\cdots D_{N-1}}$$
$$= \frac{1}{2}T_0^{N-1}(k) - \frac{1}{2}T_0^{N-1}(0) - \frac{1}{2}f_k T_0^N \tag{115}$$

Contracting Eq.114 with $p_k^{\mu_1}$, we obtain

$$T^N_{\mu_1}\cdot p_k^{\mu_1} = \sum_{i_1=1}^{N-1} T^N_{i_1} p_{i_1}\cdot p_k \tag{116}$$

where T_0^M are all scalar integrals.

Since there are $N-1$ different k's, equating Eq.115 and Eq.116 leads to a $(N-1)\times(N-1)$ linear equation system, which can be written as

$$\begin{pmatrix} \frac{1}{2}T_0^{N-1}(1)-\frac{1}{2}T_0^{N-1}(0)-\frac{1}{2}f_1T_0^N \\ \vdots \\ \frac{1}{2}T_0^{N-1}(N-1)-\frac{1}{2}T_0^{N-1}(0)-\frac{1}{2}f_{N-1}T_0^N \end{pmatrix} = \begin{pmatrix} p_1\cdot p_1 & \cdots & p_1\cdot p_{N-1} \\ \vdots & \ddots & \vdots \\ p_{N-1}\cdot p_1 & \cdots & p_{N-1}\cdot p_{N-1} \end{pmatrix} \begin{pmatrix} T_1^N \\ \vdots \\ T_{N-1}^N \end{pmatrix} \tag{117}$$

where the $N-1\times N-1$ matrix composed with $p_i\cdot p_j$ is called Gram determinant, denoted as X_{N-1}. The explicit properties of X_{N-1} give rise to three different cases for solving T_k^N.

1. $\det(X_{N-1})\neq 0$

If the Gram determinant is not equal to 0, i.e. $\{p_1,\cdots,p_{N-1}\}$ are linearly independent, the solutions of T_i^N take the form

$$\begin{pmatrix} T_1^N \\ \vdots \\ T_{N-1}^N \end{pmatrix} = \begin{pmatrix} p_1\cdot p_1 & \cdots & p_1\cdot p_{N-1} \\ \vdots & \ddots & \vdots \\ p_{N-1}\cdot p_1 & \cdots & p_{N-1}\cdot p_{N-1} \end{pmatrix}^{-1} \times \begin{pmatrix} \frac{1}{2}T_0^{N-1}(1)-\frac{1}{2}T_0^{N-1}(0)-\frac{1}{2}f_1T_0^N \\ \vdots \\ \frac{1}{2}T_0^{N-1}(N-1)-\frac{1}{2}T_0^{N-1}(0)-\frac{1}{2}f_{N-1}T_0^N \end{pmatrix} \tag{118}$$

Thus T_i are linear combinations of scalar integrals with coefficients as functions of external momenta dot product $p_i\cdot p_j$ and mass m_k.

2. $\det(X_{N-1})=0,\{p_1,\cdots,p_{N-1}\}$ **are not linearly independent**

If the Gram determinant is equal to 0, it indicates $\{p_1, \cdots, p_{N-1}\}$ are not linearly independent and Eq.116 fails. Suppose there are M linearly independent momenta, Eq.116 becomes

$$T^N_{\mu_1} \cdot p_k^{\mu_1} = \sum_{i_1=1}^{M} T^N_{i_1} p_{i_1} \cdot p_k \tag{119}$$

and the solutions of T_i^N is

$$\begin{pmatrix} T_1^N \\ \vdots \\ T_M^N \end{pmatrix} = \begin{pmatrix} p_1 \cdot p_1 & \cdots & p_1 \cdot p_M \\ \vdots & \ddots & \vdots \\ p_M \cdot p_1 & \cdots & p_M \cdot p_M \end{pmatrix}^{-1} \begin{pmatrix} \frac{1}{2} T_0^{N-1}(1) - \frac{1}{2} T_0^{N-1}(0) - \frac{1}{2} f_1 T_0^N \\ \vdots \\ \frac{1}{2} T_0^{N-1}(M) - \frac{1}{2} T_0^{N-1}(0) - \frac{1}{2} f_M T_0^N \end{pmatrix} \tag{120}$$

Since M momenta are linearly independent, other momenta can be written as a linear combination of them, $p_l = \sum_{i=1}^{M} c_M p_M$. Besides, it is easy to check that $\det(X_{L>M}) = 0$. For example, X_{M+1} can be written as

$$\begin{aligned} & \det \begin{pmatrix} p_1 \cdot p_1 & \cdots & p_1 \cdot p_M & p_1 \cdot p_{M+1} \\ \vdots & \ddots & \vdots & \vdots \\ p_M \cdot p_1 & \cdots & p_M \cdot p_M & p_M \cdot p_{M+1} \\ p_{M+1} \cdot p_1 & \cdots & p_{M+1} \cdot p_M & p_{M+1} \cdot p_{M+1} \end{pmatrix} \\ = \ & \det \begin{pmatrix} p_1 \cdot p_1 & \cdots & p_1 \cdot p_M & \sum_{i=1}^{M} c_i p_1 \cdot p_i \\ \vdots & \ddots & \vdots & \vdots \\ p_M \cdot p_1 & \cdots & p_M \cdot p_M & \sum_{i=1}^{M} c_i p_M \cdot p_i \\ \sum_{i=1}^{M} c_i p_i \cdot p_1 & \cdots & \sum_{i=1}^{M} c_i p_i \cdot \cdot p_M & \sum_{i=1}^{M} \sum_{j=1}^{M} c_i c_j p_i \cdot p_j \end{pmatrix} = 0 \end{aligned} \tag{121}$$

3. $\det(X_{N-1}) = 0, \{p_1, \cdots, p_{N-1}\}$ **are linearly independent**

It is also possible that $N-1$ momenta are linearly independent and $\det(X_{N-1}) = 0$. In this case, the previous reduction method based on finding M linearly independent momenta also fails, thus one has to use a different reduction algorithm. We will use the reduction of scalar five-point function as an example.

The scalar five-point function contains four linearly independent external momenta, then the loop momentum q is always a linear combination of four external momenta. Thus according to Eq.121, the following equation holds

$$
\begin{aligned}
0 &= \det \begin{pmatrix} q\cdot q & q\cdot p_1 & \cdots & q\cdot p_4 \\ p_1\cdot q & p_1\cdot p_1 & \cdots & p_1\cdot p_4 \\ \vdots & \vdots & \ddots & \vdots \\ p_4\cdot q & p_4\cdot p_1 & \cdots & p_4\cdot p_4 \end{pmatrix} = \det \begin{pmatrix} 2q\cdot q & 2q\cdot p_1 & \cdots & 2q\cdot p_4 \\ 2p_1\cdot q & 2p_1\cdot p_1 & \cdots & 2p_1\cdot p_4 \\ \vdots & \vdots & \ddots & \vdots \\ 2p_4\cdot q & 2p_4\cdot p_1 & \cdots & 2p_4\cdot p_4 \end{pmatrix} \\
&= \det \begin{pmatrix} 2D_0+Y_{00} & 2q\cdot p_1 & \cdots & 2q\cdot p_4 \\ D_1-D_0+Y_{10}-Y_{00} & 2p_1\cdot p_1 & \cdots & 2p_1\cdot p_4 \\ \vdots & \vdots & \ddots & \vdots \\ D_4-D_0+Y_{40}-Y_{00} & 2p_4\cdot p_1 & \cdots & 2p_4\cdot p_4 \end{pmatrix} \\
&= \frac{1}{i\pi^2}\int d^Dq \frac{1}{D_0D_1\cdots D_4} \times \det \begin{pmatrix} 2D_0+Y_{00} & 2q\cdot p_1 & \cdots & 2q\cdot p_4 \\ D_1-D_0+Y_{10}-Y_{00} & 2p_1\cdot p_1 & \cdots & 2p_1\cdot p_4 \\ \vdots & \vdots & \ddots & \vdots \\ D_4-D_0+Y_{40}-Y_{00} & 2p_4\cdot p_1 & \cdots & 2p_4\cdot p_4 \end{pmatrix}
\end{aligned}
\tag{122}
$$

Expanding the determinant along the first column we obtain

$$
0 = \frac{1}{i\pi^2}\int d^Dq \frac{1}{D_0D_1\cdots D_4} \times [2D_0+Y_{00}] \times \det \begin{pmatrix} 2p_1\cdot p_1 & \cdots & 2p_1\cdot p_4 \\ \vdots & \ddots & \vdots \\ 2p_4\cdot p_1 & \cdots & 2p_4\cdot p_4 \end{pmatrix}
$$

$$+\frac{1}{i\pi^2}\int d^Dq\frac{1}{D_0D_1\cdots D_4}\times\sum_{k=1}^{4}(-1)^k[D_k-D_0+Y_{k0}-Y_{00}]$$
$$\times\det\begin{pmatrix}2q\cdot p_1 & \cdots & 2q\cdot p_4\\ \vdots & \ddots & \vdots\\ 2p_{k-1}\cdot p_1 & \cdots & 2p_{k-1}\cdot p_4\\ 2p_{k+1}\cdot p_1 & \cdots & 2p_{k+1}\cdot p_4\\ \vdots & \ddots & \vdots\end{pmatrix} \tag{123}$$

Subtracting $p_4^\mu T_0^4(0)$ and added it back, the above equation is still invariant and obtains a new form

$$0=[2T_0^4(0)+Y_{00}T_0^5]\times\det\begin{pmatrix}2p_1\cdot p_1 & \cdots & 2p_1\cdot p_4\\ \vdots & \ddots & \vdots\\ 2p_4\cdot p_1 & \cdots & 2p_4\cdot p_4\end{pmatrix}$$
$$+\sum_{k=1}^{4}(-1)^k\times[T_\mu^4(k)-T_\mu^4(0)+(Y_{k0}-Y_{00})T_\mu^5-p_4^\mu T_0^4(0)+p_4^\mu T_0^4(0)]$$
$$\times\det\begin{pmatrix}2p_1^\mu & \cdots & 2p_4^\mu\\ \vdots & \ddots & \vdots\\ 2p_{k-1}\cdot p_1 & \cdots & 2p_{k-1}\cdot p_4\\ 2p_{k+1}\cdot p_1 & \cdots & 2p_{k+1}\cdot p_4\\ \vdots & \ddots & \vdots\end{pmatrix} \tag{124}$$

Writing in this form helps the algebraic simplification. Finally, we obtain

$$0 = (-1) \times \det \begin{pmatrix} T_0^5 & -T_0^4(0) & -T_0^4(1) & -T_0^4(2) & -T_0^4(3) & -T_0^4(4) \\ 1 & Y_{00} & Y_{01} & Y_{02} & Y_{03} & Y_{04} \\ 1 & Y_{10} & Y_{11} & Y_{12} & Y_{13} & Y_{14} \\ 1 & Y_{20} & Y_{21} & Y_{22} & Y_{23} & Y_{24} \\ 1 & Y_{30} & Y_{31} & Y_{32} & Y_{33} & Y_{34} \\ 1 & Y_{40} & Y_{41} & Y_{42} & Y_{43} & Y_{44} \end{pmatrix} \tag{125}$$

In particular, this yields T_0^5 can be reduced to a linear combination of five scalar four-point functions, which is only true if the Gram determinant vanishes. The detailed derivation from Eq.124 to Eq.125 can be found in Appendix.A.

Eq.125 is only for scalar five-point function. General formula for tensor N-point function is

$$0 = \frac{1}{i\pi^2} \int d^D q \frac{q_{\mu_1} \cdots q_{\mu_P}}{D_0 D_1 \cdots D_{N-1}} \times \det \begin{pmatrix} D_0 + Y_{00} & 2q \cdot p_1 & \cdots & 2q \cdot p_{N-1} \\ Y_{10} - Y_{00} & 2p_1 \cdot p_1 & \cdots & 2p_1 \cdot p_4 \\ \vdots & \vdots & \ddots & \vdots \\ Y_{(N-1)0} - Y_{00} & 2p_{N-1} \cdot p_1 & \cdots & 2p_{N-1} \cdot p_{N-1} \end{pmatrix} \tag{126}$$

With the same strategy, we obtain the reduction formula for tensor N-point function with vanishing Gram determinant

$$0 = \det \begin{pmatrix} T^N_{\mu_1 \cdots \mu_P} & -T^{N-1}_{\mu_1 \cdots \mu_P}(0) & -T^{N-1}_{\mu_1 \cdots \mu_P}(1) & \cdots & -T^{N-1}_{\mu_1 \cdots \mu_P}(N-1) \\ 1 & Y_{00} & Y_{01} & \cdots & Y_{0(N-1)} \\ 1 & Y_{10} & Y_{11} & \cdots & Y_{1(N-1)} \\ \vdots & \vdots & \vdots & \ddots & \vdots \\ 1 & Y_{(N-1)0} & Y_{(N-1)1} & \cdots & Y_{(N-1)(N-1)} \end{pmatrix} \tag{127}$$

which expresses T^N by T^{N-1}. The latter can be reduced to a linearly combinations of scalar integrals, which will be shown in Sec.1.3.2.2, thus T^N is also reduced to scalar integrals.

Remember that this formula is only valid for $\det y \neq 0$. If $\det y = 0$, one has to choose another reduction method.

1.3.2.2 General Formulas for the Reduction of $T^N_{\mu_1,\cdots,\mu_P}$

Sec.1.3.2.1 explicitly shows how to reduce tensor integrals with one index under various conditions for the Gram determinant. For tensor integrals with more indices $T^N_{\mu_1\cdots\mu_P}$, Eq.117 are modified due to the extra $T_{00\cdots}$ term. Assuming $M < N-1$ momenta are linearly independent, we obtain the following reduction formulas

$$\begin{aligned} T^N_{00i_1\cdots i_{P-2}} &= \frac{1}{D+P-2-M}\Big[R^{N,00}_{i_1\cdots i_{P-2}} - \sum_{k=1}^{M} R^{N,k}_{ki_1\cdots i_{P-2}}\Big], \\ T^N_{ki_1\cdots i_{P-2}} &= (X^{-1}_M)_{kk'}\Big[R^{N,k'}_{i_1\cdots i_{P-1}} - \sum_{r=1}^{P-1}\delta^{k'}_{i_r} T^N_{00i_1\cdots i_{r-1}i_{r+1}\cdots i_{P-1}}\Big]. \end{aligned} \tag{128}$$

Similar to Eq.115, $R^{N,\cdots}_{\cdots}$ can be expressed as a linear combination of scalar functions. Besides, due to the freedom to choose M linearly independent momenta, the $R^{N,\cdots}_{\cdots}$ can be obtained in different ways, i.e. linear combination of different set of scalar functions, which allows for checks on the analytical result as well as on numerical stability.

To illustrate the use of Eq.128, we explicitly show the reduction for C_μ and $C_{\mu\nu}$, which is defined as

$$\begin{aligned} C_{\mu(\nu)} &= C_{\mu(\nu)}(p_1^2, p_2^2; m_0, m_1, m_2) \\ &= \frac{(2\pi\mu)^{4-D}}{i\pi^2}\int d^Dq \frac{q_\mu(q_\nu)}{[q^2-m_0^2][(q+p_1)^2-m_1^2][(q+p_2)^2-m_2^2]} \end{aligned} \tag{129}$$

with

$$
\begin{aligned}
&p_1^2 = M_1^2 \ , \ p_2^2 = M_2^2 \ , \\
&p_{21} = (p_2 - p_1)^2 = M_0^2 \ , \\
&p_1 \cdot p_2 = -\frac{1}{2}(M_0^2 - M_1^2 - M_2^2)
\end{aligned} \tag{130}
$$

where p_1 and p_2 are linearly independent momenta, thus $M = N - 1 = 2$. Besides, the tensor decomposition of $C_{\mu(\nu)}$ can be found in Eq.106.

Eq.128 yields

$$C_k = T_k^3 = (X_2^{-1})_{kk'} R^{3,k'}, \tag{131}$$

$$C_{00} = T_{00}^3 = \frac{1}{D-1}\Big[R^{3,00} - R_1^{3,1} - R_2^{3,1}\Big], \tag{132}$$

$$C_{ki} = T_{ki}^3 = (X_2^{-1})_{kk'}\Big[R_i^{N,k'} - \delta_i^{k'} C_{00}\Big]. \tag{133}$$

The explicit form of Gram determinant is

$$X_2 = \begin{pmatrix} M_1^2 & -\frac{1}{2}(M_0^2 - M_1^2 - M_2^2) \\ -\frac{1}{2}(M_0^2 - M_1^2 - M_2^2) & M_2^2 \end{pmatrix}, \tag{134}$$

the inverse of which is

$$X_2^{-1} = \frac{4}{4M_1^2 M_2^2 - (M_1^2 + M_2^2 - M_0^2)^2} \begin{pmatrix} M_2^2 & \frac{1}{2}(M_0^2 - M_1^2 - M_2^2) \\ \frac{1}{2}(M_0^2 - M_1^2 - M_2^2) & M_1^2 \end{pmatrix} \tag{135}$$

$R^{3,k}$ is reduced to a linear combination of scalar integrals according to Eq.115,

$$
\begin{aligned}
R^{3,1} &= \frac{1}{2}B_0(p_2^2, m_0, m_2) - \frac{1}{2}B_0((p_1 - p_2)^2, m_1, m_2) - (p_1^2 - m_1^2 + m_0^2)C_0, \\
R^{3,2} &= \frac{1}{2}B_0(p_1^2, m_0, m_1) - \frac{1}{2}B_0((p_1 - p_2)^2, m_1, m_2) - (p_2^2 - m_2^2 + m_0^2)C_0.
\end{aligned} \tag{136}
$$

Thus, C_k can be simply solved using Eq.131

$$C_1 = \frac{4}{4M_1^2M_2^2 - (M_1^2 + M_2^2 - M_0^2)^2}\Big[M_2^2 R^{3,1} + \frac{1}{2}(M_0^2 - M_1^2 - M_2^2)R^{3,2}\Big],$$
$$C_2 = \frac{4}{4M_1^2M_2^2 - (M_1^2 + M_2^2 - M_0^2)^2}\Big[\frac{1}{2}(M_0^2 - M_1^2 - M_2^2)R^{3,2} + M_1^2 R^{3,2}\Big]. \quad (137)$$

$R^{3,00}$ and $R_i^{3,k}$can be derived from Eq.111 and Eq.112

$$\begin{aligned}
R^{3,00} &= B_0((p_1 - p_2)^2, m_1, m_2) + m_0^2 C_0, \\
2R_1^{3,1} &= B_1((p_1 - p_2)^2, m_1, m_2) + B_0((p_1 - p_2)^2, m_1, m_2) + (m_1^2 - p_1^2 - m_0^2)C_1, \\
2R_2^{3,1} &= B_1(p_2^2, m_1, m_2) - B_1((p_1 - p_2)^2, m_1, m_2) + (m_2^2 - p_2^2 - m_0^2)C_2, \\
2R_1^{3,2} &= B_1(p_1^2, m_0, m_2) + B_1((p_1 - p_2)^2, m_1, m_2) + B_0((p_1 - p_2)^2, m_1, m_2) \\
&\quad + (m_2^2 - p_2^2 - m_0^2)C_1, \\
2R_2^{3,2} &= -B_1((p_1 - p_2)^2, m_1, m_2) + (m_2^2 - p_2^2 - m_0^2)C_2. \quad (138)
\end{aligned}$$

combining with Eq.137 and

$$B_1(p^2, m_0, m_2) = \frac{m_0^2 - m_1^2}{2p^2}\Big[B_0(p^2, m_0, m_2) - B_0(0, m_0, m_2)\Big] - \frac{1}{2}B_0(p^2, m_0, m_2) \quad (139)$$

$R_k^{3,i}$ can be fully reduced to a linear combination of scalar integrals B_0, C_0. Thus, the solutions of C_{ij} can be obtained from Eq.133.

$C_{\mu\nu\rho}$ can also be reduced to scalar functions with the same strategy. For sake of brevity, we will not explicitly list the expressions here. Remember, there are no terms like $C_{\mu\nu\rho\sigma}$ due to renormalizability of the SM.

1.3.3 Analytical Expression for One-Loop Scalar Integrals

With the reduction method described in the last section, all one-loop integrals can be reduced to the scalar ones. Thus, the analytical solutions of one-loop scalar function is essential to obtain the analytical result for all the other tensor integrals. Besides, these scalar functions depend on the parameter $D = 4 - 2\epsilon$, where only the first few terms in the expansion of ϵ are encountered.

There are two methods for deriving expressions for the first few terms. Explicitly solve the loop integral, which leads to generalized hypergeometric functions [48], and then expand them in ϵ. Alternatively, one can first expand the loop integral and calculate the coefficients of the expansion in ϵ [45]. In this work, we adopt the latter method and list analytical expressions for A_0, B_0, C_0, and D_0 up to $\mathcal{O}(\epsilon)$. A more detailed derivation of the analytical expressions for one-loop scalar integrals as well as the analytical properties of those integrals can be found in Appendix.B and Refs. [44, 45].

For practical calculation, numerical evaluation is more straightforward. Various codes are available for the numerical evaluation of one-loop scalar integrals, such as LoopTools [49, 50], Golem95 [51, 52], Collier [53, 54], OneLoop [55], QCDLoop [56] and PackageX [57, 58].

1.3.3.1 One-Point Function

The scalar one-point function has the following form

$$\begin{aligned} A_0(m) &= (\mu^2 \pi e^{\gamma_E})^{\epsilon} \frac{1}{i\pi^2} \int d^D q \ \frac{1}{q^2 - m^2 + i\varepsilon} \\ &= \frac{m^2}{\epsilon} + A_0^{(0)}(m) + \epsilon A_0^{(1)}(m) + \mathcal{O}(\epsilon^2) \end{aligned} \tag{140}$$

with

$$A_0^{(0)}(m) = m^2 - m^2 \ln \frac{m^2}{\mu^2}$$
$$A_0^{(1)}(m) = \epsilon\big[m^2 + \frac{\pi^2}{12}m^2 - m^2 \ln \frac{m^2}{\mu^2} + \frac{1}{2}m^2 \ln^2 \frac{m^2}{\mu^2}\big] \tag{141}$$

1.3.3.2 Two-Point Function

The scalar two-point function $B_0(k^2, m_1, m_2) = B_0$ has the following form:

$$\begin{aligned} B_0 &= (\mu^2 \pi e^{\gamma_E})^\epsilon \frac{1}{i\pi^2} \int d^D q \ \frac{1}{[q^2 - m_1^2 + i\varepsilon][(q+k)^2 - m_2^2 + i\varepsilon]} \\ &= \frac{1}{\epsilon} + B_0^{(0)} + \epsilon B_0^{(1)} + \mathcal{O}(\epsilon^2) \end{aligned} \tag{142}$$

with

$$\begin{aligned} B_0^{(0)} &= -\ln\big(\frac{k^2}{\mu^2} - i\varepsilon\big) - \sum_{j=1}^{2}\big[\ln(1-x_j) - x_j \ln\frac{x_j - 1}{x_j} - 1\big] \\ B_0^{(1)} &= \frac{\pi^2}{12} + \frac{1}{2}\ln^2\big(\frac{k^2}{\mu^2} - i\varepsilon\big) + \sum_{j=1}^{2}\Big\{\frac{1}{2}\ln(1-x_j)\ln^2(1-x_j) + \frac{1}{2}x_j \ln^2(1-x_j) \\ &\quad + \big[\ln(\frac{k^2}{\mu^2} - i\varepsilon) - 2\big] \times \big[\ln(1-x_j) - x_j \ln\frac{x_j-1}{x_j} - 1\big]\Big\} \\ &\quad + (1-x_1)\ln(1-x_1)\ln(1-x_2) + x_1 \ln(-x_1)\ln(-x_2) + (x_1 - x_2) \\ &\quad \times \left[\mathrm{Li}_2\big(\frac{x_2}{x_2 - x_1}\big) - \mathrm{Li}_2\big(\frac{x_2 - 1}{x_2 - x_1}\big) + \ln(x_2 - x_1)\ln\frac{x_2 - 1}{x_2}\right] \end{aligned} \tag{143}$$

where $x_{1,2}$ are the roots of

$$k^2 x^2 + (-k^2 + m_2^2 - m_1^2)x + m_1^2 = k^2(x - x_1)(x - x_2) \tag{144}$$

The B_0 function has one threshold at $k_0^2 = (m_1 + m_2)^2$. When $k^2 < k_0^2$, the B_0 function are purely real, while the imaginary part is non-zero when $k^2 > k_0^2$.

This discontinuity can be understood as follows. Fig.3 shows the distributions of the Eq. 144 in the region $x \in \{0, 1\}$. We have set $m_1 = 4$ GeV $, m_2 = 10$ GeV . k^2 are considered with three values, $k^2 > k_0^2$, $k^2 = k_0^2$ as well as $K^2 < k_0^2$, which are represented by the blue, orange and green line respectively. As we can see from the green line, Eq. 144 is negative in the region $x \in (0.149, 0.478)$. Eq. 144 originates from the integral

$$B_0^{(0)} = \int_0^1 dx \ln\left[\frac{k^2}{\mu^2}(x - x_1)(x - x_2) - i\varepsilon\right]. \tag{145}$$

Negative value of Eq. 144, i.e. the integral of logarithm in Eq. 145 with negative argument leads to non-zero imaginary part.

The analytical formula of this discontinuity in $D = 4 - 2\epsilon$ is written as

$$\begin{aligned}\Delta B_0(k^2, m_2^2, m_2^2) &\equiv -\frac{1}{\pi}\mathrm{Im}B_0(k^2, m_2^2, m_2^2) \\ &= 2\pi i\Big(\frac{k^2}{4\pi\mu^2}\Big)^{-\epsilon}\frac{\Gamma(1-\epsilon)}{\Gamma(2-2\epsilon)}\frac{\lambda^{\frac{1}{2}-\delta}(k^2, m_1^2, m_2^2)}{(k^2)^{1-2\epsilon}}\Theta(k^2 - (m_1 + m_2)^2)\end{aligned} \tag{146}$$

where Θ is the Heaviside function and $\lambda(x, y, z) = x^2 + y^2 + z^2 - 2(xy + xz + yz)$.

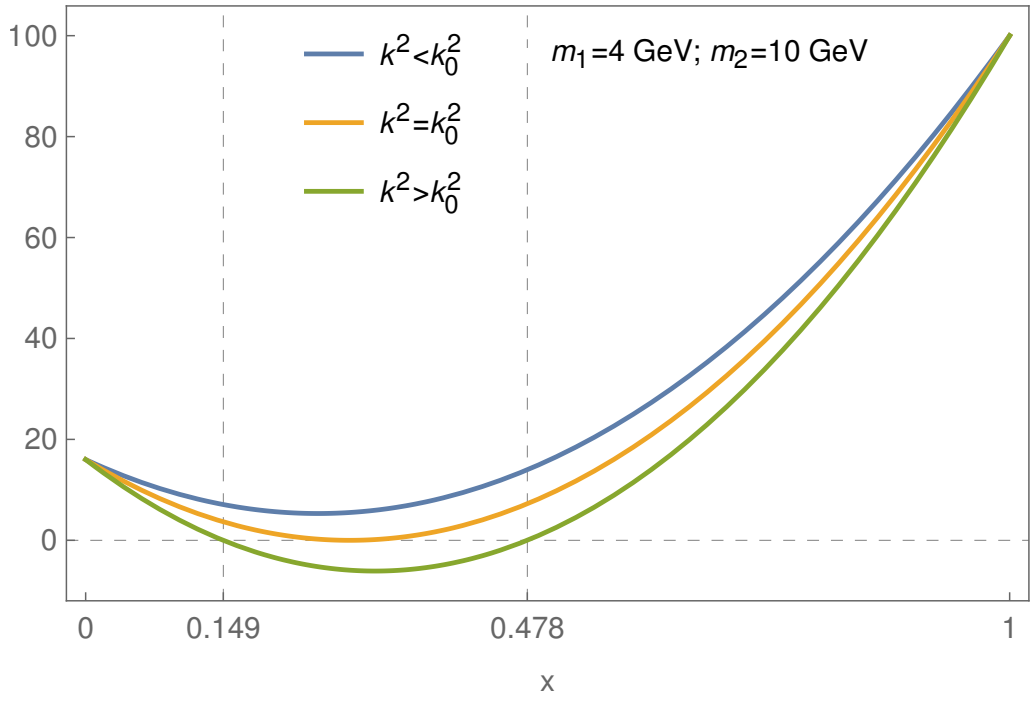

Figure 3: Distributions of Eq.145 for $m_1 = 4$ GeV, $m_2 = 10$ GeV, $\mu = 1$ GeV with $k^2 < k_0^2$(blue),$k^2 = k_0^2$(orange) and $k^2 > k_0^2$(green)

1.3.3.3 Three-Point Function

The scalar three-point function $C_0(p_1^2, p_2^2, (p_1+p_2)^2, m_1, m_2, m_3) = C_0$ has the following form:

$$C_0 = (\mu^2 \pi e^{\gamma_E})^\epsilon \frac{1}{i\pi^2} \int d^D q \; \frac{1}{[q^2 - m_1^2 + i\varepsilon][(q+p_1)^2 - m_2^2 + i\varepsilon][(q+p_1+p_2)^2 - m_2^2 + i\varepsilon]}$$
$$= C_0^{(0)} + \epsilon C_0^{(1)} \tag{147}$$

with

$$C_0^{(0)} = -\frac{1}{\mu^2}\frac{1}{c+2ab}\sum_{j=1}^{3}\sum_{k=1}^{2}\sum_{l=1}^{2}(-1)^{j+l}\mathrm{Li}_2(-r_{jk}^{(l)}), \tag{148}$$

$$\begin{aligned}
C_0^{(1)} = &-C_0^{(0)} \times \ln T + \frac{1}{\mu^2}\frac{1}{c+2ab}\sum_{j=1}^{3}\sum_{l=1}^{2}(-1)^{j+l}\Bigg\{\sum_{k=1}^{2}\Big[-\ln(-r_{jk}^{(l)})\ln^2(1+r_{jk}^{(l)}) \\
&- 2\ln(1+r_{jk}^{(l)})\mathrm{Li}_2(1+r_{jk}^{(l)}) + 2\mathrm{Li}_3(1+r_{jk}^{(l)})\Big] + \Big[\ln(1+r_{j1}^{(l)}) - \ln(1+r_{j2}^{(l)})\Big] \\
&\times \left[\frac{1}{2}\ln(r_{jk}^{(l)}) + \eta\left(-r_{jk}^{(l)}, \frac{1+r_{j2}^{(l)}}{r_{j2}^{(l)} - r_{j1}^{(l)}}\right) \times \Big[\ln(1+r_{j1}^{(l)}) - \ln(1+r_{j2}^{(l)})\Big]\right. \\
&\left. + \mathrm{Li}_2\left(\frac{1+r_{j1}^{(l)}}{1+r_{j2}^{(l)}}\right) - \mathrm{Li}_2\left(\frac{r_{j2}^{(l)}(1+r_{j1}^{(l)})}{r_{j1}^{(l)}(1+r_{j2}^{(l)})}\right)\right] \\
&- \mathrm{Li}_3\left(\frac{1+r_{j1}^{(l)}}{1+r_{j2}^{(l)}}\right) + \mathrm{Li}_3\left(\frac{r_{j2}^{(l)}(1+r_{j1}^{(l)})}{r_{j1}^{(l)}(1+r_{j2}^{(l)})}\right)\Bigg\}
\end{aligned} \tag{149}$$

where α is the root of $a + c\alpha + c\alpha^2 = 0$ and $a = p_2^2/\mu^2, b = p_1^2\mu^2, c = 2p_1 \cdot p_2/\mu^2$. The definitions of $r_{ij}^{(k)}$ can be found in Eq.379. These expressions are valid for real mass and momentum squared. For complex parameters, see Eq.4.26 of [43].

A special type of C_0 function contains soft or/and collinear IR divergence. The C_0 function with soft divergence corresponds to the vertex function with intermediate photon shown in Fig. 4. Suppose the momenta (masses) of two external fermions are $p_{1,2}$ ($m_{1,2}$). The soft divergence originates from the massless photon. To regulate the divergence, a fictitious photon mass λ is introduced, and $\lambda \to 0$ needs to be taken at the end. The corresponding C_0 function is

$$\begin{aligned}
C_0 &= \frac{1}{i\pi^2}\int d^D q \, \frac{1}{[q^2 - m_1^2][(q+p_1)^2 - \lambda^2][(q+p_1+p_2)^2 - m_2^2]} \\
&= -\frac{1}{2}(F_1 \ln\lambda^2 - F_2)
\end{aligned} \tag{150}$$

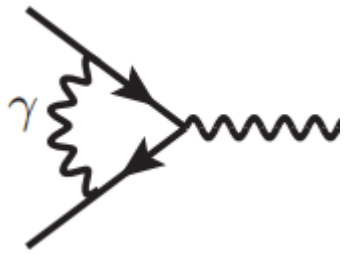

Figure 4: The example vertex diagram that contains soft IR divergence, where the fermions are massive.

with

$$
\begin{aligned}
F_1 &= \frac{1}{(p_1+p_2)^2(y_1-y_2)}\Big[\ln\frac{y_1-1}{y_1}-\ln\frac{y_2-1}{y_2}\Big],\\
F_2 &= F_1\ln((p_1+p_2)^2)+\frac{1}{(p_1+p_2)^2(y_1-y_2)}\Big[\frac{1}{2}\ln^2(1-y_1)-\frac{1}{2}\ln^2(-y_1)\\
&\quad-\frac{1}{2}\ln^2(1-y_2)+\frac{1}{2}\ln^2(-y_2)+\ln(-y_1)\ln(-y_2)+2\ln\frac{y_1-1}{y_1}\ln(y_1-y_2)\\
&\quad-2\mathrm{Li}_2\frac{y_1-1}{y_1-y_2}+2\mathrm{Li}_2\frac{y_1}{y_1-y_2}\Big] \qquad (151)
\end{aligned}
$$

where $y_{1,2}$ are the roots of $(p_1+p_2)^2y^2+y[m_2^2-m_1^2-(p_1+p_2)^2]+m_1^2=0$. $\ln\lambda^2$ regulates the soft divergence, which cancels by adding real photon emission diagrams.

1.3.3.4 Four-Point Function

The 1-loop scalar four-point function is defined as $D_0(p_1^2,p_2^2,p_3^2,p_4^2,m_1,m_2,m_3,m_4)$

$$
\begin{aligned}
D_0 = (\mu^2\pi e^{\gamma_E})^\epsilon\frac{1}{i\pi^2}\int d^Dq\ &\frac{1}{[q^2-m_1^2+i\varepsilon][(q+p_1)^2-m_2^2+i\varepsilon]}\\
&\times\frac{1}{[(q+p_1+p_2)^2-m_3^2+i\varepsilon][(q+p_1+p_2+p_3)^2-m_4^2+i\varepsilon]}
\end{aligned}
$$

$$= D_0^{(0)} + \mathcal{O}(\epsilon) \tag{152}$$

where we have only kept the finite order since the $\mathcal{O}(\epsilon)$ is usually irrelevant for $2 \to 2$ process. In addition, the D_0 function is a linear combination of two C_0 functions, as can be seen from Eq.397, thus we disregard the explicit expressions for D_0, which can be found in [44].

The D_0 function with two small and equal masses and four external on-shell momenta also contains collinear IR divergence, which takes the form

$$\begin{aligned} D_0 &= \frac{1}{i\pi^2}\int d^D q \frac{1}{[q^2 - m_1^2][(q+p_1)^2 - \lambda^2]} \\ &= \frac{1}{[(q+p_1+p_2)^2 - m_3^2][(q+p_1+p_2+p_3)^2 - \lambda^2]} \\ &= \frac{2}{t}\ln\left|\frac{t}{\lambda^2}\right| \times \frac{1}{\Lambda}\ln\left|\frac{(m_1+m_2)^2 + s + \Lambda}{(m_1+m_2)^2 + s - \Lambda}\right| - i\frac{2\pi}{t}\ln\left|\frac{t}{\lambda^2}\right| \times \frac{1}{\Lambda}\theta(-s + (m_1+m_2)^2) \end{aligned} \tag{153}$$

with

$$\begin{aligned} & p_1^2 = m_1^2 \ , \ p_2^2 = m_2^2 = p_3^2 \ , \ (p_1+p_2)^2 = s \ , \ (p_2 = p_3)^2 = t, \\ & \Lambda = \sqrt{s^2 + 2s(m_1^2 + m_2^2) + (m_1^2 - m_2^2)^2} \ , \\ & \theta(x) = \begin{cases} 0 & \text{for} \quad x \leq 0 \\ 1 & \text{for} \quad x > 0 \end{cases} \end{aligned} \tag{154}$$

1.3.4 Numerical Evaluation Method

Analytical solutions of Feynman integrals in terms of special mathematical functions are preferred from an efficiency perspective. However, the analytical solutions are challenging at two and higher loop level due to the appearance of multiple mass scale. Thus, semi-numerical or numerical methods allow broader flexibility and better automation.

Various numerical methods are developed for evaluating Feynman diagrams, and they can be broadly divided into direct and indirect evaluation methods. Direct methods such as sector decomposition[59] and Mellin-Barnes representation [60], compute Feynman integral by directly performing integration over some variables. Indirectly methods, on the other hand, compute Feynman integrals by solving differential equations[61]. A comprehensive review and comparison over a variety of numerical loop integration techniques can be found in [62].

The authors of [46, 47] have developed a new semi-numerical method corresponding to the direct evaluation method based on a combination of Feynman parametrization, dispersion relation and subtraction method. This section aims to introduce these techniques. A combination of them used for evaluating two-loop Feynman diagrams will be discussed in Sec.2.3.1, Sec.2.3.2 and Sec.2.3.3.

1.3.4.1 Feynman Parametrization

Feynman parametrization is a technique of changing an expression into a numerical integral, the general form of which is

$$\frac{1}{A_1 \cdots A_n} = \int_0^1 dx_1 \cdots \int_0^1 dx_n (n-1)! \frac{\delta(1 - x_1 \cdots x_n)}{[\alpha_1 A_1 + \cdots \alpha_n A_n]^n} \tag{155}$$

In our calculation, it is very often to use Feynman parametrization for $n \leq 4$, thus we write the formula explicitly

$$\frac{1}{AB} = \int_0^1 dx \int_0^1 dy \frac{\delta(1-x-y)}{[xA+yB]^2} = \int_0^1 dx \frac{1}{[(1-x)A+xB]^2}, \tag{156}$$

$$\begin{aligned}\frac{1}{ABC} &= \int_0^1 dx \int_0^1 dy \int_0^1 dz \frac{2\delta(1-x-y-z)}{[xA+yB+zC]^3} \\ &= \int_0^1 dx \int_0^{1-x} dy \frac{2}{[xA+yB+(1-x-y)C]^3} \qquad (157) \\ &= \int_0^1 dx \int_0^x dy \frac{2}{[(1-x)A+yB+(x-y)C]^3}, \qquad (158)\end{aligned}$$

$$\begin{aligned}\frac{1}{ABCD} &= \int_0^1 dx \int_0^{1-x} dy \int_0^{1-x-y} dz \frac{6}{[(1-x-y-z)A+xB+yC+zD]^4} \qquad (159) \\ &= \int_0^1 dx \int_0^x dy \int_0^y dz \frac{6}{[(y-z)A+(1-x)B+(x-y)C+zD]^4}. \qquad (160)\end{aligned}$$

Feynman parameterization is also very useful in deriving the analytical expressions for 1-loop scalar integrals, as shown in Appendix.B. Implementing Feynman parametrization for two-loop integrals offers several advantages. Firstly, by introducing Feynman parameters, the loop integrand becomes simple as it involves the multiplication of one-loop integrals only. This avoids the need for developing new special functions. Secondly, the integration over the parameters can carried out numerically. As stated before, numerical evaluation is more appropriate for computing two-loop Feynman integrals.

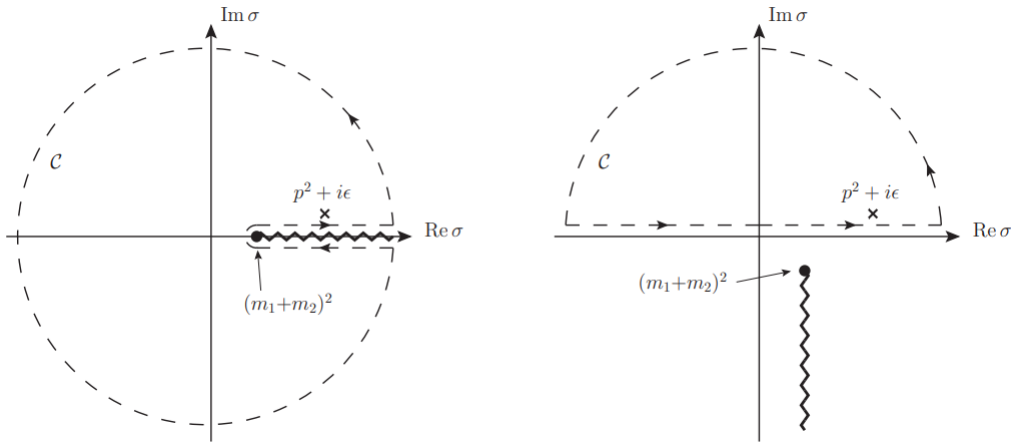

Figure 5: Integration contours for the dispersion relations for the one-loop two-point functions for the cases $\mathrm{Im}((m_1+m_2)^2) = 0$(left) and $\mathrm{Im}((m_1+m_2)^2) \neq 0$(right). The zigzag lines denote the branch cuts, ending at the branch point $(m_1 + m_2)^2$. The sircle sections are understood to have a radius $R \to \infty$

1.3.4.2 Dispersion Relation

Implementing dispersion relation is a crucial step in the evaluation of two-loop Feynman integrals. It allows for the disentanglement of the two subloops, enabling the two-loop integrals to be expressed as a product of one-loop integrals. This section presents the fundamental formulas of the dispersion relation. The application of the dispersion relation for computing two-loop Feynman integrals will be discussed in Sec. 2.3.1, Sec. 2.3.2, and Sec. 2.3.3.

The basic dispersion relation formula for the one-loop tensor two-point function,

$B_{\mu\nu\rho}(p^2, m_1^2, m_2^2) = B_{\mu\nu\rho}$, has two different forms according to the mass argument:

$$B_{\mu\nu\rho} = \int_{(m_1+m_2)^2}^{\infty} d\sigma \frac{\Delta B_{\mu\nu\rho}(\sigma, m_1^2, m_2^2)}{\sigma - p^2 - i\epsilon} \ , \ \mathrm{Im}((m_1+m_2)^2) = 0 \tag{161}$$

$$= \int_{-\infty}^{+\infty} d\sigma \frac{1}{2\pi i} \frac{B_{\mu\nu\rho}(\sigma, m_1^2, m_2^2)}{\sigma - p^2 - i\epsilon} \ , \ \mathrm{Im}((m_1+m_2)^2) \neq 0 \tag{162}$$

where

$$\Delta B_{\mu\nu\rho}(p^2, m_1^2, m_2^2) = \frac{1}{\pi} \mathrm{Im} B_{\mu\nu\rho}(p^2, m_1^2, m_2^2) \tag{163}$$

Branch points of $B_{\mu\nu\rho}$ and $\mathrm{Im}B_{\mu\nu\rho}$ are at $\mathrm{Re}(\sigma) = (m_1+m_2)^2$, which can be clearly see from $\lambda^{1/2}$. The integration contours must be chosen to circumvent the branch cuts and the one we choose correspond to the dashed curve shown in Fig.5

The analytical expressions of $B_{\mu\nu\rho}$ are

$$\begin{aligned}
B_0 =& \frac{1}{2p^2}\Bigg(2L_1(p^2, m_1^2, m_2^2)\lambda^{1/2}(p^2, m_1^2, m_2^2) \\
& + 4p^2 + (m_1^2 - m_2^2 + p^2)\log\frac{1}{m_1^2} + (-m_1^2 + m_2^2 + p^2)\log\frac{1}{m_2^2} \Bigg) \\
B_1 =& \frac{1}{2p^2}\left(m_1^2 - m_2^2 - B_0(p^2, m_1^2, m_2^2) + m_1^2\log\frac{1}{m_1^2} - m_2^2\log\frac{1}{m_2^2} \right) \\
B_{00} =& \frac{1}{6}\Bigg(2m_1^2 B_0(p^2, m_1^2, m_2^2) + (m_1^2 - m_2^2 + p^2)B_1(p^2, m_1^2, m_2^2) \\
& + \frac{3m_1^2 + 6m_2^2 - p^2}{3} + m_2^2\log\frac{1}{m_2^2} \Bigg) \\
B_{11} =& \frac{1}{6p^2}\Bigg(-2m_1^2 B_0(p^2, m_1^2, m_2^2) - 4(m_1^2 - m_2^2 + p^2)B_1(p^2, m_1^2, m_2^2) \\
& + \frac{-3m_1^2 - 3m_2^2 + p^2}{3} + 2(m_2^2 + m_2^2\log\frac{1}{m_2^2}) \Bigg) \\
B_{001} =& \frac{1}{8}\Bigg(2m_1^2 B_1(p^2, m_1^2, m_2^2) + (m_1^2 - m_2^2 + p^2)B_{11}(p^2, m_1^2, m_2^2) \\
& \frac{-2m_1^2 - 10m_2^2 + p^2}{6} - m_2^2\log\frac{1}{m_2^2} \Bigg)
\end{aligned}$$

$$B_{111} = -\frac{1}{4p^2}\Bigg(2m_1^2 B_1(p^2,m_1^2,m_2^2) + 2(m_1^2 - m_2^2 + p^2)B_{11}(p^2,m_1^2,m_2^2) + \frac{-2m_1^2 + 2m_2^2 + p^2}{6} + m_2^2 \log\frac{1}{m_2^2}\Bigg) \tag{164}$$

The L_1 and λ functions are defined as follows

$$\begin{aligned}\lambda(x,y,z) &= x^2 + y^2 + z^2 - 2(xy + xz + yz) = (x - y - z)^2 - 4yz\ , \\ L_1(x,y,z) &= \log\Bigg(\frac{(yz)^{-1/2}}{2(\lambda(x,y,z) - x + y + z)^{1/2}}\Bigg)\end{aligned} \tag{165}$$

The analytical expressions of $\mathrm{Im}B_{\mu\nu\rho}$ are

$$\begin{aligned}\mathrm{Im}B_0 =& \pi\lambda^{1/2}(1,\frac{m_1^2}{p^2},\frac{m_2^2}{p^2}) \\ \mathrm{Im}B_1 =& \frac{\pi}{2}\lambda^{1/2}(1,\frac{m_1^2}{p^2},\frac{m_2^2}{p^2})\frac{m_2^2 - m_1^2 - p^2}{p^2} \\ \mathrm{Im}B_{00} =& -\frac{\pi}{12}\lambda^{3/2}(1,\frac{m_1^2}{p^2},\frac{m_2^2}{p^2})p^2 \\ \mathrm{Im}B_{11} =& \pi\lambda^{1/2}(1,\frac{m_1^2}{p^2},\frac{m_2^2}{p^2})\Bigg(\frac{1}{3}\lambda(1,\frac{m_1^2}{p^2},\frac{m_2^2}{p^2}) + \frac{m_1^2}{p^2}\Bigg) \\ \mathrm{Im}B_{001} =& \frac{\pi}{24}\lambda^{3/2}(1,\frac{m_1^2}{p^2},\frac{m_2^2}{p^2})(p^2 + m_1^2 - m_2^2) \\ \mathrm{Im}B_{111} =& \frac{\pi}{4}\lambda^{1/2}(1,\frac{m_1^2}{p^2},\frac{m_2^2}{p^2})\Bigg((\frac{m_2^2}{p^2} - \frac{m_1^2}{p^2} - 1)(\lambda(1,\frac{m_1^2}{p^2},\frac{m_2^2}{p^2}) + \frac{2m_1^2}{p^2})\Bigg)\end{aligned} \tag{166}$$

The derivative of $B_{\mu\nu\rho}$ and $\mathrm{Im}B_{\mu\nu\rho}(p^2,m_1^2,m_2^2)$ with respect to mass will also be needed in evaluating two-loop Feynman integrals. The derivative is straightforward and list in Appendix.C and Appendix.D.

In many cases, numerical integration of the form

$$\int_a^\infty ds\ \frac{f(s)}{s - s_0 \pm i\varepsilon} \tag{167}$$

had to be handled, where one has to calculate in case of $s_0 > a$ a principal value and a residuum contribution. This can be easily coded for the numerical evaluation, resulting in

$$\int_a^\infty ds\ \frac{f(s)}{s - s_0 \pm i\varepsilon} = \int_a^{s_0} ds\ \frac{f(s) - f(2s_0 - s)}{s - s_0} \mp i\pi f(s_0) + \int_{2s_0 - a}^\infty ds\ \frac{f(s)}{s - s_0 \pm i\varepsilon} \tag{168}$$

Higher powers of propagators lead also to integration of the type

$$\int_a^\infty ds\ \frac{f(s)}{(s - s_0 \pm i\varepsilon)^2} \tag{169}$$

A formula which proved more useful for the numerical evaluation of this integral is given by

$$\int_a^\infty ds\ \frac{f(s)}{(s - s_0 \pm i\varepsilon)^2} = \int_a^{s_0} \frac{f(s) + f(2s_0 - s) - 2f(s_0)}{(s - s_0)^2} \mp i\pi f'(s_0) + \frac{2f(s_0)}{a - s_0} + \int_{2s_0 + a}^\infty ds\ \frac{f(s)}{(s - s_0)^2} \tag{170}$$

where $f'(s) = df(s)/ds$.

1.3.4.3 Subtraction Method

The numerical methods described in Sec. 1.3.4.1 and Sec. 1.3.4.2 encounter challenges when dealing with UV divergent integrals, as dimensional regularization cannot be simply applied in numerical integrals. To address these UV divergences, we employ the subtraction method. The general idea is to subtract a few simple terms from the original integral to make it UV finite, and then add back the analytical expressions of these subtracted terms to the total result. The strategy of this method can be established as follows:

$$I_{\text{UV-div}} = \underbrace{I_{\text{UV-div}} - I_{\text{subtra}}}_{\text{UV-finite}} + \underbrace{I_{\text{subtra}}}_{\text{UV-div}} \tag{171}$$

where I_{subtra} denotes the subtraction terms. The first one is evaluated numerically, while the second one is UV divergent thus must be evaluated analytically.

The number of subtracted terms needed for evaluating UV diagrams varies, and generally involves three types of subtracted terms at two-loop level: two for subloop divergences and one more for a global divergence. The global divergence refers to the highest order divergence of a given diagram, while the subloop divergence does not. In two-loop Feynman diagrams, the global (subloop) divergence is proportional to $\epsilon^{-2(-1)}$, where $\epsilon = (4 - D)/2$. The number of global and subloop divergences can be counted by power counting the explicit Feynman integrals or by counting the number of two/one-loop counterterms contained in the Feynman diagram. For instance, let's consider the box diagram with a subloop vertex shown on the left of Fig. 6. Since there is only one one-loop counterterm diagram corresponding to this diagram, as illustrated on the right, which implies that it contains only one subloop divergence.

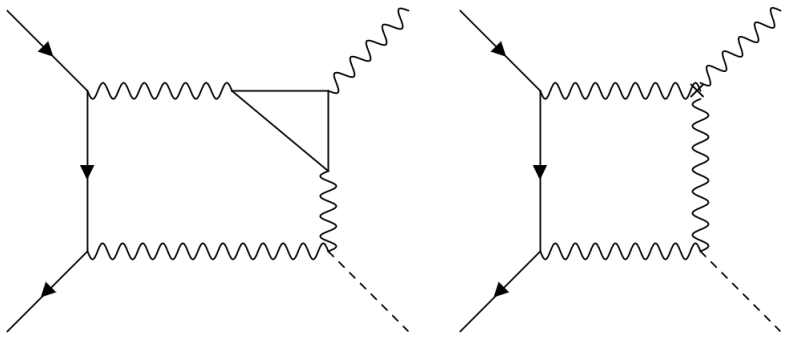

Figure 6: Box with a subloop vertex diagrams and its corresponding counterterm diagrams.

To ensure the numerical evaluation, both the global and subloop divergences need to be subtracted from the original integrand. The subtraction term for global divergence is obtained by evaluating the same diagram but setting all external momenta to zero. On the other hand, the subtraction term for subloop divergence is obtained by setting all momenta except for the loop momentum inside all propagators to zero. The practical implementation of constructing different subtraction terms is shown in Sec.2.3.2 and Sec.2.3.3.

2.0 Two-loop Electroweak Corrections for $e^+e^- \to Zh$ Process

2.1 Motivation

After the discovery of the Higgs boson in 2012 by the ATLAS[63] and CMS[64] collaboration at the Large Hadron Collider(LHC), many measurements have been performed to study its properties. As we discussed in Sec.1.1, the neutral Higgs boson is responsible for the masses of gauge boson and fermions. More importantly, the Higgs mechanism leads to a distinctive phenomenological imprint in the coupling structure between Higgs and other particles, i.e. all fermionic and bosonic couplings to the Higgs boson are proportional to the masses of the corresponding fermion and gauge boson. Thus, measuring the properties of the Higgs boson can test the SM, and deviations between experiments and SM prediction indicate the presence of new physics beyond the SM. Assuming the new physics scale Λ is at TeV range, the deviations in Higgs couplings, which can be parameterized as m_H^2/Λ^2, is at percent level, thus beyond the current experimental accuracy of the LHC. Under κ framework, the uncertainty for most of the higgs couplings is larger than 10% as shown in Fig. 7 from Ref. [65].

In order to detect the percent level deviations in the Higgs boson couplings, several proposals have been made for so-called e^+e^- Higgs factories. These facilities, including the International Linear Collider (ILC) [1, 2], the Future Circular Collider (FCC-ee) [3], and the Circular Electron-Positron Collider (CEPC) [4], are lepton colliders, thus provide a clean environment and allow for more precise and model independent measurements of the properties of the Higgs boson.

These machines are planned to operate at center-of-mass energies of 240-250 GeV,

where the dominant Higgs production channel is the Higgsstrahlung process $e^+e^- \to ZH$. Together with the recoil mass method, which can reconstruct the Higgs with leptonic decay products of Z boson, the cross section of $e^+e^- \to ZH$ is expected to be measured with an accuracy of about 1.2% at ILC, 0.4% at FCC-ee, and 0.5% at CEPC. The coupling between Higgs and Z, g_{HZZ} can be extracted by comparing the experimental result and theoretical prediction, namely $(g_{HZZ}/g^{\mathrm{SM}}_{HZZ})^2 = \sigma(e^+e^- \to ZH)^{\mathrm{exp}}/\sigma(e^+e^- \to ZH)^{\mathrm{SM}}$. With the so-called κ framework, this can be rewritten in terms of κ_Z, $\kappa_Z = g_{HZZ}/g^{\mathrm{SM}}_{HZZ}$. Thus the ratio between cross sections is directly related to κ_Z. κ_Z stands for the normalized coupling between Higgs and Z, and $\kappa_Z \neq 1$ indicate the appearance of new physics.

The interpretation of σ_{HZ} in terms of the κ_Z requires precise theoretical predictions $\sigma(e^+e^- \to ZH)^{\mathrm{SM}}$, which has been calculated up to next-to-next-to-leading order(NNLO) with mixed EW and QCD corrections[66, 67]. The numerical impact of the mixed EW and QCD corrections is around 1.4%, which is larger than the expected experimental accuracies of the Higgs factories. Thus, missing higher order corrections must be calculated.

The largest missing higher order corrections is from NNLO EW corrections, which depend on up to four independent mass scales (m_H, m_Z, m_W, m_t), as well as two additional momentum scales (which can be represented by the Mandelstam variables s and t). Therefore it is difficult to find analytical solutions, since the expressions will be impractically large and may require the development of new special functions. On the other hand, generic numerical methods (such as numerical integration over Feynman parameters [68]) are highly computationally intensive.

Due to these reasons, the evaluation of NNLO EW corrections is not only necessary to meet the precision requirements of future Higgs factories, but it also represents a significant advancement in the techniques used to perform two-loop electroweak

diagram calculations. In Sec.2.3, we outline our approach for evaluating the two-loop diagrams contributing to the process $e^+e^- \to HZ$. The numerical result and related discussion is shown in Sec.2.4

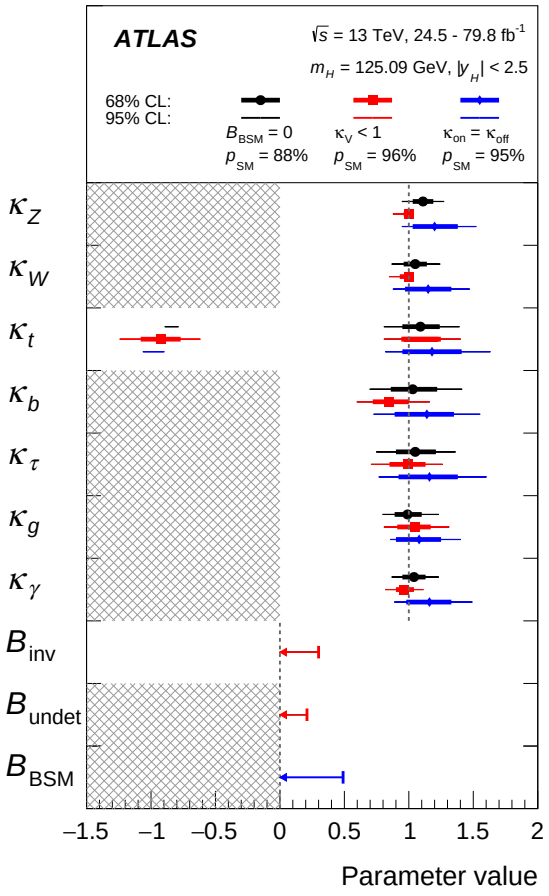

Figure 7: Best-fit values and uncertainties for Higgs boson coupling modifiers per particle type with effective photon and gluon couplings and either $\mathrm{B_{inv}} = \mathrm{B_{undet}} = 0$(black); $\mathrm{B_{inv}}$ and $\mathrm{B_{undet}}$ included as free parameters, the condition $\kappa_{\mathrm{W,Z}} \leq 1$ applied and the measurement of the Higgs boson decay rate into invisible final states included in the combination (red); or $\mathrm{B_{BSM}} = \mathrm{B_{inv}} + \mathrm{B_{undet}}$ included as a free parameter, the measurement of off-shell Higgs boson production included in the combination, and the assumptions described in the text applied to the off-shell coupling-strength scale factors (blue). The SM corresponds to $\mathrm{B_{inv}} = \mathrm{B_{undet}} = 0$ and all κ parameters set to unity. All parameters except κ_t are assumed to be positive.

2.2 Polarized and Unpolarized Cross Section

The e^+e^- Higgs factories, such as FCC-ee, CEPC, and ILC, have different strategies regarding the use of unpolarized and polarized beams. FCC-ee is primarily designed to operate with unpolarized beams, but some operation modes will employ polarized beams, which is also considered for CEPC. On the other hand, ILC plans to use polarized beams, with up to 80% longitudinal polarization for electrons and 60% for positrons. The use of polarized beams will not only enable more precise measurements but also provide a means to explore new physics beyond the Standard Model.

Thus, in order to compare the theoretical predictions of $\sigma(e^+e^- \to ZH)$ with future experimental results, it is necessary to calculate both the polarized and unpolarized cross sections.

The perturbative expansion of the matrix element $\mathcal{M}$ for $e^+e^- \to ZH$ process is obtained by expanding EW and QCD couplings, and it takes the following form:

$$\mathcal{M} = \mathcal{M}^{(0)} + \mathcal{M}^{(\alpha)} + \mathcal{M}^{(\alpha\alpha_s)} + \mathcal{M}^{(\alpha^2)} + \mathcal{M}^{(\alpha^2\alpha_s)} + \cdots \tag{172}$$

The upper indices stand for the expansion order of EW and QCD coupling. Note that there is no one-loop QCD correction $M^{(\alpha_s)}$ since the gluons do not interact with leptons and EW gauge bosons.

The matrix element has the form

$$\mathcal{M}^{(n)} = \bar{v}(p_{e^+})\Gamma^{\mu,(n)}u(p_{e^-}) \tag{173}$$

where $p_{e^\pm}$ are the momenta of incoming positron and electron, respectively, μ is the Lorentz index of the outgoing Z boson, and Γ^μ stands for the eeZ three-point function. n shows the expansion order.

For unpolarized square matrix element, one needs to average of initial spins, which is accomplished by the Carsimir trace technique

$$|M^{(m)}M^{(n)}|_{\rm unpol} = \frac{1}{4}\sum_{e^{\pm}{\rm spin}} M^{*(m)}M^{(n)} = \frac{1}{4}{\rm Tr}\Big\{\bar{\Gamma}^{\mu,(m)}\not{p}_{e^+}\Gamma^{(m)}_{\mu}\not{p}_{e^-}\Big\} \tag{174}$$

where the electron and positron mass have been neglected.

On the other hand, the squared matrix element with polarized electron and positron beam can be obtained by inserting the polarization projectors $P_{\rm R,L} = (1 \pm \gamma^5)/2$. Thus the polarized amplitude is obtained by performing the following replacement:

$$\begin{aligned}
u(p_{e^-}) &\Rightarrow u(p_{e^-})_{\rm L} = P_{\rm L} \times u(p_{e^-}) = \frac{1-\gamma_5}{2} \times u(p_{e^-}) \\
&\Rightarrow u(p_{e^-})_{\rm R} = P_{\rm R} \times u(p_{e^-}) = \frac{1+\gamma_5}{2} \times u(p_{e^-}) \\
\bar{v}(p_{e^+}) &\Rightarrow \bar{v}(p_{e^+})_{\rm L} = P_{\rm R} \times \bar{v}(p_{e^+}) = \frac{1+\gamma_5}{2} \times \bar{v}(p_{e^+}) = \bar{v}(p_{e^+}) \times \frac{1-\gamma_5}{2} \\
&\Rightarrow \bar{v}(p_{e^+})_{\rm R} = P_{\rm L} \times \bar{v}(p_{e^+}) = \frac{1-\gamma_5}{2} \times \bar{v}(p_{e^+}) = \bar{v}(p_{e^+}) \times \frac{1+\gamma_5}{2}
\end{aligned} \tag{175}$$

Thus for polarized square matrix elements, Eq.174 becomes

$$|M^{(m)}M^{(n)}|_{e^+_j,e^-_k} = M^{*(m)}_{e^+_j,e^-_k}M^{(n)}_{e^+_j,e^-_k} = {\rm Tr}\Big\{\bar{\Gamma}^{\mu,(m)}\not{p}_{e^+}P_j\Gamma^{(m)}_{\mu}P_k\not{p}_{e^-}\Big\}\ ,\ j,k = {\rm R,L} \tag{176}$$

Instead of separately going through all the steps of the computation for left- and right-handed polarized beams, one can alternatively derive the polarized matrix elements from the unpolarized one, which seems more efficient for calculating the two-loop diagrams. This is achieved by grouping certain types of diagrams. Considering a two-loop diagram where the incoming fermion line connects with N gauge bosons(γ or Z), the polarized matrix elements satisfy the relationships

$$M^{V_1\cdots V_N}_{(2)}|_{\rm LR} = g^{eeV_1}_{\rm R}\cdots g^{eeV_N}_{\rm R}\bar{v}(p_{e^+})P_{\rm L}F_{(2)}P_{\rm R}u(p_{e^-})G_{(2)}$$

$$M_{(2)}^{V_1\cdots V_N}|_{\rm RL} = g_{\rm L}^{eeV_1}\cdots g_{\rm L}^{eeV_N}\bar{v}(p_{e^+})P_{\rm R}F_{(2)}P_{\rm L}u(p_{e^-})G_{(2)}$$
$$M_{(2)}^{V_1\cdots V_N}|_{\rm LL} = M_{(2)}^{V_1\cdots V_N}|_{\rm RR} = 0 \tag{177}$$

where $g_{\rm L(R)}^{eeV}$ is the left(right)-handed coupling of eeV vertex, F denotes the matrix elements of fermion line, and G denotes the rest part of the matrix element. The tree-level matrix element can be written in the same form.

The polarized squared matrix elements are

$$\begin{aligned}
|M_{(2)}^{V_1\cdots V_N}M_{(0)}|_{\rm LR} =& g_{\rm R}^{eeZ}g_{\rm R}^{eeV_1}\cdots g_{\rm R}^{eeV_N}G_{(0)}G_{(2)}\times{\rm Tr}[\not{p}_{e^+}P_{\rm L}F_{(2)}P_{\rm R}\not{p}_{e^-}F_{(0)}],\\
|M_{(2)}^{V_1\cdots V_N}M_{(0)}|_{\rm RL} =& g_{\rm L}^{eeZ}g_{\rm L}^{eeV_1}\cdots g_{\rm L}^{eeV_N}G_{(0)}G_{(2)}\times{\rm Tr}[\not{p}_{e^+}P_{\rm R}F_{(2)}P_{\rm L}\not{p}_{e^-}F_{(0)}],\\
|M_{(2)}^{V_1\cdots V_N}M_{(0)}|_{\rm LL} =& |M_{(2)}^{V_1\cdots V_N}M_{(0)}|_{\rm RR} = 0
\end{aligned} \tag{178}$$

With $|M_{(2)}M_{(0)}|_{\rm unpol} = (|M_{(2)}M_{(0)}|_{\rm LR}+|M_{(2)}M_{(0)}|_{\rm RL}+|M_{(2)}M_{(0)}|_{\rm LL}+|M_{(2)}M_{(0)}|_{\rm RR})/4$, we obtain the relationship between polarized and unpolarized squared matrix element

$$\begin{aligned}
|M_{(2)}^{V_1\cdots V_N}M_{(0)}|_{\rm LR} &= \frac{4g_{\rm R}^{eeZ}g_{\rm R}^{eeV_1}\cdots g_{\rm R}^{eeV_N}}{g_{\rm R}^{eeZ}g_{\rm R}^{eeV_1}\cdots g_{\rm R}^{eeV_N}+g_{\rm L}^{eeZ}g_{\rm L}^{eeV_1}\cdots g_{\rm L}^{eeV_N}}\times|M_{(2)}M_{(0)}|_{\rm unpol},\\
|M_{(2)}^{V_1\cdots V_N}M_{(0)}|_{\rm RL} &= \frac{4g_{\rm L}^{eeZ}g_{\rm L}^{eeV_1}\cdots g_{\rm L}^{eeV_N}}{g_{\rm R}^{eeZ}g_{\rm R}^{eeV_1}\cdots g_{\rm R}^{eeV_N}+g_{\rm L}^{eeZ}g_{\rm L}^{eeV_1}\cdots g_{\rm L}^{eeV_N}}\times|M_{(2)}M_{(0)}|_{\rm unpol},\\
|M_{(2)}^{V_1\cdots V_N}M_{(0)}|_{\rm LL} &= |M_{(2)}^{V_1\cdots V_N}M_{(0)}|_{\rm RR} = 0
\end{aligned} \tag{179}$$

If the fermion line connects only with W bosons, which only interact with left-handed fermions, thus we end up with very simple equations

$$\begin{aligned}
|M_{(2)}^{W\cdots W}M_{(0)}|_{\rm RL} &= 4\times|M_{(2)}M_{(0)}|_{\rm unpol},\\
|M_{(2)}^{W\cdots W}M_{(0)}|_{\rm LR} &= |M_{(2)}^{W\cdots W}M_{(0)}|_{\rm LL} = |M_{(2)}^{W\cdots W}M_{(0)}|_{\rm RR} = 0
\end{aligned} \tag{180}$$

After calculating squared matrix element, the differential cross section can be directly obtained by multiplying the 2-body phase space. The differential cross section up to NNLO(EW+EW) reads

$$\begin{aligned}\frac{d\sigma}{d\cos\theta} &= \frac{1}{32\pi s}\beta(1,\frac{m_Z^2}{s},\frac{m_H^2}{s})|M^2| \\ &= \frac{1}{32\pi s}\beta(1,\frac{m_Z^2}{s},\frac{m_H^2}{s})\Bigg(\underbrace{|M^{(0)}|^2}_{\text{LO}} + \underbrace{2\text{Re}(M^{(0)*}M^{(\alpha)})}_{\text{NLO}} + \underbrace{2\text{Re}(M^{(0)*}M^{(\alpha\alpha_s)}}_{\text{NNLO(EW+QCD)}} \\ &+ \underbrace{|M^{(\alpha)}|^2 + 2\text{Re}(M^{(0)*}M^{(\alpha^2)})}_{\text{NNLO(EW+EW)}}\Bigg)\end{aligned} \tag{181}$$

where $\sqrt{s}$ is the center of mass energy, θ is the angle between outgoing Z boson and incoming electron. β functions is $\beta(x,y,z) = (x-y-z)^2 - 4yz$. The polarized and unpolarized cross sections can be obtained by substituting the polarized and unpolarized squared matrix elements, respectively, into Eq. 181.

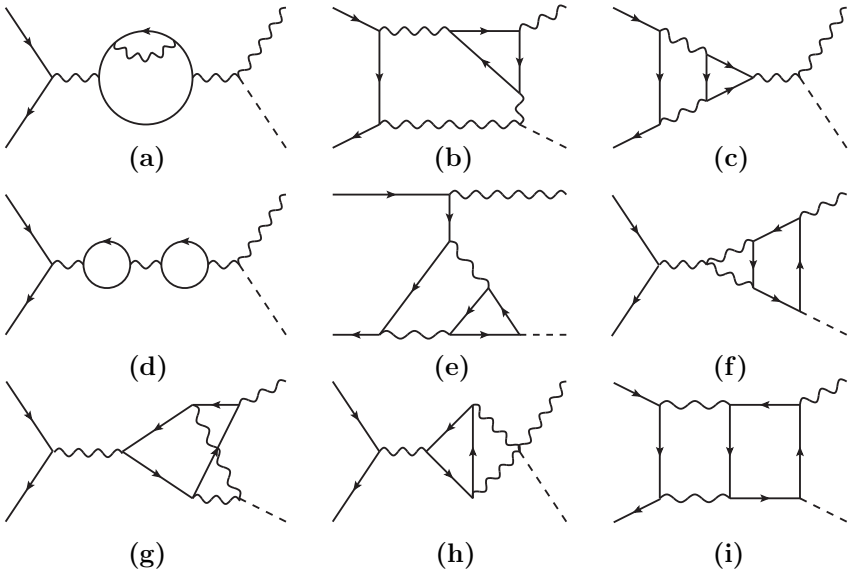

Figure 8: Examples of two-loop Feynman diagrams with at least one closed fermion loop.

2.3 Evaluation Method for Two-Loop Diagrams

As shown in Eq. 181, the NNLO EW corrections involve the interference between one-loop diagrams, $|M^{(\alpha)}|^2$ and two-loop diagrams. The former can be evaluated using the techniques described in Sec. 1.3.1 and Sec. 1.3.2, which have been implemented in modern packages for automated calculation, such as FeynCalc [69]. However, no automated packages are available for the evaluation of general two-loop diagrams due to their complexity.

Some examples of two-loop diagrams are shown in Fig.8. Two-loop self-energy

Fig.8(d) and their corresponding counterterm diagrams can be straightforwardly computed by reducing the expressions to a set of know master integrals (MIs)[70], which can be further evaluated with TVID 2.2 [71] both numerically and analytically. Two-loop vertex diagrams Fig.8(c,e,f,g) and box diagrams Fig.8(i) can also be evaluated by reducing to MIs, but this reduction process is heavily time-consuming, which is of order few thousands CPU hour[72].

Thus we have developed a new method for evaluating two-loop diagram, which is based on a semi-numerical method using a combination of Feynman parametrization and dispersion relation. This method is further developed to enable the treatment of UV divergences by constructing subtraction terms as discussed in Sec.1.3.4.3. With this approach, all relevant two-loop Feynman integrals are reduced to at most three-dimensional numerical integral, which is further evaluated with Gaussian-Kronrod quadrature integral routine.

Three different elements comprise this evaluation method, which would be hard to understand by implementing them at the same time. Sec.2.3.1 aims for evaluation of UV finite diagrams, which is a good example to show how to reduce two-loop diagrams into three-dimensional numerical integrals with Feynman parametrization and dispersion relation. Sec.sections 2.3.2 and 2.3.3 aims to show how to construct different subtraction terms according to different UV structures.

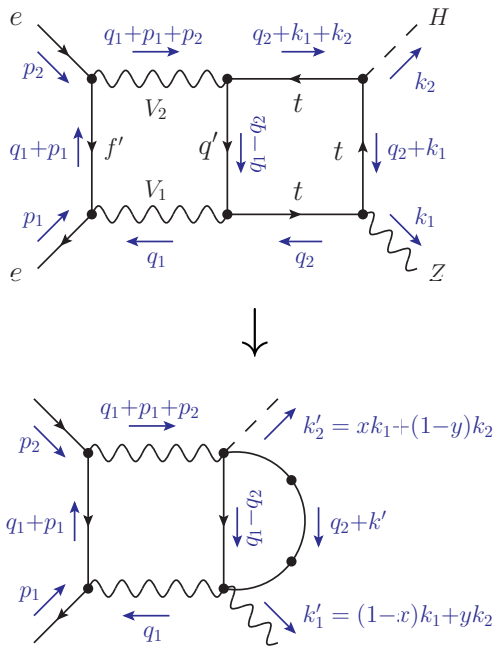

Figure 9: Planar two-loop box diagrams with top quarks in the loop. The bottom row visually illustrates the effect of introducing Feynman parameters for the top loop. If $V_{1,2} = \gamma, Z$ then $f' = e$, $q' = t$, whereas $f' = \nu_e$ and $q' = b$ for $V_{1,2} = W$.

2.3.1 UV Finite Diagram: Planar Double-Box

To illustrate the implementation of Feynman parametrization and dispersion relation, consider a planar double-box diagram, which contains the propagators of the diagram in Fig.9. Generally the numerator can be arbitrary pair product among internal and external momentum, $l_i \cdot l_j$ where $l_i = \{q_i, p_i, k_i\}$. For simplicity, let us

begin by choosing the numerator to be 1,

$$I_{\rm plan} = \int d^D q_1\, d^D q_2\, \frac{1}{[q_1^2 - m_{V_1}^2][(q_1+p_1)^2 - m_{f'}^2][(q_1+p_1+p_2)^2 - m_{V_2}^2]} \times \frac{1}{[(q_1-q_2)^2 - m_{q'}^2][q_2^2 - m_t^2][(q_2+k_1)^2 - m_t^2][(q_2+k_1+k_2)^2 - m_t^2]}\,. \quad (182)$$

Introduce Feynman parameters for the propagators that depend only on loop momemtum q_2

$$\begin{aligned} &\frac{1}{[q_2^2 - m_t^2][(q_2+k_1)^2 - m_t^2][(q_2+k_1+k_2)^2 - m_t^2]} \\ &= \int_0^1 dx \int_0^{1-x} dy\, \frac{2}{[(q_2+k')^2 - m'^2]^3} \\ &= \int_0^1 dx \int_0^{1-x} dy\, \frac{\partial^2}{\partial^2 m'^2} \frac{1}{(q_2+k')^2 - m'^2}, \end{aligned} \quad (183)$$

with

$$m'^2 = m_t^2 - xy(k_1+k_2)^2 - (1-x-y)(xk_1^2 + yk_2^2)\ ,\ k' = (1-x)k_1 + y\,k_2 \quad (184)$$

In the last line, we take derivative with respect to m'^2 twice to make the power of propagator be 1. Plugging it into Eq.182, we obtain

$$I_{\rm plan} = \int_0^1 dx \int_0^{1-x} dy \int d^D q_1\, \frac{1}{[q_1^2 - m_{V_1}^2][(q_1+p_1)^2 - m_{f'}^2][(q_1+p_1+p_2)^2 - m_{V_2}^2]} \times \int d^D q_2 \frac{\partial^2}{\partial^2 m'^2}\, \frac{1}{[(q_1-q_2)^2 - m_{q'}^2][(q_2+k')^2 - m'^2]} \quad (185)$$

Integrating the q_2 loop leads to $B_0((q_1+k)^2, m'^2, m_{q'}^2)$ function together with the dispersion relation discussed in Sec.1.3.4.2, we obtain

$$\begin{aligned} &\int dx\, dy \int d^D q_2\, \frac{2}{[(q_1-q_2)^2 - m_{q'}^2][(q_2+k')^2 - m'^2]^3} \\ &= \int dx\, dy\, \frac{\partial^2}{\partial (m'^2)^2} \int_{\sigma_0}^{\infty} d\sigma\, \frac{\Delta B_0(\sigma, m'^2, m_{q'}^2)}{\sigma - \tilde{q}_1^2} \end{aligned}$$

$$= \int dx\, dy \left\{ \int_{\sigma_0}^{\infty} d\sigma\, \frac{\partial^2_{m'} \Delta B_0(\sigma, m'^2, m^2_{q'})}{\sigma - \tilde{q}_1^2} - \left[\frac{\partial_{m'} \Delta B_0(\sigma, m'^2, m^2_{q'})}{\sigma - \tilde{q}_1^2} \right]_{\sigma \to \sigma_0} \right\}, \quad (186)$$

where we have introduced the short-hand notation

$$\sigma_0 = (m' + m_{q'})^2, \qquad \tilde{q}_1 = q_1 + k' + i\epsilon, \qquad \partial_{m'} = \frac{\partial}{\partial(m'^2)}\,, \quad (187)$$

and used the fact that $\Delta B_0(\sigma_0, m'^2, m^2_{q'}) = 0$. Unfortunately, the σ integral blows up at the lower boundary, and the term in [ ] is also divergent for $\sigma \to \sigma_0$, whereas only the sum of the two is finite. To circumvent this problem, one can modify the integrand according to

$$\int dx\, dy \left\{ \int_{\sigma_0}^{\infty} d\sigma\; \partial^2_{m'} \Delta B_0(\sigma, m'^2, m^2_{q'}) \left(\frac{1}{\sigma - \tilde{q}_1^2} - \frac{\sigma_0}{\sigma(\sigma_0 - \tilde{q}_1^2)} \right) + \frac{\sigma_0}{\sigma_0 - \tilde{q}_1^2}\, \partial^2_{m'} B_0(0, m'^2, m^2_{q'}) \right\}. \quad (188)$$

Here the extra term in the integrand of $\int d\sigma$ is added back in integrated form, where the function $\partial^2_{m'} B_0$ can be expressed in terms of basic logarithms (see appendix). With the modified integrand, the boundary term in eq. (186) evaluates to zero.

Inserting eq. (188) into the remainder of the q_1 loop integral, one obtains

$$\begin{aligned} I_{\rm plan} = -\int dx\, dy \Bigg\{ \int_{\sigma_0}^{\infty} d\sigma\; \partial^2_{m'} \Delta B_0(\sigma, m'^2, m^2_{q'}) \times \Big[& D_0(p_1^2, p_2^2, k_2'^2, k_1'^2, s, t', m^2_{V_1}, m^2_{f'}, m^2_{V_2}, \sigma) \\ & - \frac{\sigma_0}{\sigma}\, D_0(p_1^2, p_2^2, k_2'^2, k_1'^2, s, t', m^2_{V_1}, m^2_{f'}, m^2_{V_2}, \sigma_0) \Big] \\ & + \sigma_0\, \partial^2_{m'} B_0(0, m'^2, m^2_{q'})\, D_0(p_1^2, p_2^2, k_2'^2, k_1'^2, s, t', m^2_{V_1}, m^2_{f'}, m^2_{V_2}, \sigma_0) \Bigg\}, \end{aligned} \quad (189)$$

where $s = (p_1 + p_2)^2$, $t' = (p_1 - k_1')^2$, and D_0 is the well-known scalar one-loop box function.

Since the double box diagrams are UV finite, all expressions in Eq. (189) can be computed for D=4 dimensions.

The full diagram represented by Fig. 9 (top) contains additional terms with momenta $q_{1,2}$ in the numerator stemming from the Dirac propagators and vertex structures. For numerators depending on q_2, it is convenient to perform a Passarino-Veltman decomposition as discussed in Sec.1.3.2 of $\partial^2_{m'} B_0(\tilde{q}_1^2, m'^2, m_{q'}^2)$ after introduction of the Feynman parameters. As a first step, let us shift the integration momentum to $q_2' \equiv q_2 + k'$:

$$\begin{aligned} &\int d^4 q_2 \, \frac{q_2^\mu q_2^\nu \cdots}{[(q_2+k')^2 - m'^2]^3 [(q_1 - q_2)^2 - m_{q'}^2]} \\ &= \int d^4 q_2' \, \frac{(q_2' - k')^\mu (q_2' - k')^\nu \cdots}{[q_2'^2 - m'^2]^3 [(q_2' - q_1 - k')^2 - m_{q'}^2]} \, . \end{aligned} \tag{190}$$

The terms with powers of q_2' in the numerator can be decomposed according to

$$\begin{aligned} &\int d^4 q_2' \, \frac{q_2'^\mu}{[q_2'^2 - m'^2]^3 [(q_2' - q_1 - k')^2 - m_{q'}^2]} = -\tilde{q}_1^\mu \, \partial^2_{m'} B_1(\tilde{q}_1^2, m'^2, m_{q'}^2) \, , \\ &\int d^4 q_2' \, \frac{q_2'^\mu q_2'^\nu}{[q_2'^2 - m'^2]^3 [(q_2' - q_1 - k')^2 - m_{q'}^2]} \\ &\quad = g^{\mu\nu} \, \partial^2_{m'} B_{00}(\tilde{q}_1^2, m'^2, m_{q'}^2) + \tilde{q}_1^\mu \tilde{q}_1^\nu \, \partial^2_{m'} B_{11}(\tilde{q}_1^2, m'^2, m_{q'}^2) \, , \\ &\quad \text{etc.} \end{aligned} \tag{191}$$

Each of the Passarino-Veltman functions $\partial^2_{m'} B_{ij\ldots}((q_1+k')^2, m'^2, m_{q'}^2)$ can then be represented through a dispersion relation in the same manner as above:

$$\begin{aligned} \partial^2_{m'} B_{ij\ldots}(\tilde{q}_1^2, m'^2, m_{q'}^2) = \frac{1}{\pi} \int_{\sigma_0}^\infty \mathrm{d}\sigma \, [\mathrm{Im} \, \partial^2_{m'} B_{ij\ldots}(\sigma, m'^2, m_{q'}^2)] \left[\frac{1}{\sigma - \tilde{q}_1^2} - \frac{\sigma_0}{\sigma(\sigma_0 - \tilde{q}_1^2)} \right] \\ + \frac{\sigma_0}{\sigma_0 - \tilde{q}_1^2} \, \partial^2_{m'} B_{ij\ldots}(0, m'^2, m_{q'}^2) \, . \end{aligned} \tag{192}$$

Explicit expressions for $\mathrm{Im} \, \partial^2_{m'} B_{ij\ldots}(\sigma, m_1^2, m_2^2)$ and $\partial^2_{m'} B_{ij\ldots}(0, m'^2, m_{q'}^2)$ are collected in the Appendix.D.

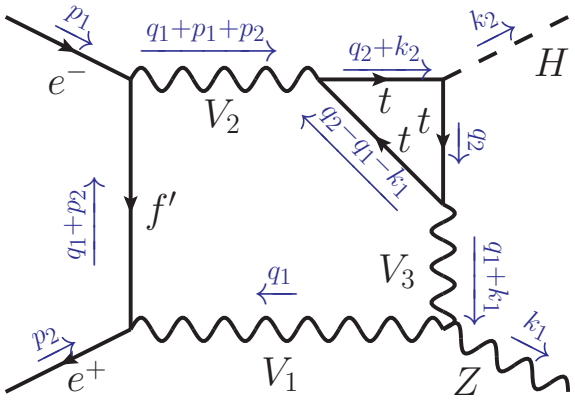

Figure 10: Feynman diagram for a box with a triangle subloop, where $V_{1,2} = \{\gamma, Z, W^{\pm}\}, V_3 = \{Z, G^0, W^{\pm}, G^{\pm}, H\}$.

Similarly, the q_1 loop will in general contain terms with different powers of q_1 in the numerator, some of which in fact originate from Eq. 191. These lead to Passarino-Veltman functions D_1, D_2, D_3, D_{00}, etc. [42], which can be evaluated numerically by using, for example, the techniques introduced in Ref. [49, 73]. In some cases, there are cancellations between terms in the numerator and denominator, resulting in C_0, C_1, C_2, C_{00}, ... and B_0, B_1, B_{00}, ... functions.

2.3.2 UV Divergent Diagram with Subloop Divergence: Box with Triangle Subloop

This section aims to illustrate the strategy of constructing subtraction term for diagrams with subloop UV divergence only. One such example is box diagram with triangle subloop as shown in Fig.10. To manifest this UV divergence, we choose

numerator to be q_2^2. The corresponding Feynman integral is

$$I_{\rm box-ver} = \int d^D q_1\, d^D q_2\, \frac{q_2^2}{[(q_1+k_1-q_2)^2-m_t^2][q_2^2-m_t^2][(q_2+k_2)^2-m_t^2]} \times \frac{1}{[q_1^2-m_{V_1}^2][(q_1+p_2)^2-m_{f'}^2][(q_1+p_1+p_2)^2-m_{V_2}^2][(q_1+k_1)^2-m_{V_3}^2]}. \quad (193)$$

For brevity, we have omitted the constant $1/(i\pi^2)$ that always accompanies loop integrals. Introduce Feynman parameters for the propagators that depend only on loop momentum q_2

$$\frac{1}{[q_2^2-m_t^2][(q_2+k_2)^2-m_t^2]} = \int_0^1 dx \frac{1}{[(q_2+k')^2-m'^2]^2} = \int_0^1 dx \frac{\partial}{\partial m'^2}\frac{1}{[(q_2+k')^2-m'^2]} \quad (194)$$

with $k' = xk_2$, $m'^2 = m_t^2 + (x^2-x)k_2^2$. Similarly, the derivative aims to make the power of propagator be 1. Plugging into Eq.193, we obtain

$$\begin{aligned} I_{\rm box-ver} =& \frac{\partial}{\partial m'^2}\int_0^1 dx \int d^D q_1 d^D q_2 \frac{1}{[q_1^2-m_{V_1}^2][(q_1+p_2)^2-m_{f'}^2][(q_1+p_1+p_2)^2-m_{V_2}^2]} \\ & \times \frac{1}{[(q_1+k_1)^2-m_{V_3}^2]} \times \frac{1}{[(q_2+k')^2-m'^2]}\frac{q_2^2}{[(q_1+k_1-q_2)^2-m_t^2]} \\ =& \frac{\partial}{\partial m'^2}\int_0^1 dx \int d^D q_1 d^D q_2 \frac{1}{[q_1^2-m_{V_1}^2][(q_1+p_2)^2-m_{f'}^2][(q_1+p_1+p_2)^2-m_{V_2}^2]} \\ & \times \frac{1}{[(q_1+k_1)^2-m_{V_3}^2]} \times \frac{1}{[q_2^2-m'^2]}\frac{(q_2-k')^2}{[(q_1+k_1+k'-q_2)^2-m_t^2]} \end{aligned} \quad (195)$$

In Eq.195, we shift the internal momentum $q_2 \to q_2 + k'$. Before integrating over q_2, tensor reduce is needed following the strategy stated in Sec.1.3.2

$$(q_2-k')^2 = q_2^2 - 2q_2\cdot k' + k'^2 = g_{\mu\nu}q_2^\mu q_2^\nu - 2q_2^\mu k'^\mu + k'^2 \quad (196)$$

$$\int d^D q_2 \frac{q_2^\mu q_2^\nu}{[q_2^2-m_1^2][(q_1+p)^2-m_2^2]} = B^{\mu\nu}(p^2,m_1^2,m_2^2) = g^{\mu\nu}B_{00} + p^\mu p^\nu B_{11} \quad (197)$$

$$\int d^D q_2 \frac{q_2^\mu}{[q_2^2 - m_1^2][(q_1+p)^2 - m_2^2]} = B^\mu(p^2, m_1^2, m_2^2) = g^\mu B_1 \tag{198}$$

After q_2 integration, we obtain

$$\begin{aligned} I_{\rm box-ver} =& \frac{\partial}{\partial_m^2} \int_0^1 dx \int d^D q_1 \; \frac{1}{[q_1^2 - m_{V_1}^2][(q_1+p_2)^2 - m_{f'}^2][(q_1+p_1+p_2)^2 - m_{V_2}^2]} \\ & \frac{1}{[(q_1+k_1)^2 - m_{V_3}^2]} \times \frac{\partial}{\partial_m^2} \Big[D B_{00}(\tilde{q}_1^2, m'^2, m_t^2) + \tilde{q}_1^2 B_{11}(\tilde{q}_1^2, m'^2, m_t^2) \\ & - 2k' \cdot \tilde{q}_1 B_1(\tilde{q}_1^2, m'^2, m_t^2) + k'^2 B_0(\tilde{q}_1^2, m'^2, m_t^2) \Big] \end{aligned} \tag{199}$$

where $\tilde{q}_1 = q_1 + k_1 + k'$. Clearly $\mathrm{Im}(m' + m_t)^2 = 0$, so we use Eq.161 as the dispersion relation formula

$$\begin{aligned} I_{\rm box-ver} =& \int_0^1 dx \int d^D q_1 \; \frac{1}{[q_1^2 - m_{V_1}^2][(q_1+p_1)^2 - m_{f'}^2][(q_1+p_1+p_2)^2 - m_{V_2}^2]} \\ & \frac{1}{[(q_1+k_1)^2 - m_{V_3}^2]} \times \frac{\partial}{\partial_m^2} \int_{\sigma_0}^\infty d\sigma \frac{1}{\sigma - \tilde{q}_1^2} \Big[D \Delta B_{00}(\sigma, m'^2, m_t^2) \\ & + \tilde{q}_1^2 \Delta B_{11}(\sigma, m'^2, m_t^2) - 2k' \cdot \tilde{q}_1 \Delta B_1(\sigma, m'^2, m_t^2) + k'^2 \Delta B_0(\sigma, m'^2, m_t^2) \Big] \\ =& I_{\rm box-ver}^{00} + I_{\rm box-ver}^{11} + I_{\rm box-ver}^{1} + I_{\rm box-ver}^{0} \; , \end{aligned} \tag{200}$$

where we have used a short notation for the inetgral with ΔB_{ij}

$$I_{\rm box-ver}^{ij} = \int_0^1 dx \int d^D q_1 \; \frac{1}{[\cdots q_1 \cdots]} \frac{\partial}{\partial_m^2} \int_{\sigma_0}^\infty d\sigma \frac{c_{ij} \Delta B_{ij}}{\sigma - \tilde{q}_1^2} \tag{201}$$

and $\sigma_0 = (m' + m_t)^2$. Before performing integration over q_1, it is crucial to check if the integrand is finite as σ goes infinity. With the help pf Eq.166, we obtain

$$\lim_{\sigma \to \infty} I_{\rm box-ver}^{00} \approx \int_{\sigma_0}^\infty d\sigma \frac{1}{\sigma} = \log \infty, \tag{202}$$

$$\lim_{\sigma \to \infty} I_{\rm box-ver}^{11} \approx \int_{\sigma_0}^\infty d\sigma \frac{1}{\sigma^3} = \frac{1}{\sigma_0^2}, \tag{203}$$

$$\lim_{\sigma\to\infty} I^{1}_{\text{box}-\text{ver}} \approx \int_{\sigma_0}^{\infty} d\sigma \frac{1}{\sigma^2} = \frac{1}{\sigma_0}, \tag{204}$$

$$\lim_{\sigma\to\infty} I^{0}_{\text{box}-\text{ver}} \approx \int_{\sigma_0}^{\infty} d\sigma \frac{1}{\sigma^2} = \frac{1}{\sigma_0}. \tag{205}$$

$I^{00}_{\text{box}-\text{ver}}$ contains logarithmic divergence, which is the local divergence in the Feynman diagram. To deal with this divergence, we subtract a term, $I^{00,\text{subt}}_{\text{box}-\text{ver}}$, to make $I^{00}_{\text{box}-\text{ver}}$ finite, and then add this term back analytically. As we can see from Eq. 205, $1/\sigma^2$ contains no divergence, thus one should expect that

$$\lim_{\sigma\to\infty}\left(I^{00}_{\text{box}-\text{ver}} - I^{00,\text{subt}}_{\text{box}-\text{ver}}\right) = \int_{\sigma_0}^{\infty} d\sigma \frac{1}{\sigma^2}. \tag{206}$$

This can be realized through

$$I^{00,\text{subt}}_{\text{box}-\text{ver}} \propto \frac{\Delta B_{00}}{\sigma}. \tag{207}$$

Thus, we obtain

$$I^{00}_{\text{box}-\text{ver}} = I^{00}_{\text{box}-\text{ver}} - I^{00,\text{subt}}_{\text{box}-\text{ver}} + I^{00,\text{subt}}_{\text{box}-\text{ver}} = I^{00,\text{finite}}_{\text{box}-\text{ver}} + I^{00,\text{subt}}_{\text{box}-\text{ver}} \tag{208}$$

$$\begin{aligned} I^{00,\text{subt}}_{\text{box}-\text{ver}} &= \int_0^1 dx \int d^D q_1 \, \frac{D}{[q_1^2 - m_{V_1}^2][(q_1+p_1)^2 - m_{f'}^2][(q_1+p_1+p_2)^2 - m_{V_2}^2]} \\ &\quad \frac{1}{[(q_1+k_1)^2 - m_{V_3}^2]} \times \frac{\partial}{\partial_m^2} \int_{\sigma_0}^{\infty} d\sigma \frac{1}{\sigma} \times \Delta B_{00}(\sigma, m'^2, m_t^2) \\ &= D \times D_0[\cdots] \times \int_0^1 dx \; \partial_{m'^2} B_{00}(0, m'^2, m_t^2) \\ &= D \times D_0[\cdots] \times \int_0^1 dx \left[\partial_{m'^2} B_{00}^{\text{div}}(0, m'^2, m_t^2) + \partial_{m'^2} B_{00}^{\text{finite}}(0, m'^2, m_t^2)\right] \end{aligned} \tag{209}$$

The analytical expressions for the last integral can be obtained by plugging in Eq.164, performing the derivative and analytical integration. The explicit result reads

$$\int_0^1 dx \; \partial_{m'^2} B_{00}^{\text{div}}(0, m'^2, m_t^2) = \frac{2}{D-4} \int_0^1 dx \frac{m'^2 + m_t^2}{4} = \frac{2}{D-4} \frac{12 m_t^2 - m_h^2}{24} \tag{210}$$

$$\int_0^1 dx\ \partial_{m'^2} B_{00}^{\text{finte}}(0, m'^2, m_t^2) = -\frac{m_t^4}{m_h^2}\Bigg[\pi \log \frac{m_h^2 - 2m_t^2 + m_h\sqrt{m_h^2 - 4m_t^2}}{4m_t^2} + \pi \log \frac{-m_h^2 + 2m_t^2 + m_h\sqrt{m_h^2 - 4m_t^2}}{m_t^2} + 2\text{Li}_2\left(\frac{2m_h}{m_h + \sqrt{m_h^2 - 4m_t^2}}\right) - 2\text{Li}_2\left(\frac{m_h^2 + m_h\sqrt{m_h^2 - 4m_t^2}}{2m_t^2}\right)\Bigg] \tag{211}$$

where $D = 4 - 2\epsilon$ is the dimension of the integral. The analytical expressions for D_0 is also known, thus we obtian analytical expressions for $I_{\text{box-ver}}^{00,\text{subt}}$.

The final expression of $I_{\text{box-ver}}$ is

$$I_{\text{box-ver}} = I_{\text{box-ver}}^{00,\text{finite}} + I_{\text{box-ver}}^{11} + I_{\text{box-ver}}^{1} + I_{\text{box-ver}}^{0} + I_{\text{box-ver}}^{00,\text{subt}} \tag{212}$$

$$= I_{\text{box-ver}}^{\text{finite}} + I_{\text{box-ver}}^{00,\text{subt}} \tag{213}$$

The first term is UV finite, thus can be evaluated numerically. More importantly, the UV divergent and finite part of $I_{\text{box-ver}}^{00,\text{subt}}$ are obtained analytically. The UV divergence cancels with the one in corresponding counterterm diagrams. Taking $V_1 = V_2 = V_3 = W, f' = b$ as an example, the UV divergent part for loop diagram and its corresponding CT diagram is

$$\begin{aligned} \text{loop diagram} &: -2.808566335 \times 10^{-6} + 1.176922426 \times 10^{-6} i \\ \text{CT diagram} &: +2.808566335 \times 10^{-6} - 1.176922426 \times 10^{-6} i \end{aligned} \tag{214}$$

Clearly, the sum of them equals 0.

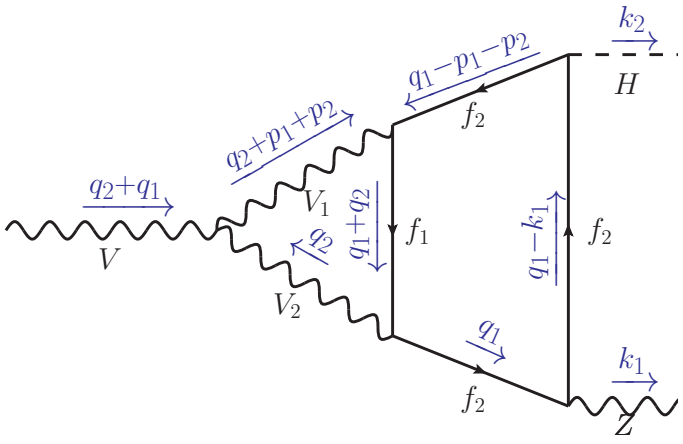

Figure 11: Feynman diagram for a 2-loop VZH vertex, where $V = \{\gamma, Z\}, f_1 = \{t, b\}, f_2 = t, V_{1,2} = \{Z, W^{\pm}\}$.

2.3.3 UV Divergent Diagrams with Global and Subloop Divergences: VZH Vertex

In this section, we discuss the evaluation method for diagrams with both global and subloop divergences, and one such example is the VZH vertex diagram shown in Fig.11. To manifest the UV divergences, we choose numerator to be $q_2^2 q_1^2 + q_1^4$:

$$I_{\text{VZH}} = \int \frac{d^D q_2}{i\pi^2} \frac{d^D q_1}{i\pi^2} \frac{q_2^2 q_1^2 + q_1^4}{[q_1^2 - m_{f_2}^2][(q_1 - p_h)^2 - m_{f_2}^2][(q_1 - p_1 - p_2)^2 - m_{f_2}^2]} \times \frac{1}{[q_2^2 - m_{V_2}^2][(q_2 + p_1 + p_2)^2 - m_{V_1}^2][(q_2 + q_1)^2 - m_{f_1}^2]} \tag{215}$$

By power counting one can see that this integral has sub-loop divergences for

both the q_1 and q_2 loops, as well as a global two-loop divergence

$$\left.\begin{aligned}\lim_{q_1\to\infty} I_{\rm VZH} &= \frac{d^4q_1}{i\pi^2}\frac{1}{q_1^4} = \log\infty \\ \lim_{q_2\to\infty} I_{\rm VZH} &= \frac{d^4q_2}{i\pi^2}\frac{1}{q_2^4} = \log\infty\end{aligned}\right\} \Rightarrow \lim_{q_1,q_2\to\infty} I_{\rm VZH} = \infty \tag{216}$$

Before we introduce Feynman parameters, this global divergence must be subtracted first. The global divergence is cancelled by subtracting the same integral with all external momenta set to zero (i.e. $p_1 = p_2 = p_z = p_h = 0$)

$$I_{\rm VZH} = I_{\rm VZH} - I_{\rm VZH}^{p_{\rm ext}=0} + I_{\rm VZH}^{p_{\rm ext}=0} = I_{\rm VZH}^1 + I_{\rm VZH}^{p_{\rm ext}=0} \tag{217}$$

$I_{\rm VZH}^{p_{\rm ext}=0}$ is equivalent to the vacuum diagram

$$\begin{aligned} I_{\rm VZH}^{p_{\rm ext}=0} &= I_{\rm VZH}(p_1 = p_2 = p_z = p_h = 0) \\ &= \int \frac{d^Dq_2}{i\pi^2}\frac{d^Dq_1}{i\pi^2}\frac{q_2^2q_1^2 + q_1^4}{[q_1^2 - m_{f_2}^2][q_1^2 - m_{f_2}^2][q_1^2 - m_{f_2}^2]} \\ &\times \frac{1}{[q_2^2 - m_{V_2}^2][q_2^2 - m_{V_1}^2][(q_2+q_1)^2 - m_{f_1}^2]} \end{aligned} \tag{218}$$

and it can be evaluated analytically by reducing it to MIs. Two subloop divergences exist in $I_{\rm VZH}^1$, the explicit form of which is

$$\begin{aligned} I_{\rm VZH}^1 = \int \frac{d^Dq_2}{i\pi^2}\frac{d^Dq_1}{i\pi^2}\Bigg\{ &\frac{q_2^2q_1^2 + q_1^4}{[q_1^2 - m_{f_2}^2][(q_1-p_h)^2 - m_{f_2}^2][(q_1-p_1-p_2)^2 - m_{f_2}^2]} \\ \times &\frac{1}{[q_2^2 - m_{V_2}^2][(q_2+p_1+p_2)^2 - m_{V_1}^2][(q_2+q_1)^2 - m_{f_1}^2]} \\ - &\frac{q_2^2q_1^2 + q_1^4}{[q_1^2 - m_{f_2}^2][q_1^2 - m_{f_2}^2][q_1^2 - m_{f_2}^2][q_2^2 - m_{V_2}^2][q_2^2 - m_{V_1}^2][(q_2+q_1)^2 - m_{f_1}^2]}\Bigg\} \end{aligned} \tag{219}$$

We introduce Feynman parameters to $I_{\rm VZH}^1$ for the propagators depending on loop momentum q_2 only, thus we obtain

$$\frac{1}{[q_2^2 - m_{V_2}^2][(q_2+p_1+p_2)^2 - m_{V_1}^2]}$$

$$= \int_0^1 dx \frac{1}{[(q_2+k')^2 - m'^2]^2} = \int_0^1 dx \frac{\partial}{\partial_{m'^2}} \frac{1}{[(q_2+k')^2 - m'^2]}$$
$$\frac{1}{[q_2^2 - m_{V_2}^2][q_2^2 - m_{V_1}^2]} = \int_0^1 dx \frac{1}{[q_2^2 - m_0'^2]^2} = \int_0^1 dx \frac{\partial}{\partial_{m_0'^2}} \frac{1}{[q_2^2 - m_0'^2]} \tag{220}$$

with

$$k' = xp_1 + xp_2 \ , \ m'^2 = (1-x)m_{V_1}^2 + xm_{V_2}^2 + (x^2 - x)(p_1+p_2)^2 \ ,$$
$$m_0'^2 = (1-x)m_{V_1}^2 + xm_{V_2}^2 \tag{221}$$

Similarly, the derivative aims to make the power of propagator to be 1. Plugging into Eq.215, we obtain

$$\begin{aligned} I^1_{\rm VZH} = &\int_0^1 dx \int \frac{d^D q_1}{i\pi^2} \frac{d^D q_2}{i\pi^2} \Bigg\{ \frac{\partial}{\partial_{m'^2}} \frac{q_2^2 q_1^2 + q_1^4}{[q_1^2 - m_{f_2}^2][(q_1 - p_h)^2 - m_{f_2}^2][(q_1 - p_1 - p_2)^2 - m_{f_2}^2]} \\ &\times \frac{1}{[(q_2+k')^2 - m'^2]^2 [(q_2+q_1)^2 - m_{f_1}^2]} \\ &- \frac{\partial}{\partial_{m_0'^2}} \frac{q_2^2 q_1^2 + q_1^4}{[q_1^2 - m_{f_2}^2][q_1^2 - m_{f_2}^2][q_1^2 - m_{f_2}^2][q_2^2 - m_0'^2][(q_2+q_1)^2 - m_{f_1}^2]} \Bigg\} \end{aligned} \tag{222}$$

$$\begin{aligned} = &\int_0^1 dx \int \frac{d^D q_1}{i\pi^2} \frac{d^D q_2}{i\pi^2} \Bigg\{ \frac{\partial}{\partial_{m'^2}} \frac{(q_2 - k')^2 q_1^2 + q_1^4}{[q_1^2 - m_{f_2}^2][(q_1 - p_h)^2 - m_{f_2}^2][(q_1 - p)^2 - m_{f_2}^2]} \\ &\times \frac{1}{[q_2^2 - m'^2]^2 [(q_2+q_1-k')^2 - m_{f_1}^2]} \\ &- \frac{\partial}{\partial_{m_0'^2}} \frac{q_2^2 q_1^2 + q_1^4}{[q_1^2 - m_{f_2}^2][q_1^2 - m_{f_2}^2][q_1^2 - m_{f_2}^2][q_2^2 - m_0'^2][(q_2+q_1)^2 - m_{f_1}^2]} \Bigg\} \end{aligned} \tag{223}$$

Similarly, we need to perform tensor decomposition. The numerator involving q_2 is same as the one in Eq.193, so we can directly use the result therein. We obtain

$$\begin{aligned} I^1_{\rm VZH} = &\int_0^1 dx \int \frac{d^D q_1}{i\pi^2} \Bigg\{ \frac{\partial}{\partial_{m'^2}} \frac{1}{[q_1^2 - m_{f_2}^2][(q_1 - p_h)^2 - m_{f_2}^2][(q_1 - p)^2 - m_{f_2}^2]} \\ &\times \big[q_1^2 D B_{00}(\tilde{q}_1^2, m'^2, m_{f_1}^2) + q_1^2 \tilde{q}_1^2 B_{11}(\tilde{q}_1^2, m'^2, m_{f_1}^2) \\ &- 2q_1^2 k' \cdot \tilde{q}_1 B_1(\tilde{q}_1^2, m'^2, m_{f_1}^2) + q_1^2 (k'^2 + q_1^2) B_0(\tilde{q}_1^2, m'^2, m_{f_1}^2) \big] \end{aligned}$$

$$
\begin{aligned}
&- \frac{\partial}{\partial_{m_0'^2}} \frac{1}{[q_1^2 - m_{f_2}^2][q_1^2 - m_{f_2}^2][q_1^2 - m_{f_2}^2]} \\
&\times \big[q_1^2 D B_{00}(q_1^2, m_0'^2, m_{f_1}^2) + q_1^4 B_{11}(q_1^2, m_0'^2, m_{f_1}^2) \\
&- 2q_1^2 k' \cdot q_1 B_1(q_1^2, m_0'^2, m_{f_1}^2) + q_1^2 (k'^2 + q_1^2) B_0(q_1^2, m_0'^2, m_{f_1}^2) \big] \Bigg\} \qquad (224)
\end{aligned}
$$

where $\tilde{q_1} = q_1 - k'$. Since $\mathrm{Im}\{(m' + m_{f_1})^2\} = \mathrm{Im}\{(m_0' + m_{f_1})^2\} = 0$, we use Eq.161 as the dispersion relation formula. I^1_{VZH} becomes

$$
\begin{aligned}
I^1_{\mathrm{VZH}} = &\int_0^1 dx \int \frac{d^D q_1}{i\pi^2} \Bigg\{ \frac{1}{[q_1^2 - m_{f_2}^2][(q_1 - p_h)^2 - m_{f_2}^2][(q_1 - p)^2 - m_{f_2}^2]} \frac{\partial}{\partial_{m'^2}} \int_{\sigma_0}^{\infty} d\sigma \frac{1}{\sigma - \tilde{q}_1^2} \\
&\times \big[q_1^2 D \Delta B_{00}(\sigma, m'^2, m_{f_1}^2) + q_1^2 \tilde{q}_1^2 \Delta B_{11}(\sigma, m'^2, m_{f_1}^2) \\
&- 2q_1^2 k' \cdot \tilde{q}_1 \Delta B_1(\sigma, m'^2, m_{f_1}^2) + q_1^2 (k'^2 + q_1^2) \Delta B_0(\sigma, m'^2, m_{f_1}^2) \big] \\
&- \frac{1}{[q_1^2 - m_{f_2}^2][q_1^2 - m_{f_2}^2][q_1^2 - m_{f_2}^2]} \frac{\partial}{\partial_{m_0'^2}} \int_{\sigma_0'}^{\infty} d\sigma \frac{1}{\sigma - q_1^2} \\
&\times \big[q_1^2 D \Delta B_{00}(\sigma, m_0'^2, m_{f_1}^2) + q_1^4 \Delta B_{11}(\sigma, m_0'^2, m_{f_1}^2) \\
&- 2q_1^2 k' \cdot q_1 \Delta B_1(\sigma, m_0'^2, m_{f_1}^2) + q_1^2 (k'^2 + q_1^2) \Delta B_0(\sigma, m_0'^2, m_{f_1}^2) \big] \Bigg\} \\
= &I^{1,00}_{\mathrm{VZH}} + I^{1,11}_{\mathrm{VZH}} + I^{1,1}_{\mathrm{VZH}} + I^{1,0}_{\mathrm{VZH}} \qquad (225)
\end{aligned}
$$

where $\sigma_0 = (m' + m_{f_1})^2, \sigma_0' = (m_0' + m_{f_1})^2$. The short notation $I^{1,ij}_{\mathrm{VZH}}$ reads

$$
\begin{aligned}
I^{1,ij}_{\mathrm{VZH}} = \int_0^1 dx \int \frac{d^D q_1}{i\pi^2} \Bigg\{ &\frac{1}{[\cdots q_1 \cdots]} \frac{\partial}{\partial_{m'^2}} \int_{\sigma_0}^{\infty} d\sigma \frac{c_{ij} \Delta B_{ij}(\sigma, m'^2, m_{f_1}^2)}{\sigma - \tilde{q}_1^2} \\
&- \frac{1}{[\cdots q_1 \cdots]} \frac{\partial}{\partial_{m_0'^2}} \int_{\sigma_0'}^{\infty} d\sigma \frac{c_{ij}' \Delta B_{ij}(\sigma, m_0'^2, m_{f_1}^2)}{\sigma - q_1^2} \Bigg\} \qquad (226)
\end{aligned}
$$

Same as what we shown in Sec.2.3.2, $I^{1,00}_{\mathrm{VZH}}$ contains logarithmic divergence, which can be taken care of by constructing subtraction terms

$$
I^{1,00}_{\mathrm{VZH}} = I^{1,00}_{\mathrm{VZH}} - I^{1,00,\mathrm{subt}}_{\mathrm{VZH}} + I^{1,00\mathrm{subt}}_{\mathrm{VZH}} = I^{1,00\mathrm{finite}}_{\mathrm{VZH}} + I^{1,00\mathrm{subt}}_{\mathrm{VZH}} \qquad (227)
$$

with

$$I_{\rm VZH}^{1,00{\rm subt}} = \int_0^1 dx \int \frac{d^D q_1}{i\pi^2} \Big\{ \frac{q_1^2}{[q_1^2 - m_{f_2}^2][(q_1 - p_h)^2 - m_{f_2}^2][(q_1 - p)^2 - m_{f_2}^2]} \frac{\partial}{\partial_{m'^2}} \int_{\sigma_0}^{\infty} d\sigma \frac{D\Delta B_{00}(\sigma, m'^2, m_{f_1}^2)}{\sigma} \times \frac{q_1^2}{[q_1^2 - m_{f_2}^2][q_1^2 - m_{f_2}^2][q_1^2 - m_{f_2}^2]} \frac{\partial}{\partial_{m_0'^2}} \int_{\sigma_0'}^{\infty} d\sigma \frac{D\Delta B_{00}(\sigma, m_0'^2, m_{f_1}^2)}{\sigma} \Big\} \tag{228}$$

$$= F_{00} \times \int_0^1 dx \ \partial_{m'^2} \ B_{00}(0, m'^2, m_{f_1}^2) - F_{00}' \times \int_0^1 dx \ \partial_{m_0'^2} \ B_{00}(0, m_0'^2, m_{f_1}^2) \tag{229}$$

where F_{00} and F_{00}' are the integral related to loop momentum q_1. They are linear combinations of 1-loop scalar functions

$$F_{00} = D \times \left[B_0(pz^2, m_{f_2}^2, m_{f_2}^2) + m_{f_2}^2 C_0(ph^2, (p_1 + p_2)^2, pz^2, m_{f_2}^2, m_{f_2}^2, m_{f_2}^2) \right] \tag{230}$$

$$F_{00}' = D \times \left[B_0(0, m_{f_2}^2, m_{f_2}^2) + m_{f_2}^2 C_0(0, 0, 0, m_{f_2}^2, m_{f_2}^2, m_{f_2}^2) \right] = \frac{D^2(D-2)}{8m_{f_2}^2} A_0(m_{f_2}^2) \tag{231}$$

Besides the subloop divergence originates from $I_{\rm VZH}^{1,00}$, there is a subloop divergence from $I_{\rm VZH}^{1,11}$ and $I_{\rm VZH}^{1,0}$ term. Although they behave like $1/\sigma^2$ as σ goes to infinity, these two terms contains logrithmic divergence as q_1 tends to infinity, which can be clearly seen by power counting

$$\lim_{q_1 \to \infty} I_{\rm VZH}^{1,11} = \int d^4 q_1 \ \frac{1}{q_1^4} = \log \infty \tag{232}$$

$$\lim_{q_1 \to \infty} I_{\rm VZH}^{1,0} = \int d^4 q_1 \ \frac{1}{q_1^4} = \log \infty \tag{233}$$

To make it UV finite as $q_1 \to \infty$, we can subtract a term that same as $I^{1,11}_{\rm VZH}$ and $I^{1,0}_{\rm VZH}$ except setting all momenta inside q_1 propagators to zero. This term is written as

$$\begin{aligned}
I^{1,11+0,\rm subt}_{\rm VZH} =& \int \frac{d^Dq_1}{i\pi^2}\frac{d^Dq_2}{i\pi^2}\Bigg\{\frac{q_1^4}{[q_1^2-m_{f_2}^2][q_1^2-m_{f_2}^2][q_1^2-m_{f_2}^2][q_1^2-m_{f_1}^2]} \\
&\times \frac{1}{[q_2^2-m_{V_2}^2][(q_2+p_1+p_2)^2-m_{V_1}^2]} \\
&- \frac{q_1^4}{[q_1^2-m_{f_2}^2][q_1^2-m_{f_2}^2][q_1^2-m_{f_2}^2][q_1^2-m_{f_1}^2][q_2^2-m_{V_2}^2][q_2^2-m_{V_1}^2]}\Bigg\} \\
=& \frac{1}{8(m_{f_1}^2-m_{f_2})^3(m_{V_1}^2-m_{V_2}^2)}\Bigg\{8m_{f_1}^4A_0(m_{f_1}^2) \\
&- \left[-2(D^2-4)m_{f_1}^2m_{f_2}^2+D(D+2)m_{f_1}^4+D(D-2)m_{f_2}^4\right]A_0(m_{f_2}^2)\Bigg\} \\
&\times\left\{\left[m_{V_1}^2-m_{V_2}^2\right]B_0((p_1+p_2)^2,m_{V_1}^2,m_{V_2}^2)-A_0(m_{V_1}^2)+A_0(m_{V_2}^2)\right\} \quad (234)
\end{aligned}$$

By subtracting this term and add it back, we obtain

$$\begin{aligned}
I^{1,11}_{\rm VZH}+I^{1,0}_{\rm VZH} &= I^{1,11}_{\rm VZH}+I^{1,0}_{\rm VZH}-I^{1,11+0,\rm subt}_{\rm VZH}+I^{1,11+0,\rm subt}_{\rm VZH} \\
&= I^{1,11+0,\rm finite}_{\rm VZH}+I^{1,11+0,\rm subt}_{\rm VZH} \qquad (235)
\end{aligned}$$

After constructing subtraction terms for one global and two subloop divergence, the final expressions of $I_{\rm VZH}$ becomes

$$\begin{aligned}
I_{\rm VZH} =& I^{1,00,\rm finite}_{\rm VZH}+I^{1,11+0,\rm finite}_{\rm VZH}+I^{1,1}_{\rm VZH}+I^{p_{\rm ext}=0}_{\rm VZH}+I^{1,00,\rm subt}_{\rm VZH}+I^{1,11+0,\rm subt}_{\rm VZH} \\
=& I^{\rm finite}_{\rm VZH}+I^{p_{\rm ext}=0}_{\rm VZH}+I^{1,00,\rm subt}_{\rm VZH}+I^{1,11+0,\rm subt}_{\rm VZH} \qquad (236)
\end{aligned}$$

The strategy for constructing subtraction terms is diagrammatically illustrated in Fig.12.

The diagram labeled by $[\cdots]_{\rm finite}$ corresponds to $I^{\rm finite}_{\rm VZH}$. The vacuum diagram corresponds to $I^{p_{\rm ext}=0}_{\rm VZH}$. The diagrams shown in the second and third line correspond to $I^{1,00,\rm subt}_{\rm VZH}$ and $I^{1,11+0,\rm subt}_{\rm VZH}$ separately.

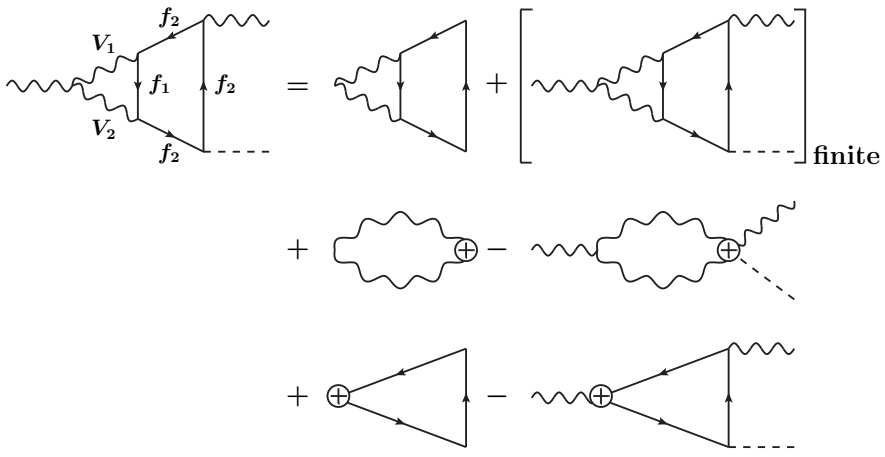

Figure 12: Diagrammatical domenstration of VZH divergence separation.

2.3.4 Strategy for Constructing Subtraction Terms

In Sec.2.3.2 and Sec.2.3.3, we demonstrated the process of constructing the subtraction terms by explicitly choosing the numerators. However, it is worth noting that this process does not need to be carried out case-by-case. In practice, it is relatively easy to construct the subtraction term for any arbitrary diagram. We will demonstrate the automation by taking the two-loop vertex diagram Fig. 11 as an example. The general tensor integral can be written as

$$\begin{aligned} I = \int \frac{d^D q_2}{i\pi^2} \frac{d^D q_1}{i\pi^2} \sum_{n_0,n_1,n_2,i,j} c_{ij}^{n_0,n_1,n_2} \times \{p_i^{n_0}, q_1^{n_1}, q_2^{n_2}\}_j \\ \times \frac{1}{(q_2^2 - m_{V_2}^2)((q_2+p)^2 - m_{V_1}^2)((q_2+q_1)^2 - m_{f_1}^2)} \\ \times \frac{1}{(q_1^2 - m_{f_2}^2)((q_1-p_h)^2 - m_{f_2}^2)((q_1-p)^2 - m_{f_2}^2)} , \end{aligned} \tag{237}$$

where $\{p_i^{n_0}, q_1^{n_1}, q_2^{n_2}\}$ denotes dot products among external momentum p_i and loop momentum $q_{1,2}$, and n_i denote the power of each of them. The index j labels all possible dot product conditions. For example for $n_0 = 0, n_1 = n_2 = 2$, the possible dot products read

$$\begin{aligned}\{p_i^0, q_1^2, q_2^2\}_1 &= (q_1 \cdot q_1)(q_2 \cdot q_2),\\ \{p_i^0, q_1^2, q_2^2\}_2 &= (q_1 \cdot q_2)(q_1 \cdot q_2).\end{aligned} \tag{238}$$

The SM Feynman rules require that $n_1 \leq 4, n_2 \leq 2, n_0 + n_1 + n_2 \leq 6$. $c_{ij}^{n_0,n_1,n_2}$ is the coefficient of a dot product, and it is a function of masses and dimension D. The integral Eq.237 contains a subloop divergence from the q_1 loop, which originate from the numerators $q_1^{n_1}$ with $n_1 \geq 4$. To make the q_1 integral UV finite, the following subtraction term is constructed:

$$\begin{aligned}I_{\text{subtr}}^{q_1} = \int \frac{d^D q_2}{i\pi^2} \frac{d^D q_1}{i\pi^2} \sum_{i,j} \Big[& c_{ij}^{2,4,0} \times \{p_i^2, q_1^4, q_2^0\}_j + c_{ij}^{1,4,1} \times \{p_i^1, q_1^4, q_2^1\}_j \\ & + c_{ij}^{0,4,2} \times \{p_i^0, q_1^4, q_2^2\}_j + c_{ij}^{1,4,0} \times \{p_i^1, q_1^4, q_2^0\}_j \\ & + c_{ij}^{0,4,1} \times \{p_i^0, q_1^4, q_2^1\}_j + c_{ij}^{0,4,0} \times \{p_i^0, q_1^4, q_2^0\}_j \Big] \\ & \times \frac{1}{(q_2^2 - m_{V_2}^2)((q_2+p)^2 - m_{V_1}^2)(q_1^2 - m_{f_1}^2)} \\ & \times \frac{1}{(q_1^2 - m_{f_2}^2)(q_1^2 - m_{f_2}^2)(q_1^2 - m_{f_2}^2)} \,.\end{aligned} \tag{239}$$

From Eq. 239, one can see that the loop integrals of q_1 and q_2 are disentangled. After performing the loop integration, one obtains

$$I_{\text{subtr}}^{q_1} = B_0(p^2, m_{V_2}^2, m_{V_1}^2) \times \Big[a_1 A_0(m_{f_1}^2) + a_2 A_0(m_{f_2}^2) \Big] \tag{240}$$

where a_i are functions of masses, external momenta and dimension D. A similar subloop subtraction term needs to be introduced in the vacuum integrals for the global divergence. Combining the two subloop subtraction terms, we obtain

$$\begin{aligned} I_{\text{subtr}} = &\Big[B_0(p^2, m_{V_2}^2, m_{V_1}^2) - B_0(0, m_{V_2}^2, m_{V_1}^2)\Big] \\ &\times \Big[a_1 A_0(m_{f_1}^2) + a_2 A_0(m_{f_2}^2)\Big]. \end{aligned} \tag{241}$$

This term can now be expanded in powers of $\epsilon = (4 - D)/2$, resulting in the expressions

$$\begin{aligned} I_{\text{subtr}}^{\text{div}} = &\Big[B_0^{(0)}(p^2, m_{V_2}^2, m_{V_1}^2) - B_0^{(0)}(0, m_{V_2}^2, m_{V_1}^2)\Big] \\ &\times \Big[a_1^{(0)} A_0^{(-1)}(m_{f_1}^2) + a_2^{(0)} A_0^{(-1)}(m_{f_2}^2)\Big], \end{aligned} \tag{242}$$

$$\begin{aligned} I_{\text{subtr}}^{\text{fin}} = &\Big[B_0^{(0)}(p^2, m_{V_2}^2, m_{V_1}^2) - B_0^{(0)}(0, m_{V_2}^2, m_{V_1}^2)\Big] \\ &\times \Big[a_1^{(0)} A_0^{(0)}(m_{f_1}^2) + a_2^{(0)} A_0^{(0)}(m_{f_2}^2) \\ &\quad + a_1^{(1)} A_0^{(-1)}(m_{f_1}^2) + a_2^{(1)} A_0^{(-1)}(m_{f_2}^2)\Big] \\ &+ \Big[B_0^{(1)}(p^2, m_{V_2}^2, m_{V_1}^2) - B_0^{(1)}(0, m_{V_2}^2, m_{V_1}^2)\Big] \\ &\times \Big[a_1^{(0)} A_0^{(-1)}(m_{f_1}^2) + a_2^{(0)} A_0^{(-1)}(m_{f_2}^2)\Big]. \end{aligned} \tag{243}$$

where (n) denote the expansion order in ϵ. Eq. 243 indicates that $\mathcal{O}(\epsilon)$ parts of one-loop scalar functions must be taken into account. Analytical expressions for these can be found in Ref. [45].

2.4 Numerical Results for Two-Loop EW Corrections to $\sigma(e^+e^- \to ZH)$

The analytical expressions for the LO cross section can be found in [74]. For the NLO cross section, both unpolarized and polarized beams are available. The NLO result for unpolarized beams can be found in [75, 76, 78], while the polarized beam result is presented in [79]. The NNLO mixed EW+QCD corrections were calculated by two groups, with [66] presenting an analytical result [80] and [67] presenting a numerical result.

The NNLO EW corrections to the process $e^+e^- \to HZ$ were estimated be on the order of 1%, and can be decomposed into contributions with and without closed fermionic loops. The contribution with closed fermionic loops is expected to dominate due to the large Yukawa coupling and large flavour numbers. While it would be ideal to calculate both contributions, it may not be necessary since the expected experimental precision is also of around 1%. In this case, including only the fermionic contribution may be sufficient to meet the required level of accuracy.

Thus in this section we only present results for two-loop EW diagrams with fermionic loops. However, the evaluation method discussed in Sec.2.3 can also be employed to evaluate diagrams without fermionic loops. Besides, the numerical results presented do not include QED initial-state radiation (ISR). At the order that we are working, QED ISR factorizes and can be taken into account through convolution with a universal structure function, see *e.g.* Ref. [81].

The following input parameters are used for the numerical evaluation:

$$m_W^{\text{exp}} = 80.379 \text{ GeV} \quad \Rightarrow \quad m_W = 80.352 \text{ GeV},$$
$$m_Z^{\text{exp}} = 91.1876 \text{ GeV} \quad \Rightarrow \quad m_Z = 91.1535 \text{ GeV},$$
$$m_H = 125.1 \text{ GeV}, \qquad m_t = 172.76 \text{ GeV},$$

$$\alpha^{-1} = 137.036, \qquad \Delta\alpha = 0.059,$$
$$\sqrt{s} = 240 \text{ GeV}. \tag{244}$$

where $\sqrt{s}$ represents the center-of-mass energy, and the masses of all other fermions are set to be 0. The discussion of differences between experimental and the on-shell $m_{Z,W}, \Gamma_{Z,W}$ can be found in Appendix.E.

2.4.1 Unpolarized Beam

Table.3 lists the results for the integrated unpolarized cross section at LO,NLO and NNLO, where corrections are further divided according to the number of fermion loops, denoted by N_f. Besides, it is worth mention that the corrections with fermion loops are gauge invariant, thus the comparison between them are meaningful. This is also the reason that we didn't list the corrections from different vertices or self-energies, which is gauge invariant by summing all corrections.

One can see that corrections with more fermion loops dominate, the reasons of which are the large top mass and large falvour number dependence. Taking the self-energy corrections as an example, the ratio between the cross section of diagrams with one and two top-quark self-energy loop behaves approximately as

$$R = \frac{\sigma(N_t = 1)}{\sigma(N_t = 2)} \approx \frac{m_Z^2 m_t^2 B_0(s, m_t^2, m_t^2) B_0(s, m_Z^2, m_Z^2)}{m_t^4 B_0^2(s, m_t^2, m_t^2)} \approx \frac{m_Z^2}{m_t^2} \tag{245}$$

Similarly, the ratio between the cross section of diagrams with one and two light-fermion self-energy loop behaves approximately as

$$R = \frac{\sigma(N_{f\neq t} = 1)}{\sigma(N_{f\neq t} = 2)} \approx \frac{N_f B_0(s, 0, 0) B_0(s, m_Z^2, m_Z^2)}{N_f^2 B_0^2(s, 0, 0)} \approx \frac{1}{N_f} \tag{246}$$

Thus, the cross sections with more fermion loops dominate.

Table 3: Numerical results for the integrated cross section at LO, NLO and NNLO. Electroweak one-loop and two-loop corrections are also provided and divided according to the number of fermion loops symbolized as N_f.

	(fb)	Contribution	(fb)
σ^{LO}	222.958		
σ^{NLO}	229.893		
		$\mathcal{O}(\alpha_{N_f=1})$	21.130
		$\mathcal{O}(\alpha_{N_f=0})$	-14.195
σ^{NNLO}	231.546		
		$\mathcal{O}(\alpha^2_{N_f=2})$	1.881
		$\mathcal{O}(\alpha^2_{N_f=1})$	-0.226

From Table.3, one can see that NLO corrections increases σ_{LO} by 3%, which is due to the cancellation between fermionic $N_f = 1$ and bosonic $N_f = 0$ contributions. The NNLO(EW+EW) corrections turns out to be 0.7% of the NLO correction, where the contribution with two fermionic loops is much greater than the one with one fermion loop. Besides the top-quark and flavor number enhancement, another reason is accidental numerical cancellation in the contribution with one femrion loop. This can be clearly seen from the plot of differential cross section, which is shown in Fig.13.

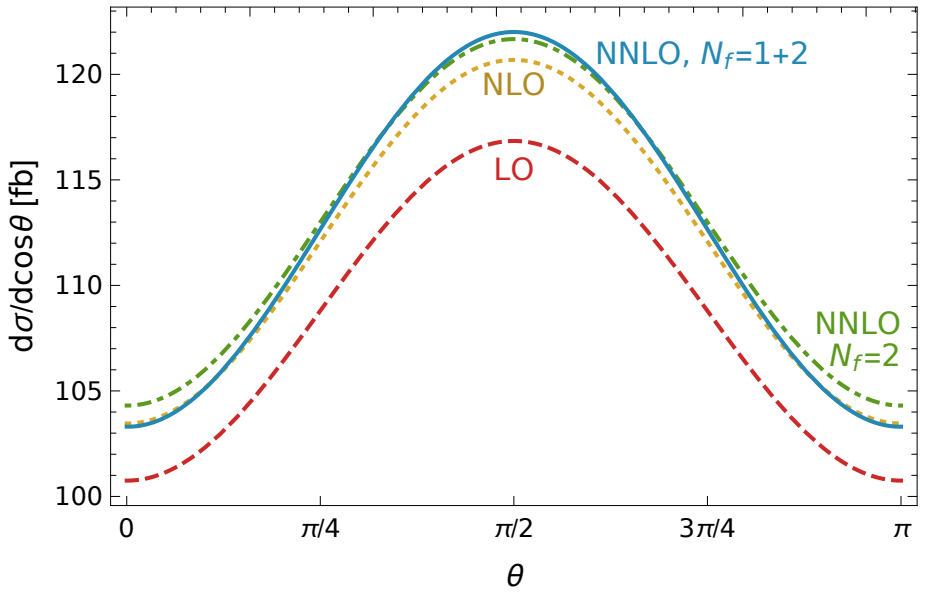

Figure 13: Angular distribution of differential cross section for $e^+e^- \to ZH$ at leading order("LO"), next-to-leading order("NLO"), next-to-next-to-leading order with two closed fermion loops("NNLO $N_f = 2$), and next-to-next-to-leading order with closed fermion loops("NNLO $N_f = 1 + 2$).

In Fig.13, the contributions of two fermion loops is the dashed green curve, and the sum of one and two fermion loop is denoted with blue curve. Thus the contributions due to one fermion loop is the difference between the green and blue curve, which is positive in the region $|\cos\theta| < 0.59$, and negative when $|\cos\theta| > 0.59$. Thus integrating over the whole angle regions leads to small total cross section of contributions due to one fermion loop.

Another interesting feature of the angular distribution of the differential cross section is its slight shape change, which arises from the appearance of new Lorentz structures at the loop level that are not present at tree level. These structures include

the ZZH, γZH vertices, and box diagram. At tree level, they can be written as

$$\begin{aligned}\Gamma^{\mu\nu}_{\text{ZZH,tree}} &= \frac{e\cos\theta_W}{\sin\theta_W} m_Z g^{\mu\nu} \\ \Gamma^{\mu\nu}_{\gamma\text{ZH,tree}} &= 0 \\ \Gamma^{\mu}_{\text{box,tree}} &= 0 \end{aligned} \tag{247}$$

where the indices represent the polarization vectors of gauge boson. Scalar particles contain no indices. At higher loop level, the general form of ZZH, γZH vertices are

$$\begin{aligned}\Gamma^{\mu\nu}_{\text{ZZH,loop}} &= F_1 g^{\mu\nu} + F_2 k_1^\mu k_2^\nu + F_3 k_2^\mu k_1^\nu + F_4 k_{1\rho} k_{2\sigma} \epsilon^{\mu\nu\rho\sigma} \\ \Gamma^{\mu\nu}_{\gamma\text{ZH,loop}} &= G_1 g^{\mu\nu} + G_2 k_1^\mu k_2^\nu + G_3 k_2^\mu k_1^\nu + G_4 k_{1\rho} k_{2\sigma} \epsilon^{\mu\nu\rho\sigma} \end{aligned} \tag{248}$$

where k_i is the momenta of Z and photon. The Lorentz structure for box diagram can be written as

$$\Gamma^{\mu}_{\text{box,loop}} = K_1 p_1^\mu + K_2 p_2^\mu + K_3 p_z^\mu \tag{249}$$

Clearly, there are new Lorentz structure, which is responsible for shape change.

Moreover, the angular distribution is maximum at $\cos\theta = 0$, which is due to longitudinal Z boson. This can be seen from tree level cross section. The tree level cross section for longitudinal and transverse Z boson is:

$$\frac{d\sigma_T^{\text{tree}}}{d\Omega} = \sum_{\sigma=\pm1}\sum_{\lambda=\pm1}\frac{d\sigma}{d\Omega} = \frac{\alpha^2\beta}{16}\frac{m_Z^2}{(s-m_Z^2)^2}\frac{s_W^4+(s_W^2-\frac{1}{2})^2}{c_W^4 s_W^4}(\cos\theta^2+1), \tag{250}$$

$$\Rightarrow\ \sigma_T^{\text{tree}} = \frac{\alpha^2\beta\pi}{4}\frac{m_Z^2}{(s-m_Z^2)^2}\frac{s_W^4+(s_W^2-\frac{1}{2})^2}{c_W^4 s_W^4}\frac{2}{3}, \tag{251}$$

$$\frac{d\sigma_L^{\text{tree}}}{d\Omega} = \sum_{\sigma=\pm1}\sum_{\lambda=0}\frac{d\sigma}{d\Omega} = \frac{\alpha^2\beta}{8}\frac{m_Z^2}{(s-m_Z^2)^2}\frac{s_W^4+(s_W^2-\frac{1}{2})^2}{c_W^4 s_W^4}\frac{3}{2}(\frac{\beta^2 s}{6m_Z^2}+\frac{2}{3})(\sin\theta^2), \tag{252}$$

$$\Rightarrow\ \sigma_L^{\text{tree}} = \frac{\alpha^2\beta\pi}{4}\frac{m_Z^2}{(s-m_Z^2)^2}\frac{s_W^4+(s_W^2-\frac{1}{2})^2}{c_W^4 s_W^4}(\frac{\beta^2 s}{6m_Z^2}+\frac{2}{3}). \tag{253}$$

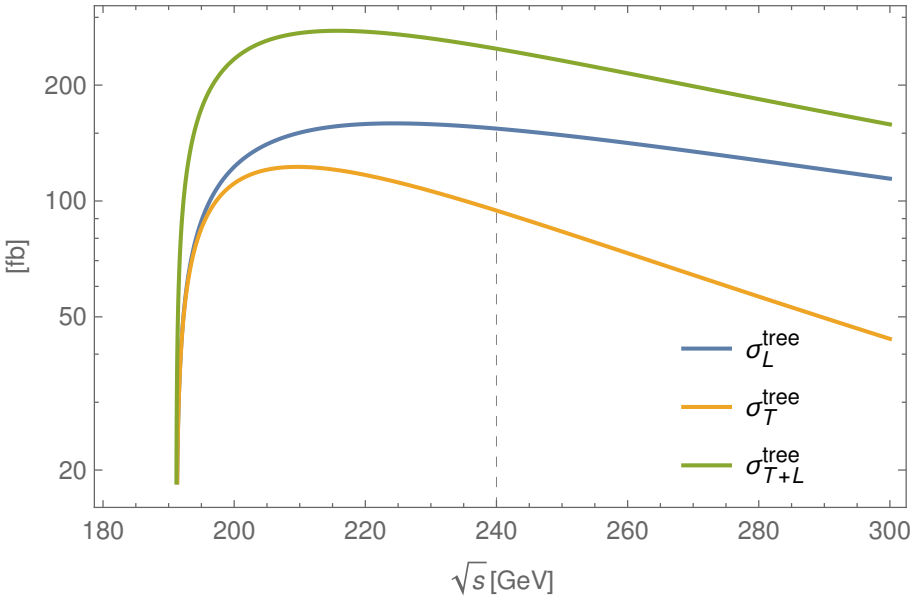

Figure 14: Distribution of $\sigma^{\text{tree}}(e^+e^- \to ZH)$ at different center-of-mass energy, $\sqrt{s}$, for unpolarized electron-positron bea,. "L(T)" represents the contribution from longitudinal(transverse) Z boson.

Fig. 14 shows the distribution of $\sigma^{\text{tree}}(e^+e^- \to ZH)$ at different center-of-mass energy, $\sqrt{s}$, for unpolarized electron-positron bea,. "L(T)" represents the contribution from longitudinal(transverse) Z boson. As one can read from this figure, the longitudinal mode dominates at $\sqrt{s} = 240\text{GeV}$, so the differential cross section peaks at $\pi/2$.

2.4.2 Polarized Beam

Numerical result of $\sigma(e^+e^- \to ZH)$ with polarized beam is listed in Table. 4. As can be seen from this table, the electroweak NNLO corrections depend strongly on

Table 4: Numerical results for the integrated ZH production cross section, in fb, at LO, NLO and fermionic electroweak NNLO, for different beam polarizations. The electroweak NNLO corrections are also listed individually according to the number of fermion loops symbolized as N_f.

		$e^+_{\mathrm{R}}e^-_{\mathrm{L}}$	$e^+_{\mathrm{L}}e^-_{\mathrm{R}}$
σ^{LO}	[fb]	541.28	350.55
σ^{NLO}	[fb]	507.92	411.66
σ^{NNLO}	[fb]	507.51	418.68
	$\mathcal{O}(\alpha^2_{N_f=2})$	1.75	5.77
	$\mathcal{O}(\alpha^2_{N_f=1})$	-2.15	1.25

the beam polarization.

The contributions with two closed fermions loops ($N_f = 2$) are significantly larger for right-handed electron polarization and left-handed positron polarization than for the opposite case. The contribution with one closed fermion loop ($N_f = 1$) has opposite signs for the two polarization, which leads to an accidental cancellation for the unpolarized cross-section.

2.4.3 Multiple Renormalization Schemes and Missing Higher Order Corrections

In this section, we display the numerical result of two different schemes of electric charge. One scheme, called the $\alpha(0)$ scheme, defines $\alpha = e^2/(4\pi)$ as the electromagnetic coupling at zero momentum, and the second scheme, called the G_μ scheme,

relates the weak coupling to the Fermi coupling G_μ,

$$\frac{G_\mu}{\sqrt{2}} = \frac{g^2}{8m_W^2}(1 + \Delta r). \tag{254}$$

Details of electric charge renormalization schemes can be found in Sec.1.2.3.

The input value of $\alpha(0)$ scheme has been shown in Eq.244. In G_μ scheme, we use the input parameters in eq. (244), together with $G_\mu = 1.1663787 \times 10^{-5}$. The numerical results for total cross section obtained in the two renormalization schemes are shown in Tab 5.

One can realize that the total cross section of G_μ scheme is always greater than $\alpha(0)$ scheme due to the larger effective fine structure constant. However, the radiative corrections in G_μ scheme is smaller. The one-loop EW radiative corrections in G_μ scheme can be parametrized as [76]

$$\delta_{\text{weak}}^{G_\mu} = \delta_{\text{weak}}^{\alpha(0)} - 2\Delta r \tag{255}$$

The fermionic contributions in $\delta_{\text{weak}}^{G_\mu}$ are reduced by Δr, while bosonic contribution hardly changes, which leads to a reduction of radiative corrections.

Another feature from the table is that the numerical difference between two schemes, i.e. dependence on renormalization schemes, decreases as more and more radiative contributions are included, which is expected by perturbative theory.

In fact, this convergence is further improved when including the mixed electroweak-QCD two-loop corrections [66, 67]. We use numerical results for this contribution from Ref. [67]. In order to do so, we have to compute our electroweak corrections for the same input parameters used there. The results are shown in Table. 6.

The prediction for the cross-section including all available results agrees very well between the two renormalization schemes, with a difference of 0.12 fb. As we discussed in Sec.1.2, renormalization scheme difference can be utilized to estimate

Table 5: Numerical results for the unpolarized integrated ZH production cross section, in fb, for two different renormalization schemes. Results are given at LO, NLO and fermionic electroweak NNLO. For the latter, the contributions from two ($N_f = 2$) and one ($N_f = 1$) closed fermion loops are also shown individually.

	$\alpha(0)$ scheme	G_μ scheme	scheme dependence
σ^{LO} [fb]	222.96	239.18	16.22
σ^{NLO} [fb]	229.89	232.08	2.19
σ^{NNLO} [fb]	231.55	232.74	1.19
$\mathcal{O}(\alpha^2_{N_f=2})$	1.88	0.73	
$\mathcal{O}(\alpha^2_{N_f=1})$	-0.23	-0.07	

Table 6: Similar to Table. 5, but using input values and mixed EW-QCD corrections from Ref. [67].

	$\alpha(0)$ scheme	G_μ scheme	scheme dependence
σ^{LO} [fb]	223.14	239.64	16.50
σ^{NLO} [fb]	229.78	232.46	2.68
$\sigma^{\text{NNLO,EW}\times\text{QCD}}$ [fb]	232.21	233.29	1.08
$\sigma^{\text{NNLO,EW}}$ [fb]	233.86	233.98	0.12

missing higher-order corrections, where the dominant impact is expected from the bosonic electroweak NNLO corrections, *i.e.* from two-loop contributions without closed fermion loops.

Therefore, one can use the difference between the two renormalization schemes as an order-of-magnitude estimate of the perturbative theory uncertainty. Since this estimate is only a lower bound on the size of missing higher-order contributions, we conservatively multiply it by a factor 2, thus arrive at an error estimate of 0.24 fb.

The alternative estimation is obtained from $2\,\mathrm{Re}\{\mathcal{M}^*_{(0)}\mathcal{M}_{(2,\mathrm{bos})}\} \lesssim |\mathcal{M}_{(1,\mathrm{bos})}|^2$, where $\mathcal{M}_{(1,\mathrm{bos})}$ is the matrix element of the bosonic NLO corrections. This leads to a contribution of 0.65 fb to the cross-section. One may expect that the unknown $2\,\mathrm{Re}\{\mathcal{M}^*_{(0)}\mathcal{M}_{(2,\mathrm{bos})}\}$ is smaller is due to several suppression factors in the Born matrix element $\mathcal{M}_{(0)}$: (a) the e-e-Z couplings in the initial state are smaller than the e-ν-W couplings, which appear in the 1-loop box diagrams, by a factor $2^{-3/2} \sim 0.35$; (b) the s-channel Z propagator produces a factor $m_Z^2/(s - m_Z^2) \sim 0.17$ for $\sqrt{s} = 240$ GeV.

Thus it seems plausible that the missing bosonic electroweak NNLO corrections have an impact between 0.24 and 0.65 fb on the SM prediction for the ZH production cross-section. These theory error estimates, $0.1 - 0.3\%$ are lower than the anticipated experimental precision (0.4–1%), but a direct calculation of these missing contributions is still desirable.

2.4.4 Treatment of Z Decay

Both the Z and Higgs bosons are unstable particles, so we must take into account their decays when calculating the cross section. Due to the small width-to-mass ratio of Higgs boson, $\Gamma_H/m_H = \mathcal{O}(10^{-5})$, the Narrow-Width-Approximation (NWA) can be used to treat Higgs decay. In this approximation, the cross section for the

process $e^+e^- \to ZH \to ZX$ can be written as the product of the cross section for $e^+e^- \to ZH$ and the branching ratio of $H \to X$, namely

$$\sigma(e^+e^- \to ZX)\Big|_{\text{NWA}} = \sigma(e^+e^- \to ZH) \times \text{Br}(H \to X) \tag{256}$$

However, the width-to-mass ratio of Z boson, $\Gamma_Z/m_Z = \mathcal{O}(10^{-2})$, is much larger. In Ref. [77], the authors calculated the mixed EW+QCD corrections for the process $e^+e^- \to ZH \to \mu^+\mu^- H$ by employing the NWA for the Z decay as well as using a fixed width. Their result shows that the cross section obtained using the NWA deviates from the one obtained with a fixed width by 4%. Consequently, NWA is not a suitable method for treating Z boson decay, especially considering the anticipated high precision measurements at future Higgs factories, which is around 1%.

Since the implementation of NWA is relatively simple, we first consider the treatment of the Z boson. Considering outgoing Z boson decaying into $\mu^+\mu^-$ pair, the complete all-orders matrix element for the process $e^+e^- \to \mu^+\mu^- H$ can be written as

$$\mathcal{M}_{ee\to\mu\mu H} = \Gamma_{\text{prod}} \frac{1}{p_z^2 - m_Z^2 + \Sigma_Z(p_z^2)} \Gamma_{\text{dec}} + \mathcal{M}_{\text{bkgd}} \tag{257}$$

The first term is the matrix element with on-shell Z decay, where Γ_{prod} and Γ_{dec} are the e^+e^-ZH and $Z\mu^+\mu^-$ Green's function, respectively, and Σ_Z is the Z-boson self-energy. $\mathcal{M}_{\text{bkgd}}$ denotes the contribution to $e^+e^- \to \mu^+\mu^- H$ process without Z resonance.

When expanding the above matrix element perturbatively without breaking gauge invariance, we adopt the complex pole method. The complex pole, $s_0 = m_Z^2 - i m_Z \Gamma_Z$, of Z propagator satisfies the following equation

$$s_0 - m_Z^2 + \Sigma(s0) = 0 \;\Rightarrow\; m_Z^2 = s_0 + \Sigma(s0) \tag{258}$$

Plugging Eq (258) into Eq (257)

$$\mathcal{M}_{ee\to\mu\mu H} = \Gamma_{\text{prod}} \frac{1}{p_z^2 - s_0 - \Sigma(s0) + \Sigma_Z(p_z^2)} \Gamma_{\text{dec}} + \mathcal{M}_{\text{bkgd}} \tag{259}$$

$$= \frac{\Gamma_{\text{prod}}\Gamma_{\text{dec}}}{(p_z^2 - s_0)(1 + \frac{-\Sigma(s0)+\Sigma_Z(p_z^2)}{p_z^2 - s0})} + \mathcal{M}_{\text{bkgd}} \tag{260}$$

Expanding Γ and Σ around complex mass

$$\Gamma(p_z^2) = \Gamma(s_0) + (p_z^2 - s_0)\Gamma^{'}(s_0) + \frac{1}{2}(p_z^2 - s_0)^2\Gamma^{''}(s_0) \tag{261}$$

$$\Sigma_Z(p_z^2) = \Sigma_Z(s_0) + (p_z^2 - s_0)\Sigma_Z^{'}(s_0) + \frac{1}{2}(p_z^2 - s_0)^2\Sigma_Z^{''}(s_0) + (...) \tag{262}$$

Plugging these into Eq (260), we obtain

$$\begin{aligned}
\mathcal{M}_{ee\to\mu\mu H} &= \frac{(\Gamma_{\text{prod}}(s_0) + (p_Z^2 - s_0)\Gamma^{'}_{\text{prod}}(s_0))(\Gamma_{\text{dec}}(s_0) + (p_Z^2 - s_0)\Gamma^{'}_{\text{dec}}(s_0)}{(p_Z^2 - s_0)(1 + \Sigma_Z^{'}(s_0) + \frac{1}{2}(p_Z^2 - s_0)\Sigma_Z^{''}(s_0)} + \mathcal{M}_{\text{bkgd}} \\
&= \frac{1}{p_Z^2 - s_0}\frac{\Gamma_{\text{prod}}(s_0)\Gamma_{\text{dec}}(s_0)}{1 + \Sigma_Z^{'}(s_0)} + \mathcal{M}_{\text{bkgd}} + \frac{\Gamma_{\text{prod}}(s_0)\Gamma^{'}_{\text{dec}}(s_0) + \Gamma^{'}_{\text{prod}}(s_0)\Gamma_{\text{dec}}(s_0)}{1 + \Sigma_Z^{'}(s_0)} \\
&- \frac{\Gamma_{\text{prod}}(s_0)\Gamma_{\text{dec}}(s_0)\Sigma_Z^{''}(s_0)}{2(1 + \Sigma_Z^{'}(s_0))^2} + \mathcal{O}(p_Z^2 - s_0) \\
&= \frac{1}{p_Z^2 - s_0}R(s_0) + S(s_0) + (p_Z^2 - s_0)S^1
\end{aligned} \tag{263}$$

Given that $\Gamma_Z \ll m_Z$, we can expand R,S around $s_0 = m_Z^2$, thus

$$\mathcal{M}_{ee\to\mu\mu H} = \frac{1}{p_Z^2 - s_0}R(s_0) + \frac{p_Z^2 - s_0}{p_Z^2 - s_0}S(s_0) \tag{264}$$

$$\begin{aligned}
&= \frac{1}{p_Z^2 - s_0}(R(m_Z^2) + (s_0 - m_Z^2)R^{'}(m_Z^2)) \\
&+ \frac{p_Z^2 - m_Z^2 - (s_0 - m_Z^2)}{p_Z^2 - s_0}(S(m_Z^2) + (s_0 - m_Z)S^{'}(m_Z^2))
\end{aligned} \tag{265}$$

$$= \frac{1}{p_Z^2 - s_0}R(m_Z^2) + \frac{p_Z^2 - m_Z^2}{p_Z^2 - s_0}S(m_Z^2) + \mathcal{O}(s_0 - m_Z^2) \tag{266}$$

Each of the terms is separately gauge invariant. Since the experimental analysis will select $\mu^+\mu^-$ pair with invariant mass close to the Z resonance, $p_Z^2 \sim m_Z^2$, which leads to $p_Z - s_0 \sim \Gamma_Z$, thus the terms in the series expansion in Eq. 266 decrease in numerical magnitude. If one seeks NNLO accuracy in leading R term, NLO accuracy is sufficient in subleading S terms and LO precision for the following term.

Focusing on the leading R term, the different cross section is written as

$$d\sigma = \frac{1}{2s} d\Phi_3 |\mathcal{M}_{ee\to\mu\mu H}|^2 \tag{267}$$

where Φ_3 is the three-body phase space, plugging the explicit form we get

$$\frac{d\sigma}{d\cos\theta_{12} d\phi_{12} ds_{12} d\cos\theta_H d\phi_H} = \frac{1}{16s}\frac{1}{(2\pi)^5}\frac{\sqrt{\lambda(s, s_{12}, m_H^2)}}{8s} \times \left|\frac{\Gamma_{\rm prod}\Gamma_{\rm dec}}{1+\Sigma_Z'}\frac{1}{p_z^2 - s0}\right|^2 \tag{268}$$

where $s_{12}, \theta_{12}, \phi_{12}$ is the invariant mass, polar angle and azimuthal angle of the $\mu^+\mu^-$ pair. θ_H, ϕ_H is the polar and azimuthal angle between outgoing Higgs and incoming electron beam. After integrating all variables except s_{12}, θ_{12}, we obtain

$$\begin{aligned}
\frac{d\sigma}{d\cos\theta_{12} ds_{12}} &= \frac{1}{2s}\frac{1}{(2\pi)^5} 4\pi \frac{1}{8} 2\pi \frac{\sqrt{\lambda(s, s_{12}, m_H^2)}}{8s} \times \left(\frac{\Gamma_{\rm prod}^2 \Gamma_{\rm dec}^2}{(1+\Sigma_Z')^2}\frac{1}{(p_z^2 - m_z^2)^2 + m_z^2\Gamma_Z^2}\right) \\
&= \frac{\sqrt{\lambda(s, s_{12}, m_H^2)}}{32\pi s^2}\frac{1}{16\pi^2}\frac{\Gamma_{\rm prod}^2}{1+\Sigma_Z'}\frac{\Gamma_{\rm dec}^2}{1+\Sigma_Z'}\frac{1}{(p_z^2 - m_z^2)^2 + m_z^2\Gamma_Z^2} \\
&= \underbrace{\frac{\lambda(1, s_{12}/s, m_H^2/s)}{32\pi s}|M_{\rm pro}|^2}_{d\sigma(e^+e^-\to ZH)} \frac{m_Z^{-1}\Gamma_{\rm dec}^2}{16\times 3\pi(1+\Sigma_Z')}\frac{\pi^{-1} m_Z}{(p_z^2 - m_z^2)^2 + m_z^2\Gamma_Z^2}
\end{aligned} \tag{269}$$

To obtain the cross section for $e^+e^- \to \mu^+\mu^- H$, we should replace $p_Z^2 = s_{12}$ of $\sigma(e^+e^- \to ZH)$ and performing the integration over it.

The additional factor of 1/3 in the last line of the calculation comes from the unstable Z boson. When we break down a $2 \to 3$ process into a $2 \to 2$ and a $1 \to 2$

process, we need to sum over all possible Z boson polarizations. This summation gives rise to a factor

$$g^{\mu_1\mu_2} - \frac{p_Z^{\mu_1} p_Z^{\mu_2}}{m_Z^2}, \tag{270}$$

Multiplying the $2 \to 2$ and $1 \to 2$ processes give rise an additional constant

$$= (g^{\mu_1\mu_2} - \frac{p_z^{\mu_1\mu_2}}{m_z^2}) g_{\mu_1\mu_2} (g^{\nu_1\nu_2} - \frac{p_z^{\nu_1\nu_2}}{m_z^2}) g_{\nu_1\nu_2} \tag{271}$$

$$= (4 - 2\frac{p_z^2}{p_z^2} + \frac{p_z^4}{p_z^4}) \tag{272}$$

$$= 3 \tag{273}$$

However, for a $2 \to 3$ process, Z boson polarization only appears in the intermediate state, and we need to multiply an extra factor of $1/3$ to account for all possible polarizations.

3.0 Probing Dark Sector Fermions through Higgs Precision Study

3.1 Motivation

Although the discovery of the Higgs boson at the LHC by the ATLAS and CMS collaborations confirmed all particle contents of the SM, it is clear that this theory is not a complete description of nature, and one such evidence is dark matter. The existence of dark matter was first proposed by Fritz Zwicky in the 1930s [82], based on his observations that the velocity dispersion of galaxies in the Coma cluster of galaxies was far too large to be supported by the luminous matter. Since then, numerous studies have confirmed the presence of dark matter at various scales, from individual galaxies to the entire universe. In fact, dark matter is believed to make up about 27% of the total mass-energy content of the universe, with ordinary matter comprising only about 5%.

In particle physics, dark matter is the leading empirical evidence for new particles, and dark matter candidates are motivated not only by cosmology, but also by robust problems in particle physics. There are striking hints that it may be linked to attempts to understand electroweak symmetry breaking, the leading puzzle in the field today. Dark matter includes WIMPs, hidden dark matter, sterile neutrinos, and axions, etc. Besides, supersymmetry and models with extra dimensions also provide a dark matter candidate.

The search for dark matter has been pursued through direct detection, which measures the cross section for dark matter scattering off atomic nuclei, sets strong bounds on dark matter properties. Meanwhile, collider searches for dark matter typically focus on events with missing energy/momentum, providing a complementary

approach to direct detection. Despite many years of searches, neither approach has yielded any conclusive evidence of dark matter.

With the high experimental accuracy expected at future colliders, precision measurements of Higgs boson properties may reveal deviations that must be attributed to new physics, such as SM extension with extra scalars [83, 84] or fermions [85, 86, 87, 88, 89]. The effect of SM with extended scalar on Higgs physics has been studied comprehensively in Refs. [90, 91, 92, 93, 94, 95, 96, 97, 98, 99, 100], while the studies with extended fermions [101, 102, 103] focus on how to create a dark matter candidate satisfying all relevant constraints. Since the possible deviation on Higgs boson properties will also put stringent bound on these new fermions, it is important to understand how precision measurements will constrain these new fermions.

In this section, our focus is on the Higgs portal with fermionic dark matter, which is one of the simplified dark matter models [1]. We will investigate this model from both indirect and direct perspectives. In the indirect search, we will study its impact on Higgs precision studies, with a primary focus on $\sigma(e^+e^- \to ZH)$, which is anticipated to be measurable with a precision of about 1.2% at ILC [1, 2], 0.4% at FCC-ee [3] and 0.5% at CEPC [4], and explore the parameter space that leads to deviations greater than 0.5%. In the direct search, we examine the direct production of the new fermions associated with this model at the (HL-)LHC. By considering both aspects, we can obtain implication on whether the parameter regions associated with deviations greater than 0.5% have been and can be covered by the direct searches for new physics at the (HL)-LHC.

[1] In simplified dark matter models, the new fermions may belong to a larger dark sector. Without assuming any specifics about this larger dark sector, we do not incorporate constraints from dark matter relic density and direct detection, as done in previous studies [101, 102, 103].

3.2 The Models

We start by introducing two UV complete models that extend the SM with vector fermions: the singlet-doublet model[85, 86, 87, 101, 103] and the doublet-triplet model[88, 89, 101, 103]. Both models contains two fermion multiplets to form a Yukawa interaction term. Besides, we impose the Z_2 symmetry, under which the new fermion multiplets are odd while the SM particles are even. This Z_2 symmetry ensures the lightest dark matter stable, thus become a dark matter candidate and escapes detection giving signatures of missing energy and momentum. Besides, both models are treated as simplified models rather than full theories, i.e. the fermions could be part of a larger dark sector thus we do not expect our model can satisfy the constraints from the dark matter relic density and direct detection.

3.2.1 Singlet-Double Model

The SM is extended with one fermion singlet χ_S and one doublet χ_D, which transform under the Electroweak gauge group $\mathrm{SU(2)_L \times U(1)_Y}$ as

$$\chi_D = \begin{pmatrix} \chi_D^+ \\ \chi_D^0 \end{pmatrix} \sim (2, \frac{1}{2}) \ , \ \chi_S \sim (1, 0). \tag{274}$$

Both fields are vector-like fermions. Since the hypercharge of the singlet χ_S equals zero, it can be either a Dirac or a Majorana fermion. We discuss both of these possibilities.

3.2.1.1 Dirac Singlet-Double Model (DSDM)

We start from the Dirac case. The Lagrangian for the dark sector is

$$\mathcal{L}_{\rm DM} \supset -m_S \bar{\chi}_S \chi_S - m_D \bar{\chi}_D \chi_D - (y \chi_S \bar{\chi}_D H + \text{h.c.}), \tag{275}$$

where y is the Yukawa coupling. In general, the Yukawa coupling y are complex, but the complex phase can be absorbed into the Fermion spinors. Therefore, y can always be chosen to be real. Discussions of the consequences of introducing a non-zero phase can be found in Refs. [104, 105].

After the electroweak symmetry breaking (EWSB), the neutral component of dark matter acquires extra mass from Yukawa interaction term, thus the mass matrix of neutral component obtains non-diagonal elements. The new Lagrangian of the mass term can be written as

$$\mathcal{L}_{\rm DM}^{\rm mass,N} = -\begin{pmatrix} \bar{\chi}_S & \bar{\chi}_D^0 \end{pmatrix} \mathcal{M}_N \begin{pmatrix} \chi_S \\ \chi_D^0 \end{pmatrix} \tag{276}$$

with

$$\mathcal{M}_N = \begin{pmatrix} m_S & y\nu/\sqrt{2} \\ y\nu/\sqrt{2} & m_D \end{pmatrix} \tag{277}$$

where N stands for the neutral. The mass matrix can be diagonalized by the following rotational matrix

$$R_2 = \begin{pmatrix} \cos\theta_2 & \sin\theta_2 \\ -\sin\theta_2 & \cos\theta_2 \end{pmatrix}, \tag{278}$$

where

$$\sin^2\theta_2 = \frac{1}{2}\Big(1 + \frac{m_D - m_S}{\Delta m_2}\Big),\ (\Delta m_2)^2 = (m_S - m_D)^2 + 2y^2v^2 \tag{279}$$

The heavy and light mass eigenstates, χ_h and χ_l, are given by

$$\chi_h^0 = \cos\theta_2 \chi_D^0 + \sin\theta_2 \chi_S \ , \ \chi_l^0 = -\sin\theta_2 \chi_D^0 + \cos\theta_2 \chi_S \tag{280}$$

with corresponding mass eigenvalues

$$m_{h,l}^0 = \frac{1}{2}(m_S + m_D \pm \Delta m_2) \tag{281}$$

The charged state $\chi^+ = \chi_D^+$ is pure doublet with mass equal to m_D. The mass distributions of three mass eigenstates at different values of $m_D - m_S$ are shown in Fig.15, where m_l^0, m_h^0 and m_D are represented by the blue, yellow and green lines respectively. We have chosen $m_S = 500\text{GeV}$ and $y = 1(1.5)$ for the solid(dashed) curve. The χ_l^0 is the lightest particle thus become a dark matter candidate. As the Yukawa coupling increasing, $m_l^0(m_h^0)$ decreases(increases) since it depends on y negatively(positively). When $m_S \ll m_D$, χ_l^0 is singlet-dominant, and χ_h^0 are doublet-dominant thus has the same mass as χ^+. When $m_S \gg m_D$, χ_l^0 are doublet-dominant thus $m_l^0 \approx m_D$.

In the mass eigenstate basis, the interactions between new fermions and SM particles are

$$\begin{aligned}
\hat{\mathcal{L}} \supset & \frac{e}{\sqrt{2}s_W}\Big[\sin\theta_2 \bar{\chi}_h^0 \gamma^\mu \chi^+ + \cos\theta_2 \bar{\chi}_l^0 \gamma^\mu \chi^+\Big] W_\mu^+ + \frac{e(c_W^2 - s_W^2)}{2 s_W c_W} \bar{\chi}^+ \gamma^\mu \chi^+ Z_\mu \\
& - \frac{e}{2 s_W c_W}\Big[\sin^2\theta_2 \bar{\chi}_h^0 \gamma^\mu \chi_h^0 + \cos^2\theta_2 \bar{\chi}_l^0 \gamma^\mu \chi_l^0 + \frac{1}{2}\sin(2\theta_2)(\bar{\chi}_h^0 \gamma^\mu \chi_l^0 + \bar{\chi}_l^0 \gamma^\mu \chi_h^0)\Big] Z_\mu \\
& - \frac{y}{\sqrt{2}}\Big[\sin(2\theta_2)(\bar{\chi}_h^0 \chi_h^0 - \bar{\chi}_l^0 \chi_l^0) + \cos(2\theta_2)(\bar{\chi}_h^0 \chi_l^0 + \bar{\chi}_l^0 \chi_h^0)\Big] h
\end{aligned} \tag{282}$$

where $\hat{\mathcal{L}}$ denotes the unrenormalized Lagrangian. Since new fermions are vector-like, the couplings of left-handed and right-handed fermion are same. Besides, the coupling with weak gauge boson is proportional to its coefficient of doublet component. Charged component does not interact with Higgs boson since its mass is not changed after EWSB.

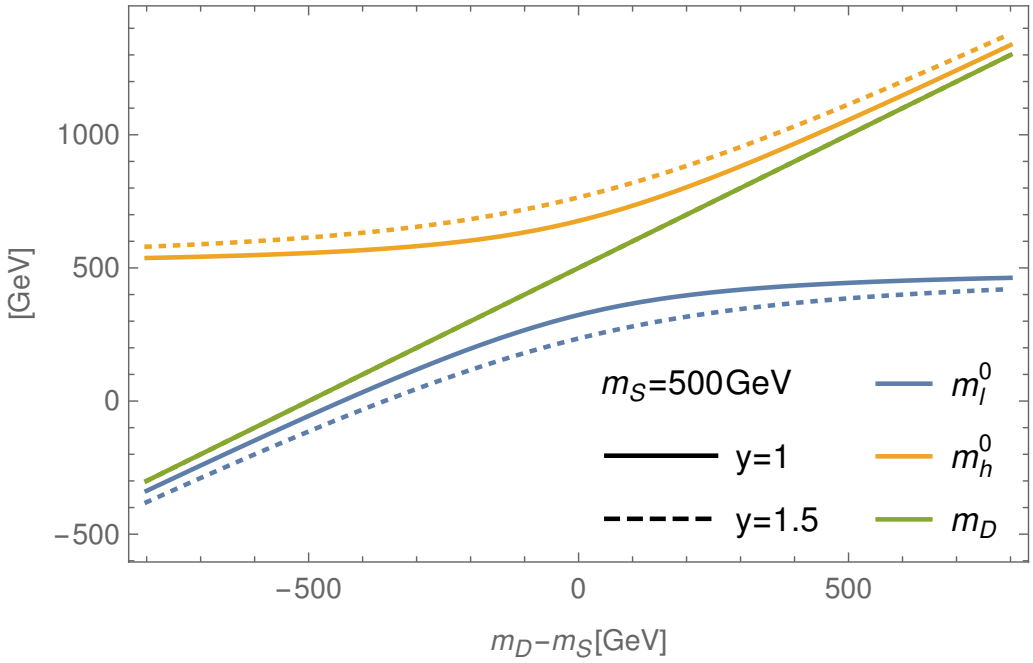

Figure 15: The mass distributions of three mass eigenstates in the Dirac singlet-doublet model at different values of $m_D - m_S$. m_l^0, m_h^0 and m_D are represented by the blue, yellow and green lines respectively. We have chosen $m_S = 500\text{GeV}$ and $y = 1(1.5)$ for the solid(dashed) curve.

3.2.1.2 Majorana Singlet-Double Model (MSDM)

The SM is extended with a Majorana singlet and a Dirac doublet fermion, and it is more convenient to express them in terms of Weyl spinors. The Dirac doublet corresponds to two left-handed Weyl doublets with opposite hypercharge. Under the

Electroweak gauge group $\mathrm{SU(2)_L} \times \mathrm{U(1)_Y}$, they transform according to

$$\chi_D = \begin{pmatrix} \chi_D^+ \\ \chi_D^0 \end{pmatrix} \sim (2, \frac{1}{2}) \ , \ \chi_D^c = \begin{pmatrix} \chi_D^{c0} \\ \chi_D^{c-} \end{pmatrix} \sim (2, -\frac{1}{2}) \tag{283}$$

The two-component Weyl fermion form a Dirac fermion by $(\chi_D, \epsilon\chi_D^{c*}) \to \chi_D$, where ϵ is 2×2 antisymmetric tensor. Additionally, we assume that the two Weyl spinors couple to the Higgs field with equal but opposite strengths. This particular coupling choice forbids any new physics contributions to the oblique T parameter due to the custodial symmetry. Other coupling choices can be found in the literature, such as [101, 102]. Under this assumption, the dark sector Lagrangian in two-component notation is expressed as

$$\mathcal{L}_{\mathrm{DM}} \supset -\frac{1}{2} m_S \chi_S \chi_S + m_D \chi_D^c \epsilon \chi_D - y(\chi_S H^\dagger \chi_D - \chi_S \chi_D^c \epsilon H) + \mathrm{h.c.} \tag{284}$$

After the EWSB, the neutral components acquire additional mass contributions from the non-zero Higgs vacuum expectation value (vev), which results in the Lagrangian of the mass term expressed as

$$\mathcal{L}_{\mathrm{DM}}^{\mathrm{mass,N}} = (-\frac{1}{2} \bar{\chi}_i \mathcal{M}_{ij}^N \chi_j + \mathrm{h.c.}), \tag{285}$$

where $\chi = (\chi_S, \chi_D^{c0}, \chi_D^0)^T$ and

$$\mathcal{M}^N = \begin{pmatrix} m_S & -yv/\sqrt{2} & yv/\sqrt{2} \\ -yv/\sqrt{2} & 0 & -m_D \\ yv/\sqrt{2} & -m_D & 0 \end{pmatrix} \tag{286}$$

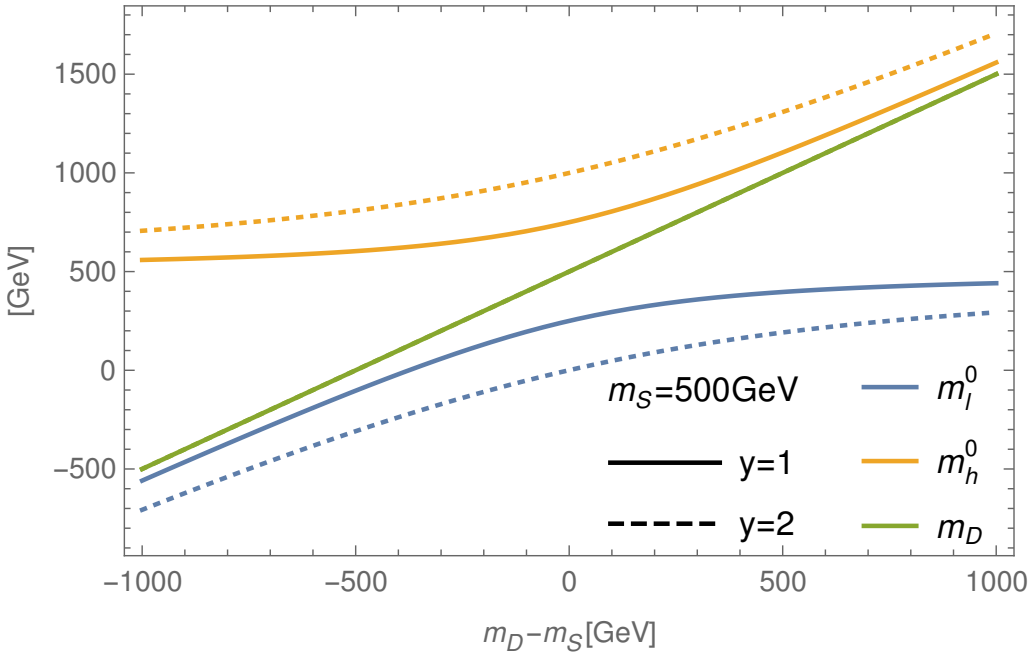

Figure 16: The mass distributions of four mass eigenstates in the Majorana singlet-doublet model at different values of $m_D - m_S$. m_l^0, m_h^0 and $m_m^0 = m^+ = m_D$ are represented by the blue, yellow and green lines respectively. We have chosen $m_S =$ 500GeV and $y = 1(2)$ for the solid(dashed) curve.

The mass matrix can be diagonalized by the following transformation

$$\begin{pmatrix} \chi_h^0 \\ \chi_m^0 \\ \chi_l^0 \end{pmatrix} = \begin{pmatrix} \cos\theta_4 & -\frac{1}{\sqrt{2}}\sin\theta_4 & \frac{1}{\sqrt{2}}\sin\theta_4 \\ 0 & \frac{i}{\sqrt{2}} & \frac{i}{\sqrt{2}} \\ \sin\theta_4 & \frac{1}{\sqrt{2}}\cos\theta_4 & -\frac{1}{\sqrt{2}}\cos\theta_4 \end{pmatrix} \begin{pmatrix} \chi_S \\ \chi_D^{c0} \\ \chi_D^0 \end{pmatrix}, \tag{287}$$

The mixing angle can be obtained from Eq. 279 by performing the replacement

$2 \to 4$. The corresponding mass eigenvalues are

$$m^0_{h,l} = \frac{1}{2}(m_S + m_D \pm \Delta m_4) \ , \ m^0_m = m_D \tag{288}$$

where $(\Delta m_4)^2 = (m_S - m_D)^2 + 4y^2v^2$.

The charged components remain pure doublet with mass $m^+ = m_D$. The mass distribution of four mass eigenstates as a function of $m_D - m_S$ is shown in Fig.16, where m^0_l, m^0_h and $m^0_m = m^+ = m_D$ are represented by the blue, yellow and green line respectively. We have chosen $m_S = 500$GeV , and the Yukawa coupling are considered with values $y = 1$ and $y = 2$. The χ^0_l is the lightest particle thus become a dark matter candidate. The relationship between masses and Yukawa coupling is same as the Dirac singlet-doublet model.

In the mass eigenstate basis, the interactions between new fermions and SM particles are

$$\begin{aligned}\hat{\mathcal{L}} \supset & \frac{e}{2s_W}\Big[\sin\theta_4\chi^0_h\gamma^\mu\chi^+ - \cos\theta_2\chi^0_l\gamma^\mu\chi^+ + \chi^0_m\gamma^\mu\chi^+\Big]W^+_\mu \\ & + \frac{e(c^2_W - s^2_W)}{2s_Wc_W}\chi^-\gamma^\mu\chi^+Z_\mu - \frac{e}{2s_Wc_W}\Big[\sin\theta_4\chi^0_h\gamma^\mu\chi^0_m - \cos\theta_4\chi^0_l\gamma^\mu\chi^0_m\Big]Z_\mu \\ & - \frac{y}{2}\Big[\sin(2\theta_4)(\chi^0_h\chi^0_h - \chi^0_l\chi^0_l) - 2\cos(2\theta_2)\chi^0_h\chi^0_l\Big]h \end{aligned} \tag{289}$$

Comparing with Dirac singlet case, one find that the $\chi^0_i\chi^\pm_jW^\pm$ coupling for Majorana singlet case is suppressed by $1/\sqrt{2}$. Similar to DSDM, χ^0_m and χ^+ does not interact with Higgs boson since its mass is not changed after EWSB.

The extension of the SM with a Majorana singlet and a Dirac doublet fermions corresponds to the Bino-Higgsino system[2] with decoupled Wino in Minimal Supersymmetric Model (MSSM) with $\tan\beta = 1, y = g'/\sqrt{2}$. The search for Higgsino pair production has been explored at the LHC, and the search results can be implemented

[2]Bino is the dark matter candidate, and Higgsinos are heavier thus can decay into Bino.

in our model. The implementation of LHC search result will be discussed with more details in Sec. 3.4.

3.2.2 Doublet-Triplet Model

In this model, the SM is extended with one fermion doublet, χ_D and one fermion triplet χ_T, which transforms under the Electroweak gauge group $\mathrm{SU(2)_L \times U(1)_Y}$ as

$$\chi_D = \begin{pmatrix} \chi_D^{r+1} \\ \chi_D^{r} \end{pmatrix} \sim (2, \frac{1}{2} + r) \ , \ \chi_T = \begin{pmatrix} \chi_T^{r+1} \\ \chi_T^{r} \\ \chi_T^{r-1} \end{pmatrix} \sim (3, r) \tag{290}$$

where the superscript denotes the charge. We consider the cases $r = 0, -1$, thus both multiplets contain a neutral component. For $r = 0$, the triplet can be either a Dirac or Majorana fermion, while the doublet is always a Dirac fermions. Thus, there are three possible cases: $r = -1$ with Dirac triplet, $r = 0$ with Dirac triplet, and $r = 0$ with Majorana triplet.

3.2.2.1 Dirac Doublet-Triplet Model with $r = -1$ (DDTM1)

For $r = -1$, the doublet and triplet components are

$$\chi_D = \begin{pmatrix} \chi_D^0 \\ \chi_D^- \end{pmatrix} \ , \ \chi_T = \begin{pmatrix} \chi_T^-/\sqrt{2} & \chi_T^0 \\ \chi_T^{--} & -\chi_T^-/\sqrt{2} \end{pmatrix} \tag{291}$$

where the triplet is expressed in its adjoint representation.

The Lagrangian of dark sector is

$$\mathcal{L}_{\mathrm{DM}} = -m_D \bar{\chi}_D \chi_D - m_T \mathrm{Tr}(\bar{\chi}_T \chi_T) - (y \bar{\chi}_D \chi_T H + \mathrm{h.c.}) \tag{292}$$

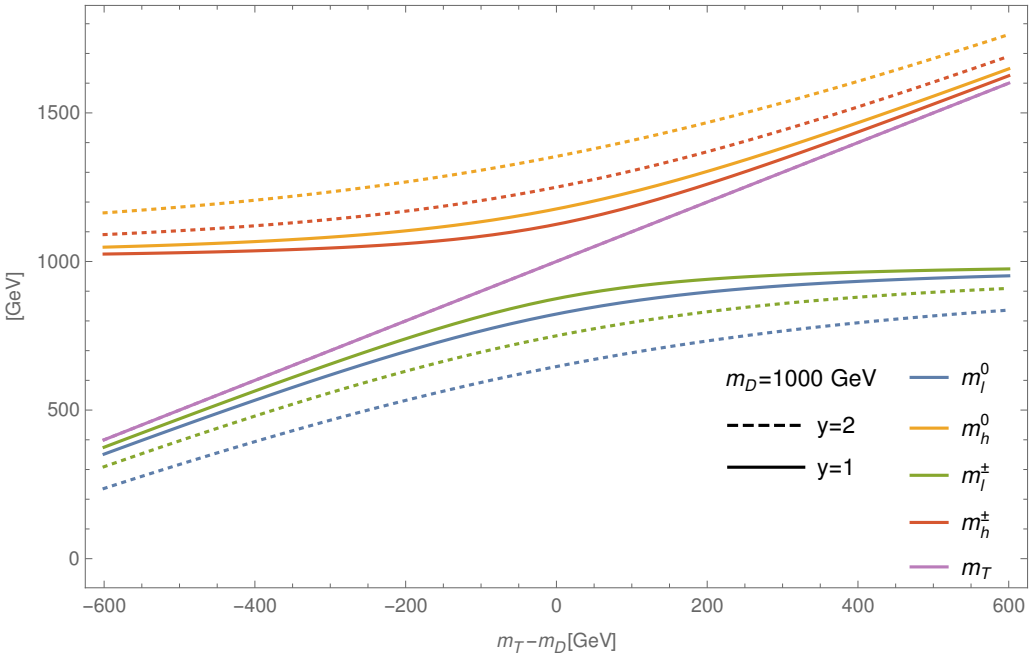

Figure 17: The mass distributions of five mass eigenstates in the Dirac doublet-triplet model with $r = -1$ at different values of $m_T - m_D$. $m_l^0, m_h^0, m_l^\pm, m_h^\pm$ and m_T are represented by the blue, yellow, green, red and purple lines respectively. We have chosen $m_D = 1000\text{GeV}$ and $y = 1(2)$ for the solid(dashed) curve.

After EWSB, the mass matrices for charged and charged neutral fermions in the bases (χ_T^0, χ_D^0) and (χ_T^-, χ_D^-) are

$$\mathcal{M}^N = \begin{pmatrix} m_T & yv/\sqrt{2} \\ yv/\sqrt{2} & m_D \end{pmatrix} \ , \ \mathcal{M}^C = \begin{pmatrix} m_T & -yv/2 \\ -yv/2 & m_D \end{pmatrix} \tag{293}$$

where $C(N)$ denotes the charged(charged neutral) components. They can be diagonalized with the following transformations

$$\begin{pmatrix}\chi_h^0\\ \chi_l^0\end{pmatrix}=\begin{pmatrix}\cos\theta_2 & \sin\theta_2\\ -\sin\theta_2 & \cos\theta_2\end{pmatrix}\begin{pmatrix}\chi_T^0\\ \chi_D^0\end{pmatrix}\ ,\ \begin{pmatrix}\chi_h^-\\ \chi_l^-\end{pmatrix}=\begin{pmatrix}\cos\theta_1 & \sin\theta_1\\ -\sin\theta_1 & \cos\theta_1\end{pmatrix}\begin{pmatrix}\chi_T^-\\ \chi_D^-\end{pmatrix} \quad (294)$$

where $\sin^2\theta_{2(1)} = 1/2 + (m_T - m_D)/(2\Delta m_{2(1)})$ and $(\Delta m_{2(1)})^2 = (m_D - m_T)^2 + 2(1)y^2v^2$. The masses for charged and charged neutral mass eigenstates are

$$m_{h,l}^0 = \frac{1}{2}(m_D + m_T \pm \Delta m_2)\ ,\ m_{h,l}^- = \frac{1}{2}(m_D + m_T \pm \Delta m_1) \quad (295)$$

while χ_T^{--} remains pure triplet with mass $m^{--} = m_T$. The physical mass spectrum is shown in Fig. 17 for two different Yukawa couplings, $y = 1$ and $y = 2$. χ_l^0 is lightest thus becomes a dark matter candidate. As Yukawa coupling increasing, the masses for $\chi_h^{0,\pm}$ increase, while decrease for $\chi_l^{0,\pm}$, which can be understood from Eq. 295. The pure triplet particle χ_T^{--} is independent on the Yukawa coupling. As $m_T - m_D \gg yv$, $\sin\theta_{1,2} = 0$, $\chi_l^{0,\pm}$ becomes doublet-dominate, which behaves like m_D, thus the curve tends to $m_D = 1000$GeV. As $m_T - m_D \gg yv$, $\chi_h^{0,\pm}$ becomes triplet-dominate, thus $m_h^{0,\pm} \approx m_T$.

The interactions between extra fermions and EW gauge bosons are

$$\begin{aligned}\hat{\mathcal{L}} \supset +\frac{e}{2s_W}\Big[&(-2\cos\theta_1\cos\theta_2+\sqrt{2}\sin\theta_1\sin\theta_2)\chi_h^+\gamma^\mu\chi_h^0\\ &+(\sqrt{2}\cos\theta_2\sin\theta_1+2\cos\theta_1\sin\theta_2)\chi_h^+\gamma^\mu\chi_l^0\\ &+(2\cos\theta_2\sin\theta_1+\sqrt{2}\cos\theta_1\sin\theta_2)\chi_l^+\gamma^\mu\chi_h^0\\ &+(\sqrt{2}\cos\theta_1\cos\theta_2-2\sin\theta_1\sin\theta_2)\chi_l^+\gamma^\mu\chi_l^0\\ &+\chi_T^{++}\gamma^\mu(2\sin\theta_1\chi_l^- - 2\cos\theta_1\chi_h^-)\Big]W_\mu^-\\ +\frac{e}{2s_Wc_W}\Big[&(\cos^2\theta_2+1)\bar{\chi}_h^0\gamma^\mu\chi_h^0+(\sin^2\theta_2+1)\bar{\chi}_l^0\gamma^\mu\chi_l^0\end{aligned}$$

$$
\begin{aligned}
&- \frac{1}{2}\sin 2\theta_2(\bar{\chi}_h^0\gamma^\mu\chi_l^0 + \bar{\chi}_l^0\gamma^\mu\chi_h^0) - (\sin^2\theta_2 - 2s_W^2)\bar{\chi}_h^+\gamma^\mu\chi_h^- \\
&- (\cos^2\theta_2 - 2s_W^2)\bar{\chi}_l^+\gamma^\mu\chi_l^- - \frac{1}{2}\sin 2\theta_1(\bar{\chi}_h^+\gamma^\mu\chi_l^- + \bar{\chi}_l^+\gamma^\mu\chi_h^-) \\
&- (1 - 2s_W^2)\chi_T^{++}\gamma^\mu\chi_T^{--}\Big] Z_\mu \\
&+ \frac{1}{\sqrt{2}}y\Big[\sin 2\theta_2(\bar{\chi}_l^0\chi_l^0 - \bar{\chi}_h^0\chi_h^0) - \cos 2\theta_2(\bar{\chi}_h^0\chi_l^0 + \bar{\chi}_l^0\chi_h^0) \\
&+ \frac{\sin 2\theta_1}{\sqrt{2}}(\chi_h^+\chi_h^- - \chi_l^+\chi_l^-) + \frac{\cos 2\theta_1}{\sqrt{2}}(\chi_h^+\chi_l^- + \chi_l^+\chi_h^-)\Big] h
\end{aligned}
\tag{296}
$$

Both doublet and triplet fermions interact with weak gauge bosons, thus the couplings are more complicated compared with the singlet-doublet case. χ_T^{--} does not interact with Higgs since its mass does not change after EWSB.

3.2.2.2 Dirac Doublet-Triplet Model with $r = 0$ (DDTM0)

For $r = 0$, the doublet and triplet have the following components

$$
\chi_D = \begin{pmatrix} \chi_D^+ \\ \chi_D^0 \end{pmatrix} \ , \ \chi_T = \begin{pmatrix} \chi_T^0/\sqrt{2} & \chi_T^+ \\ \chi_T^{-\prime} & \chi_T^0/\sqrt{2} \end{pmatrix} \tag{297}
$$

The Lagrangian for dark sector is same as the one with $r = -1$, which is shown in Eq.292. After EWSB, the mass matrices for charged and neutral fermions are

$$
\mathcal{M}^N = \begin{pmatrix} m_T & yv/2 \\ yv/2 & m_D \end{pmatrix} \ , \ \mathcal{M}^C = \begin{pmatrix} m_T & -yv/\sqrt{2} \\ -yv/\sqrt{2} & m_D \end{pmatrix} \tag{298}
$$

in the bases (χ_T^0, χ_D^0) and (χ_T^+, χ_D^+). Clearly, the mass matrices for neutral and charged states are same as the one with $r = -1$ by interchange the charged and

charged neutral component $\mathcal{M}^C \leftrightarrow \mathcal{M}^N$. Thus we obtain the following rotational matrices

$$\begin{pmatrix} \chi_h^0 \\ \chi_l^0 \end{pmatrix} = \begin{pmatrix} \cos\theta_1 & \sin\theta_1 \\ -\sin\theta_1 & \cos\theta_1 \end{pmatrix} \begin{pmatrix} \chi_T^0 \\ \chi_D^0 \end{pmatrix} \ , \ \begin{pmatrix} \chi_h^+ \\ \chi_l^+ \end{pmatrix} = \begin{pmatrix} \cos\theta_2 & \sin\theta_2 \\ -\sin\theta_2 & \cos\theta_2 \end{pmatrix} \begin{pmatrix} \chi_T^+ \\ \chi_D^+ \end{pmatrix} \quad (299)$$

and the corresponding masses

$$m_{h,l}^0 = \frac{1}{2}(m_D + m_T \pm \Delta m_1) \ , \ m_{h,l}^- = \frac{1}{2}(m_D + m_T \pm \Delta m_2) \quad (300)$$

The negative charged component $\chi_T^{-'}$ is pure triplet with mass m_T. If $m_{D,T} > 0$, $m_l^0 > m_l^\pm$, i.e. the lightest particle is not charged neutral. To address this problem, we perform the transformation, $\chi_l^{0,\pm} \to i\gamma^5 \chi_l^{0,\pm}$, which cause $m_l^{0,\pm} \to -m_l^{0,\pm}$. The mass difference becomes

$$\begin{aligned} |m_l^0| - |m_l^\pm| &= \frac{1}{2}\Big(\Delta m_1 - \Delta m_2\Big) \\ &= \frac{1}{2}\Big(\sqrt{(m_D - m_T)^2 + y^2 v^2} - \sqrt{(m_D - m_T)^2 + 2y^2 v^2}\Big) \leq 0. \end{aligned} \quad (301)$$

The the mass distributions of all five particles in this model after this transformation is shown in Fig. 18. $m_l^0, m_h^0, m_l^\pm, m_h^\pm$ and m_T are represented by the blue, yellow, green, red and purple lines respectively. We have chosen $m_D = -100\text{GeV}$ and considered two values for the Yukawa coupling, $y = 1$ (solid) and $y = 2$ (dashed). As one can read from this figure, the lightest particle is charged neutral. One can also notice that $m_h^0 \approx m_h^\pm \approx m_T$, which indicates that these three particles are triplet dominant, while $m_l^{0,\pm}$ are doublet-dominant.

The interactions between $\chi_{l,h}^{0,+}$ and W,h are same as the $y = -1$ case by interchanging $\theta_1 \leftrightarrow \theta_2$. The interactions involving χ_T^- are

$$\hat{\mathcal{L}} \supset + \frac{e}{2s_W}\Big[+ \chi_T^+ \gamma^\mu (\sin\theta_1 \chi_l^0 + \cos\theta_1 \chi_h^0)\Big] W_\mu^- \quad (302)$$

Due to the change of hypercharge, simply interchanging the mixing angle does not lead to the correct interaction between new fermions and Z boson. The Lagrangian involving new fermions and Z boson has the following form

$$\begin{aligned}\hat{\mathcal{L}} \supset -\frac{e}{2s_W c_W}\Big[&\sin^2\theta_1 \bar{\chi}_h^0\gamma^\mu\chi_h^0 + \cos^2\theta_1\bar{\chi}_l^0\gamma^\mu\chi_l^0 + \frac{1}{2}\sin 2\theta_1(\bar{\chi}_h^0\gamma^\mu\chi_l^0 + \bar{\chi}_l^0\gamma^\mu\chi_h^0)\\ &-(1+\cos^2\theta_2 - 2s_W^2)\bar{\chi}_h^+\gamma^\mu\chi_h^- - (1+\sin^2\theta_2-2s_W^2)\bar{\chi}_l^+\gamma^\mu\chi_l^-\\ &+\frac{1}{2}\sin 2\theta_2(\bar{\chi}_h^+\gamma^\mu\chi_l^- + \bar{\chi}_l^+\gamma^\mu\chi_h^-) + 2\bar{\chi}_T^+\chi_T^-\Big]Z_\mu \end{aligned} \tag{303}$$

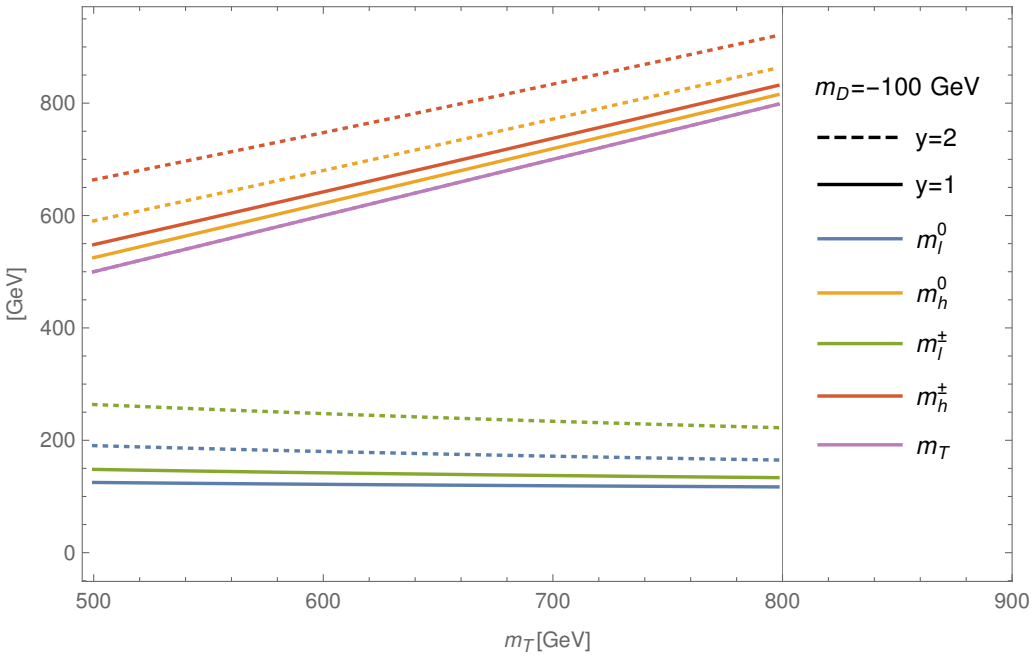

Figure 18: The mass distributions of five mass eigenstates in the Dirac doublet-triplet model with $r = 0$ at different values of m_T. $m_l^0, m_h^0, m_l^\pm, m_h^\pm$ and m_T are represented by the blue, yellow, green, red and purple lines respectively. We have chosen $m_D = -100\text{GeV}$ and $y = 1(2)$ for the solid(dashed) curve.

3.2.2.3 Majorana Doublet-Triplet Model (MDTM)

Same as Majorana singlet Model, we rewrite the Lagrangian in terms of Weyl spinors. The doublets have the same form with Eq.283, and the triplet is

$$\chi_T = \begin{pmatrix} \chi_T^0/\sqrt{2} & \chi_T^+ \\ \chi_T^- & \chi_T^0/\sqrt{2} \end{pmatrix} \tag{304}$$

With two-component notation, the Lagrangian of the mass and Yukawa interactions terms is

$$\mathcal{L}_{\rm DM} \supset m_D \chi_D^c \epsilon \chi_D - \frac{1}{2} m_T {\rm Tr}(\chi_T \chi_T) - y(H^\dagger \chi_T \chi_D - \chi_D^{cT} \epsilon \chi_T H) + {\rm h.c.} \tag{305}$$

As for the Majorana singlet-doublet model, we assume the Yukawa couplings for two doublets are same but with opposite sign. After EWSB, the Lagrangian for the mass terms is

$$\mathcal{L}_{\rm DM}^{\rm mass} = -\frac{1}{2} \begin{pmatrix} \chi_T^0 & \chi_D^{c0} & \chi_D^0 \end{pmatrix} \mathcal{M}^N \begin{pmatrix} \chi_T^0 \\ \chi_D^{c0} \\ \chi_D^0 \end{pmatrix} - \begin{pmatrix} \chi_T^- & \chi_D^{c-} \end{pmatrix} \mathcal{M}^C \begin{pmatrix} \chi_T^+ \\ \chi_D^+ \end{pmatrix} + {\rm h.c.}, \tag{306}$$

and the mass matrices are

$$\mathcal{M}^N = \begin{pmatrix} m_T & yv/2 & -yv/2 \\ yv/2 & 0 & -m_D \\ -yv/2 & -m_D & 0 \end{pmatrix} \ , \ \mathcal{M}^C = \begin{pmatrix} m_T & yv/\sqrt{2} \\ yv/\sqrt{2} & m_D \end{pmatrix} \tag{307}$$

The mass matrices can be diagonalized by

$$\begin{pmatrix} \chi_h^0 \\ \chi_m^0 \\ \chi_l^0 \end{pmatrix} = \begin{pmatrix} \cos\theta_2 & \sin\theta_2/\sqrt{2} & -\sin\theta_2/\sqrt{2} \\ 0 & i/\sqrt{2} & i/\sqrt{2} \\ \sin\theta_2 & -\cos\theta_2/\sqrt{2} & \cos\theta_2/\sqrt{2} \end{pmatrix} \begin{pmatrix} \chi_T^0 \\ \chi_D^{c0} \\ \chi_D^0 \end{pmatrix} \ ,$$

$$\begin{pmatrix}\chi_h^+\\ \chi_l^+\end{pmatrix} = \begin{pmatrix}\cos\theta_2 & \sin\theta_2\\ -\sin\theta_2 & \cos\theta_2\end{pmatrix}\begin{pmatrix}\chi_T^+\\ \chi_D^+\end{pmatrix} \tag{308}$$

The corresponding masses are

$$m_{h,l}^0 = m_{h,l}^+ = \frac{1}{2}(m_D + m_T \pm \Delta m_2)\ ,\ m_m^0 = m_D \tag{309}$$

The mass distribution of five mass eigenstates in the Majorana doublet-triplet model at different values of $m_D - m_T$ is shown in Fig.19. One can notice that $\chi_l^{0,\pm}$ are both lightest and mass degenerate, while this mass degeneracy if lifted by one-loop corrections involving gauge bosons [106, 107, 108, 109], and only the neutral becomes dark matter candidate. When $m_D \gg m_T$, all three heavy particles are triplet dominant, and two light particles are doublet dominant. One the other hand, when $m_T \gg m_D$, light particles become triplet dominant. Heavy particles, explicitly $\chi_h^\pm$ and χ_h^0 become doublet-dominant. Therefore, $m_h^{0,\pm} \approx m_D$.

The interaction between new fermions and SM particles is

$$\begin{aligned}\hat{\mathcal{L}} \supset &+ \frac{e}{2s_W}\Big[-\chi_h^+\gamma^\mu\Big((1+\cos^2\theta_2)\chi_h^0 + i\sin\theta_2\chi_m^0 + \frac{\sin 2\theta_2}{2}\chi_l^0\Big)\\
&\qquad + \chi_l^+\gamma^\mu\Big((1+\sin^2\theta_2)\chi_l^0 + i\cos\theta_2\chi_m^0 + \frac{\sin 2\theta_2}{2}\chi_h^0\Big)\Big]W_\mu^-\\
&+ \frac{e}{2s_W c_W}\Big[(i\cos\theta_2\chi_l^0 - i\sin\theta_2\chi_h^0)\gamma^\mu\chi_m^0 - \frac{1}{2}\sin 2\theta_2(\bar{\chi}_a^+\gamma^\mu\chi_l^- + \bar{\chi}_c^+\gamma^\mu\chi_h^-)\\
&\qquad + (1+\cos^2\theta_2 - 2s_W^2)\bar{\chi}_a^+\gamma^\mu\chi_h^- + (1+\sin^2\theta_2 - 2s_W^2)\bar{\chi}_c^+\gamma^\mu\chi_l^-\Big]Z_\mu\\
&+ \frac{1}{\sqrt{2}}y\Big[\sin 2\theta_2(\bar{\chi}_c^0\chi_l^0 - \bar{\chi}_a^0\chi_h^0) + \cos 2\theta_2(\bar{\chi}_a^0\chi_l^0 + \bar{\chi}_c^0\chi_h^0)\\
&\qquad + \sin 2\theta_2(\chi_l^+\chi_l^- - \chi_h^+\chi_h^-) + \cos 2\theta_2(\chi_h^+\chi_l^- + \chi_l^+\chi_h^-)\Big]h\end{aligned} \tag{310}$$

The extension of the SM with Dirac doublet and Majorana triplet fermion corresponds to the Higgsino-Wino system(with decoupled bino) in MSSM for $\tan\beta =$

$1, y = g$. The experimental constraints on this scenario can be used to constrain parameters of MDTM, which will be discussed more in Sec. 3.4.

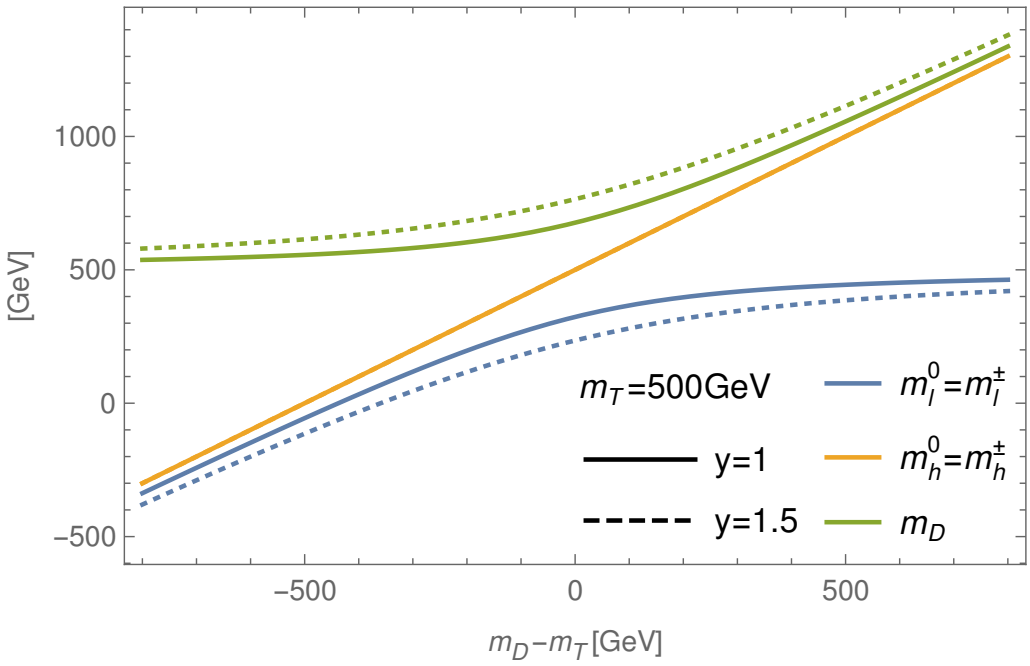

Figure 19: The mass distributions of five mass eigenstates in the Majorana doublet-triplet model at different values of $m_D - m_T$. $m_l^{0,\pm}, m_h^{0,\pm}$ and m_D are represented by the blue, yellow and green lines respectively. We have chosen $m_T = 500\text{GeV}$ and $y = 1(2)$ for the solid(dashed) curve.

3.2.3 Model Summary

In Table.7, we summarized the gauge, mass eigenstates as well as the free parameter set that we will implemented for calculate $\sigma(e^+e^- \to ZH)$ for models introduced in Sec. 3.2.1 and Sec. 3.2.2.

models	gauge states	mass states	free parameters
DSDM	$\chi_S = \chi_S^0, \chi_D = \begin{pmatrix} \chi_D^+ \\ \chi_D^0 \end{pmatrix}$	$\chi_{h,l}^0, \chi^+$	$y, m_l^0, \Delta m_{\rm hl} = m_h^0 - m_l^0$
MSDM	$\chi_S = \chi_S^0, \chi_D = \begin{pmatrix} \chi_D^+ \\ \chi_D^0 \end{pmatrix}$	$\chi_{h,l}^0, \chi_D^0, \chi_D^+$	$y, m_l^0, \Delta m_{\rm hl} = m_h^0 - m_l^0$
DDTM1	$\chi_D = \begin{pmatrix} \chi_D^0 \\ \chi_D^- \end{pmatrix}, \chi_T = \begin{pmatrix} \chi_T^0 \\ \chi_T^- \\ \chi_T^{--} \end{pmatrix}$	$\chi_{h,l}^0, \chi_{h,l}^-, \chi^{--}$	$y, m_l^0, \Delta m_{\rm ll} = m_l^+ - m_l^0$
DDTM0	$\chi_D = \begin{pmatrix} \chi_D^+ \\ \chi_D^0 \end{pmatrix}, \chi_T = \begin{pmatrix} \chi_T^+ \\ \chi_T^0 \\ \chi_T^{'-} \end{pmatrix}$	$\chi_{h,l}^0, \chi_{h,l}^+, \chi^-$	$y, m_l^0, \Delta m_{\rm hl} = m_h^0 - m_l^0$
MDTM	$\chi_D = \begin{pmatrix} \chi_D^+ \\ \chi_D^0 \end{pmatrix}, \chi_T = \begin{pmatrix} \chi_T^+ \\ \chi_T^0 \\ \chi_T^- \end{pmatrix}$	$\chi_l^{0,\pm}, \chi_h^{0,\pm}, \chi_m^0$	$y, m_l^0, \Delta m_{\rm hl} = m_h^0 - m_l^0$

Table 7: Summary table of gauge, mass eigenstates and free parameter set for the five models introduced in Sec. 3.2.1 and Sec. 3.2.2.

3.3 Constraints

Before implementing any constraints, we restrict the free parameters introduced in Table.7 to the following ranges:

- $m_l^0 < 1$ TeV, $m_l^\pm \geq 103.5$ GeV

  m_l^0 is the mass of lightest charged neutral particle. We are interested in the dark

matter candidate with mass below TeV range, which is possible to be found at colliders. The lower bound on $m_l^{\pm}$, which is the mass of the lightest charged particle, comes from the exclusion limit searching for charginos at LEP [110].

- $\Delta m_{\mathrm{Xl}} = m_X - m_l^0 < 1.5$ TeV

  Δm_{Xl} (introduced in Table.7) is the mass difference between heavy particle with mass m_X and the lightest dark matter. The sensitivity of the collider searches depends on the visible energy released in the decay process. The mass difference range at the order of TeV covers all phenomenological possibilities: (a) non-compressed spectra, $\Delta M > M_{Z,W,h}$; (b) compressed spectra $\Delta M \sim \mathcal{O}(1\mathrm{GeV})$; (c) nearly-degenerate spectra $\Delta M \sim \mathcal{O}(100\mathrm{MeV})$. Each scenario corresponds to different final states, which will be discussed more in Sec.3.3.2.

- $0 < y < 3$

  Large values of Yukawa coupling are constrained by perturbativity, i.e. the corrections from higher order loops should be suppressed, which requires $y/\pi < 1$.

Besides, all parameters are chosen to be real since the complex phase vanishes with field redefinition.

While one could impose the relic density as a constraint on the parameter space, in the spirit of simplified models we will not do this here in order not to cut away regions of parameter space that might be interesting from a collider perspective. Instead we note that there are several alternate possibilities to avoid a too large relic density in this case. For example, First, if $\tilde{\chi}_1^0$ is not absolutely stable, but just long lived enough to escape the detectors, the relic density constraint can be satisfied while the collider phenomenology is unchanged. Another possibility is a non-standard cosmological history, for example late decaying particles can inject additional entropy after $\tilde{\chi}_1^0$ freezes out, such that its relic density is diluted.

Instead, the constraints we implemented include oblique parameters, current and expected dark matter search results at the LEP, LHC as well as HL-LHC, and the relative decay ratio of Higgs to diphotons with respect to the SM result $R_\gamma = \Gamma(H \to \gamma\gamma)/\Gamma_{\rm SM}(H \to \gamma\gamma)$.

3.3.1 Oblique Parameters

Given that new physics is heavier than the W and Z boson, the new physics indirectly contribute to the propagators of gauge boson, i.e. the so-called oblique corrections[111, 112, 113]. The effects of oblique corrections are parameterized into six oblique parameters: S,T,U,V,X and W, but only the first three parameters contribute to electroweak precision observables. Furthermore, we fix U=0, which is motivated by the fact that U is suppressed by an additional factor $M^2_{\rm new}/M^2_Z$ compared to S and T where $M_{\rm new}$ is the energy scale of new physics. This suppression can also be understood from EFT: S and T correspond to dimension-6 operator $H^\dagger W^a_{\mu\nu}\sigma^a H B^{\mu\nu}$ and $H^\dagger (D_\mu H)(D^\mu H)^\dagger H$, while the operator contributing to U in the lowest order is a dimension-8 operator $H^\dagger W^a_{\mu\nu}\sigma^a H H^\dagger W^{b\mu\nu}\sigma^b H$ [114].

The definitions of S and T at one-loop level are

$$\frac{\alpha}{4s^2_W c^2_W} S = \frac{\Pi^{\rm new}_{ZZ}(M^2_Z) - \Pi^{\rm new}_{ZZ}(0)}{M^2_Z} - \frac{c^2_W - s^2_W}{c_W s_W}\frac{\Pi^{\rm new}_{Z\gamma}(M^2_Z)}{M^2_Z} - \frac{\Pi^{\rm new}_{\gamma\gamma}(M^2_Z)}{M^2_Z} \tag{311}$$

$$\alpha T = -\frac{s^2_W}{c^2_W M^2_Z}\Sigma^{AA}_T(0) + \frac{1}{M^2_W}\Sigma^{WW}_T(0) - \frac{2s_W}{c_W M^2_Z}\Sigma^{ZA}_T(0) - \frac{1}{M^2_Z}\Sigma^{ZZ}_T(0) \tag{312}$$

where $\Sigma^{\rm new}$ stands for the self-energy corrections from new physics, and $\Pi(p^2) = \Sigma(p^2)/p^2$. Under the assumption $U = 0$, the numerical value of S and T from multiparameter fit at 95% CL are [41]

$$S = -0.01 \pm 0.14\ ,\ T = 0.04 \pm 0.12. \tag{313}$$

3.3.2 LHC Search

Due to the Z_2 symmetry, fermionic dark matter must be produced in pairs, and particles heavier than χ_l^0 eventually decay into χ_l^0. The dark matter pair production channels at hadron colliders include

$$q\bar{q}' \to W^{*-} \to \chi^{\pm}(\to \chi_l^0 W^{*\pm}) + \chi^0(\to \chi_l^0 + Z^*/H), \tag{314}$$

$$q\bar{q}' \to Z^* \to \chi^0(\to \chi_l^0 + Z^*/H) + \chi^0(\to \chi_l^0 + Z^*/H) \tag{315}$$

$$q\bar{q}' \to Z^* \to \chi^{\pm}(\to \chi_l^0 W^{\pm *}) + \chi^{\mp}(\to \chi_l^0 W^{\mp *}), \tag{316}$$

where $\chi^{\pm,0}$ denote the heavier charged and charged neutral particles, and they eventually devay to the lightest charged neutral particle through W,Z or H [3]. The fist production channel leads to the strongest constraints since the production cross section is largest. The reason is that Zff vertex is suppressed by weak mixing angle. The final Z, W and Higgs can decay either leptonically or hadronically, which lead to the signatures with hadronic, semi-leptonic and fully leptonic final states plus missing energy.

Fully hadronic final states benefit from large SM gauge boson decay branching ratios, thus this search channel is sensitive to the scenarios with large mass splitting. Multi lepton final state is sensitive to the scenario with moderate mass splitting, while this search fails in the compressed mass scenario, since the leptons from the decays become too soft to pass the event selection trigger. In such case, an energetic jet from initial state radiation can help enhance the detectability of the signal. The final state particles recoil against the ISR jet, i.e. the missing transverse momenta is at the same order as the jet, thus the signal can be detected. According to [115], the

[3]The heavier charged neutral particles can also decay via photon through loop-induced interaction, which is suppressed thus not included.

final state with a soft photon, jet and missing energy can also improve sensitivity of compressed mass scenario.

Fig. 20 from Ref. [116] illustrates the analysis conducted to search for Supersymmetry in the Bino-Wino simplified scenario. The figure displays the best exclusion limit achieved for each point in the mass plane $\{m_{\tilde{\chi}_1^0}, m_{\tilde{\chi}_1^\pm} = m_{\tilde{\chi}_2^0}\}$, where $m_{\tilde{\chi}_1^0}$ represents the Bino mass, and $m_{\tilde{\chi}_1^\pm} = m_{\tilde{\chi}_2^0}$ corresponds to the mass-degenerate Wino mass. It is evident from the plot that the fully hadronic final state provides the best sensitivity at large mass difference, and the semi-leptonic final state also shows comparable sensitivity in this scenario. On the other hand, the soft-lepton final state can reach the scenario where mass different is of tens of GeV.

3.3.3 Higgs Decays

In the doublet-triplet model, the decay rate of Higgs to di-photons is changed at one-loop level due to the presence of virtual charged fermions. The decay ratio with respect to the SM rate is given by

$$R_\gamma = \frac{\Gamma(h \to \gamma\gamma)}{\Gamma_{\rm SM}(h \to \gamma\gamma)} = \left|1 + \frac{A_\chi}{A_{\rm SM}}\right|^2 \tag{317}$$

The one-loop corrections for the SM, $A_{\rm SM}$ and the fermionic dark matter A_χ are defined as

$$A_{\rm SM} = \sum_f N_c A_f^2 A_F(\tau_F) + A_B(\tau_W)\ ,\ A_\chi = \sum_\chi Q_\chi^2 y_\chi \frac{v}{m_\chi} A_F(\tau_\chi) \tag{318}$$

with $\tau_i = m_H^2/4m_i^2$. N_c is the color number of SM fermions, and m_H is the Higgs mass. Q_χ and y_χ are the charge number and Yukawa coupling of new fermions. The loop functions $A_{f,B}$ for $\tau \leq 1$ are given by [103, 117, 118, 119]

$$A_F(\tau) = \frac{2}{\tau^2}\Big\{\tau + (\tau - 1)\arcsin^2\sqrt{\tau}\Big\},$$

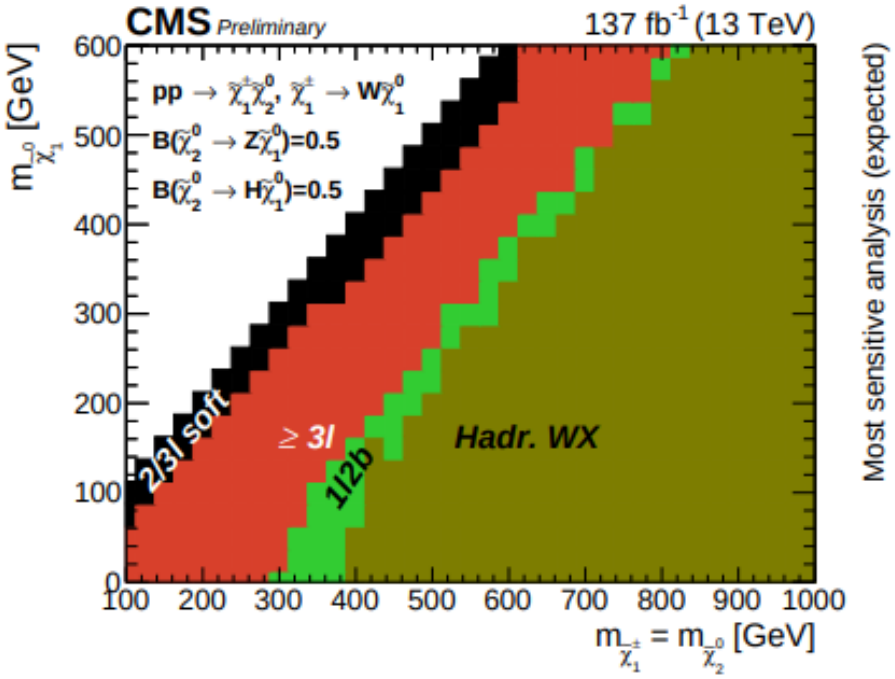

Figure 20: The analysis of searching for Suppersymmetry in Bino-Wino simplified scenario with the best exclusion limit for each point in the mass plane $\{m_{\tilde{\chi}_1^0}, m_{\tilde{\chi}_1^\pm} = m_{\tilde{\chi}_2^0}\}$, where $m_{\tilde{\chi}_1^0}$ is the Bino mass, and $m_{\tilde{\chi}_1^\pm} = m_{\tilde{\chi}_2^0}$ is the mass degenerate Wino mass. The charged Wino decays through W boson. The charge neutral Wino can decay via either Z or Higgs, and the branching ratio is assumed to be equal.

$$A_B(\tau) = -\frac{1}{\tau^2}\Big\{2\tau^2 + 3\tau + (6\tau - 2)\arcsin^2\sqrt{\tau}\Big\} \tag{319}$$

If the new fermions are light such that $\tau > 1$, then A_F becomes[117, 118, 119]

$$A_F(\tau) = \frac{2}{\tau^2}\Big\{\tau - \frac{\tau - 1}{4}\Big[\ln\frac{1+\sqrt{1-\tau^{-1}}}{1-\sqrt{1-\tau^{-1}}} - i\pi\Big]^2\Big\}. \tag{320}$$

However, the case of $\tau > 1$ has been excluded by LEP search [110] since $m_{\tilde{\chi}_1^\pm} > 103.5$ GeV $> m_H/2$.

For the three doublet-triplet models discussed in Section 3.2.2, the expression for A_χ is given by

$$A_\chi = \frac{v^2 y^2}{2(m_h^\pm - m_l^\pm)}\Big(\frac{1}{m_h^\pm}A_F(\tau_{\chi_h^\pm}) - \frac{1}{m_l^\pm}A_F(\tau_{\chi_l^\pm})\Big) \times \begin{cases} 1 & \text{for DDTM} \\ 2 & \text{for DDTM0, MDTM} \end{cases} \tag{321}$$

The current measurements of R_γ from the ATLAS and CMS experiments at 95% CL are $R_\gamma^{\rm ATLAS} = 1.04^{+0.20}_{-0.18}$ [120] and $R_\gamma^{\rm CMS} = 1.12 \pm 0.18$ [121], respectively. The projected result at HL-LHC can be found in Ref. [122], in which the uncertainties are expected to reduced to 8% by combining ggF and bbH channel. The expected result at FCC-ee is $R_\gamma^{\rm FCC-ee} = 1 \pm 0.18$[123]. However, this precision is comparatively lower than the projected HL-LHC result thus implementing the FCC-ee experiment for studying R_γ may not be necessary.

3.4 Impact on $\sigma(e^+e^- \to ZH)$

The deviation of $\sigma(e^+e^- \to ZH)$ due to new fermions is defined as

$$\delta = \frac{\sigma^{\rm FDM}(e^+e^- \to ZH)}{\sigma^{\rm SM}(e^+e^- \to ZH)}, \tag{322}$$

where $\sigma^{\rm FDM}$ considers the contribution from new fermions only. Both integrated cross sections are computed assuming unpolarized electron-positron beams. The inclusion of polarized beams does not introduce any changes, as all dark sector fermions are considered to be vector fermions. The Standard Model contribution, $\sigma^{\rm SM}(e^+e^- \to$

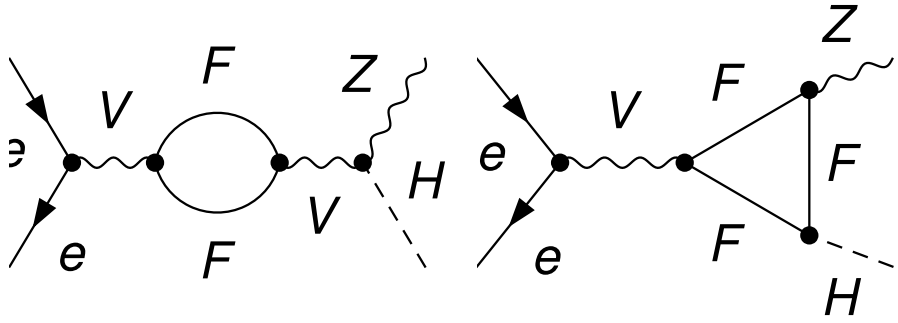

Figure 21: Self-energy (left) and vertex (right) Feynman diagrams with new fermions, denoted as F, and $V = \gamma, Z$.

ZH), takes into account one-loop EW as well as fermionic two-loop electroweak corrections, and the corresponding result is obtained from Table 3. On the other hand, the cross section for the process involving dark sector fermions, $\sigma^{\rm FDM}(e^+e^- \to ZH)$, incorporates one-loop electroweak corrections only.

At the one-loop level, the inclusion of new fermions contributes to $\sigma^{\rm FDM}(e^+e^- \to ZH)$ through self-energy and vertex contributions. The corresponding Feynman diagrams illustrating these contributions are depicted in Fig. 21. It is worth noting that the vertex contributions with $V = A$ dominate in this case. This dominance arises from the large Yukawa coupling and the less $\chi\overline{\chi}Z$ couplings, which is suppressed by weak mixing angle.

Input parameters used are same as Eq.244, and on-shell renormalization scheme is employed for fields, mass and electromagnetic coupling e. The $\alpha(0)$ scheme is used

for the latter, i.e. e is renormalized to its value in Thomson limit. In Sec.1.2.3.1, we discussed that the SM electromagnetic renormalization constant $\delta Z_e^{\rm SM}$ shown in Eq.81 is ill-defined due to light fermions, while this problem does not appear in calculating the contributions from dark sector fermions, $\delta Z_e^{\rm FDM}$, since new charged fermions are all massive. Besides, dark fermions are intermediate states so dark matter fields and masses do not need to be renormalized.

3.4.1 Majorana Singlet-Double Model (MSDM)

For Majorana singlet-doublet model, we choose $y, m_h^0, \Delta m_{hl} = m_h^0 - m_l^0$ as free parameters. There are two solutions to the relations between the Lagrangian parameter set, $\{m_S, m_D, y\}$, and the free parameter set we chosen, which originate from the mixing angle, $\sin^2\theta_4$. In terms of free parameters, it is written as

$$\sin^2\theta_4 = \frac{1}{2}\Big(1 \pm \sqrt{1 - \frac{4}{x^2}}\Big), \tag{323}$$

where $x = \Delta m/(vy)$. The positive solution leads to doublet-dominant χ_h^0, thus we refer this solution as doublet-dominant scenario, and the other as singlet-dominant scenario. Besides, $x \geq 2$ is required to satisfy the condition $\sin^2\theta_2 \leq 1$, which gives rises to large mass difference between χ_h^0 and χ_l^0 assuming $y = \mathcal{O}(1)$, $\Delta m = \mathcal{O}(\ 500\ \text{GeV}\ )$. To constrain dark matter particles with large mass difference, we implement the collider search with energetic leptonic and hadronic final states [116, 124, 125, 126, 127].

In the doublet-dominant scenario, the dark matter candidate remains mostly a singlet, and all three heavy particles are nearly degenerate masses doublets. This scenario is similar to the Bino-Higgsino system (with decoupled Wino) in the Minimal Supersymmetric Standard Model (MSSM) for $\tan\beta = 1$ and $y = g$. Fig. 22

displays the results of a parameter scan for $y = 1$ (upper plot) and $y = 1.5$ (lower plot). In each plot, different size of the cross section relative deviation is illustrated with different colored stars. The green, yellow, red, and purple stars represent deviations of $\{0, 0.5\%\}$, $\{0.5\%, 1\%\}$, $\{1\%, 3\%\}$, and $\{3\%, \infty\}$ respectively. Parameter space points excluded by oblique parameters is indicated by gray stars, but they do not appear in the Majorana singlet-doublet model due to custodial symmetry. The most stringent constraint in current LHC data arises from searches of Higgsino pair production with fully hadronic final state, denoted as "4q, ATLAS" in Fig.. 22. For massless dark matter, mass differences smaller than 900 GeV are excluded at 95% confidence level (CL). The expected 95% CL exclusion region at HL-LHC, focusing on the final state with 1 lepton and 2 b-jets, places an upper limit on Δm_{hl} around 1100 GeV. For $y = 1$, only a small part of the survived parameter space points yields deviations greater than 1%. More parameter points lead to deviations greater than 3% for $y = 1.5$.

In singlet-dominant scenario, $m_h^0 \approx m_S \gg m_D \approx m_l^0$, thus the production channel from $pp \to \chi_D^{0,\pm}\chi_D^{0,\mp}$. Due to the small mass difference between pure doublet and the dark matter candidate, we implement the collider search for compressed Higgsinos [124, 129, 130, 131, 132, 133] and replace Δm_{hl} by $\Delta m_{Dl} = m_D - m_l^0$. The result of a parameter scan in the singlet-dominant region with $y = 1$ fixed is shown in Fig. 23. Two regions exhibit $\delta \geq 0.5\%$: $m_l^0 \leq 50, \text{GeV}$ and $m_l^0 \approx 100, \text{GeV}$. The first region leads to large relative deviations due to the threshold effects and has already been excluded by LEP. In the second region, m_h^0 reaches its minimum value. The LHC search with three soft lepton in the final states excludes mass difference up to 60 GeV at 95% CL. Increasing the Yukawa coupling to 1.5 does not cause any qualitative differences thus not shown.

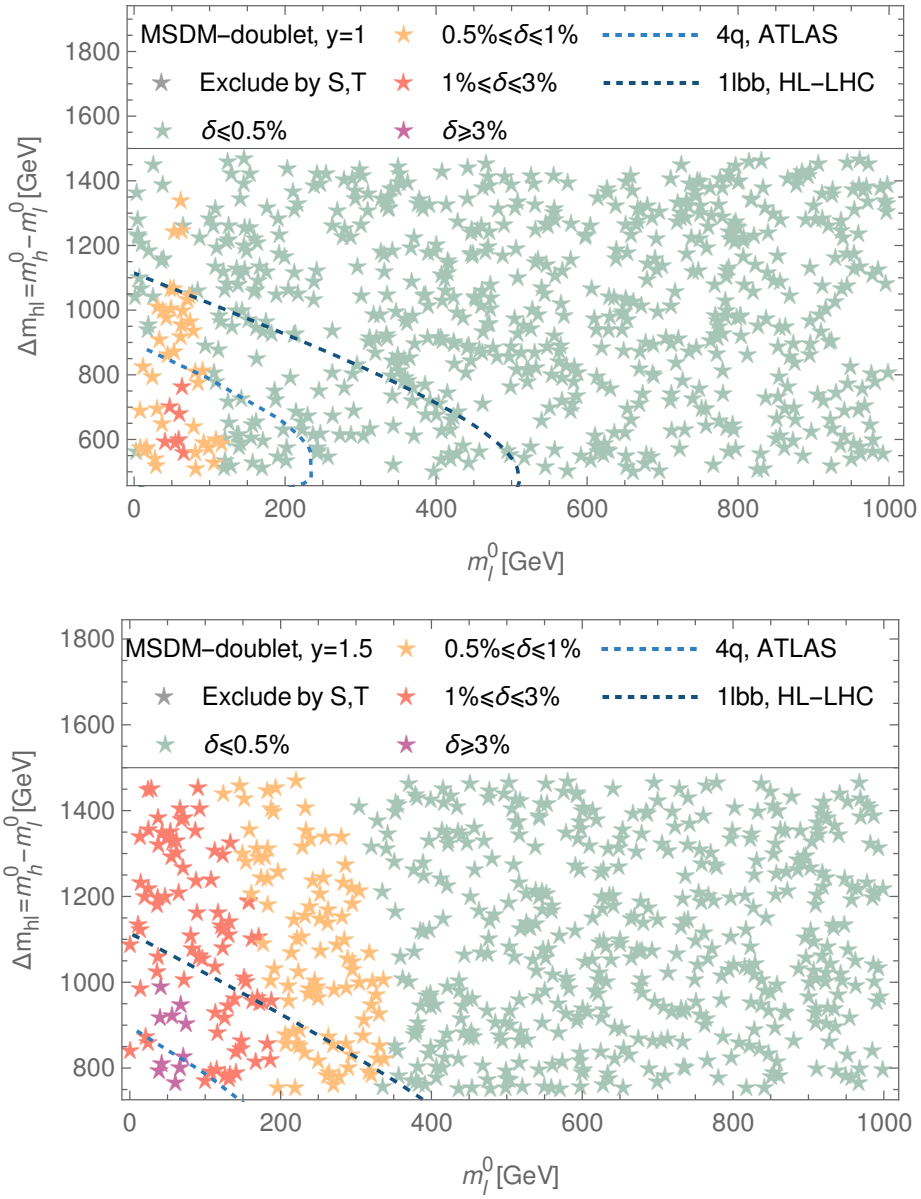

Figure 22: Parameter scan result for Majorana singlet-doublet model with $y = 1$ and $y = 1.5$ in doublet-dominant scenario, together with current and projected LHC constraints from Refs. [125] ("4q, ATLAS") and [127], ("1lbb, HL-LHC"), respectively.

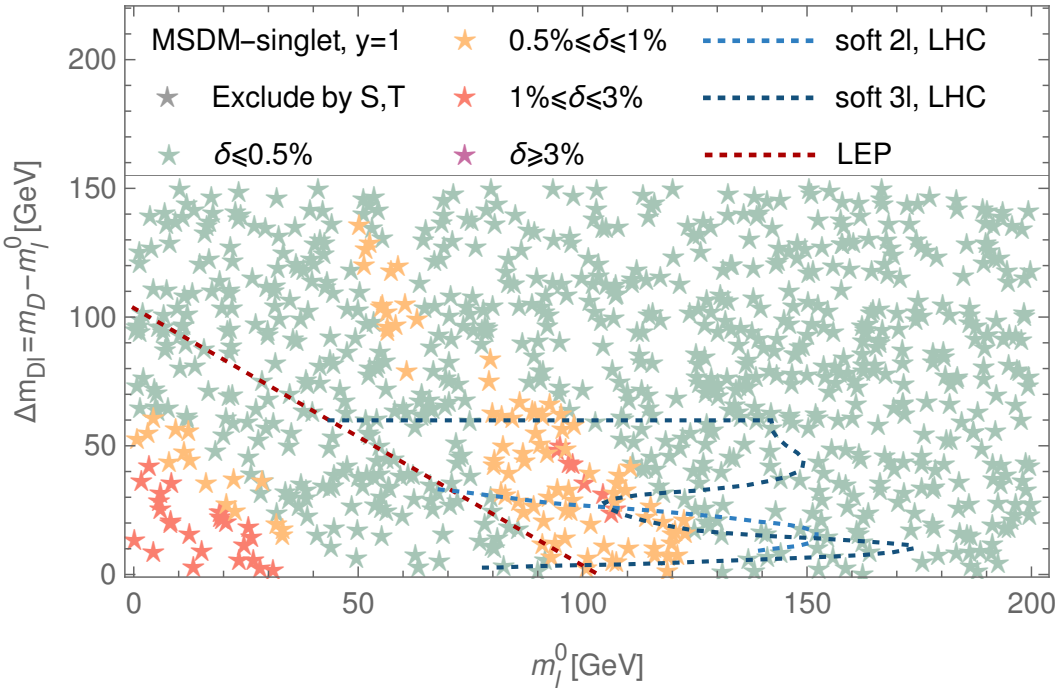

Figure 23: Parameter scan result for Majorana singlet-doublet model with $y = 1$ in singlet-dominant scenario, together with direct search constraints from LEP [110] and LHC [129, 131].

3.4.2 Dirac Singlet-Double Model (DSDM)

In the Dirac singlet-doublet model, the chosen set of free parameters consists of y, m_l^0 and $\Delta m_{\rm hl} = m_h^0 - m_l^0$. Similar to the MSDM, the chosen free parameters lead to the doublet-dominant and singlet-dominant scenario, according to the two solutions of the mixing angle

$$\sin^2\theta_2 = \frac{1}{2}\left(1 \pm \sqrt{1 - \frac{2}{x^2}}\right) \tag{324}$$

where $x = \Delta m_{\rm hl}/(vy) \geq \sqrt{2}$. Besides, it also give rise to $\mathcal{O}$(350GeV mass differences between χ_h^0 and χ_l^0 assuming $y = \mathcal{O}(1)$.

Fig. 24 displays the distribution of δ in the doublet-dominant scenario for two different values of y, $y = 1$ and $y = 1.5$. For $y = 1$, the oblique parameters exclude heavy neutral particle mass below 750 GeV. As for $y = 1.5$, $m_h^0 \lesssim 1500$GeV is excluded. The dashed lines correspond to the constraints from collider search, which are identical to the MSDM in doublet-dominant scenario. The DSDM in the doublet-dominant scenario is also similar to the Bino-Higgsino scenario, thus these constraints can be directly incorporated. For $y = 1$, most of the parameter space points survive, while only a few points lead to $\delta \geq 0.5\%$. These points are sssociated with TeV scale mass difference, while relatively light χ_l^0. For $y = 1.5$, survived parameter space points with $\delta \geq 0.5\%$ corresponds to much heavier χ_l^0.

In the singlet-dominant scenario, heavy neutral particle, χ_h^0, is singlet-dominant thus the production channel involving χ_h^0 is suppressed. The relevant channel is $pp \to \chi^{\pm}\chi^{\mp}$, which is equivalent to charged Higgsino pair production [134]. Therefore, in this scenario, it is more convenient to use $\Delta m_{\rm Dl} = m_D - m_l^0$ as free parameters. The expected 95% CL exclusion contours from the search for charged Higgsino pair production at the LHC (assuming 100 fb^{-1} at 13 TeV) and HL-LHC (assuming 3 ab^{-1} at 13 TeV) are implemented in Fig. 25 and excludes the mass difference below 20 GeV for $m_l^0 \leq 190$GeV . The region where $m_D \leq 103.5$GeV , indicated by the red dashed line, has been excluded by LEP [110]. For $y = 1.5$, most points in the region $\Delta m_{\rm Dl} \geq 20$GeV are excluded by the oblique parameters, resulting in the survived points with $\delta \geq 0.5\%$ concentrate in the region $\Delta m_{\rm Dl} \approx 20$GeV . For $y = 1$, more points are survived, and they can have various different mass differences. In both plots, survived points can lead to $\delta \geq 0.5\%$, which indicate that the future Higgs factories can probe the parameter space not covered at the LHC.

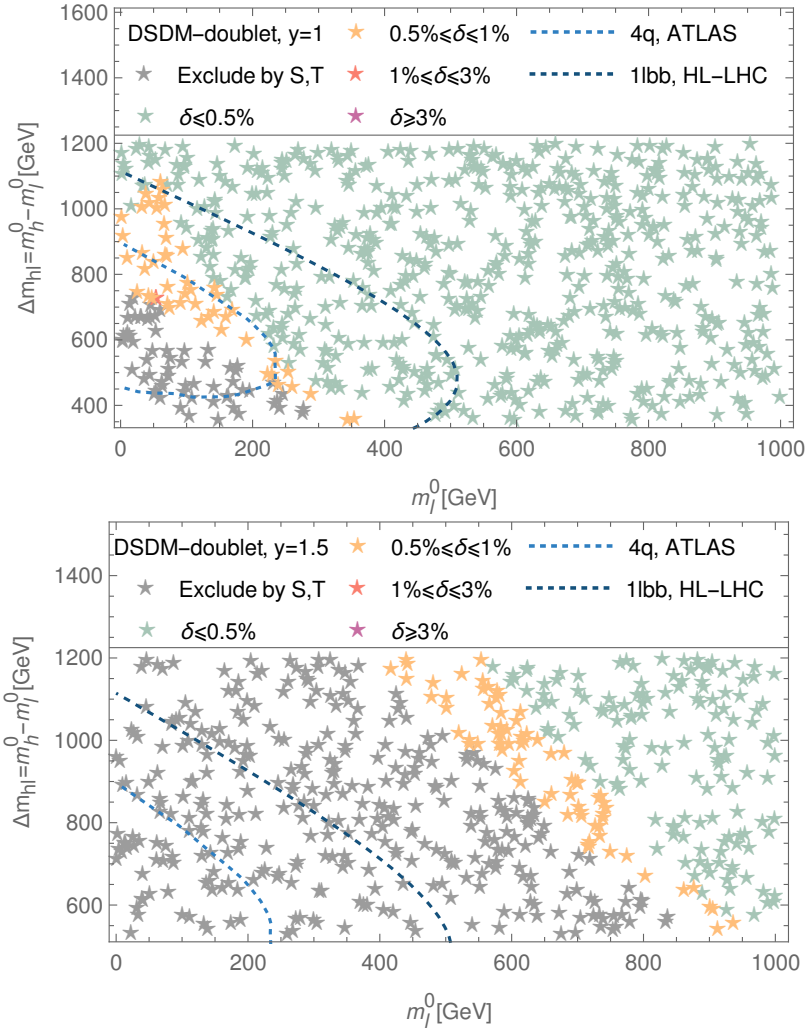

Figure 24: Parameter scan result of the DSDM in the doublet-dominant scenario at different values of m_l^0 and $\Delta m_{\rm hl}$, where the Yukawa coupling is chosen to be $y = 1$ in the upper plot and $y = 1.5$ in the lower one. The dashed lines are the 95% CL exclusion contour based on Refs. [125] ("4q, ATLAS") and [127], ("1lbb, HL-LHC"), respectively.

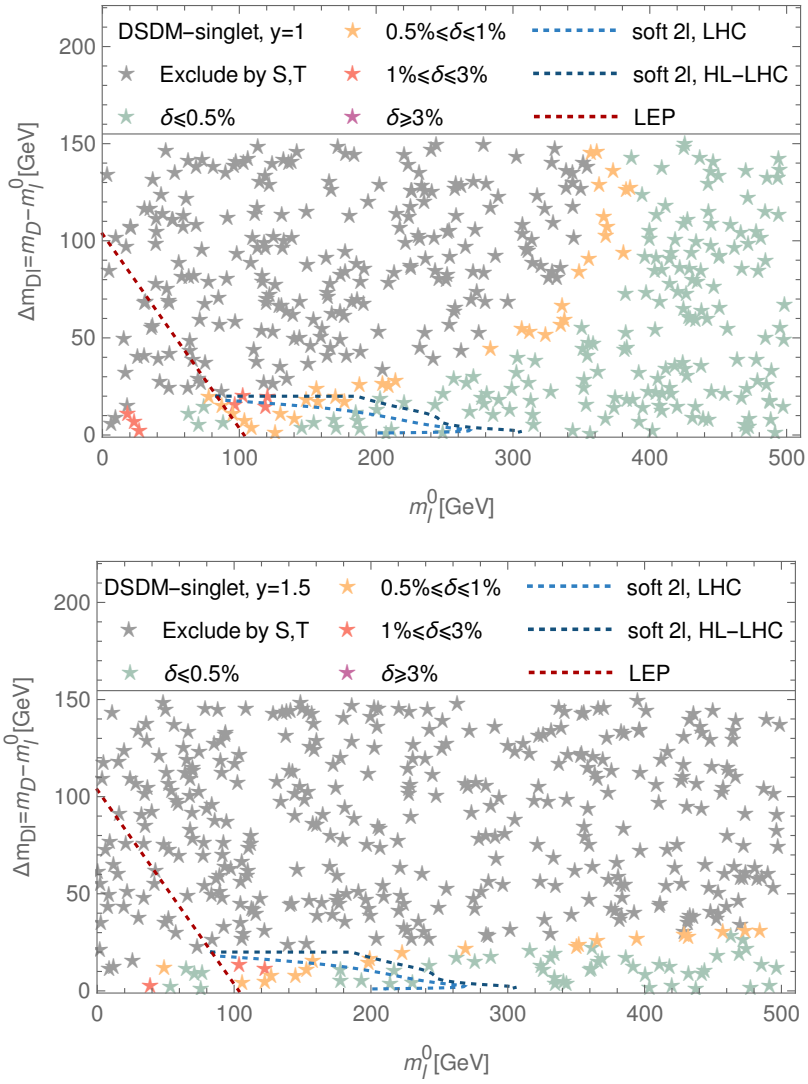

Figure 25: Parameter scan result of the DSDM in the singlet-dominant scenario with Yukawa coupling $y = 1$ (upper) and $y = 1.5$ (lower). The LHC exclusion curves from direct searches for the new fermions are based on Ref. [134].

3.4.3 Majorana Doublet-Triplet Model (MDTM)

For Majorana doublet-triplet model, y, m_l^0 and $\Delta m_{\rm hl} = m_h^0 - m_l^0$ are chosen as free parameters. Similar to the Majorana singlet-doublet model, for each choice of free parameters $\{y, \Delta m_{\rm hl}\}$, the mixing angle has two different values

$$\sin^2\theta_2 = \frac{1}{2}\Big(1 \pm \sqrt{1 - \frac{2}{x^2}}\Big), \tag{325}$$

where $x = \Delta m_{\rm hl}/(vy) \geq \sqrt{2}$ to ensure all parameters are real. Following what we did in the Majorana singlet-doublet model, we will refer the positive solution as " doublet-dominant " scenario, under which $\chi_h^{0,+}$ is doublet-dominant, and the second as " triplet-dominant " scenario. Besides, $x \geq \sqrt{2}$, which corresponds to a mass difference of the order $\Delta m_{\rm hl} = \mathcal{O}(400\ \text{GeV})$, must be satisfied to ensure all parameters are real. As discussed in Sec. 3.4.1, collider search through energetic leptons and hadronic jets can put stringent bound on dark matter with large mass differences. These searches has been performed in [124, 125, 126, 127, 116].

In the doublet-dominant scenario, three heavy particles are all doublets and nearly mass degenerate, while two light particles are triplets, which is similar to the Wino-Higgsinos scenario (with decoupled Bino) in MSSM. In the Wino-Higgsino scenario, it is typically assumed that the three Higgsino components are mass degenerate, namely $m_{\tilde{\chi}_1^\pm} = m_{\tilde{\chi}_1^0} = m_{\tilde{\chi}_2^0}$. However, in our model, the mass ordering is such that $m_m^0 < m_h^0 = m_h^\pm$. Despite this difference, when considering the effects of mixing angles and mass differences, the modifications to the cross section are found to be less than 10%. Consequently, the bounds on the mass difference are adjusted by approximately $\mathcal{O}(10\text{GeV})$, which is very small and causes no qualitative difference. Thus the results in Wino-Higgsino scenario can be directly implemented. Moreover, it is worth mentioning that the exclusion limits for Bino-Higgsino scenario [124, 126, 127, 116]

can also be implemented, which is due to the observation that exclusion limit for Wino-Higgsino scenario is almost same as the one for Bino-Higgsino scenario [125].

In the triplet-dominant scenario, the dark matter production channels include $pp \to \chi_h^{\pm}\chi_h^{\mp}, \chi_h^0\chi_h^{\pm}, \chi_m^0\chi_h^{0,\pm}$, where $\chi_h^{0,\pm}$ are mass degenerate triplet-dominant states, and χ_m^0 is pure doublet. Production channels involving χ_m^0 are suppressed by $\sin^2\theta_2 \approx 0$. Thus the dominant production channels are $pp \to \chi_h^{\pm}\chi_h^{\mp}, \chi_h^0\chi_h^{\pm}$, which is equivalent to Higgsino-Wino scenario. Additionally according to the analysis in Ref. [125], the exclusion limits for the Higgsino-Wino scenario are found to be very similar to those of the Bino-Wino scenario. Therefore, we also incorporate the exclusion contours obtained from studies on the Bino-Wino scenario [126, 127, 116].

Fig. 26 and Fig. 27 display the scan result in doublet- and triplet-dominant scenario respectively, together with the constraints from oblique parameters, branching fraction of the Higgs boson to di-photons, as well as the collider searches. The constraints of Higgs boson's branching fraction are denoted by the black solid, dashed and dot-dashed lines, which represent the upper limits of R_γ at the CMS, ATLAS as well as HL-LHC, respectively. The arrows point to the allowed regions.

The constraints from oblique parameter and R_γ exhibit similar behavior in both scenarios for a same Yukawa coupling. The oblique parameters exclude m_l^0 up to 50 GeV for $y = 1$, while exclude m_l^0 up to 150 GeV for $y = 2$. The constraint from R_γ covers a larger region, and the most stringent one comes from the projected result at the HL-LHC. The mass of χ_l^0 up to 300 GeV is excluded for a 1.5 TeV χ_h^0 in the case of $y = 1$, and $m_{\chi_l^0} \leq 800$ GeV is excluded in the case of $y = 2$.

The constraint from LHC collider searches in the doublet-dominant scenario is different from the triplet-dominant case. The exclusion contour in the triplet-dominant scenario is more stringent due to the higher pair production cross section of Winos compared to Higgsinos. The most stringent constraint comes from the

expected exclusion contour at the HL-LHC, excluding triplet masses up to 1.3 TeV and doublet masses up to 1.1 TeV, assuming a massless χ_l^0. For $y = 1$, all surviving points with $\delta \geq 0.5\%$ are expected to be excluded at 95% at the HL-LHC. Increasing y to 2 allows for more surviving points that satisfy $\delta \geq 0.5\%$, and the precise measurement of $\sigma(e^+e^- \to ZH)$ as well as R_γ can cover a larger region compared to the direct searches at the LHC and HL-LHC.

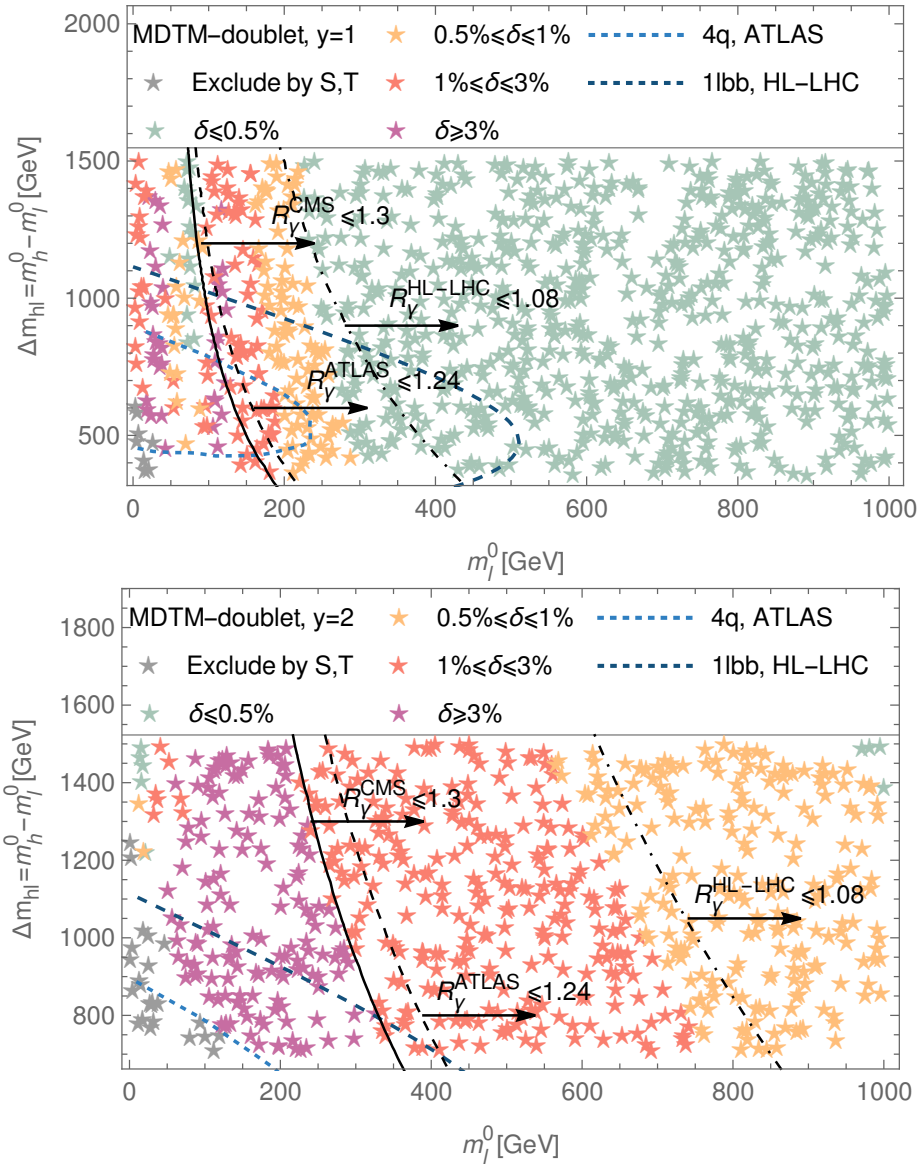

Figure 26: Parameter scan result for Majorana doublet-triplet model with $y = 1$ and $y = 2$ in doublet-dominant scenario, together with current and projected LHC constraints from Refs. [125] ("4q, ATLAS") and [127], ("1lbb, HL-LHC"), respectively. The upper bounds on R_γ at LHC and HL-LHC are from Refs.[120, 121, 122].

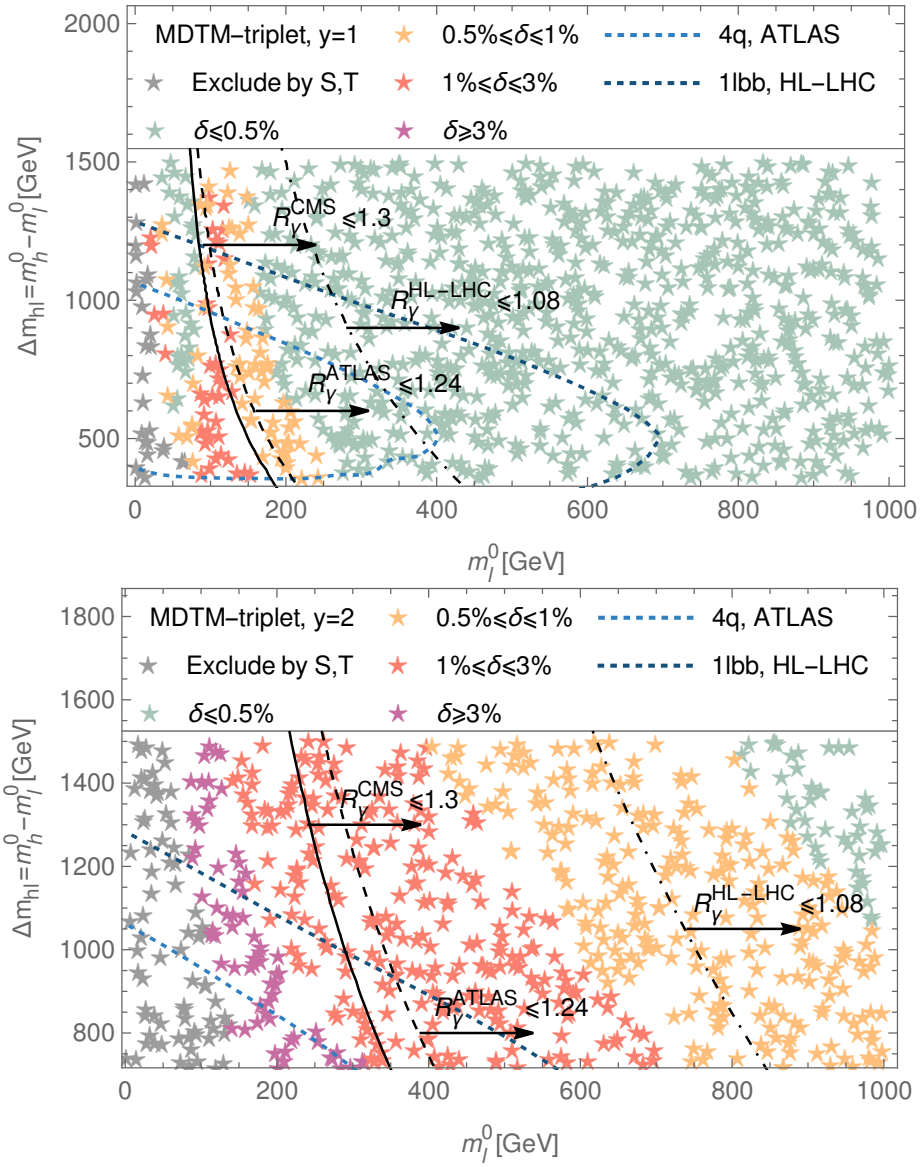

Figure 27: Parameter scan result for Majorana doublet-triplet model with $y = 1$ and $y = 2$ in triplet-dominant scenario, together with current and projected LHC constraints from Refs. [125] ("4q, ATLAS") and [127], ("1lbb, HL-LHC"), as well as the constraint from branching fraction of the Higgs boson to di-photons from Refs.[120, 121, 122].

3.4.4 Dirac Doublet-Triplet Model with $r = 0$ (DDTM0)

For Dirac doublet-triplet model with zero hypercharge, the free parameter set is $\{y, m_l^0, \Delta m_{\rm hl} = m_h^0 - m_l^0\}$. Similar to the Majorana singlet-doublet model, the mixing angles defined in Eq.299 have two different values for each choice of free parameters $\{y, m_{\rm hl}\}$, and are written as

$$\sin^2\theta_1 = \frac{1}{2}\Big(1 \pm \sqrt{1 - x^{-2}}\Big), \tag{326}$$

$$\sin^2\theta_2 = \frac{1}{2}\Big(1 \pm \frac{\sqrt{1 - x^{-2}}}{\sqrt{1 + x^{-2}}}\Big), \tag{327}$$

where $x = (m_h^0 + m_l^0)/(vy)$.[4] We refer to the positive solution as the "doublet-dominated scenario," in which $\chi_h^{0,\pm}$ are mainly doublets, and the other solution stands for the "triplet-dominated scenario."

Fig. 28 shows the mass distributions of the five particles as a function of $\Delta m_{\rm hl}$ for two Yukawa coupling choices, $y = 1$ and $y = 1.5$, with m_l^0 set to 300 GeV. In the doublet-dominant scenario, the lightest particle, $\chi_m^{\pm}$, is charged, resulting in the exclusion of the entire doublet-dominant scenario. However, in the triplet-dominated scenario, χ_l^0 can be the lightest particle if $\Delta m_{\rm hl} > v^2y^2/8m_l^0$. The figure also reveals that $m_l^0 \approx m_l^{\pm}$ and $m_T \approx m_h^0 \approx m_h^{\pm}$, as previously demonstrated in Fig. 18. This behavior can be further explained by Fig. 29, which displays the mixing angle distributions in the triplet-dominated scenario. The plot clearly illustrates that $\cos\theta_2 \approx \cos\theta_1 \approx 1$. According to Eq.299, large values of $\cos\theta_{2,1}$ indicate that the heavy particles, $\chi_h^{0,\pm}$, are predominantly triplets, resulting in their masses being close to m_T.

[4]The definition of x differs from other models, which is defined as $x = \Delta m/(vy)$, due to the replacement of m_l^0 with $-m_l^0$ to ensure that χ_l^0 is the lightest particle.

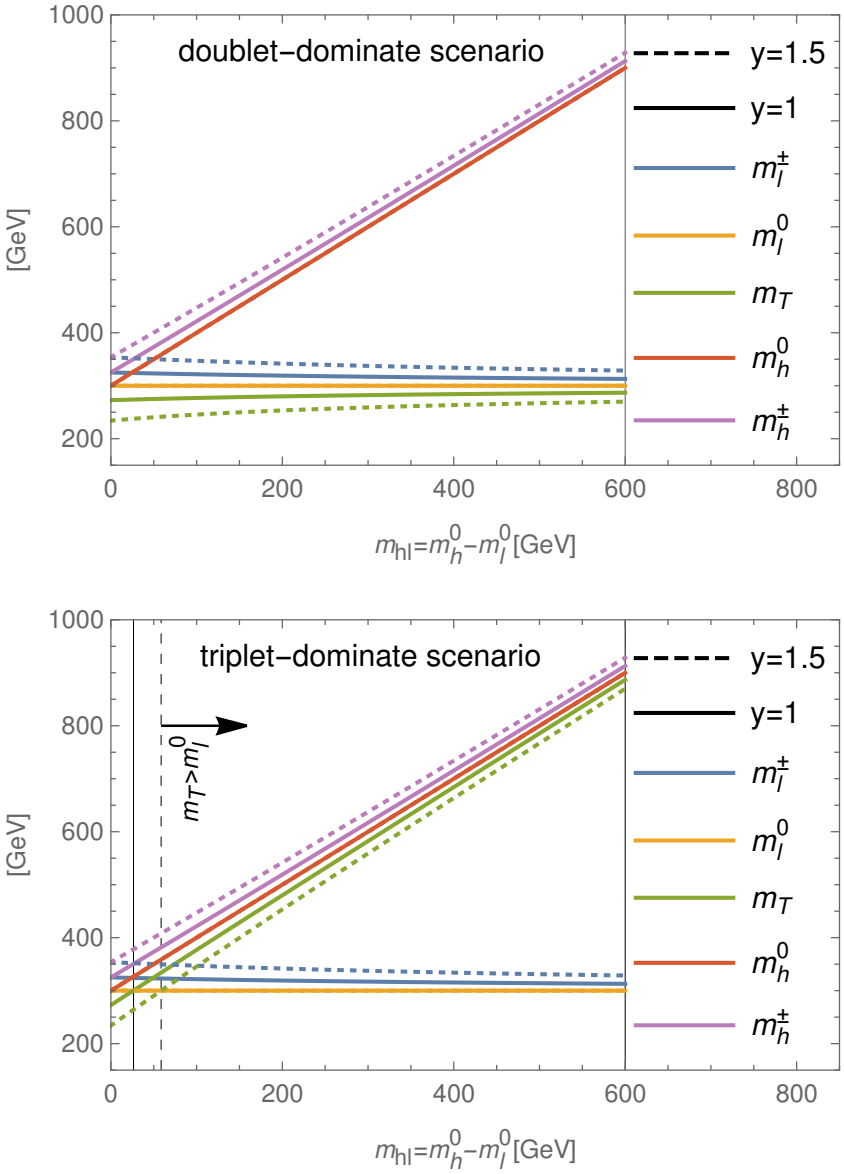

Figure 28: The mass distribution of five particles in the Dirac doublet-triplet model with $r = 0$, as functions of $\Delta m_{\rm hl}$ in the doublet-dominate scenario(upper) and triplet-dominate scenario(lower). The Yukawa coupling is chosen to be: $y = 1$ (solid) and $y = 1.5$ (dashed), and $m_l^0 = 300$ GeV in both plots.

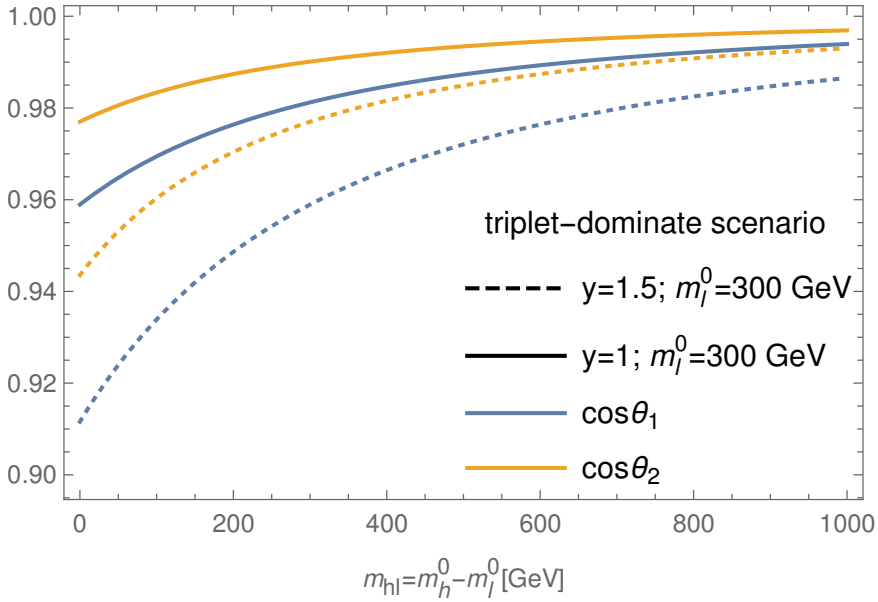

Figure 29: The distributions of charged neutral states mixing angle (blue), denoted as $\cos\theta_2$, and charged states mixing angle (yellow), denoted as $\cos\theta_1$, at different values of $\Delta m_{\rm hl}$ in the triplet-dominate scenario. The Yukawa coupling is chosen to be: $y = 1$ (solid) and $y = 1.5$ (dashed), and $m_l^0 = 300$ GeV in both plots.

Fig. 30 displays δ in triplet-dominant scenario at different values of m_l^0 and $\Delta m_{\rm hl}$, and the Yukawa coupling is chosen to be $y = 1(2)$ in the upper(lower) plot. In this figure, a new type of point is introduced and represented by dark gray stars. These points correspond to parameter choices that result in complex masses or $m_T < m_l^0$, and they are unphysical thus excluded. This condition removes a few points in the region of small mass differences both for $y = 1$ and $y = 2$, while more points are excluded due to oblique parameters for $y = 1$. As the Yukawa coupling increasing to 2, only a few points are not excluded by the oblique parameter.

For both Yukawa couplings, the parameter space points with $\delta \geq 0.5\%$ concentrate in the region with large mass difference, which can be best constrained through collider searches using energetic leptons and hadronic jets in the final states. The relevant channels includes the production of charged states pairs, $pp \to \chi_h^\pm \chi_h^\mp, \chi_m^\pm \chi_m^\mp$,[5], as well as the production of charged-neutral pairs, $pp \to \chi_h^0 \chi_h^\pm, \chi_h^0 \chi_m^\pm$.[6] The cross section of summing over all channels are approximately twice the cross section of Wino-pair productions, namely $pp \to \tilde{W}^\pm \tilde{W}^\mp + \tilde{W}^0 \tilde{W}^\pm$. Consequently, the 95% CL contour in this model corresponds to the 1σ exclusion region in the search for Wino-pair production, which can be obtained through extrapolation.

The results from the collider searches for Wino-pair production, as analyzed in Refs. [125, 127], are incorporated into Fig. 30. The most stringent constraint, from the expected 95% CL contour at the HL-LHC, excludes mass differences up to 1.3 TeV assuming a massless dark matter candidate. Combining the constraint from the Higgs diphoton decay branching fraction [120, 121, 122], all parameter points with $\delta \geq 0.5\%$ are excluded for $y = 1$. However, a few surviving points with $\delta \geq 0.5\%$ exist in the $y = 2$ case, resulting in TeV-scale heavy fermions. In Fig.31, the scan result for $y = 2.5$ is shown. The entire parameter region with $m_l^0 \leq 1$TeV is excluded by oblique parameters, necessitating an extension of m_l^0. Similar to the $y = 2$ case, the surviving parameter space points with $\delta \geq 0.5\%$ concentrate in the region where new fermions have TeV-scale masses. This region can be explored at a 100 TeV hadron collider, as analyzed in Ref. [128]. Additionally, precision measurements of the cross section for $e^+e^- \to ZH$ can provide complementary information to the direct searches conducted at a 100 TeV hadron collider.

[5]The production channel $pp \to \chi_l^\pm \chi_l^\mp$ is not taken into account since $m_l^\pm - m_l^0 = \mathcal{O}(20\text{ GeV})$.

[6]The production of neutral pairs, $pp \to \chi_h^0 \chi_h^0$, can also contribute. However, this channel is significantly suppressed by the factor $\sin^2\theta_1 \approx 0$.

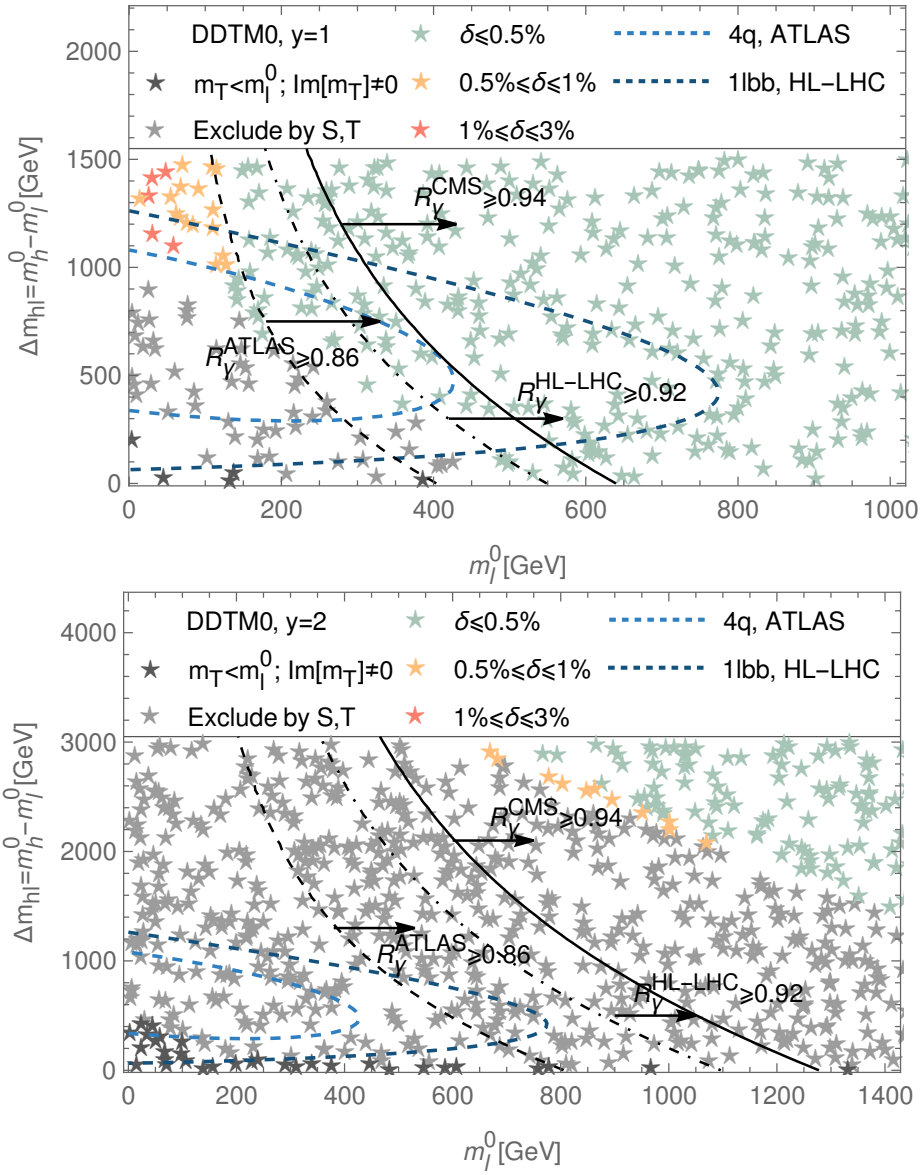

Figure 30: Parameter scan result for DDTM0 with $y = 1$ and $y = 2$ in the large mass difference region, together with current and projected LHC constraints from Refs. [125] ("4q, ATLAS") and [127], ("1lbb, HL-LHC"), respectively. The lower bounds on R_γ at LHC and HL-LHC are from Refs.[120, 121, 122].

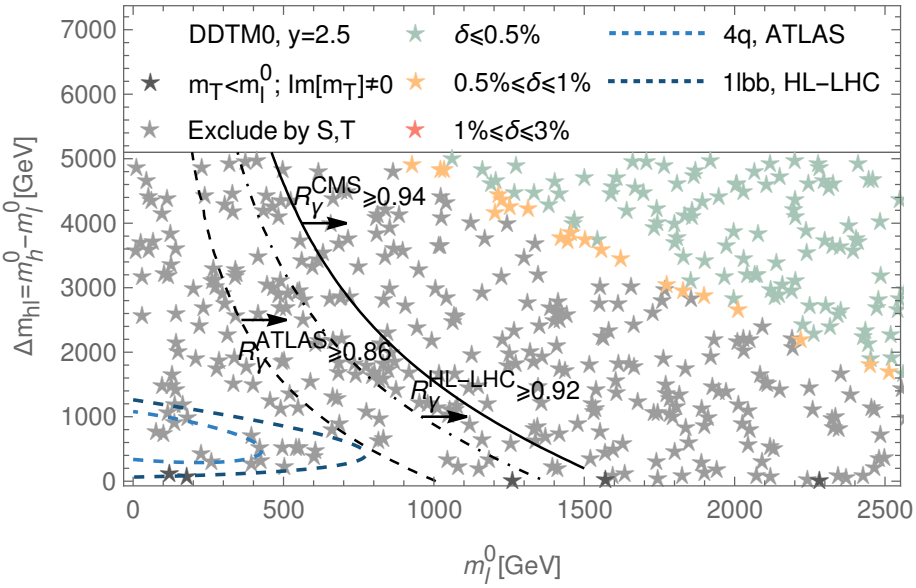

Figure 31: Parameter scan result for DDTM0 with $y = 2.5$ in the large mass difference region, together with current and projected LHC constraints from Refs. [125] ("4q, ATLAS") and [127], ("1lbb, HL-LHC"), respectively. The lower bounds on R_γ at LHC and HL-LHC are from Refs.[120, 121, 122].

3.4.5 Dirac Doublet-Triplet Model with $r = -1$ (DDTM1)

In the Dirac doublet-triplet model with $r = -1$, we consider the following free parameters: $\{y, m_l^0, \Delta m_{ll} = m_l^\pm - m_l^0\}$. Similar to the Majorana case, two solutions for the mixing angle in terms of these free parameters leads to two scenario: the doublet dominate scenario and triplet dominate scenario. In the doublet(triplet)-dominate scenario, m_l^+ is almost doublet(triplet). In both scenarios, the production

channel is limited to $pp \to m_l^\pm m_l^\mp$ [7] for two reasons: (a) $m_l^\pm$ is the lightest heavy particle; (b) all the other heavy particles are much heavier and effectively decouple. To illustrate the latter explicitly, we can express the masses of decoupled heavy particles in terms of Δm,

$$\begin{aligned}
&\frac{m_h^0 - m_l^0}{\Delta m_{ll}} = 1 + \frac{1}{4x^2} \ , \\
&\frac{m_h^\pm - m_l^0}{\Delta m_{ll}} = \frac{1}{4x^2} \ , \\
&\frac{m^{--} - m_l^0}{\Delta m_{ll}} = \frac{1}{2} + \frac{1}{8x^2} + \frac{1}{8}\sqrt{16 - \frac{24}{x} + \frac{1}{x^2}},
\end{aligned} \tag{328}$$

where $x = \Delta m_{ll}/(vY)$. To ensure all parameters real, the condition $x^2 \leq (3/4 - 1/\sqrt{2}) = 0.043$, is imposed, which leads to relative heavy m_h^0, m^{--} and $m_h^\pm$. Thus the production cross section involving those particles can be ignored.

For a doublet $\chi_l^\pm$, the production channel, $pp \to \chi_l^\pm \chi_l^\mp$, is equivalent to charged Higgsinos pair production. Besides, the condition $x^2 \leq 0.043$ causes Δm_{ll} of order 50 GeV for a $\mathcal{O}(1)$ Yukawa coupling. As explained in the previous section, scenarios with such small mass differences can be best searched for by using the hard jet plus soft leptons signature at the LHC. The expected 95% CL reach of LHC13 with 100fb^{-1} and 3ab^{-1} from the analysis in Ref.[134] is shown by the light and dark blue dotted lines in Fig. 32 respectively. The exclusion contour from LEP [110] (red dotted line) is also shown in the figure. These bounds are also imposed for the triplet $\chi_l^\pm$. To account for the differences of the production cross section between the doublet- and triplet-dominant scenario, the following recast was performed:

$$\mathcal{S}^{\text{Triplet}} = \mathcal{S}^{\text{Doublet}} \times \frac{\sigma^{\text{Triplet}(pp \to \chi_l^\pm \chi_l^\mp)}}{\sigma^{\text{Doublet}(pp \to \chi_l^\pm \chi_l^\mp)}} \approx \mathcal{S}^{\text{Doublet}} \times \frac{1}{5} \tag{329}$$

[7] The production channel, $pp \to \chi_l^\pm \chi_l^0$, can also contribute, and leads the final states with soft lepton and jet [135]. However, the exclusion region from this channel is weaker than $pp \to m_l^\pm m_l^\mp$ thus not included.

where "Triplet(Doublet)" stands for the triplet(doublet)-dominant scenario. This equation implies that the 95% C.L. exclusion contour for a triplet $\chi_l^{\pm}$ corresponds to 10σ exclusion contour in the doublet case, which is realized by extrapolating Table. 4 of Ref. [134].

The distributions of δ in the doublet- and triplet-dominate scenario are shown in Fig. 32 and Fig. 33 respectively. In both scenarios, the Yukawa coupling is considered with values 1 and 2, and δ exhibits similar distributions for a same Yukawa coupling.

In the doublet-dominant scenario for the case of $y = 1$, the oblique parameters exclude the region of large mass differences for small m_l^0. The constraint from R_γ at HL-LHC excludes a few more points at small mass difference. As the Yukawa coupling increasing to 2, all parameter points with $\Delta m_{ll} \geq 16$GeV are ruled out by the oblique parameters. The constraint from collider search for charged Higgsino pair productions, which is complementary to the constraints from oblique parameters, and R_γ, can in addition exclude masses of χ_l^0 up to 200GeV for $\Delta m_{ll} \leq 20$GeV. As a consequence in the case of $y = 2$, the survived points focus in the region with $\Delta m_{ll} \leq 20$GeV and $m_l^0 \geq 200$ GeV . While for $y = 1$, the survived points are also in the region $m_l^0 \geq 200$ GeV , but there is less stringent bound on $\Delta m_{\rm ll}$.

The scan result in the triplet-dominant scenario exhibit a similar behavior compared to the doublet case. Although the collider search is not as strong as the charged Higgsino case due to the suppression of production cross section, the oblique parameters exclude more points. As a consequence, less points are survived, but they can also yield $\delta \geq 0.5\%$.

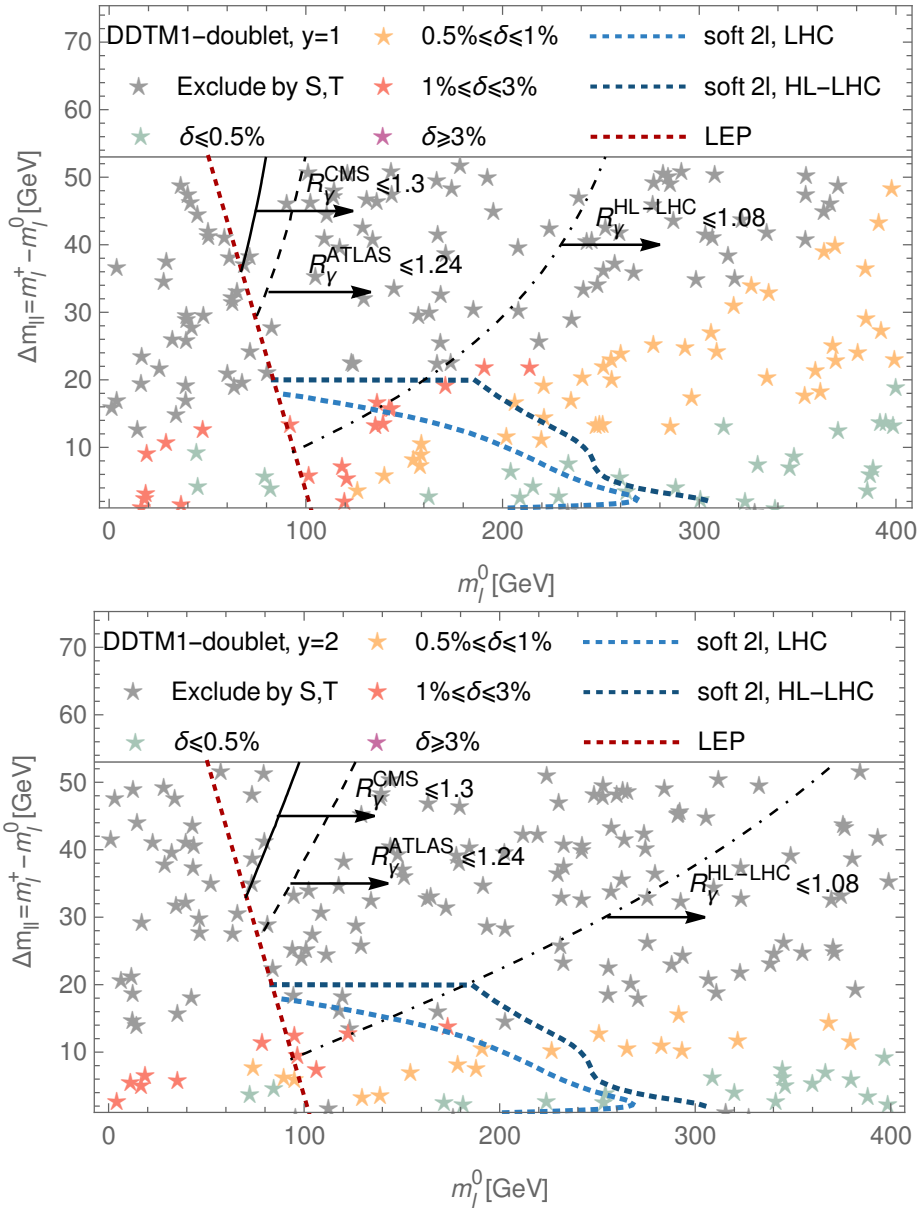

Figure 32: Parameter scan result for DDTM with $y = 1$(upper) and $y = 2$(lower) in the doublet-dominant scenario together with the constraint from LEP [110], the expected 95% C.L. reach at LHC and HL-LHC from Ref.[134], and upper bounds of R_γ at LHC and HL-LHC from Refs.[120, 121, 122].

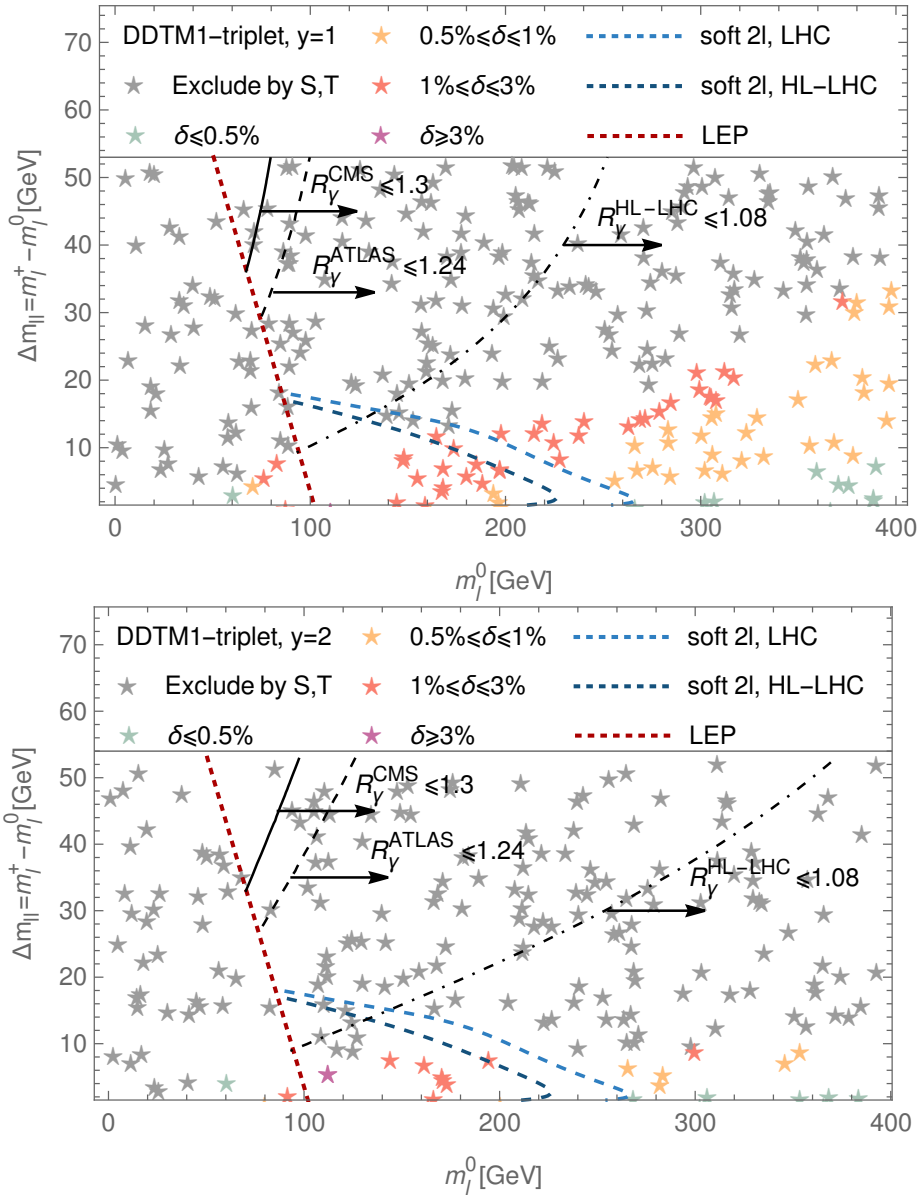

Figure 33: Parameter scan result for DDTM with $y = 1$(upper) and $y = 2$(lower) in the triplet-dominant scenario together with the constraint from LEP [110], the expected 95% C.L. reach at LHC and HL-LHC from Ref.[134], and upper bounds of R_γ at LHC and HL-LHC from Refs.[120, 121, 122].

4.0 Conclusions

The future Higgs factories, such as the International Linear Collider (ILC), Future Circular Collider electron-positron (FCC-ee), and Circular Electron Positron Collider (CEPC), are poised to provide unprecedented experimental accuracy in measuring the properties of the Higgs boson. Among the dominant production channels, the Higgsstrahlung process $e^+e^- \to ZH$ plays a critical role in extracting the Higgs to Z-boson coupling. However, to fully exploit the potential of these experimental facilities, it is imperative that theoretical uncertainties do not surpass the experimental ones.

To achieve this, the theoretical precision of the Higgsstrahlung process must be at least comparable to the anticipated experimental accuracy of 1.2% at ILC, 0.4% at FCC-ee, and 0.5% at CEPC. The inclusion of Next-to-Next-to-Leading Order Electroweak (NNLO EW) corrections has paved the way towards achieving such a goal. With the addition of these corrections, the theoretical uncertainty is reduced to about 0.7%, making it comparable to the experimental accuracy. The attainment of such a level of theoretical and experimental precision is a major milestone in the pursuit of precision measurements of the Higgs boson, and opens up new avenues for exploring the properties of the Standard Model and beyond.

In the pursuit of high-precision measurements at future Higgs factories, it is expected that deviations in the cross section measurements of the Higgsstrahlung process may become apparent. These deviations, if observed, would need to be explained by new physics beyond the Standard Model. To address this possibility, we explore the Higgs portal models with fermion multiplets as a potential source of such new physics and investigate the resulting deviations on the cross section of the

Higgsstrahlung process. We specifically focus on regions of the parameter space that exhibit significant deviations and find that some portions of this parameter space may be accessible to future hadron colliders. Our investigation sheds light on the potential implications of these new models and the potential for their detection in future experiments.

Appendix A One-Loop Tensor Integral Reduction

This Appendix illustrates the deviation from Eq. 124 to Eq. 125. Start with Eq. 124, which has the following form

$$
\begin{aligned}
0 = & [2T_0^4(0) + Y_{00}T_0^5] \times \det \begin{pmatrix} 2p_1 \cdot p_1 & \cdots & 2p_1 \cdot p_4 \\ \vdots & \ddots & \vdots \\ 2p_4 \cdot p_1 & \cdots & 2p_4 \cdot p_4 \end{pmatrix} \\
& + \sum_{k=1}^{4} (-1)^k \times [T_\mu^4(k) - (T^{4\mu}(0) + p_4^\mu T_0^4(0)) + p_{4\mu} T_0^4(0) + (Y_{k0} - Y_{00}) T_\mu^5] \\
& \times \det \begin{pmatrix} 2p_1^\mu & \cdots & 2p_4^\mu \\ \vdots & \ddots & \vdots \\ 2p_{k-1} \cdot p_1 & \cdots & 2p_{k-1} \cdot p_4 \\ 2p_{k+1} \cdot p_1 & \cdots & 2p_{k+1} \cdot p_4 \\ \vdots & \ddots & \vdots \end{pmatrix}
\end{aligned} \tag{330}
$$

Writing in this form helps the algebraic simplification: (1) $T_\mu^4(k) \times \det(\cdots) = 0$; (2) $T_\mu^4(0) + p_{4\mu} T_0^4(0) \times \det(\cdots) = 0$; (3) $\sum_{k=1}^{3} p_{4\mu} T_0^4(0) \times \det(\cdots) = 0$. Thus, Eq.330 becomes

$$
\begin{aligned}
0 = & [2T_0^4(0) + Y_{00}T_0^5] \times \det \begin{pmatrix} 2p_1 \cdot p_1 & \cdots & 2p_1 \cdot p_4 \\ \vdots & \ddots & \vdots \\ 2p_4 \cdot p_1 & \cdots & 2p_4 \cdot p_4 \end{pmatrix} \\
& + T_0^4(0) \times \det \begin{pmatrix} 2p_1 \cdot p_4 & \cdots & 2p_4 \cdot p_4 \\ \vdots & \ddots & \vdots \\ 2p_3 \cdot p_1 & \cdots & 2p_3 \cdot p_4 \end{pmatrix}
\end{aligned}
$$

$$+\sum_{k=1}^{4}(-1)^k(Y_{k0}-Y_{00})T_\mu^5\times\det\begin{pmatrix}2p_1^\mu & \cdots & 2p_4^\mu\\ \vdots & \ddots & \vdots\\ 2p_{k-1}\cdot p_1 & \cdots & 2p_{k-1}\cdot p_4\\ 2p_{k+1}\cdot p_1 & \cdots & 2p_{k+1}\cdot p_4\\ \vdots & \ddots & \vdots\end{pmatrix} \tag{331}$$

According to the property

$$\begin{pmatrix}2p_1\cdot p_4 & \cdots & 2p_4\cdot p_4\\ \vdots & \ddots & \vdots\\ 2p_3\cdot p_1 & \cdots & 2p_3\cdot p_4\end{pmatrix}=(-1)\times\det\begin{pmatrix}2p_1\cdot p_1 & \cdots & 2p_1\cdot p_4\\ \vdots & \ddots & \vdots\\ 2p_4\cdot p_1 & \cdots & 2p_4\cdot p_4\end{pmatrix} \tag{332}$$

Eq.331 can be further simplified to

$$\begin{aligned}0=&[T_0^4(0)+Y_{00}T_0^5]\times\det\begin{pmatrix}2p_1\cdot p_1 & \cdots & 2p_1\cdot p_4\\ \vdots & \ddots & \vdots\\ 2p_4\cdot p_1 & \cdots & 2p_4\cdot p_4\end{pmatrix}\\ &+\sum_{k=1}^{4}(-1)^k(Y_{k0}-Y_{00})T_\mu^5\times\det\begin{pmatrix}2p_1^\mu & \cdots & 2p_4^\mu\\ \vdots & \ddots & \vdots\\ 2p_{k-1}\cdot p_1 & \cdots & 2p_{k-1}\cdot p_4\\ 2p_{k+1}\cdot p_1 & \cdots & 2p_{k+1}\cdot p_4\\ \vdots & \ddots & \vdots\end{pmatrix}\\ &=\frac{1}{i\pi^2}\int d^Dq\frac{1}{D_0D_1\cdots D_4}\times\det\begin{pmatrix}D_0+Y_{00} & 2q\cdot p_1 & \cdots & 2q\cdot p_4\\ Y_{10}-Y_{00} & 2p_1\cdot p_1 & \cdots & 2p_1\cdot p_4\\ \vdots & \vdots & \ddots & \vdots\\ Y_{40}-Y_{00} & 2p_4\cdot p_1 & \cdots & 2p_4\cdot p_4\end{pmatrix}\end{aligned} \tag{333}$$

Using

$$2p_i \cdot p_j = Y_{ij} - Y_{i0} - Y_{0j} + Y_{00} \ , \ 2q \cdot p_j = D_j - D_0 + Y_{0j} - Y_{00} \tag{334}$$

Eq.333 becomes

$$\begin{aligned}
0 &= \frac{1}{i\pi^2} \int d^D q \frac{1}{D_0 D_1 \cdots D_4} \\
&\times \det \begin{pmatrix} D_0 + Y_{00} & D_1 - D_0 + Y_{01} - Y_{00} & \cdots & D_4 - D_0 + Y_{04} - Y_{00} \\ Y_{10} - Y_{00} & Y_{11} - Y_{10} - Y_{01} + Y_{00} & \cdots & Y_{14} - Y_{10} - Y_{04} + Y_{00} \\ \vdots & \vdots & \ddots & \vdots \\ Y_{40} - Y_{00} & Y_{41} - Y_{40} - Y_{01} + Y_{00} & \cdots & Y_{44} - Y_{40} - Y_{04} + Y_{00} \end{pmatrix} \\
&= \frac{1}{i\pi^2} \int d^D q \frac{1}{D_0 D_1 \cdots D_4} \times \det \begin{pmatrix} D_0 + Y_{00} & D_1 + Y_{01} & \cdots & D_4 + Y_{04} \\ Y_{10} - Y_{00} & Y_{11} - Y_{01} & \cdots & Y_{14} - Y_{04} \\ \vdots & \vdots & \ddots & \vdots \\ Y_{40} - Y_{00} & Y_{41} - Y_{01} & \cdots & Y_{44} - Y_{04} \end{pmatrix} \\
&= \det \begin{pmatrix} T_0^4(0) + Y_{00} T_0^5 & T_0^4(1) + Y_{01} T_0^5 & \cdots & T_0^4(4) + Y_{04} T_0^5 \\ Y_{10} - Y_{00} & Y_{11} - Y_{01} & \cdots & Y_{14} - Y_{04} \\ \vdots & \vdots & \ddots & \vdots \\ Y_{40} - Y_{00} & Y_{41} - Y_{01} & \cdots & Y_{44} - Y_{04} \end{pmatrix}
\end{aligned} \tag{335}$$

where we have used the property that the matrix determinant does not change by adding the first column to each of the other columns. We can also enlarge this 5×5 matrix determinant by adding one column and one row, which is chosen to be

$$0 = \det \begin{pmatrix} 1 & Y_{00} & Y_{01} & \cdots & Y_{04} \\ 0 & T_0^4(0) + Y_{00} T_0^5 & T_0^4(1) + Y_{01} T_0^5 & \cdots & T_0^4(4) + Y_{04} T_0^5 \\ 0 & Y_{10} - Y_{00} & Y_{11} - Y_{01} & \cdots & Y_{14} - Y_{04} \\ \vdots & \vdots & \vdots & \ddots & \vdots \\ 0 & Y_{40} - Y_{00} & Y_{41} - Y_{01} & \cdots & Y_{44} - Y_{04} \end{pmatrix} \tag{336}$$

Adding the first row to each of the other rows and exchanging the first and second rows, we end up with

$$
\begin{aligned}
0 = \det & \begin{pmatrix}
0 & T_0^4(0) & T_0^4(0) & T_0^4(0) & T_0^4(0) & T_0^4(0) \\
1 & Y_{00} & Y_{01} & Y_{02} & Y_{03} & Y_{04} \\
1 & Y_{10} & Y_{11} & Y_{12} & Y_{13} & Y_{14} \\
1 & Y_{20} & Y_{21} & Y_{22} & Y_{23} & Y_{24} \\
1 & Y_{30} & Y_{31} & Y_{32} & Y_{33} & Y_{34} \\
1 & Y_{40} & Y_{41} & Y_{42} & Y_{43} & Y_{44}
\end{pmatrix} \\
+ \det & \begin{pmatrix}
0 & Y_{00}T_0^5 & Y_{01}T_0^5 & Y_{02}T_0^5 & Y_{03}T_0^5 & Y_{04}T_0^5 \\
0 & 0 & 0 & 0 & 0 & 0 \\
0 & 0 & 0 & 0 & 0 & 0 \\
0 & 0 & 0 & 0 & 0 & 0 \\
0 & 0 & 0 & 0 & 0 & 0 \\
0 & 0 & 0 & 0 & 0 & 0
\end{pmatrix} \qquad (337) \\
= (-1) \times \det & \begin{pmatrix}
T_0^5 & -T_0^4(0) & -T_0^4(1) & -T_0^4(2) & -T_0^4(3) & -T_0^4(4) \\
1 & Y_{00} & Y_{01} & Y_{02} & Y_{03} & Y_{04} \\
1 & Y_{10} & Y_{11} & Y_{12} & Y_{13} & Y_{14} \\
1 & Y_{20} & Y_{21} & Y_{22} & Y_{23} & Y_{24} \\
1 & Y_{30} & Y_{31} & Y_{32} & Y_{33} & Y_{34} \\
1 & Y_{40} & Y_{41} & Y_{42} & Y_{43} & Y_{44}
\end{pmatrix} \qquad (338)
\end{aligned}
$$

The equivalence between Eq.337 and Eq.338 can be easily checked with Mathematica. Eq.338 is exactly Eq.125 and can be solved for the scalar five-point function T_0^5. In particular this yields T_0^5 can be reduced to a linear combination of five scalar four-point functions, which is only true if the Gram determinant vanishes.

Appendix B Analytical Expressions for $T_0^{N\leq 4}$

In this appendix, we will provide a detailed derivation of the analytical expressions for $T_0^{N\leq 4}$. As mentioned in Sec. 1.3.2, all one-loop tensor integrals can be reduced to scalar integrals. Therefore, by obtaining analytical expressions for scalar integrals, the one-loop tensor integrals are also known analytically. Remember that

$$T_0^1 = A_0, T_0^2 = B_0, T_0^3 = C_0, T_0^4 = D_0. \tag{339}$$

B.1 Preliminary

To derive the analytical expressions for one-loop scalar integral, the following property is crucial

$$\begin{aligned} I_n(A) &= \int d^D q \frac{1}{[q^2 - A + i\varepsilon]^n} \\ &= \int d^D q \frac{1}{[(q+p)^2 - A + i\varepsilon]^n}, \end{aligned} \tag{340}$$

which follows the Lorentz invariance of Feynman integral. The analytical expression for I_n reads

$$I_n(A) = i(-1)^n \pi^{\frac{D}{2}} \frac{\Gamma(n - \frac{D}{2})}{\Gamma(n)} (A - i\varepsilon)^{\frac{D}{2} - n} \tag{341}$$

We also list some important integrals, which are related to logarithmic log, di-logarithmic Li_2 and tri-logarithmic functions Li_3,

$$I(a,b) = \int_0^1 dx \ \frac{1}{ax+b} = \frac{1}{a} \ln \frac{a+b}{b}, \tag{342}$$

$$I(a,x_i) = \int_0^1 dx\ \ln\big[a(x-x_1)(x-x_2)-i\varepsilon\big]$$
$$= \ln(a-i\varepsilon) + \sum_{i=1}^{2}\left(\ln(1-x_i) - x_i \ln\frac{x_i-1}{x_i} - 1\right), \tag{343}$$

$$\mathrm{Li}_2(x) = -\int_0^x dt \frac{\ln(1-t)}{t} = -\int_0^1 dt \frac{\ln(1-xt)}{t}, \tag{344}$$

$$\mathrm{Li}_3(x) = \int_0^x dt \frac{Li_2(t)}{t}, \tag{345}$$

$$\int_0^1 \frac{dt}{t}\ln^2(1+at) = \ln(-a)\ln^2(1+a)$$
$$+ 2\ln(1+a)\mathrm{Li}_2(1+a) - 2\mathrm{Li}_2(1+a) + 2\mathrm{Li}_3(1) \tag{346}$$

$$\int_0^1 \frac{dt}{t}\ln^2\frac{1+a_1t}{1+a_2t} = [\ln(1+a_1) - \ln(1+a_2)]$$
$$\times\left\{\left[\ln\frac{a_2-a_1}{1+a_2} - \ln\left(1-\frac{a_2(1+a_1)}{a_1(1+a_2)} \pm i\varepsilon\right)\right]\times[\ln(1+a_1)\right.$$
$$\left. - \ln(1+a_2)] + 2\mathrm{Li}_2\frac{1+a_1}{1+a_2} - 2\mathrm{Li}_2\left(\frac{a_2(1+a_1)}{a_1(1+a_2)} \mp i\varepsilon\right)\right\}$$
$$- 2\mathrm{Li}_3\frac{1+a_1}{1+a_2} + 2\mathrm{Li}_3\left(\frac{a_2(1+a_1)}{a_1(1+a_2)} \mp i\varepsilon\right) \tag{347}$$

B.2 One-Point Function

The scalar one-point function reads:

$$A_0(m) = (\mu^2\pi e^{\gamma_E})^\epsilon \frac{1}{i\pi^2}\int d^Dq\ \frac{1}{q^2-m^2+i\varepsilon}$$
$$= (\mu^2\pi e^{\gamma_E})^\epsilon \frac{1}{i\pi^2} I_1(m^2) \tag{348}$$

Plugging in Eq. 341 and expanding $D = 4-2\epsilon$ up to $\mathcal{O}(\epsilon)$, we obtain

$$A_0(m) = -m^2\big(\frac{m^2}{\mu^2}\big)^{-\epsilon} e^{\gamma_E\epsilon}\Gamma(\epsilon-1) \tag{349}$$

$$= m^2\left\{\frac{1}{\epsilon} + 1 - \ln\frac{m^2}{\mu^2} + \epsilon\big[1 + \frac{\pi^2}{12} - \ln\frac{m^2}{\mu^2} + \frac{1}{2}\ln^2\frac{m^2}{\mu^2}\big]\right\} + \mathcal{O}(\epsilon^2) \qquad (350)$$

B.3 Two-Point Function

The scalar two-point function $B_0(k^2, m_1, m_2) = B_0$ has the following form:

$$\begin{aligned} B_0 &= (\mu^2\pi e^{\gamma_E})^\epsilon \frac{1}{i\pi^2}\int d^D q\ \frac{1}{[q^2 - m_1^2 + i\varepsilon][(q+k)^2 - m_2^2 + i\varepsilon]} \\ &= (\mu^2\pi e^{\gamma_E})^\epsilon \frac{1}{i\pi^2}\int_0^1 dx\ \int d^D q \frac{1}{[(q+xk)^2 - (x^2k^2 + x(-k^2 - m_1^2 + m_2^2) + m_1^2 - i\varepsilon]^2} \\ &= (\mu^2\pi e^{\gamma_E})^\epsilon \frac{1}{i\pi^2}\int_0^1 dx\ I_2(x^2k^2 + x(-k^2 - m_1^2 + m_2^2) + m_1^2 - i\varepsilon) \end{aligned} \qquad (351)$$

where we have used Feynman parametrization. Plugging in Eq. 341 and expanding $D = 4 - 2\epsilon$ up to $\mathcal{O}(\epsilon)$, we obtain

$$\begin{aligned} B_0 &= e^{\gamma_E\epsilon}\Gamma(\epsilon)\int_0^1 dx\left[\frac{k^2}{\mu^2}x^2 + \frac{-k^2 + m_2^2 - m_1^2}{\mu^2}x + \frac{m_1^2}{\mu^2} - i\varepsilon\right]^{-\epsilon} \\ &= e^{\gamma_E\epsilon}\Gamma(\epsilon)\int_0^1 dx\left[\frac{k^2}{\mu^2}(x - x_1)(x - x_2) - i\varepsilon\right]^{-\epsilon} \\ &= \frac{1}{\epsilon} + B_0^{(0)} + \epsilon B_0^{(1)} \end{aligned} \qquad (352)$$

where

$$B_0^{(0)} = -\int_0^1 dx \ln\left[\frac{k^2}{\mu^2}(x - x_1)(x - x_2) - i\varepsilon\right] \qquad (353)$$

$$B_0^{(1)} = \int_0^1 dx\frac{\pi^2}{12}x + \int_0^1 dx\frac{1}{2}\ln^2\left[\frac{k^2}{\mu^2}(x - x_1)(x - x_2) - i\varepsilon\right] \qquad (354)$$

and we define $x_{1,2}$ as follows

$$\frac{k^2}{\mu^2}x^2 + \frac{-k^2 + m_2^2 - m_1^2}{\mu^2}x + \frac{m_1^2}{\mu^2} - i\varepsilon = \frac{k^2}{\mu^2}(x - x_1)(x - x_2) - i\varepsilon \qquad (355)$$

With Eq.343, we obtain

$$\begin{aligned} B_0^{(0)} &= -\ln\big(\frac{k^2}{\mu^2} - i\varepsilon\big) - \int_0^1 dx \ln\big[(x-x_1)(x-x_2)\big] \\ &= -\ln\big(\frac{k^2}{\mu^2} - i\varepsilon\big) - \sum_{j=1}^{2}\int_0^1 dx \ln\big[(x-x_j)\big] \\ &= -\ln\big(\frac{k^2}{\mu^2} - i\varepsilon\big) - \sum_{j=1}^{2}\big[\ln(1-x_j) - x_j \ln\frac{x_j-1}{x_j} - 1\big] \end{aligned} \tag{356}$$

where we have imposed $\ln(ab) = \ln a + \ln b$ in the second line because the imaginary part of x_1 and x_2 has opposite sign, i.e. $x_1 x_2 = -i\varepsilon$.

Similarly, $B_0^{(1)}$ is

$$\begin{aligned} B_0^{(1)} &= \frac{\pi^2}{12} + \frac{1}{2}\ln^2\big(\frac{k^2}{\mu^2} - i\varepsilon\big) + \ln\big(\frac{k^2}{\mu^2} - i\varepsilon\big) \times \int_0^1 dx \ln\big[(x-x_1)(x-x_2)\big] \\ &+ \frac{1}{2}\int_0^1 dx \ln^2\big[(x-x_1)(x-x_2)\big] \\ &= \frac{\pi^2}{12} + \frac{1}{2}\ln^2\big(\frac{k^2}{\mu^2} - i\varepsilon\big) + \ln\big(\frac{k^2}{\mu^2} - i\varepsilon\big) \times \sum_{j=1}^{2}\int_0^1 dx \ln\big[(x-x_j)\big] \\ &+ \frac{1}{2}\int_0^1 dx \ln^2\big[(x-x_1)\big] + \frac{1}{2}\int_0^1 dx \ln^2\big[(x-x_2)\big] + \int_0^1 dx \ln(x-x_1)\ln(x-x_2) \\ &= \frac{\pi^2}{12} + \frac{1}{2}\ln^2\big(\frac{k^2}{\mu^2} - i\varepsilon\big) + \sum_{j=1}^{2}\Big\{\frac{1}{2}\ln(1-x_j)\ln^2(1-x_j) + \frac{1}{2}x_j \ln^2(1-x_j) \\ &+ \big[\ln(\frac{k^2}{\mu^2} - i\varepsilon) - 2\big] \times \big[\ln(1-x_j) - x_j \ln\frac{x_j-1}{x_j} - 1\big]\Big\} \\ &+ (1-x_1)\ln(1-x_1)\ln(1-x_2) + x_1\ln(-x_1)\ln(-x_2) + (x_1 - x_2) \\ &\times \left[\mathrm{Li}_2\big(\frac{x_2}{x_2-x_1}\big) - \mathrm{Li}_2\big(\frac{x_2-1}{x_2-x_1}\big) + \ln(x_2-x_1)\ln\frac{x_2-1}{x_2}\right] \end{aligned} \tag{357}$$

B.4 Three-Point Function

The scalar three-point function $C_0(p_1^2, p_2^2, (p_1+p_2)^2, m_1, m_2, m_3) = C_0$ has the following form:

$$\begin{aligned} C_0 &= (\mu^2\pi e^{\gamma_E})^\epsilon \frac{1}{i\pi^2}\int d^Dq\ \frac{1}{[q^2-m_1^2+i\varepsilon][(q+p_1)^2-m_2^2+i\varepsilon][(q+p_1+p_2)^2-m_2^2+i\varepsilon]} \\ &= (\mu^2\pi e^{\gamma_E})^\epsilon \frac{1}{i\pi^2}\int_0^1 dx\int_0^x dy\int d^Dq\ \frac{2}{[(q_1+xp_2+yp_1-p_1-p_2)^2-m_{xy}^2]^3} \\ &= (\mu^2\pi e^{\gamma_E})^\epsilon \frac{2}{i\pi^2}\int_0^1 dx\int_0^x dy\ I_3(m_{xy}^2) \end{aligned} \tag{358}$$

where we have used Feynman parametrization and m_{xy}^2 is

$$\begin{aligned} m_{xy}^2 &= (xp_2+yp_1-p_1-p_2)^2-(1-x)(p_1+p_2)^2 \\ &\quad -(x-y)p_1^2+(1-x)m_3^2+ym_1^2+(x-y)m_2^2-i\varepsilon \\ &= x^2p_2^2+y^2p_1^2+2xyp_1\cdot p_2+x(-p_2^2+m_2^2-m_3^2) \\ &\quad +y(-p_1^2-2p_1\cdot p_2+m_1^2-m_3^2)+m_3^2-i\varepsilon \end{aligned} \tag{359}$$

According to Eq.341, we get

$$C_0 = \mu^{-2}e^{\gamma_E\epsilon}\Gamma(1+\epsilon)\int_0^1 dx\int_0^x dy\big[ax^2+by^2+cxy+dx+ey+f\big]^{-1-\epsilon} \tag{360}$$

where

$$\begin{aligned} &a=\frac{p_2^2}{\mu^2}\ ,\ b=\frac{p_1^2}{\mu^2}\ ,\ c=\frac{2p_1p_2}{\mu^2}\ ,\ d=\frac{-p_2^2+m_2^2-m_3^2}{\mu^2}\ , \\ &e=\frac{-p_1^2-2p_1p_2+m_1^2-m_2^2}{\mu^2}\ ,\ f=\frac{m_3^2}{\mu^2}-i\varepsilon \end{aligned} \tag{361}$$

Transforming y to $\alpha x+y$, the integrand becomes

$$(a+\alpha c+\alpha^2 b)x^2+by^2+(2\alpha b+c)xy+(d+\alpha e)x+ey+f$$

$$= by^2 + (2\alpha b + c)xy + (d + \alpha e)x + ey + f \tag{362}$$

We choose α, which obeys $a + \alpha c + \alpha^2 b = 0$, such that the term proportional x^2 vanishes. Since α obeys a quartic function, the solution of α can be real or imaginary depends on if $b^2 - 4ac$ is positive or negative. At first, we restrict $b^2 - 4ac > 0$, i.e. α is real. So the three-point function becomes

$$C_0 = \mu^{-2} e^{\gamma_E \epsilon} \Gamma(1+\epsilon) \int_0^1 dx \int_{-\alpha x}^{(1-\alpha)x} dy \big[by^2 + (2\alpha b + c)xy + (d + \alpha e)x + ey + f \big]^{-1-\epsilon} \tag{363}$$

Thus, the integration over x can be done easily if we interchange the integration order between x and y, which can be realized with the following trick

$$\begin{aligned} \int_0^1 dx \int_{-\alpha x}^{(1-\alpha)x} dy &= \int_0^1 dx \int_0^{(1-\alpha)x} dy \; - \int_0^1 dx \int_0^{-\alpha x} dy \\ &= \int_0^{1-\alpha} dy \int_{y/(1-\alpha)}^1 dx - \int_0^{-\alpha} dy \int_{-y/\alpha}^1 dx \end{aligned} \tag{364}$$

It is evident that this transformation requires either α real, or more precisely that there are no singularities in the complex y plane in the triangle. Plugging in this transformation, the three-point function becomes

$$\begin{aligned} C_0 = {} & \mu^{-2} e^{\gamma_E \epsilon} \Gamma(1+\epsilon) \\ & \times \left\{ \int_0^{1-\alpha} dy \int_{y/(1-\alpha)}^1 dx \big[(2\alpha b y + cy + d + \alpha e)x + by^2 + ey + f \big]^{-1-\epsilon} dx \right. \\ & \left. - \int_0^{-\alpha} dy \int_{-y/\alpha}^1 dx \big[(2\alpha b y + cy + d + \alpha e)x + by^2 + ey + f \big]^{-1-\epsilon} \right\} \end{aligned} \tag{365}$$

The x integral can be integrated easily. Define $N(y)$ be the coefficient of x, i.e. $N(y) = (2\alpha b + c)y + d + \alpha e$, we obtain

$$C_0 = -\mu^{-2} e^{\gamma_E \epsilon} \frac{\Gamma(1+\epsilon)}{\epsilon} \left\{ \int_0^{1-\alpha} dy \frac{1}{N(y)} \big[N(y) + by^2 + ey + f \big]^{-\epsilon} \right.$$

$$
\begin{aligned}
&- \int_0^{1-\alpha} dy \frac{1}{N(y)} \big[\frac{y}{1-\alpha} N(y) + by^2 + ey + f \big]^{-\epsilon} \\
&- \int_0^{-\alpha} dy \frac{1}{N(y)} \big[N(y) + by^2 + ey + f \big]^{-\epsilon} \\
&+ \int_0^{-\alpha} dy \frac{1}{N(y)} \big[-\frac{y}{\alpha} N(y) + by^2 + ey + f \big]^{-\epsilon} \Big\} \qquad (366) \\
&= C_0^{(0)} + \epsilon C_0^{(1)} \qquad (367)
\end{aligned}
$$

where in the last line, we have expanded $D = 4 - 2\epsilon$ up to $\mathcal{O}(\epsilon)$. The zeroth order of three-point function reads

$$
\begin{aligned}
-\mu^2 C_0^{(0)} = &\int_{-\alpha}^{1-\alpha} dy \ \frac{\ln[by^2 + ey + f + N(y)]}{N(y)} - \int_0^{1-\alpha} dy \ \frac{\ln\big[by^2 + ey + f + \frac{y}{1-\alpha} N(y)\big]}{N(y)} \\
&- \int_{-\alpha}^{0} dy \ \frac{\ln\big[by^2 + ey + f - \frac{y}{\alpha} N(y)\big]}{N(y)} \qquad (368)
\end{aligned}
$$

The three-point function of order $\mathcal{O}(\epsilon)$ is

$$
\begin{aligned}
2\mu^2 C_0^{(1)} = &\int_{-\alpha}^{1-\alpha} dy \ \frac{\ln^2[by^2 + ey + f + N(y)]}{N(y)} - \int_0^{1-\alpha} dy \ \frac{\ln^2\big[by^2 + ey + f + \frac{y}{1-\alpha} N(y)\big]}{N(y)} \\
&- \int_{-\alpha}^{0} dy \ \frac{\ln^2\big[by^2 + ey + f - \frac{y}{\alpha} N(y)\big]}{N(y)} \qquad (369)
\end{aligned}
$$

Note that extra constant term also appears when performing the expansion, but the integral of such constant term over y leads to zero, namely

$$
\int_{-\alpha}^{1-\alpha} dy - \int_0^{1-\alpha} dy \int_{-\alpha}^{0} dy = 0 \qquad (370)
$$

The integrand in Eq.368 and Eq.369 contains a first order pole as $N(y_0) = 0$. To let the residue of the pole vanishes, we introduce a constant term to Eq.368

$$
\begin{aligned}
-\mu^2 C_0^{(0)} = &\int_{-\alpha}^{1-\alpha} dy \ \frac{1}{N(y)} \Big\{ \ln[by^2 + ey + f + N(y)] - \ln[by_0^2 + ey_0 + f] \Big\} \\
&- \int_0^{1-\alpha} dy \ \frac{1}{N(y)} \Big\{ \ln\big[by^2 + ey + f + \frac{y}{1-\alpha} N(y)\big] - \ln\big[by_0^2 + ey_0 + f\big] \Big\}
\end{aligned}
$$

$$- \int_{-\alpha}^{0} dy \ \frac{1}{N(y)} \Big\{ \ln\big[by^2 + ey + f - \frac{y}{\alpha} N(y)\big] - \ln\big[by_0^2 + ey_0 + f\big] \Big\} \quad (371)$$

and Eq.369

$$\begin{aligned} 2\mu^2 C_0^{(1)} = & \int_{-\alpha}^{1-\alpha} dy \ \frac{1}{N(y)} \Big\{ \ln^2[by^2 + ey + f + N(y)] - \ln^2[by_0^2 + ey_0 + f] \Big\} \\ & - \int_{0}^{1-\alpha} dy \ \frac{1}{N(y)} \Big\{ \ln^2\big[by^2 + ey + f + \frac{y}{1-\alpha} N(y)\big] - \ln^2\big[by_0^2 + ey_0 + f\big] \Big\} \\ & - \int_{-\alpha}^{0} dy \ \frac{1}{N(y)} \Big\{ \ln^2\big[by^2 + ey + f - \frac{y}{\alpha} N(y)\big] - \ln^2\big[by_0^2 + ey_0 + f\big] \Big\} \quad (372) \end{aligned}$$

Note that the integral of this constant term vanish, thus adding this constant term does not change the value of $C_0^{(0)}$. The explicit expression for this constant term is

$$\begin{aligned} T &\equiv by_0^2 + ey_0 + f \\ &= b\big(\frac{-d - e\alpha}{2\alpha b + c}\big)^2 + e\big(\frac{-d - e\alpha}{2\alpha b + c}\big) + f = \frac{(2bd - ec)^2}{4b(c^2 - 4ab)} - \frac{e^2}{4b} + f \end{aligned} \quad (373)$$

where $\alpha = (-c \pm \sqrt{c^2 - 4ab})/(2b)$.

The variable transformation $y = y' - \alpha, y = (1-\alpha)y', y = -\alpha y'$ of Eq.368 leads to the following expression

$$\begin{aligned} -\mu^2 C_0^{(0)} = & \int_0^1 dy \ \frac{\ln[by^2 + (c+e)y + a + d + f] - \ln T}{(c + 2\alpha b)y + d + e\alpha + 2a + c\alpha} \\ & - \int_0^1 dy \ \frac{\ln\big[(a+b+c)y^2 + (e+d)y + f\big] - \ln T}{(c + 2\alpha b)(1-\alpha)y + d + e\alpha} \times (1 - \alpha) \\ & + \int_0^1 dy \ \frac{\ln\big[ay^2 + dy + f\big] - \ln T}{(c + 2ab)\alpha y - d - e\alpha} \times \alpha \\ = & \int_0^1 dy \ \Big\{ \frac{\ln Q_1(y) - \ln T}{(c + 2\alpha b)(y - y_1)} - \frac{\ln Q_2(y) - \ln T}{(c + 2\alpha b)(y - y_2)} + \frac{\ln Q_3(y) - \ln T}{(c + 2\alpha b)(y - y_3)} \Big\} \\ = & \frac{1}{c + 2\alpha b}(S_1 - S_2 + S_3) \end{aligned} \quad (374)$$

Following same steps, Eq.369 becomes

$$
\begin{aligned}
2\mu^2 C_0^{(1)} &= \int_0^1 dy\ \frac{\ln^2[by^2+(c+e)y+a+d+f]-\ln^2 T}{(c+2\alpha b)y+d+e\alpha+2a+c\alpha} \\
&- \int_0^1 dy\ \frac{\ln^2\big[(a+b+c)y^2+(e+d)y+f\big]-\ln^2 T}{(c+2\alpha b)(1-\alpha)y+d+e\alpha}\times 1-\alpha \\
&- \int_0^1 dy\ \frac{\ln^2\big[ay^2+dy+f\big]-\ln^2 T}{-(c+2ab)\alpha y+d+e\alpha}\times \alpha \\
&= \int_0^1 dy\ \left\{\frac{\ln^2 Q_1(y)-\ln^2 T}{(c+2\alpha b)(y-y_1)} - \frac{\ln^2 Q_2(y)-\ln^2 T}{(c+2\alpha b)(y-y_2)} + \frac{\ln^2 Q_3(y)-\ln^2 T}{(c+2\alpha b)(y-y_3)}\right\} \\
&= \frac{1}{c+2\alpha b}(J_1-J_2+J_3)
\end{aligned}
\tag{375}
$$

Keep in mind that the residue of the pole vanishes since $Q_i(y_i)=T$. $Q_i(y)$ are defined as

$$
\begin{aligned}
Q_1(y) &= by^2+(c+e)y+a+d+f \\
&= \frac{p_1^2y^2+(-p_1^2+m_1^2-m_2^2)y+m_2^2-i\varepsilon}{\mu^2} \\
Q_2(y) &= (a+b+c)y^2+(e+d)y+f \\
&= \frac{(p_1+p_2)^2y^2+(-(p_1+p_2)+m_1^2-m_3^2)y+m_3^2-i\varepsilon}{\mu^2} \\
Q_3(y) &= ay^2+dy+f \\
&= \frac{p_2^2y^2+(-p_2^2+m_2^2-m_3^2)y+m_3^2-i\varepsilon}{\mu^2}
\end{aligned}
\tag{376}
$$

y_i are

$$
\begin{aligned}
y_1 &= -\frac{d+e\alpha+2a+c\alpha}{c+2\alpha b}, \\
y_2 &= -\frac{d+e\alpha}{(c+2\alpha b)(1-\alpha)}, \\
y_3 &= -\frac{(d+e\alpha)\alpha}{c+2\alpha b}.
\end{aligned}
\tag{377}
$$

Q_i's are quadratic functions of y, the roots are labelled by y_{i1} and y_{i2}, and $Q_i(y_i) = T$, thus we can express $\ln Q_i$ in the form

$$\begin{aligned}\ln Q_i &= \ln\left[T\big(1-\frac{y-y_i}{y_{i1}-y_i}\big)\big(1-\frac{y-y_i}{y_{i2}-y_i}\big)\right] \\ &= \ln T + \ln\big(1-\frac{y-y_i}{y_{i1}-y_i}\big) + \ln\big(1-\frac{y-y_i}{y_{i2}-y_i}\big)\end{aligned} \tag{378}$$

where we have used the properties that: (a) the imaginary part of T and Q_i are same; (b) $y-y_i/y_{i1}-y_i$ and $y-y_i/y_{i2}-y_i$ are opposite.

For later use, we define two new variables

$$r_{ij}^{(1)} = \frac{y_i}{y_{ij}-y_i}\ ,\ r_{ij}^{(2)} = \frac{y_i-1}{y_{ij}-y_i} \tag{379}$$

Now it remains to calculate the integrals S_i, J_i

$$\begin{aligned}S_i &= \int_0^1 dy\ \frac{1}{y-y_i}\Big\{\ln Q_i - \ln T\Big\} \\ &= \int_0^1 dy\ \frac{1}{y-y_i}\Big\{\Big[\ln T + \ln\big(1-\frac{y-y_i}{y_{i1}-y_i}\big) + \ln\big(1-\frac{y-y_i}{y_{i2}-y_i}\big)\Big] - \ln T\Big\} \\ &= \Big(\int_0^{y_i} + \int_{y_i}^1\Big) dy\ \frac{1}{y-y_i}\Big\{\Big[\ln T + \ln\big(1-\frac{y-y_i}{y_{i1}-y_i}\big) + \ln\big(1-\frac{y-y_i}{y_{i2}-y_i}\big)\Big] - \ln T\Big\}\end{aligned} \tag{380}$$

$$\begin{aligned}J_i &= \int_0^1 dy\ \frac{1}{y-y_i}\Big\{\ln^2 Q_i - \ln^2 T\Big\} \\ &= \int_0^1 dy\ \frac{1}{y-y_i}\Big\{\Big[\ln T + \ln\big(1-\frac{y-y_i}{y_{i1}-y_i}\big) + \ln\big(1-\frac{y-y_i}{y_{i2}-y_i}\big)\Big]^2 - \ln^2 T\Big\} \\ &= \Big(\int_0^{y_i} + \int_{y_i}^1\Big) dy\ \frac{1}{y-y_i}\Big\{\Big[\ln T + \ln\big(1-\frac{y-y_i}{y_{i1}-y_i}\big) + \ln\big(1-\frac{y-y_i}{y_{i2}-y_i}\big)\Big]^2 - \ln^2 T\Big\}\end{aligned} \tag{381}$$

Transforming $y = y_i(1-s)$ for the first integration contour and $y = y_i + t(1-y_i)$ for the second, we obtain

$$
\begin{aligned}
S_i &= \int_0^1 \frac{dt}{t}\Bigg\{\Bigg[\ln T + \ln(1+tr_{i1}^{(2)}) + \ln(1+tr_{i2}^{(2)})\Bigg] - \ln T\Bigg\} \\
&- \int_0^1 \frac{ds}{s}\Bigg\{\Bigg[\ln T + \ln(1+sr_{i1}^{(1)}) + \ln(1+sr_{i2}^{(1)})\Bigg] - \ln T\Bigg\} \\
&= \mathrm{Li}_2(-r_{i1}^{(1)}) + \mathrm{Li}_2(-r_{i2}^{(1)}) - \mathrm{Li}_2(-r_{i1}^{(2)}) - \mathrm{Li}_2(-r_{i2}^{(2)}) \qquad (382) \\
J_i &= \int_0^1 \frac{dt}{t}\Bigg\{\Bigg[\ln T + \ln(1+tr_{i1}^{(2)}) + \ln(1+tr_{i2}^{(2)})\Bigg]^2 - \ln^2 T\Bigg\} \\
&- \int_0^1 \frac{ds}{s}\Bigg\{\Bigg[\ln T + \ln(1+sr_{i1}^{(1)}) + \ln(1+sr_{i2}^{(1)})\Bigg]^2 - \ln^2 T\Bigg\} \\
&= \int_0^1 \frac{du}{u}\Bigg\{2\ln T\Bigg[-\ln(1+ur_{i1}^{(1)}) - \ln(1+ur_{i2}^{(1)}) + \ln(1+ur_{i1}^{(2)}) + \ln(1+ur_{i2}^{(2)})\Bigg] \\
&+ \Bigg[\ln(1+ur_{i1}^{(2)}) + \ln(1+ur_{i2}^{(2)})\Bigg]^2 - \Bigg[\ln(1+ur_{i1}^{(1)}) + \ln(1+ur_{i2}^{(1)})\Bigg]^2\Bigg\} \\
&= 2\ln T\Bigg[\mathrm{Li}_2(-r_{i1}^{(1)}) + \mathrm{Li}_2(-r_{i2}^{(1)}) - \mathrm{Li}_2(-r_{i1}^{(2)}) - \mathrm{Li}_2(-r_{i2}^{(2)})\Bigg] \\
&+ \int_0^1 \frac{du}{u}\Bigg\{\Bigg[\ln(1+ur_{i1}^{(2)}) + \ln(1+ur_{i2}^{(2)})\Bigg]^2 - \Bigg[\ln(1+ur_{i1}^{(1)}) + \ln(1+ur_{i2}^{(1)})\Bigg]^2\Bigg\} \\
&= 2\ln T\Bigg[\mathrm{Li}_2(-r_{i1}^{(1)}) + \mathrm{Li}_2(-r_{i2}^{(1)}) - \mathrm{Li}_2(-r_{i1}^{(2)}) - \mathrm{Li}_2(-r_{i2}^{(2)})\Bigg] \\
&+ \int_0^1 \frac{du}{u}\Bigg\{2\ln^2(1+ur_{i1}^{(2)}) + 2\ln^2(1+ur_{i2}^{(2)}) - 2\ln^2(1+ur_{i1}^{(1)}) - 2\ln^2(1+ur_{i2}^{(1)}) \\
&- \Bigg[\ln(1+ur_{i1}^{(2)}) - \ln(1+ur_{i2}^{(2)})\Bigg]^2 + \Bigg[\ln(1+ur_{i1}^{(1)}) - \ln(1+ur_{i2}^{(1)})\Bigg]^2\Bigg\} \qquad (383)
\end{aligned}
$$

The expression for last integral can be obtained with Eq.346 and Eq.347.

With the analytical expressions of S_i and J_i, we can write the analytical expressions for $C_0^{(0)}, C_0^{(1)}$

$$
C_0^{(0)} = -\frac{1}{\mu^2}\frac{1}{c+2ab}\sum_{j=1}^{3}\sum_{k=1}^{2}\sum_{l=1}^{2}(-1)^{j+l}\mathrm{Li}_2(-r_{jk}^{(l)}), \qquad (384)
$$

$$
\begin{aligned}
C_0^{(1)} &= \frac{1}{2\mu^2}\frac{1}{c+2ab}\sum_{j=1}^{3}(-1)^{j+1}J_j \\
&= -C_0^{(0)} \times \ln T + \frac{1}{\mu^2}\frac{1}{c+2ab}\sum_{j=1}^{3}\sum_{l=1}^{2}(-1)^{j+l}\Bigg\{\sum_{k=1}^{2}\Big[-\ln(-r_{jk}^{(l)})\ln^2(1+r_{jk}^{(l)}) \\
&- 2\ln(1+r_{jk}^{(l)})\mathrm{Li}_2(1+r_{jk}^{(l)}) + 2\mathrm{Li}_3(1+r_{jk}^{(l)})\Big] + \Big[\ln(1+r_{j1}^{(l)}) - \ln(1+r_{j2}^{(l)})\Big] \\
&\times \left[\frac{1}{2}\ln(r_{jk}^{(l)}) + \eta\left(-r_{jk}^{(l)}, \frac{1+r_{j2}^{(l)}}{r_{j2}^{(l)} - r_{j1}^{(l)}}\right) \times \Big[\ln(1+r_{j1}^{(l)}) - \ln(1+r_{j2}^{(l)})\Big]\right. \\
&\left. + \mathrm{Li}_2\left(\frac{1+r_{j1}^{(l)}}{1+r_{j2}^{(l)}}\right) - \mathrm{Li}_2\left(\frac{r_{j2}^{(l)}(1+r_{j1}^{(l)})}{r_{j1}^{(l)}(1+r_{j2}^{(l)})}\right)\right] - \mathrm{Li}_3\left(\frac{1+r_{j1}^{(l)}}{1+r_{j2}^{(l)}}\right) + \mathrm{Li}_3\left(\frac{r_{j2}^{(l)}(1+r_{j1}^{(l)})}{r_{j1}^{(l)}(1+r_{j2}^{(l)})}\right)\Bigg\}
\end{aligned}
\tag{385}
$$

These expressions are valid for real mass and momentum squared. For complex parameters, the expressions can be found in Eq.4.26 of [43].

B.5 Four-Point Function

The 1-loop scalar four-point function, $D_0(p_1^2, p_2^2, p_3^2, p_4^2, m_1, m_2, m_3, m_4) = D_0$, is defined as

$$
\begin{aligned}
D_0 &= (\mu^2\pi e^{\gamma_E})^{\epsilon}\frac{1}{i\pi^2}\int d^Dq\ \frac{1}{[q^2 - m_1^2 + i\varepsilon][(q+p_1)^2 - m_2^2 + i\varepsilon]} \\
&\qquad \times \frac{1}{[(q+p_1+p_2)^2 - m_3^2 + i\varepsilon][(q+p_1+p_2+p_3)^2 - m_4^2 + i\varepsilon]} \\
&= (\mu^2\pi e^{\gamma_E})^{\epsilon}\frac{1}{i\pi^2}\int_0^1 dx\int_0^x dy\int_0^y dz\int d^Dq\ \frac{6}{D_{xyz}^4} \\
&= (\mu^2\pi e^{\gamma_E})^{\epsilon}\frac{6}{i\pi^2}\int_0^1 dx\int_0^x dy\int_0^y dz\ I_4(m_{xyz}^2)
\end{aligned}
\tag{386}
$$

with

$$D_{xyz} =[(q_1 + (y-z)p_1 + (x-y)(p_1+p_2) + (1-x)(p_1+p_2+p_3))^2 - m_{xyz}^2] \quad (387)$$

$$\begin{aligned} m_{xyz}^2 =& ax^2 + by^2 + gz^2 + cxy + hxz + jyz + dx + ey + kz + f \\ =& p_3^2x^2 + p_2^2y^2 + p_1^2z^2 + (2p_2\cdot p_3)xy + (2p_1\cdot p_3)xz + (2p_1\cdot p_2)yz \\ &+(m_3^2 - m_4^2 - p_3^2)x + (m_2^2 - m_3^2 - p_2^2 - 2p_2\cdot p_3)y \\ &+ (m_1^2 - m_2^2 - p_1^2 - 2p_1\cdot p_2 - 2p_1\cdot p_3)z + m_4^2 - i\varepsilon \end{aligned} \quad (388)$$

According to Eq.341, we obtain

$$\begin{aligned} D_0 &= (\mu^2\pi e^{\gamma_E})^\epsilon \Gamma(2+\epsilon)\int_0^1 dx\int_0^x dy\int_0^y dz\ [m_{xyz}^2]^{-2-\epsilon} && (389)\\ &= D_0^{(0)} + \mathcal{O}(\epsilon) \\ &= \int_0^1 dx\int_0^x dy\int_0^y dz\ [m_{xyz}^2]^{-2} && (390) \end{aligned}$$

where we have only kept the finite order since the $\mathcal{O}(\epsilon)$ is usually irrelevant for $2\to 2$ process.

Performing projective transformation, where A_i are all positive, we obtain

$$D_0^{(0)} = \int_0^1 dx\int_0^x dy\int_0^y dz\ [A_1A_2A_3A_4]\times[M_{xyz}^2]^{-2} \quad (391)$$

with

$$M_{xyz}^2 = m_{xyz}^2(p_{ij}\to q_{ij}, m_i\to M_i). \quad (392)$$

p_{ij} and M_i are

$$\begin{aligned} q_{ij} &= (p_{ij}^2 + m_i^2 + m_j^2)A_iA_j - m_i^2A_i^2 - m_j^2A_j^2 \\ &= l_{ij}A_iA_j - m_i^2A_i^2 - m_j^2A_j^2, && (393)\\ M_i^2 &= m_i^2A_i^2. && (394) \end{aligned}$$

The A_i are chosen in such a way that the coefficients of z^2, xz and yz disappear, which is equivlant to

$$\begin{aligned} q_{12}^2 = 0 \ &\rightarrow \ l_{12}A_1A_2 - m_1^2A_1^2 - m_2^2A_2^2, \\ q_{13}^2 = q_{23}^2 \ &\rightarrow \ l_{13}A_1A_3 - m_1^2A_1^2 = l_{23}A_2A_3 - m_2^2A_2^2, \\ q_{14}^2 = q_{24}^2 \ &\rightarrow \ l_{14}A_1A_4 - m_1^2A_1^2 = l_{24}A_2A_4 - m_2^2A_2^2 \end{aligned} \tag{395}$$

The solutions for the coefficients A_i are

$$\begin{aligned} \frac{A_1}{A_2} &= \frac{l_{12} \pm \sqrt{l_{12}^2 - 4m_1^2m_2^2}}{2m_1^2}, \\ A_3 &= \frac{m_2^2A_2^2 - m_1^2A_1^2}{l_{23}A_2 - l_{13}A_1}, \\ A_4 &= \frac{m_2^2A_2^2 - m_1^2A_1^2}{l_{24}A_2 - l_{14}A_1} \end{aligned} \tag{396}$$

Note that there is a freedom for choosing A_1 since we solved four variables through three linear equations. Thus Eq.391 becomes

$$\begin{aligned} D_0^{(0)} &= \int_0^1 dx \int_0^x dy \int_0^y dz \ [A_1A_2A_3A_4] \times [a'x^2 + b'y^2 + c'xy + d'x + e'y + k'z + f]^{-2} \\ &= [A_1A_2A_3A_4] \times \int_0^1 dx \int_0^x dy \ \frac{1}{k'} \Big[\frac{1}{a'x^2 + b'y^2 + c'xy + d'x + e'y + f} \\ &- \frac{1}{a'x^2 + b'y^2 + c'xy + d'x + e'y + k'y + f} \Big] \end{aligned} \tag{397}$$

where $a' = a((p_{ij} \rightarrow q_{ij}, m_i \rightarrow M_i)$ and it is same for all the other variables. Clearly, Eq.397 is the sum of two three-point functions, thus it is straightforward to derive the analytical expression for $D_0^{(0)}$ with Eq.360.

Appendix C Analytical Expressions of $\partial_{m_1^2} B_{ijk}(\sigma, m_1^2, m_2^2)$

In this appendix, explicit expressions of $\partial_{m_1^2} B_{ijk}(p^2, m_1^2, m_2^2)$ as well as its imaginary part for various tensor integrals are listed. As before, we use the notation $\partial_{m_i} \equiv \partial/\partial(m_i^2)$, and we also make use of the abbreviations

$$\lambda = \sigma^2 + m_1^4 + m_2^4 - 2(\sigma m_1^2 + \sigma m_2^2 + m_1^2 m_2^2), \tag{398}$$

$$l_1 = \log\left[\frac{m_1^2 + m_2^2 - s + \lambda^{1/2}}{2}\sqrt{\frac{1}{m_1^2 m_2^2}}\right] \tag{399}$$

Expressions of $\partial_{m_1^2} B_{ijk}(p^2, m_1^2, m_2^2)$ as well as its imaginary part for various tensor integrals are

$$\mathrm{Im}\,\partial_{m_1} B_0(\sigma, m_1^2, m_2^2) = -\pi\,\frac{\sigma - m_1^2 + m_2^2}{\sigma\lambda^{1/2}}\,, \tag{400}$$

$$\mathrm{Im}\,\partial_{m_1} B_1(\sigma, m_1^2, m_2^2) = \pi\,\frac{\sigma(m_1^2 + m_2^2 - \sigma) + \lambda}{\sigma^2\lambda^{1/2}}\,, \tag{401}$$

$$\mathrm{Im}\,\partial_{m_1} B_{00}(\sigma, m_1^2, m_2^2) = -\pi\,\frac{\lambda^{1/2}(m_1^2 - m_2^2 - \sigma)}{4\sigma^2}\,, \tag{402}$$

$$\mathrm{Im}\,\partial_{m_1} B_{11}(\sigma, m_1^2, m_2^2) = \pi\,\frac{m_1^4\sigma - m_1^2 m_2^2\sigma - m_1^2\sigma^2 + m_1^2\lambda - m_2^2\lambda}{\sigma^3\lambda^{1/2}}\,, \tag{403}$$

$$\mathrm{Im}\,\partial_{m_1} B_{001}(\sigma, m_1^2, m_2^2) = \pi\,\frac{\lambda^{1/2}(3m_1^2\sigma + 3m_2^2\sigma - 3\sigma^2 + 2\lambda)}{2\sigma^3}\,, \tag{404}$$

$$\begin{aligned}\mathrm{Im}\,\partial_{m_1} B_{111}(\sigma, m_1^2, m_2^2) = \frac{\pi}{\sigma^4\lambda^{1/2}}\big\{&-m_1^6\sigma + m_1^2\sigma(3m_2^2 + 4m_2^2\sigma + \sigma^2 - 5\lambda)\\ &- 2(m_2^6\sigma - 2m_2^4\sigma^2 + m_2^2\sigma^3 + \lambda^2 - \lambda\sigma^2)\big\}\,,\end{aligned} \tag{405}$$

$$\partial_{m_1} B_0(\sigma, m_1^2, m_2^2) = -\frac{1}{2\sigma}\Big(\log\frac{1}{m_1^2} - \log\frac{1}{m_2^2} - 2\frac{2l_1(\sigma - m_1^2 + m_2^2)}{\lambda^{1/2}}\Big)\,, \tag{406}$$

$$\begin{aligned}\partial_{m_1} B_1(\sigma, m_1^2, m_2^2) = -\frac{1}{\sigma} + \frac{1}{2\sigma\sigma}\Big(&(m_2^2 - m_1^2) \times (\log\frac{1}{m_1^2} - \log\frac{1}{m_2^2})\\ &+ \frac{l_1}{\lambda^{1/2}}((\sigma - m_1^2 + m_2^2)(\sigma + m_1^2 - m_2^2) - \lambda\Big)\,,\end{aligned} \tag{407}$$

$$\partial_{m_1} B_{00}(\sigma, m_1^2, m_2^2) = \frac{1}{4}\log\frac{1}{m_1^2} + \frac{1}{4\sigma^2}\Big(\sigma(2\sigma - m_1^2 + m_2^2) - \frac{\lambda + 2\sigma m_2^2}{2}$$
$$\times (\log\frac{1}{m_1^2} - \log\frac{1}{m_2^2}) + l_1\sqrt{\lambda}(\sigma - m_1^2 + m_2^2)\Big)\,, \tag{408}$$

$$\partial_{m_1} B_{11}(\sigma, m_1^2, m_2^2) = \frac{1}{\sigma^3}\Big(\sigma(1.5\sigma - m_1^2 + m_2^2) - \frac{\lambda + 3\sigma m_2^2}{2}$$
$$\times (\log\frac{1}{m_1^2} - \log\frac{1}{m_2^2}) + \frac{(\sigma - m_1^2 + m_2^2)(\lambda + \sigma m_2^2)}{l_1\sqrt{\lambda}}\Big)\,, \tag{409}$$

$$\partial_{m_1} B_{001}(\sigma, m_1^2, m_2^2) = -\frac{1}{12}\log\frac{1}{m_1^2} + \frac{1}{24\sigma^3}\Big((2(m_1^2 - m_2^2)^3 + \sigma^3 + 3\sigma m_2^4 - 3\sigma m_1^4)$$
$$\times (\log\frac{1}{m_1^2} - \log\frac{1}{m_2^2}) + l_1\lambda^{1/2}\frac{2(m_1^2 - m_2^2)^2 - \sigma(\sigma + m_1^2 + m_2^2)}{12\sigma^3}\Big)$$
$$+ \frac{6m_1^4 - 12m_1^2m_2^2 + 6m_2^4 - 6m_1^2\sigma - 6m_2^2\sigma - 5\sigma^2}{36\sigma^2}\,, \tag{410}$$

$$\partial_{m_1} B_{111}(\sigma, m_1^2, m_2^2) = -\frac{6(m_1^2 - m_2^2)^2 + 3m_1^2\sigma - 9m_2^2\sigma + 2\sigma^2}{6\sigma^3}$$
$$- \frac{(m_1^2 - m_2^2)^3 + m_2^2\sigma(2m_1^2 - 2m_2^2 + \sigma)}{2\sigma^4}(\log\frac{1}{m_1^2} - \log\frac{1}{m_2^2})$$
$$\frac{l_1}{\sigma^4\lambda^{1/2}} \times \Big((m_1^2 - m_2^2)^4 - (m_1^2 - m_2^2)^2(m_1^2 + 3m_2^2)\sigma$$
$$- m_1^2m_2^2\sigma^2 + 3m_2^4\sigma^2 - m_2^2\sigma^3\Big)\,. \tag{411}$$

Appendix D Analytical Expressions of $\partial_{m_i^2}\partial_{m_j^2}B_{ijk}(\sigma, m_1^2, m_2^2)$

In this appendix, explicit expressions of $\partial_{m_i^2}\partial_{m_j^2}B_{ijk}(\sigma, m_1^2, m_2^2)$ as well as its imaginary part for various tensor integrals are listed.

$$\mathrm{Im}\,\partial^2_{m_1}B_0(\sigma, m_1^2, m_2^2) = -\pi\,\frac{4m_2^2}{\sigma\lambda^{1/2}}\,, \tag{412}$$

$$\mathrm{Im}\,\partial^2_{m_1}B_1(\sigma, m_1^2, m_2^2) = \pi\,\frac{4m_2^2\sigma^2 - (m_1^2 - m_2^2 - \sigma)(\lambda - 2m_2^2\sigma)}{\sigma^2\lambda^{3/2}}\,, \tag{413}$$

$$\mathrm{Im}\,\partial^2_{m_1}B_{00}(\sigma, m_1^2, m_2^2) = -\pi\,\frac{\lambda + 2m_1^2\sigma}{2\sigma^2\lambda^{1/2}}\,, \tag{414}$$

$$\mathrm{Im}\,\partial^2_{m_1}B_{11}(\sigma, m_1^2, m_2^2) = 2\pi\,\frac{\lambda[\lambda + \sigma(m_1^2 + m_2^2 - \sigma)] - 2\sigma^2 m_1^2 m_2^2}{\sigma^3\lambda^{3/2}}\,, \tag{415}$$

$$\mathrm{Im}\,\partial^2_{m_1}B_{001}(\sigma, m_1^2, m_2^2) = \pi\,\frac{(m_1^2 - m_2^2)(\lambda + m_2^2\sigma) + m_2^2\sigma^2}{2\sigma^3\lambda^{1/2}}\,, \tag{416}$$

$$\begin{aligned}\mathrm{Im}\,\partial^2_{m_1}B_{111}(\sigma, m_1^2, m_2^2) = \frac{\pi}{\sigma^4\lambda^{3/2}}\,\big\{&(m_1^2 - m_2^2 - \sigma)[3\lambda^2 + 4m_2^2\sigma\lambda \\ &+ \sigma^2(3(m_1^2 - m_2^2 - \sigma)(m_1^2 + m_2^2 + \sigma) - 2m_1^2m_2^2)] \\ &+ 12\sigma^3[m_1^4 + m_2^4 - \sigma(m_1^2 + m_2^2)]\big\}\,,\end{aligned} \tag{417}$$

$$\mathrm{Im}\,\partial_{m_1}\partial_{m_2}B_0(\sigma, m_1^2, m_2^2) = \pi\,\frac{2(m_1^2 + m_2^2 - \sigma)}{\lambda^{3/2}}\,, \tag{418}$$

$$\mathrm{Im}\,\partial_{m_1}\partial_{m_2}B_1(\sigma, m_1^2, m_2^2) = \pi\,\frac{4m_1^2\sigma^2 - (m_2^2 - m_1^2 - \sigma)(\lambda - 2m_1^2\sigma)}{\sigma^2\lambda^{3/2}}\,, \tag{419}$$

$$\mathrm{Im}\,\partial_{m_1}\partial_{m_2}B_{00}(\sigma, m_1^2, m_2^2) = \pi\,\frac{(m_1^2 - m_2^2)^2 - \sigma(m_1^2 + m_2^2)}{2\sigma^2\lambda^{1/2}}\,, \tag{420}$$

$$\begin{aligned}\mathrm{Im}\,\partial_{m_1}\partial_{m_2}B_{11}(\sigma, m_1^2, m_2^2) = \pi\,\frac{1}{\sigma^3\lambda^{3/2}}\Big(&2m_1^2\sigma^2(m_1^2 + m_2^2 - \sigma) - \lambda[2\lambda \\ &+ \sigma(3m_1^2 + m_2^2 - \sigma)]\Big)\,,\end{aligned} \tag{421}$$

$$\partial_{m_1}\partial_{m_2}B_0(\sigma, m_1^2, m_2^2) = \frac{2}{\lambda}\Bigg\{-1 + \frac{m_1^2 + m_2^2 - s}{\lambda^{1/2}}$$

$$\times \log \frac{-m_1^2 - m_2^2 + \sigma - \lambda^{1/2}}{2\sqrt{m_1^2 m_2^2}} \Bigg\}, \tag{422}$$

$$\partial_{m_1}\partial_{m_2} B_1(\sigma, m_1^2, m_2^2) = \frac{1}{\sigma}\Bigg\{ \frac{\sigma - m_1^2 + m_2^2}{\lambda} + \frac{1}{2\sigma}\Big(\log\frac{1}{m_1^2} - \log\frac{1}{m_2^2}\Big) + \frac{l_1}{\lambda^{1/2}}\Big(\frac{\sigma - m_1^2 + m_2^2}{\sigma} + \frac{2m_2^2(\sigma - m_1^2 + m_2^2)}{\lambda}\Big)\Bigg\}, \tag{423}$$

$$\partial_{m_1}\partial_{m_2} B_{00}(\sigma, m_1^2, m_2^2) = \frac{1}{2\sigma}\Bigg\{ 1 + \frac{m_1^2 - m_2^2}{2\sigma}\Big(\log\frac{1}{m_1^2} - \log\frac{1}{m_2^2}\Big) + \frac{l_1}{\lambda^{1/2}}\Big(\frac{(m_1^2 - m_2^2)^2}{\sigma} - m_1^2 - m_2^2\Big)\Bigg\}, \tag{424}$$

$$\partial_{m_1}\partial_{m_2} B_{11}(\sigma, m_1^2, m_2^2) = \frac{1}{\sigma^2}\Bigg\{ -2\Big(2 + \frac{m_2^2\sigma}{\lambda}\Big) - \Big(\frac{1}{2} - \frac{m_1^2 - m_2^2}{\sigma}\Big)\Big(\log\frac{1}{m_1^2} - \log\frac{1}{m_2^2}\Big) + \frac{l_1}{\sigma\lambda^{3/2}}\Big(-2(m_1^2 - m_2^2)^4 + (m_1^2 - m_2^2)^2(7m_1^2 + 5m_2^2)\sigma - 3\sigma^2(3m_1^4 + m_2^4) + \sigma^3(5m_1^2 + m_2^2) - \sigma^4\Big)\Bigg\}, \tag{425}$$

$$\partial_{m_1}\partial_{m_2} B_{001}(\sigma, m_1^2, m_2^2) = \frac{1}{4\sigma^2}\Bigg\{ 2(m_1^2 - m_2^2) - \sigma + \Big(\frac{(m_1^2 - m_2^2)^2}{\sigma} - m_1^2\Big) \times \Big(\log\frac{1}{m_1^2} - \log\frac{1}{m_2^2}\Big) + \frac{2l_1}{\sigma\lambda^{1/2}}\Big(\lambda(m_1^2 - m_2^2) + \sigma m_2^2(\sigma + m_1^2 - m - 2^2)\Big)\Bigg\}, \tag{426}$$

$$\partial_{m_1}\partial_{m_2} B_{111}(\sigma, m_1^2, m_2^2) = \frac{1}{2\sigma^3}\Bigg\{ (\sigma - m_1^2 + m_2^2) \times (6 + \frac{2m_2^2\sigma}{\lambda}) - \sigma - \Big(\frac{3(m_2^2 - m_1^2)^2}{\sigma} + 2m_2^2 - 4m_1^2 + \sigma\Big) \times \Big(\log\frac{1}{m_1^2} - \log\frac{1}{m_2^2}\Big) \frac{2l_1}{\sigma\lambda^{1/2}}\Big((m_2^2 - m_1^2) \times (3\lambda + 4\sigma m_2^2) + \sigma\lambda + \frac{2m_2^4\sigma^2(m_1^2 - m_2^2 + s)}{\lambda}\Big)\Bigg\}. \tag{427}$$

The integrated functions for zero momentum are given by, in terms of $r = m_2^2/m_1^2$,

$$\partial^2_{m_1} B_0(0, m_1^2, m_2^2) = \frac{m_1^{-4}}{(1-r)^2}\left[1 + r + 2r\frac{\ln r}{1-r}\right], \tag{428}$$

$$\partial^2_{m_1} B_1(0, m_1^2, m_2^2) = \frac{m_1^{-4}}{2(1-r)^3}\left[-1 - 5r - 2r(2+r)\frac{\ln r}{1-r}\right], \tag{429}$$

$$\partial^2_{m_1} B_{00}(0, m_1^2, m_2^2) = \frac{m_1^{-2}}{4(1-r)^2}\left[-1 + 3r + 2r^2\frac{\ln r}{1-r}\right], \tag{430}$$

$$\partial^2_{m_1} B_{11}(0, m_1^2, m_2^2) = \frac{m_1^{-4}}{3(1-r)^4}\left[1 + 10r + r^2 + 6r(1+r)\frac{\ln r}{1-r}\right], \tag{431}$$

$$\partial^2_{m_1} B_{001}(0, m_1^2, m_2^2) = \frac{m_1^{-2}}{12(1-r)^3}\left[1 - 5r - 2r^2 - 6r^2\frac{\ln r}{1-r}\right], \tag{432}$$

$$\partial^2_{m_1} B_{111}(0, m_1^2, m_2^2) = \frac{m_1^{-4}}{12(1-r)^5}\left[-3 + 47r - 11r^2 + r^3 - 12r(2+3r)\frac{\ln r}{1-r}\right], \tag{433}$$

$$\partial_{m_1}\partial_{m_2} B_0(0, m_1^2, m_2^2) = \frac{m_1^{-4}}{(1-r)^2}\left[-2 - (1+r)\frac{\ln r}{1-r}\right], \tag{434}$$

$$\partial_{m_1}\partial_{m_2} B_1(0, m_1^2, m_2^2)) = \frac{m_1^{-4}}{2(1-r)^3}\left[5 + r + (2+4r)\frac{\ln r}{1-r}\right], \tag{435}$$

$$\partial_{m_1}\partial_{m_2} B_{00}(0, m_1^2, m_2^2) = \frac{m_1^{-2}}{4(1-r)^2}\left[-1 - r - 2r\frac{\ln r}{1-r}\right], \tag{436}$$

$$\partial_{m_1}\partial_{m_2} B_{11}(0, m_1^2, m_2^2) = \frac{m_1^{-4}}{6(1-r)^4}\left[-17 - 8r + r^2 - 6(1+3r)\frac{\ln r}{1-r}\right]. \tag{437}$$

Appendix E Running Z Width and Fixed Z Width

Z propagator under Dyson resummation follows the Breit-Wigner form

$$D_Z(s) = \frac{1}{s - m_Z^2 + i m_Z \Gamma_Z}. \tag{438}$$

In terms of this expression, the corresponding cross section with intermediate Z boson can be written as

$$\sigma \sim \frac{s}{(s - m_Z^2)^2 + m_Z^2 \Gamma_Z^2} \tag{439}$$

One can simply derive that σ becomes maximal at $\sqrt{s} = m_Z(1+\gamma^2)^{1/4}$, where $\gamma = m_Z/\Gamma_Z$. However in experiment, the peak of the cross section shifts with energy about $\Delta E \sim 34$ MeV. The experimental data is better fitted with running width, which is written as

$$\sigma \sim \frac{s}{(s - m_Z^2)^2 + s^2 \gamma^2} \tag{440}$$

The maximum corresponding to this running width cross section is $\sqrt{s} = m_Z(1+\gamma^2)^{-1/4}$, and the energy difference between fixed width and running width is

$$\Delta E = m_Z(1+\gamma^2)^{1/4} - m_Z(1+\gamma^2)^{-1/4} \underset{\gamma \to 0}{\simeq} \frac{1}{2}\gamma^2 m_Z \simeq 34 \text{ MeV} \tag{441}$$

which explains this peak shift.

To produce the correct peak in theoretical calculation, the energy dependent Z boson width with arbitrary EW corrections can be safely taken care of by performing the following transformation

$$G_\mu D_Z(s) = G_\mu^{'} D_Z^{'}(s) \tag{442}$$

where G_μ is the fermi constant and

$$D'_Z(s) = \frac{1}{s - m'^2_Z + i m'_Z \Gamma'_Z}, \tag{443}$$

$$m'_Z = m_Z(1+\gamma^2)^{-1/2}, \tag{444}$$

$$\Gamma'_Z = \Gamma_Z(1+\gamma^2)^{-1/2}, \tag{445}$$

$$G'_\mu = \frac{G_\mu}{1+i\gamma}. \tag{446}$$

m'_Z, Γ'_Z are formal parameters without physical interpretation.

Under this transformation, position of the new peak can be correctly reproduced

$$s = m'_Z(1+\gamma^2)^{1/4} = m_Z(1+\gamma^2)^{-1/2}(1+\gamma^2)^{1/4} = m_Z(1+\gamma^2)^{-1/4} \tag{447}$$

More details can be found in [136].

Bibliography

[1] H. Baer *et al.* "The International Linear Collider Technical Design Report - Volume 2: Physics," [arXiv:1306.6352 [hep-ph]].

[2] P. Bambade *et al.* "The International Linear Collider: A Global Project," [arXiv:1903.01629 [hep-ex]].

[3] A. Abada *et al.* [FCC Collaboration], "FCC-ee: The Lepton Collider : Future Circular Collider Conceptual Design Report Volume 2," Eur. Phys. J. ST **228**, 261 (2019).

[4] J. B. Guimarães da Costa *et al.* [CEPC Study Group], "CEPC Conceptual Design Report: Volume 2 - Physics & Detector," arXiv:1811.10545 [hep-ex].

[5] H. Fritzsch, M. Gell-Mann and H. Leutwyler, Phys. Lett. B **47**, 365-368 (1973) doi:10.1016/0370-2693(73)90625-4

[6] D. J. Gross and F. Wilczek, Phys. Rev. D **8**, 3633-3652 (1973) doi:10.1103/PhysRevD.8.3633

[7] H. D. Politzer, Phys. Rev. Lett. **30**, 1346-1349 (1973) doi:10.1103/PhysRevLett.30.1346

[8] D. J. Gross and F. Wilczek, Phys. Rev. D **9**, 980-993 (1974) doi:10.1103/PhysRevD.9.980

[9] S. L. Glashow, Nucl. Phys. **22**, 579-588 (1961) doi:10.1016/0029-5582(61)90469-2

[10] A. Salam, Conf. Proc. C **680519**, 367-377 (1968) doi:10.1142/9789812795915_0034

[11] S. Weinberg, Phys. Rev. Lett. **19**, 1264-1266 (1967) doi:10.1103/PhysRevLett.19.1264

[12] F. Englert and R. Brout, Phys. Rev. Lett. **13**, 321-323 (1964) doi:10.1103/PhysRevLett.13.321

[13] P. W. Higgs, Phys. Rev. Lett. **13**, 508-509 (1964) doi:10.1103/PhysRevLett.13.508

[14] G. S. Guralnik, C. R. Hagen and T. W. B. Kibble, Phys. Rev. Lett. **13**, 585-587 (1964) doi:10.1103/PhysRevLett.13.585

[15] P. W. Higgs, Phys. Rev. **145**, 1156-1163 (1966) doi:10.1103/PhysRev.145.1156

[16] N. Cabibbo, Phys. Rev. Lett. **10**, 531-533 (1963) doi:10.1103/PhysRevLett.10.531

[17] M. Kobayashi and T. Maskawa, Prog. Theor. Phys. **49**, 652-657 (1973) doi:10.1143/PTP.49.652

[18] y. Fukuda *et al.* [Super-Kamiokande], Phys. Rev. Lett. **82**, 2644-2648 (1999) doi:10.1103/PhysRevLett.82.2644 [arXiv:hep-ex/9812014 [hep-ex]].

[19] Q. R. Ahmad *et al.* [SNO], Phys. Rev. Lett. **89**, 011301 (2002) doi:10.1103/PhysRevLett.89.011301 [arXiv:nucl-ex/0204008 [nucl-ex]].

[20] K. Eguchi *et al.* [KamLAND], Phys. Rev. Lett. **90**, 021802 (2003) doi:10.1103/PhysRevLett.90.021802 [arXiv:hep-ex/0212021 [hep-ex]].

[21] Peskin, M. E. & Schroeder, " An Introduction to Quantum Field Theory , Westview Press" doi:10.1201/9780429503559

[22] M.D. Schwartz, " Quantum Field Theory and the Standard Model, Cambridge University Press, Cambridge, " doi: 10.1080/00107514.2014.970232

[23] J. F. Gunion, H. E. Haber, G. L. Kane and S. Dawson, Front. Phys. **80**, 1-404 (2000) SCIPP-89/13.

[24] J. C. Romao and J. P. Silva, Int. J. Mod. Phys. A **27**, 1230025 (2012) doi:10.1142/S0217751X12300256 [arXiv:1209.6213 [hep-ph]].

[25] S. Weinberg, Phys. Rev. Lett. **43**, 1566-1570 (1979) doi:10.1103/PhysRevLett.43.1566

[26] G. 't Hooft, Nucl. Phys. B **35**, 167-188 (1971) doi:10.1016/0550-3213(71)90139-8

[27] G. 't Hooft and M. J. G. Veltman, Nucl. Phys. B **44**, 189-213 (1972) doi:10.1016/0550-3213(72)90279-9

[28] B. W. Lee and J. Zinn-Justin, Phys. Rev. D **5**, 3121-3137 (1972) doi:10.1103/PhysRevD.5.3121

[29] B. W. Lee and J. Zinn-Justin, Phys. Rev. D **5**, 3137-3155 (1972) [erratum: Phys. Rev. D **8**, 4654 (1973)] doi:10.1103/PhysRevD.5.3137

[30] B. W. Lee and J. Zinn-Justin, Phys. Rev. D **5**, 3155-3160 (1972) doi:10.1103/PhysRevD.5.3155

[31] B. W. Lee and J. Zinn-Justin, Phys. Rev. D **7**, 1049-1056 (1973) doi:10.1103/PhysRevD.7.1049

[32] A. Denner and S. Dittmaier, Phys. Rept. **864**, 1-163 (2020) doi:10.1016/j.physrep.2020.04.001 [arXiv:1912.06823 [hep-ph]].

[33] A. Freitas, W. Hollik, W. Walter and G. Weiglein, Nucl. Phys. B **632**, 189-218 (2002) [erratum: Nucl. Phys. B **666**, 305-307 (2003)] doi:10.1016/S0550-3213(02)00243-2 [arXiv:hep-ph/0202131 [hep-ph]].

[34] M. Awramik, M. Czakon, A. Onishchenko and O. Veretin, Phys. Rev. D **68**, 053004 (2003) doi:10.1103/PhysRevD.68.053004 [arXiv:hep-ph/0209084 [hep-ph]].

[35] A. Sirlin, Phys. Rev. D **22**, 971-981 (1980) doi:10.1103/PhysRevD.22.971

[36] M. Steinhauser, Phys. Lett. B **429**, 158-161 (1998) doi:10.1016/S0370-2693(98)00503-6 [arXiv:hep-ph/9803313 [hep-ph]].

[37] C. Sturm, Nucl. Phys. B **874**, 698-719 (2013) doi:10.1016/j.nuclphysb.2013.06.009 [arXiv:1305.0581 [hep-ph]].

[38] A. Blondel, J. Gluza, S. Jadach, P. Janot, T. Riemann, S. Abreu, J. J. Aguilera-Verdugo, A. B. Arbuzov, J. Baglio and S. D. Bakshi, *et al.* CERN, 2020, ISBN 978-92-9083-560-8, 978-92-9083-559-2 doi:10.23731/CYRM-2020-003 [arXiv:1905.05078 [hep-ph]].

[39] M. Davier, A. Hoecker, B. Malaescu and Z. Zhang, Eur. Phys. J. C **80**, no.3, 241 (2020) [erratum: Eur. Phys. J. C **80**, no.5, 410 (2020)] doi:10.1140/epjc/s10052-020-7792-2 [arXiv:1908.00921 [hep-ph]].

[40] A. Keshavarzi, D. Nomura and T. Teubner, Phys. Rev. D **101**, no.1, 014029 (2020) doi:10.1103/PhysRevD.101.014029 [arXiv:1911.00367 [hep-ph]].

[41] R. L. Workman *et al.* [Particle Data Group], "Review of Particle Physics," PTEP **2022**, 083C01 (2022).

[42] G. Passarino and M. J. G. Veltman, Nucl. Phys. B **160**, 151-207 (1979) doi:10.1016/0550-3213(79)90234-7

[43] A. Denner, Fortsch. Phys. **41**, 307-420 (1993) doi:10.1002/prop.2190410402 [arXiv:0709.1075 [hep-ph]].

[44] G. 't Hooft and M. J. G. Veltman, Nucl. Phys. B **153**, 365-401 (1979) doi:10.1016/0550-3213(79)90605-9

[45] U. Nierste, D. Muller and M. Bohm, Z. Phys. C **57**, 605-614 (1993) doi:10.1007/BF01561479

[46] Q. Song and A. Freitas, JHEP **04**, 179 (2021) doi:10.1007/JHEP04(2021)179 [arXiv:2101.00308 [hep-ph]].

[47] A. Freitas and Q. Song, Phys. Rev. Lett. **130**, no.3, 031801 (2023) doi:10.1103/PhysRevLett.130.031801 [arXiv:2209.07612 [hep-ph]].

[48] J. Fleischer, F. Jegerlehner and O. V. Tarasov, Nucl. Phys. B **672**, 303-328 (2003) doi:10.1016/j.nuclphysb.2003.09.004 [arXiv:hep-ph/0307113 [hep-ph]].

[49] G. J. van Oldenborgh, Comput. Phys. Commun. **66**, 1-15 (1991) doi:10.1016/0010-4655(91)90002-3

[50] T. Hahn and M. Perez-Victoria, Comput. Phys. Commun. **118**, 153-165 (1999) doi:10.1016/S0010-4655(98)00173-8 [arXiv:hep-ph/9807565 [hep-ph]].

[51] T. Binoth, J. P. Guillet, G. Heinrich, E. Pilon and T. Reiter, Comput. Phys. Commun. **180**, 2317-2330 (2009) doi:10.1016/j.cpc.2009.06.024 [arXiv:0810.0992 [hep-ph]].

[52] J. P. Guillet, G. Heinrich and J. F. von Soden-Fraunhofen, Comput. Phys. Commun. **185**, 1828-1834 (2014) doi:10.1016/j.cpc.2014.03.009 [arXiv:1312.3887 [hep-ph]].

[53] A. Denner, S. Dittmaier and L. Hofer, PoS **LL2014**, 071 (2014) doi:10.22323/1.211.0071 [arXiv:1407.0087 [hep-ph]].

[54] A. Denner, S. Dittmaier and L. Hofer, Comput. Phys. Commun. **212**, 220-238 (2017) doi:10.1016/j.cpc.2016.10.013 [arXiv:1604.06792 [hep-ph]].

[55] A. van Hameren, Comput. Phys. Commun. **182**, 2427-2438 (2011) doi:10.1016/j.cpc.2011.06.011 [arXiv:1007.4716 [hep-ph]].

[56] S. Carrazza, R. K. Ellis and G. Zanderighi, Comput. Phys. Commun. **209**, 134-143 (2016) doi:10.1016/j.cpc.2016.07.033 [arXiv:1605.03181 [hep-ph]].

[57] H. H. Patel, Comput. Phys. Commun. **197**, 276-290 (2015) doi:10.1016/j.cpc.2015.08.017 [arXiv:1503.01469 [hep-ph]].

[58] H. H. Patel, Comput. Phys. Commun. **218**, 66-70 (2017) doi:10.1016/j.cpc.2017.04.015 [arXiv:1612.00009 [hep-ph]].

[59] T. Binoth and G. Heinrich, Nucl. Phys. B **585**, 741-759 (2000) doi:10.1016/S0550-3213(00)00429-6 [arXiv:hep-ph/0004013 [hep-ph]].

[60] E. E. Boos and A. I. Davydychev, Theor. Math. Phys. **89**, 1052-1063 (1991) doi:10.1007/BF01016805

[61] A. V. Kotikov, Phys. Lett. B **254**, 158-164 (1991) doi:10.1016/0370-2693(91)90413-K

[62] A. Freitas, Prog. Part. Nucl. Phys. **90**, 201-240 (2016) doi:10.1016/j.ppnp.2016.06.004 [arXiv:1604.00406 [hep-ph]].

[63] G. Aad *et al.* [ATLAS], "Observation of a new particle in the search for the Standard Model Higgs boson with the ATLAS detector at the LHC," Phys. Lett. B **716**, 1 (2012) [arXiv:1207.7214 [hep-ex]].

[64] S. Chatrchyan *et al.* [CMS], "Observation of a New Boson at a Mass of 125 GeV with the CMS Experiment at the LHC," Phys. Lett. B **716**, 30 (2012) [arXiv:1207.7235 [hep-ex]].

[65] G. Aad *et al.* [ATLAS], Phys. Rev. D **101**, no.1, 012002 (2020) doi:10.1103/PhysRevD.101.012002 [arXiv:1909.02845 [hep-ex]].

[66] y. Gong, Z. Li, X. Xu, L. L. Yang and X. Zhao, "Mixed QCD-EW corrections for Higgs boson production at e^+e^- colliders," Phys. Rev. D **95**, 093003 (2017) [arXiv:1609.03955 [hep-ph]].

[67] Q. F. Sun, F. Feng, y. Jia and W. L. Sang, "Mixed electroweak-QCD corrections to e+e-→HZ at Higgs factories," Phys. Rev. D **96**, no.5, 051301(R) (2017) [arXiv:1609.03995 [hep-ph]].

[68] F. Yuasa, E. de Doncker, N. Hamaguchi, T. Ishikawa, K. Kato, y. Kurihara, J. Fujimoto and y. Shimizu, Comput. Phys. Commun. **183**, 2136-2144 (2012) doi:10.1016/j.cpc.2012.05.018 [arXiv:1112.0637 [hep-ph]].

[69] V. Shtabovenko, R. Mertig and F. Orellana, "New Developments in FeynCalc 9.0," Comput. Phys. Commun. **207**, 432 (2016)

[70] G. Weiglein, R. Scharf and M. Bohm, Nucl. Phys. B **416**, 606-644 (1994) doi:10.1016/0550-3213(94)90325-5 [arXiv:hep-ph/9310358 [hep-ph]].

[71] S. Bauberger, A. Freitas and D. Wiegand, JHEP **01**, 024 (2020) doi:10.1007/JHEP01(2020)024 [arXiv:1908.09887 [hep-ph]].

[72] X. Chen, X. Guan, C. Q. He, Z. Li, X. Liu and y. Q. Ma, [arXiv:2209.14953 [hep-ph]].

[73] G. J. van Oldenborgh and J. A. M. Vermaseren, Z. Phys. C **46**, 425 (1990).

[74] B. W. Lee, C. Quigg and H. B. Thacker, Phys. Rev. D **16**, 1519 (1977).

[75] J. Fleischer and F. Jegerlehner, "Radiative Corrections to Higgs Production by $e^+e^- \to ZH$ in the {Weinberg-Salam} Model," Nucl. Phys. B **216**, 469 (1983).

[76] B. A. Kniehl, "Radiative corrections for associated ZH production at future e^+e^- colliders," Z. Phys. C **55**, 605 (1992).

[77] W. Chen, F. Feng, y. Jia and W. L. Sang, Chin. Phys. C **43**, no.1, 013108 (2019) doi:10.1088/1674-1137/43/1/013108 [arXiv:1811.05453 [hep-ph]].

[78] A. Denner, J. Küblbeck, R. Mertig and M. Böhm, "Electroweak radiative corrections to $e^+e^- \to ZH$," Z. Phys. C **56**, 261 (1992).

[79] S. Bondarenko, y. Dydyshka, L. Kalinovskaya, L. Rumyantsev, R. Sadykov and V. Yermolchyk, "One-loop electroweak radiative corrections to polarized $e^+e^- \to ZH$," Phys. Rev. D **100**, 073002 (2019). [arXiv:1812.10965 [hep-ph]].

[80] y. Wang, X. Xu and L. L. Yang, Phys. Rev. D **100**, no.7, 071502 (2019) doi:10.1103/PhysRevD.100.071502 [arXiv:1905.11463 [hep-ph]].

[81] M. Greco, G. Montagna, O. Nicrosini, F. Piccinini and G. Volpi, Phys. Lett. B **777**, 294-297 (2018) doi:10.1016/j.physletb.2017.12.056 [arXiv:1711.00826 [hep-ph]].

[82] F. Zwicky, Helv. Phys. Acta **6**, 110-127 (1933) doi:10.1007/s10714-008-0707-4

[83] M. J. Dolan, J. L. Hewett, M. Krämer and T. G. Rizzo, JHEP **07**, 039 (2016) doi:10.1007/JHEP07(2016)039 [arXiv:1601.07208 [hep-ph]].

[84] G. C. Branco, P. M. Ferreira, L. Lavoura, M. N. Rebelo, M. Sher and J. P. Silva, Phys. Rept. **516**, 1-102 (2012) doi:10.1016/j.physrep.2012.02.002 [arXiv:1106.0034 [hep-ph]].

[85] C. E. Yaguna, Phys. Rev. D **92**, no.11, 115002 (2015) doi:10.1103/PhysRevD.92.115002 [arXiv:1510.06151 [hep-ph]].

[86] L. Calibbi, A. Mariotti and P. Tziveloglou, JHEP **10**, 116 (2015) doi:10.1007/JHEP10(2015)116 [arXiv:1505.03867 [hep-ph]].

[87] T. Cohen, J. Kearney, A. Pierce and D. Tucker-Smith, Phys. Rev. D **85**, 075003 (2012) doi:10.1103/PhysRevD.85.075003 [arXiv:1109.2604 [hep-ph]].

[88] C. Cai, Z. H. Yu and H. H. Zhang, Nucl. Phys. B **921**, 181-210 (2017) doi:10.1016/j.nuclphysb.2017.05.015 [arXiv:1611.02186 [hep-ph]].

[89] A. Dedes and D. Karamitros, Phys. Rev. D **89**, no.11, 115002 (2014) doi:10.1103/PhysRevD.89.115002 [arXiv:1403.7744 [hep-ph]].

[90] M. Aiko, S. Kanemura and K. Mawatari, Eur. Phys. J. C **81**, no.11, 1000 (2021) doi:10.1140/epjc/s10052-021-09764-8 [arXiv:2109.02884 [hep-ph]].

[91] J. Gu, H. Li, Z. Liu, S. Su and W. Su, JHEP **12**, 153 (2017) doi:10.1007/JHEP12(2017)153 [arXiv:1709.06103 [hep-ph]].

[92] S. Kanemura, M. Kikuchi, K. Mawatari, K. Sakurai and K. Yagyu, Phys. Lett. B **783**, 140-149 (2018) doi:10.1016/j.physletb.2018.06.035 [arXiv:1803.01456 [hep-ph]].

[93] F. Bojarski, G. Chalons, D. Lopez-Val and T. Robens, JHEP **02**, 147 (2016) doi:10.1007/JHEP02(2016)147 [arXiv:1511.08120 [hep-ph]].

[94] T. Han, S. Li, S. Su, W. Su and y. Wu, JHEP **01**, 045 (2021) doi:10.1007/JHEP01(2021)045 [arXiv:2008.05492 [hep-ph]].

[95] A. Arhrib, M. Capdequi Peyranere, W. Hollik and S. Penaranda, Phys. Lett. B **579**, 361-370 (2004) doi:10.1016/j.physletb.2003.10.006 [arXiv:hep-ph/0307391 [hep-ph]].

[96] S. Kanemura, M. Kikuchi and K. Yagyu, Nucl. Phys. B **896**, 80-137 (2015) doi:10.1016/j.nuclphysb.2015.04.015 [arXiv:1502.07716 [hep-ph]].

[97] N. Chen, T. Han, S. Li, S. Su, W. Su and y. Wu, JHEP **08**, 131 (2020) doi:10.1007/JHEP08(2020)131 [arXiv:1912.01431 [hep-ph]].

[98] N. Chen, T. Han, S. Su, W. Su and y. Wu, JHEP **03**, 023 (2019) doi:10.1007/JHEP03(2019)023 [arXiv:1808.02037 [hep-ph]].

[99] F. Kling, H. Li, A. Pyarelal, H. Song and S. Su, JHEP **06**, 031 (2019) doi:10.1007/JHEP06(2019)031 [arXiv:1812.01633 [hep-ph]].

[100] B. Coleppa, F. Kling and S. Su, JHEP **01**, 161 (2014) doi:10.1007/JHEP01(2014)161 [arXiv:1305.0002 [hep-ph]].

[101] Q. F. Xiang, X. J. Bi, P. F. Yin and Z. H. Yu, Phys. Rev. D **97**, no.5, 055004 (2018) doi:10.1103/PhysRevD.97.055004 [arXiv:1707.03094 [hep-ph]].

[102] J. W. Wang, X. J. Bi, Q. F. Xiang, P. F. Yin and Z. H. Yu, Phys. Rev. D **97**, no.3, 035021 (2018) doi:10.1103/PhysRevD.97.035021 [arXiv:1711.05622 [hep-ph]].

[103] A. Freitas, S. Westhoff and J. Zupan, JHEP **09**, 015 (2015) doi:10.1007/JHEP09(2015)015 [arXiv:1506.04149 [hep-ph]].

[104] R. Mahbubani and L. Senatore, Phys. Rev. D **73**, 043510 (2006) doi:10.1103/PhysRevD.73.043510 [arXiv:hep-ph/0510064 [hep-ph]].

[105] F. D'Eramo, Phys. Rev. D **76**, 083522 (2007) doi:10.1103/PhysRevD.76.083522 [arXiv:0705.4493 [hep-ph]].

[106] G. F. Giudice and A. Pomarol, Phys. Lett. B **372**, 253-258 (1996) doi:10.1016/0370-2693(96)00060-3 [arXiv:hep-ph/9512337 [hep-ph]].

[107] H. C. Cheng, B. A. Dobrescu and K. T. Matchev, Nucl. Phys. B **543**, 47-72 (1999) doi:10.1016/S0550-3213(99)00012-7 [arXiv:hep-ph/9811316 [hep-ph]].

[108] J. L. Feng, T. Moroi, L. Randall, M. Strassler and S. f. Su, Phys. Rev. Lett. **83**, 1731-1734 (1999) doi:10.1103/PhysRevLett.83.1731 [arXiv:hep-ph/9904250 [hep-ph]].

[109] T. Gherghetta, G. F. Giudice and J. D. Wells, Nucl. Phys. B **559**, 27-47 (1999) doi:10.1016/S0550-3213(99)00429-0 [arXiv:hep-ph/9904378 [hep-ph]].

[110] J. Abdallah *et al.* [DELPHI], Eur. Phys. J. C **31**, 421-479 (2003) doi:10.1140/epjc/s2003-01355-5 [arXiv:hep-ex/0311019 [hep-ex]].

[111] M. E. Peskin and T. Takeuchi, Phys. Rev. Lett. **65**, 964-967 (1990) doi:10.1103/PhysRevLett.65.964

[112] M. E. Peskin and T. Takeuchi, Phys. Rev. D **46**, 381-409 (1992) doi:10.1103/PhysRevD.46.381

[113] I. Maksymyk, C. P. Burgess and D. London, Phys. Rev. D **50**, 529-535 (1994) doi:10.1103/PhysRevD.50.529 [arXiv:hep-ph/9306267 [hep-ph]].

[114] Z. Han, Int. J. Mod. Phys. A **23**, 2653-2685 (2008) doi:10.1142/S0217751X08041384 [arXiv:0807.0490 [hep-ph]].

[115] A. Ismail, E. Izaguirre and B. Shuve, Phys. Rev. D **94**, no.1, 015001 (2016) doi:10.1103/PhysRevD.94.015001 [arXiv:1605.00658 [hep-ph]].

[116] [CMS], CMS-PAS-SUS-21-008.

[117] M. A. Shifman, A. I. Vainshtein, M. B. Voloshin and V. I. Zakharov, Sov. J. Nucl. Phys. **30**, 711-716 (1979) ITEP-42-1979.

[118] R. Gastmans, S. L. Wu and T. T. Wu, [arXiv:1108.5872 [hep-ph]].

[119] D. Huang, Y. Tang and Y. L. Wu, Commun. Theor. Phys. **57**, 427-434 (2012) doi:10.1088/0253-6102/57/3/14 [arXiv:1109.4846 [hep-ph]].

[120] [ATLAS], [arXiv:2207.00348 [hep-ex]].

[121] A. M. Sirunyan *et al.* [CMS], JHEP **07**, 027 (2021) doi:10.1007/JHEP07(2021)027 [arXiv:2103.06956 [hep-ex]].

[122] M. Cepeda, S. Gori, P. Ilten, M. Kado, F. Riva, R. Abdul Khalek, A. Aboubrahim, J. Alimena, S. Alioli and A. Alves, *et al.* CERN Yellow Rep. Monogr. **7**, 221-584 (2019) doi:10.23731/CYRM-2019-007.221 [arXiv:1902.00134 [hep-ph]].

[123] A. Abada *et al.* [FCC], Eur. Phys. J. ST **228**, no.2, 261-623 (2019) doi:10.1140/epjst/e2019-900045-4

[124] J. Liu, N. McGinnis, C. E. M. Wagner and X. P. Wang, JHEP **09**, 073 (2020) doi:10.1007/JHEP09(2020)073 [arXiv:2006.07389 [hep-ph]].

[125] G. Aad *et al.* [ATLAS], Phys. Rev. D **104**, no.11, 112010 (2021) doi:10.1103/PhysRevD.104.112010 [arXiv:2108.07586 [hep-ex]].

[126] A. Tumasyan *et al.* [CMS], Phys. Lett. B **842**, 137460 (2023) doi:10.1016/j.physletb.2022.137460 [arXiv:2205.09597 [hep-ex]].

[127] [ATLAS], ATL-PHYS-PUB-2018-048.

[128] S. Gori, S. Jung, L. T. Wang and J. D. Wells, JHEP **12**, 108 (2014) doi:10.1007/JHEP12(2014)108 [arXiv:1410.6287 [hep-ph]].

[129] A. M. Sirunyan *et al.* [CMS], Phys. Lett. B **782**, 440-467 (2018) doi:10.1016/j.physletb.2018.05.062 [arXiv:1801.01846 [hep-ex]].

[130] G. Aad *et al.* [ATLAS], Phys. Rev. D **101**, no.5, 052005 (2020) doi:10.1103/PhysRevD.101.052005 [arXiv:1911.12606 [hep-ex]].

[131] G. Aad *et al.* [ATLAS], Eur. Phys. J. C **81**, no.12, 1118 (2021) doi:10.1140/epjc/s10052-021-09749-7 [arXiv:2106.01676 [hep-ex]].

[132] N. Cardona, F. Andrés, G. Alfredo, J. Will, S. Paul and T. cheng, JHEP **11**, 026 (2022) doi:10.1007/JHEP11(2022)026 [arXiv:2102.10194 [hep-ph]].

[133] [ATLAS], ATL-PHYS-PUB-2018-031.

[134] H. Zhou and N. Liu, JHEP **10**, 092 (2022) doi:10.1007/JHEP10(2022)092 [arXiv:2208.10406 [hep-ph]].

[135] P. Schwaller and J. Zurita, JHEP **03**, 060 (2014) doi:10.1007/JHEP03(2014)060 [arXiv:1312.7350 [hep-ph]].

[136] Bardin, D. y., Leike, A., Riemann, T., & Sachwitz, M. (1988). Physics Letters B, 206(3), 539-542.